

POLITECNICO DI TORINO



Master of Science in CIVIL ENGINEERING
Structures and Infrastructures

Optimization Strategy for Guyed Radio Mast System
based on SAP2000-OAPI

Master's Degree Thesis

Supervisors

Prof. G. C. Marano

Eng. S. G. Lenti

Candidate

Mario Lo Giudice

Co-Supervisors

Ph.D. Candidate R. Cucuzza

Ph.D. Student M. M. Rosso

Ph.D. Student J. Melchiorre

March 2022
A.Y. 2021/2022

Abstract

In this thesis a size optimization of a guyed radio mast used for radiocommunications is performed. The analyzed case study almost represents a widely industrial solution thanks to the 5G and 6G mobile networks evolution. For these reasons, this particular type of structure was adopted as the main focus of this dissertation.

The first great challenge was to manage the Application Programming Interface, or API, to create the structural model in a FEM Software, starting from an external routine performed with Matlab®. Moreover, non-linear behaviour of cable elements is taken into account during the analysis. From a structural point of view, the structure investigated has been studied according to the current standards, NTC2018. Despite that, it is important to notice that the goal of this study is not to conduct a too accurate and rigorous structural analysis, but to obtain relevant results in terms of structural optimization. However, static and dynamic analysis were investigated with the aim to provide realistic scenarios during the external effects evaluation and verification phase. By the way, just to highlight the coherence of this work, wind action has been evaluated adopting more specific technical standards, according to “Consiglio Nazionale delle Ricerche” (CNR).

The second challenge was to perform multiple analysis to find the optimal solution using Genetic Algorithm (GA). GA has been embedded into the API code, and once runned it, at each iteration, structural analysis was performed using SAP2000. At that point, the main difficulty was represented by the computational effort of the entire procedure. To overcome the problem it was possible to avoid the opening of the Graphical Interface of Sap2000 and improve a slimmer script version of the optimization process.

In the introduction section, a theoretical discussion about compressed steel members and theory of elastic stability is proposed. More details are explained about elastic stability of columns with intermediate elastic bracings.

In the second chapter, an overview of structural optimization and the most famous optimization strategies were described.

In the chapter 5, evaluation of external load for static and dynamic analysis was conducted in compliance with the current technical regulations.

In the chapter 7, several optimization scenarios are investigated with the aim to minimize the total weight of the structure. A sensitivity analysis is herein conducted with the purpose to investigate which are the variables that mainly affect the analysis. Hereafter, a preliminary discussion about the results achieved was exposed.

Finally, once the case study has been evaluated and the structural optimization has been performed as well, a deep discussion is dedicated to comparison between the not-optimized structure and the optimized one obtained from different scenarios. In the chapter 9 dedicated to the final conclusions, some considerations regarding the future developments of the thesis are proposed.

Sommario

In questa tesi viene eseguita una size-optimization di una torre strallata utilizzata per le radiocomunicazioni. Il caso studio analizzato rappresenta una soluzione di notevole interesse ingegneristico grazie all'evoluzione delle reti mobili 5G e 6G. Per questa ragione, questo particolare tipo di struttura è stato adottato come focus principale di questa tesi.

La prima grande sfida è stata quella di gestire l'Application Programming Interface, o API, per creare il modello strutturale in un software FEM, partendo da una routine esterna gestita con Matlab®. Inoltre, il comportamento non lineare degli stralli è stato preso in considerazione durante l'analisi. Da un punto di vista strutturale, la struttura è stata studiata secondo le norme attuali vigenti, le NTC2018. Nonostante ciò, è importante notare che l'obiettivo di questo studio non è quello di condurre un'analisi strutturale troppo rigorosa, ma bensì di ottenere risultati rilevanti in termini di ottimizzazione strutturale. Tuttavia, l'analisi statica e dinamica è stata condotta con lo scopo di fornire scenari realistici durante la fase di valutazione e verifica degli effetti esterni. D'altronde, proprio per evidenziare la coerenza di questo lavoro, l'azione del vento è stata valutata adottando norme tecniche più specifiche, secondo il Consiglio Nazionale delle Ricerche (CNR).

La seconda sfida è stata quella di eseguire analisi multiple per trovare la soluzione ottimale utilizzando l'Algoritmo Genetico (GA). Il GA è stato incorporato nel codice API, e una volta eseguito, ad ogni iterazione, l'analisi strutturale è stata eseguita utilizzando SAP2000. A quel punto, la difficoltà principale era rappresentata dallo sforzo computazionale dell'intera procedura. Per ovviare al problema è stato possibile evitare l'apertura dell'interfaccia grafica di Sap2000 ottenendo uno script, utilizzato per il processo di ottimizzazione, più leggero e veloce.

Nella sezione introduttiva, viene proposta una discussione teorica sulle membrature in acciaio compresse e la teoria della stabilità elastica. Sono inoltre forniti maggiori dettagli sulla stabilità elastica delle colonne con controventi elastici intermedi.

Nel secondo capitolo, è riportata una panoramica sui principi dell'ottimizzazione strutturale, in cui vengono descritte le tecniche e le strategie di ottimizzazione più famose.

Nel capitolo 5, la valutazione dei carichi gravanti sulla struttura e l'analisi statica e dinamica sono state condotte in conformità con le attuali normative tecniche.

Nel capitolo 7 vengono analizzati diversi scenari di ottimizzazione con l'obiettivo di minimizzare il peso totale della struttura. È complessivamente eseguita una analisi di sensibilità al fine di indagare quali sono le variabili che influenzano il comportamento e l'analisi strutturale stessa. Dopodiché, segue una discussione preliminare sui risultati ottenuti.

Infine, una volta che il caso studio è stato valutato e l'ottimizzazione strutturale è stata eseguita, si procede ad una discussione approfondita dedicata al confronto tra la struttura di partenza e quella ottimizzata

ottenuta dai diversi scenari. Nel capitolo 9, dedicato alle conclusioni, vengono proposte alcune considerazioni relative agli sviluppi futuri della tesi.

Ringraziamenti

Prima di tutto, vorrei ringraziare il professor G.C. Marano per avermi dato la possibilità di sviluppare la tesi su un argomento che inizialmente conoscevo poco, e con il quale ho preso gradualmente confidenza fino ad appassionarmi. Allo stesso modo, ci tengo a ringraziare l'ingegnere S.G. Lenti, che oltre ad avermi ospitato presso il suo studio, ha fornito il caso studio del presente lavoro. Sarò sempre grato all'ingegnere, e dottorando, R. Cucuzza per la sua professionalità, per il tempo che mi ha dedicato, ma soprattutto per avermi supportato quando ne avevo più bisogno. Ricorderò sempre l'espressione "Mario, noi siamo ingegneri". Un doveroso ringraziamento al dottorando M.M. Rosso, per il prezioso aiuto profuso, per la sua gentilezza, e per avermi introdotto al mondo dell'ottimizzazione strutturale. Un sincero grazie al dottorando J. Melchiorre, che ha fornito analisi critiche e costruttive, utili a rendere il mio lavoro migliore. Ne approfitto inoltre per ringraziare i membri del T-REM3DIE che mi hanno accolto nel loro laboratorio. A loro vorrei fare un grande in bocca al lupo.

Vorrei dedicare la presente tesi alla mia famiglia, in particolare a mio papà Salvatore e a mia mamma Silvia, per avermi sempre supportato incondizionatamente durante questi anni. A mia sorella Serena, da sempre punto di riferimento, alla quale auguro il meglio. Ai miei nonni, che sarebbero fieri di me. Ringrazio la mia madrina Antonietta e mio zio Giovanni per avermi sempre incoraggiato.

Sarò sempre riconoscente alla mia ragazza, Sara, che in questi anni è stata per me fondamentale. Lei è, ed è stata la persona che fin da subito è riuscita a mettere insieme i pezzi e a ricomporre la mia vita. Questo giorno lo dedico anche, ma soprattutto a te.

Un sincero grazie al mio migliore amico Demetrio, compagno di avventura, ma divisi dall'università e dal lavoro, con l'auspicio di "tornare grandi".

Infine, vorrei ringraziare me stesso per tutti i sacrifici che ho fatto, per aver stretto i denti e per non essermi mai arreso.

Contents

1	Theoretical references of elastic stability	18
1.1	Historical developments	18
1.2	The steel today. Eurocodes and NTC2018.....	19
1.2.1	The role of imperfection in structural members.....	19
1.2.2	Classification of instability phenomena.....	24
1.2.3	Design and verifications of compressed columns at Eurocodes and NTC18.....	26
1.3	Concepts of Theory of Elastic Stability.....	29
1.3.1	Elastic buckling of bars	29
1.3.2	Buckling of bars with multiple intermediate supports	33
1.3.3	Buckling of bars with elastic supports.....	36
1.3.4	Buckling of bars with multiple elastic supports.....	40
2	Bracing of columns.....	47
2.1	Overview	47
2.2	Bracing at the end of a bar.....	47
2.3	Bracing at the middle of a bar	51
2.4	Imperfections in braced columns	53
2.5	Discrete Bracing System for columns.....	54
2.6	Continuous Bracing System for Columns and Beams	58
3	Basic of Structural Optimization	62
3.1	Evolutionary Algorithms.....	65
3.1.1	Genetic Algorithm (GA).....	67
3.1.2	Differential Evolution (DE)	69
3.1.3	Genetic Programming (GP)	71
3.1.4	Evolutionary Strategy (ES)	74
4	Optimization Strategy	76
4.1	Interaction Matlab® - SAP2000® and integration of the Genetic Algorithm (GA).....	76
4.2	Optimization Problem	76
4.3	Optimization problem for the case study	79
4.4	Investigated Scenarios	82
4.4.1	Scenario A	82
4.4.2	Scenario B	83
4.4.3	Scenario C	84

4.4.4	Scenario D	85
4.4.5	Scenario E	86
4.4.6	Scenario F.....	87
4.4.7	Scenario G	88
4.4.8	Scenario H	89
5	Case Study: Structural Analysis of a Guyed Radio Mast.....	90
5.1	General description of the structure.....	90
5.2	Load Analysis	95
5.2.1	Permanent loads (Dead) G1	95
5.2.2	Non-structural permanent loads G2.....	97
5.2.3	Variable loads.....	99
5.2.3.1	Wind load.....	99
5.2.3.2	Maintenance load	115
5.2.3.3	Ice Load.....	115
5.2.4	Seismic action.....	117
5.2.4.1	Geotechnical information of the site.....	117
5.2.4.2	Design Response Spectrum.....	117
5.2.4.3	Vibration Modes	118
5.2.5	Combinations of actions.....	120
5.2.6	Verification Criteria.....	122
5.3	Structural Analysis	123
5.3.1	Modelling solution.....	123
5.3.2	G2 loads	126
5.3.3	Maintenance load.....	127
5.3.4	Wind action	128
5.3.5	Results	131
6	How API operates	139
7	Case Study: Structural Optimization.....	149
7.1	Scenario ‘A’.....	151
7.2	Scenario ‘B’.....	155
7.3	Scenario ‘C’.....	159
7.4	Scenario ‘D’	163
7.5	Scenario ‘E’.....	167
7.6	Scenario ‘F’.....	171
7.7	Scenario ‘G’	175
7.8	Scenario ‘H’	179

8	Discussions and Results	183
9	Conclusions and future developments	194
10	References	196

List of Figures

Figure 1. Influence of the variable yielding. Image taken by [2].	20
Figure 2. Stability curves about strong axis (- - -) and weak axis. Image taken by [2].	20
Figure 3. Influence of cross-sectional shape on stability curves. Image taken by [2].	21
Figure 4. Influence of initial curvature and residual stresses in steel members. Image taken by [2].	21
Figure 5. Influence of initial curvature in circular steel profiles. Image taken by [2].	22
Figure 6. Influence of different imperfections on IPE profile. Image taken by [2].	22
Figure 7. The first three stability curves proposed by CECM-ECCS. Image taken by [2].	23
Figure 8. The five stability curves proposed by CECM-ECCS. Image taken by [2].	24
Figure 9. Pure flexural instability.	25
Figure 10. Pure torsional instability.	25
Figure 11. Lateral-torsional instability.	25
Figure 12. Local instability.	26
Figure 13. Typical shapes of local instability and below distortional instability. Image taken by [2].	26
Figure 14. Typical deformed configuration for stability. Image taken by [2].	27
Figure 15.	28
Figure 16.	29
Figure 17.	31
Figure 18.	31
Figure 19.	33
Figure 20.	33
Figure 21.	34
Figure 22.	36
Figure 23.	36
Figure 24.	37
Figure 25.	38
Figure 26.	38

Figure 27. As the stiffness of intermediate support increases, the critical load increases as well. For $K_2 = 0$ the critical load is the same for a simply supported beam, and $P_{cr} = P_e$.	39
Figure 28.	40
Figure 29.	41
Figure 30. As the stiffness of intermediate support increases, the critical load increases as well. For $K_2 = 0$ the critical load is the same for a simply supported beam, and $P_{cr} = P_e$.	43
Figure 31	44
Figure 32	45
Figure 33.	47
Figure 34. Inadequate stiffness gives sidesway (Helwig & Yura, 1996).	48
Figure 35. The equilibrium state is controlled by the equilibrium rotation (Helwig & Yura, 1996).	48
Figure 36. Relation between the stiffness and critical load when bracing at the top (Helwig & Yura, 1996).	49
Figure 37.	50
Figure 38. Effect of initial out of plumb.	50
Figure 39. Column with sinusoidal shaped curvature (Helwig & Yura, 1996).	51
Figure 40. Inadequate stiffness (Helwig & Yura, 1996)	51
Figure 41. Illustrating column that is subjected to column buckling with a minuscule unyielding support verses a hinge in the middle (Winkler, 1958).	52
Figure 42. Moment equilibrium (Helwig & Yura, 1996).	52
Figure 43.	53
Figure 44. Equilibrium with initial curvature (Winter, 1958).	53
Figure 45. Different types of bracing systems.	54
Figure 46.	55
Figure 47.	55
Figure 48.	55
Figure 49.	56
Figure 50.	56
Figure 51.	57
Figure 52. Continuous bracing system.	58
Figure 53. Continuous inelastic lateral column bracing solutions.	59
Figure 54. Modelling point bracing.	60
Figure 55. Point and continuous lateral column bracing-elastic.	60

Figure 56. Point and continuous lateral column bracing-inelastic.....	61
Figure 57: Images taken by [12]. Initial designs and optimized solutions are proposed. (a) Size optimization; (b) Shape optimization with the function $\eta(x)$; (c) Topology optimization saving 50% of structural material.....	63
Figure 58: Classification of meta-heuristic algorithms. Image taken by [16].	65
Figure 59. Image taken by [21].	66
Figure 60.	67
Figure 61. Population, Chromosome and Alleles (genes). Image taken by [24].	68
Figure 62. Crossover point. Image taken by [24].	68
Figure 63. Exchanging alleles. Image taken by [24].	68
Figure 64. New offspring. Image taken by [24].	68
Figure 65. Mutation: Before and After. Image taken by [24].	69
Figure 66. Differential Evolution flow chart. Image taken by [25].	70
Figure 67. An example of Genetic Programming flow chart. Image taken by [28].	72
Figure 68. Crossover. Image taken by [28].	72
Figure 69. Mutation. Image taken by [28].	73
Figure 70. Workflow adopted for the case study.	76
Figure 71. Linear interpolation used to determine pole-diameter.	79
Figure 72. Flowchart of the optimization procedure using GA.....	81
Figure 73. Conceptual scheme of Scenario A.....	82
Figure 74. From initial to optimized solution. A conceptual scheme.	83
Figure 75. Scenario C.	84
Figure 76. Scenario D.	85
Figure 77. Scenario E.	86
Figure 78. Performance ratios. Adapting segments 2 and 3 means performing a poor optimization of the elements at the ends.	87
Figure 79. Scenario G.	88
Figure 80. Scenario H.	89
Figure 81. Render model realized using Tekla Structures.	90
Figure 82. Other points of view. Tekla Structures.	91
Figure 83. Technical drawing of the structure investigated [mm].	92
Figure 84. Technical drawing of the Shelter.	93
Figure 85. Photographic material of the site	94
Figure 86. Constitutive law stress-strain	95
Figure 87. Rotation capacity of steel members.....	96

Figure 88. Huawei antenna.....	98
Figure 89. Amphenol antenna.....	98
Figure 90. Actions per unit length on slender structures [36].....	101
Figure 91. Reynolds number.	102
Figure 92. Force coefficients c_{fx0} for circular elements.....	103
Figure 93. Slenderness coefficient $\psi\lambda$	104
Figure 94. Force coefficients.....	105
Figure 95. Peak longitudinal aerodynamic actions.	105
Figure 96. Drag and Lift forces	112
Figure 97. Drag and Lift forces. Combo 1.....	113
Figure 98. Drag and Lift forces. Combo 2.....	113
Figure 99. Drag and Lift forces. Combo 3.....	114
Figure 100. Wind action on electronic equipment.....	114
Figure 101. Example of ice formation on different shape section [36].	115
Figure 102. Influence of ice formation.	116
Figure 103. Elastic Response Spectrum Acceleration at SLV	118
Figure 104. Mode 10 – Ts = 0.437s – Mass Participant X = 9.6% Y = 26.2%	118
Figure 105. Mode 11 - Ts = 0.434s - Mass Participant X = 26.4% Y = 9.2%	119
Figure 106. Mode 12 - Ts = 0.206s - Mass Participant X = 7.2% Y = 4.4%	119
Figure 107. Example of beam element in SAP2000.	124
Figure 108. Example of cable modelling in SAP2000.....	124
Figure 109. 3D model in SAP2000.	125
Figure 110. G2 loads.....	126
Figure 111. Maintenance load.....	127
Figure 112. On the left, the distribution of wind load, on the right, the distribution of wind action due to presence of ice sleeves at ULS.....	130
Figure 113. Axial forces diagram.	131
Figure 114. On the left the shear force V2, On the righth the bending moment M2.....	132
Figure 115. On the left the shear force V3, On the righth the bending moment M3.....	132
Figure 116. Perfomance Ratios.	135
Figure 117. Displacements vs elevation at SLS.	138
Figure 118. SAP2000 opening.	139
Figure 119. Define material properties in SAP2000.....	140

Figure 120. Define section properties in SAP2000.....	141
Figure 121. 3D model in SAP2000.	141
Figure 122. Define constraints in SAP2000.	142
Figure 123. Define load patterns in SAP2000.....	142
Figure 124. Define mass-source in SAP2000.....	143
Figure 125. Set a non-linear case in SAP2000.	144
Figure 126. Add load combinations and assign load pattern in SAP2000.	145
Figure 127. Define which load cases must be run in SAP2000.	146
Figure 128. Scenario 'A'. Decay of the Objective Function OF.	151
Figure 129. Scenario 'A' - PRs-trend. In blue are illustrated the Performance Ratios of each pole at the initial situation, in orange at the optimized solution. In green are represented PRs at a design configuration according to the product list.....	153
Figure 130. Scenario 'A'. In blue are illustrated the maximum values of Axial, Shear forces and Bending Moment at the initial situation, in orange at the optimized solution. In green they are represented at a design configuration according to the product list. Moreover they are reported the maximum deformation at the top of the structure.....	154
Figure 131. Scenario 'B'. Decay of the Objective Function OF.	155
Figure 132. Scenario 'B' - PRs-trend. In blue are illustrated the Performance Ratios of each pole at the initial situation, in orange at the optimized solution. In green are represented PRs at a design configuration according to the product list.....	157
Figure 133. Scenario 'B'. In blue are illustrated the maximum values of Axial, Shear forces and Bending Moment at the initial situation, in orange at the optimized solution. In green they are represented at a design configuration according to the product list. Moreover they are reported the maximum deformation at the top of the structure.....	158
Figure 134. Scenario 'C'. Decay of the Objective Function OF.	159
Figure 135. Scenario 'C' - PRs-trend. In blue are illustrated the Performance Ratios of each pole at the initial situation, in orange at the optimized solution. In green are represented PRs at a design configuration according to the product list.....	161
Figure 136. Scenario 'C'. In blue are illustrated the maximum values of Axial, Shear forces and Bending Moment at the initial situation, in orange at the optimized solution. In green they are represented at a design configuration according to the product list.....	162
Figure 137. Scenario 'D'. Decay of the Objective Function OF.	163
Figure 138. Scenario 'D' - PRs-trend. In blue are illustrated the Performance Ratios of each pole at the initial situation, in orange at the optimized solution. In green are represented PRs at a design configuration according to the product list.....	165

Figure 139. Scenario 'D'. In blue are illustrated the maximum values of Axial, Shear forces and Bending Moment at the initial situation, in orange at the optimized solution. In green they are represented at a design configuration according to the product list.....	166
Figure 140. Scenario 'E'. Decay of the Objective Function OF.	167
Figure 141. Scenario 'E' - PRs-trend. In blue are illustrated the Performance Ratios of each pole at the initial situation, in orange at the optimized solution. In green are represented PRs at a design configuration according to the product list.....	169
Figure 142. Scenario 'E'. In blue are illustrated the maximum values of Axial, Shear forces and Bending Moment at the initial situation, in orange at the optimized solution. In green they are represented at a design configuration according to the product list.....	170
Figure 143. Scenario 'F'. Decay of the Objective Function OF.	171
Figure 144. Scenario 'F' - PRs-trend. In blue are illustrated the Performance Ratios of each pole at the initial situation, in orange at the optimized solution. In green are represented PRs at a design configuration according to the product list.....	173
Figure 145. Scenario 'F'. In blue are illustrated the maximum values of Axial, Shear forces and Bending Moment at the initial situation, in orange at the optimized solution. In green they are represented at a design configuration according to the product list.....	174
Figure 146. Scenario 'G'. Decay of the Objective Function OF.	175
Figure 147. Scenario 'G' - PRs-trend. In blue are illustrated the Performance Ratios of each pole at the initial situation, in orange at the optimized solution. In green are represented PRs at a design configuration according to the product list.....	177
Figure 148. Scenario 'G'. In blue are illustrated the maximum values of Axial, Shear forces and Bending Moment at the initial situation, in orange at the optimized solution. In green they are represented at a design configuration according to the product list.....	178
Figure 149. Scenario 'H'. Decay of the Objective Function OF.....	179
Figure 150. Scenario 'H' - PRs-trend. In blue are illustrated the Performance Ratios of each pole at the initial situation, in orange at the optimized solution. In green are represented PRs at a design configuration according to the product list.....	181
Figure 151. Scenario 'H'. In blue are illustrated the maximum values of Axial, Shear forces and Bending Moment at the initial situation, in orange at the optimized solution. In green they are represented at a design configuration according to the product lists.	182
Figure 152. Influence of the number of Optimization Parameters. Average Performance Ratios.....	185
Figure 153. Influence of the number of Optimization Parameters. Mass of the main pole.....	185

Figure 154. In blue, orange and green, the average PRs respectively at initial condition, after optimization, and design solution.	186
Figure 155. Increasing the number of design variables the final mass becomes gradually smaller until 385 kg (scenario H).	187
Figure 156. Computational efforts, knowing $t = 18$ seconds for each iteration	189
Figure 157. Mass Reduction $\Delta M = M_0 - M_{opt}$	189
Figure 158. Providing the ratio between the mass reduction and the computational time, the quantity of structural material saved per unit of time is founded.	190
Figure 159. Objective Function for the single trial. Figure taken from Scenario 'G'	191
Figure 160.	193

List of Tables

Table 1.....	95
Table 2. Technical specifications of steel ropes. Tecnofuni®	96
Table 3. Computation of Dead Loads.....	97
Table 4. Weight of equipment.	99
Table 5. G2 loads.....	99
Table 6.....	100
Table 7.....	101
Table 8. Most common surface roughness.	104
Table 9. Effective slenderness λ [36].....	104
Table 10. Main quantities calculated for this case study.....	106
Table 11. Evaluation of the longitudinal dynamic coefficient for the case study.....	109
Table 12. Evaluation of the transverse dynamic coefficient for the case study.....	112
Table 13. Combinations according to [36].....	112
Table 14. Equipment.....	114
Table 15. Maintenance Load.	115
Table 16. Computation of wind action on ice-sleeves.....	116
Table 17. Combination coefficients.	120
Table 18. Partial factor for the actions at ULS	121
Table 19. Combinations of actions.	121
Table 20. Input parameters for verifications.....	123
Table 21. G2 loads.....	126
Table 22. Maintenance load.	127
Table 23. Drag and Lift forces according to [36] at ULS.....	128
Table 24. Drag and Lift forces according to [36] at SLS.	129
Table 25. Static quantities at Envelope Combination.....	134
Table 26. Performance Ratios (Efficiency indexes) at Envelope Combination.	137
Table 27. Deformability limits for structures subjected to horizontal actions.	137
Table 28. Displacements of the structure along the main pole. From base to top.....	137
Table 29. Total Mass of the main pole.	149
Table 30. Scenario 'A', best solutions.....	151

Table 31. Scenario ‘A’, Optimized solution. The optimization suggests to reduce D to 121 mm that causes a reduction of 437 kg.....	152
Table 32. Scenario ‘A’, Design solution. In this case, industrial product list has available just D=139.7 that is quite similar to 121 mm, suggested by optimizer. For this reason the mass reduction is lower, 264 kg.	152
Table 33. Scenario ‘B’, best solutions.....	155
Table 34. Scenario ‘B’, Optimized solution. At the base D=149 mm, progressively the tapering produces a reduction of D until 103 mm, achieving a mass reduction equal to 389 kg.	156
Table 35. Scenario ‘B’, Design solution. In this case, industrial product list fit quite well the solution proposed by the optimizer, infact the mass reducaiton is similar (329 kg).....	156
Table 36. Scenario ‘C’, best solutions.....	159
Table 37. Scenario ‘C’, Optimized solution. At the base D=147 mm, progressively the tapering produces a reduction of D until 103 mm, achieving a mass reduction equal to 400 kg.	160
Table 38. Scenario ‘C’, Design solution. In this case, industrial product list fit quite well the solution proposed by the optimizer, infact the mass reducaiton is similar (392 kg).....	160
Table 39.....	163
Table 40. Optimized solution. At the base D=161 mm, progressively the tapering produces a reduction of D until 106 mm, achieving a mass reduction equal to 875 kg. The thickness is set to 6 mm.	164
Table 41. Design solution. Industrial product list fit well the optimize solution, in fact the mass reduction is 853kg.	164
Table 42. Scenario ‘E’, best solutions.....	167
Table 43. Scenario ‘E’, Optimized solution.	168
Table 44. Scenario ‘D’, Design solution.....	168
Table 45. Scenario ‘F’, best solutions.	171
Table 46. Scenario ‘E’, Optimized solution. It is evident how introducing two different thickness means adapting better to the problem of interest (-1025kg).....	172
Table 47. Scenario ‘F’, Design solution.	172
Table 48. Scenario ‘G’, best solutions.....	175
Table 49. Scenario ‘G’. Optimized solution. Keeping the same diameter at each segment and just managing the thickness of each segments the mass reduction is equal to 1050kg.....	176
Table 50. Scenario ‘G’. Design solution. Industrial product list has available for a specific diameter, a large number of different thickness. This is reflected in this table, where the mass variation is similar to the optimized solution (-1026kg).	176
Table 51. Scenario ‘H’, best solutions.....	179

Table 52. Scenario 'H', Optimized solution. Coupling tapering and 5 different thickness we obtain an hybrid solution that results in a reduction of 1055 kg.	180
Table 53. Scenario 'H'. Design solution.....	180
Table 54. Summary of the different scenarios.....	184
Table 55. How the number of design variables employed in the structural optimization affects the performance ratios of structural members.	184
Table 56. How the number of design variables employed in the structural optimization affects the performance ratios of structural members.	184
Table 57. Computational Time $T = \text{Pop.Size} \cdot \text{Max.Generations} \cdot \text{Ntrial} \cdot t$	188
Table 58.....	190
Table 59.....	192

1 Theoretical references of elastic stability

1.1 Historical developments

Steel material exhibits high mechanic characteristics and it affects the structures slender and light. However, these aspects influence the design due to the important role of the instability phenomena. The most used theoretical model to study instability is the “compressed bar” or “ideal column” model, which consists into a fixed constrained rod at the base, free at the end, and made of elastic and isotropic material.

The study of the compressed column goes back to Erone of Alexandria (75 A.C.) and in the modern age by Leonardo Da Vinci (1453- 1519). It was P. Van Musschenbroek (1693-1761) who came up with the first empirical formulas and defining the critical load as value inversely proportional to the length of the span. The formulas that we know today, are due to the studies of D. Bernoulli (1700-1782) on the elastic line that inspired the researches of L. Euler (1707-1783) who came up with the well-known formula of the elastic critical load and the critical stress.

$$N_{cr} = \frac{\pi^2 EI}{L^2}$$

$$\sigma_{cr} = \frac{\pi^2 EA}{\lambda^2}$$

Two century later L. Navier (1785-1829) discovered that the Euler’s critical load represented a major limit of the exact solution, Therefore he defined a limit of its applicability in relation to the elastic limit f_e of the structural material through the so-called slenderness limit λ_e , different from the slenderness λ which contains only geometric properties:

$$\lambda_e = \pi \sqrt{\frac{E}{f_e}}$$

$$\lambda = \frac{L}{i}$$

T. Young (1773-1829) observing differences between experimental data, he understood that geometrical imperfections of the columns influenced the carrying capacity. A bar, having width v_0 and subjected to an axial load N , with an initial sinusoidal imperfection was considered. In the middle of the span, the bar is inflected by a moment of the second order:

$$M = \frac{Nv_0}{1 - \frac{N}{N_{cr}}}$$

Young declared that the problem of instability was due to a resistance problem, arguing that the limit load is reached when the normal stress at the most stressed fiber reaches the limit value of the resistance f_{lim} :

$$\frac{N_c}{A} + \frac{N_c v_0}{(1 - N_c/N_{cr})W} = f_{lim}$$

Several years later, R.H. Smith (1878), W.E. Ayrton and J. Perry (1886) and then A. Robertson (1925) gave probabilistic interpretations about the concept of imperfection, while other researchers followed the path traced by Euler introducing the elastoplastic behavior of the material and rejecting the theory related to the imperfections (F. Engesser (1889)). J. Dutheil (1946) was inspired by Young's concepts, treating the behavior of the compressed real bar as a strength problem in which the actions are related to the deformed configuration. Many factors are taken into account, such as geometric imperfections (e.g. initial curvature), and the effect of structural imperfections (e.g. residual stresses and elastic limit variation).

1.2 The steel today. Eurocodes and NTC2018

1.2.1 The role of imperfection in structural members

Due to imperfections, there are differences between ideal and real columns. Overall we can have several conditions that must be taken into account, for instance

- Inhomogeneity in material properties;
- Residual stresses;
- Initial curvature;
- Eccentricity of axial load point of application;

The need to consider the imperfections in the calculation is due to differences between experimental data and theoretical results provided by Euler. However, the implementation of numerical methods combined with calculator have allowed to study the problem in depth, raising the degree of discretization of the column dividing in many small sections (e.g. Finite Element Method). In order to describe the effects of such imperfections in the bar behaviour, it is useful to represent the stability curves in the dimensionless plane $(N ; \lambda)$

$$\bar{N} = \frac{\sigma_c}{f_y} \quad \bar{\lambda} = \frac{\lambda}{\pi\sqrt{E/f_y}}$$

Typically the yielding strength of the material does not affect the behaviour of the bar, as indicated in Figure 1

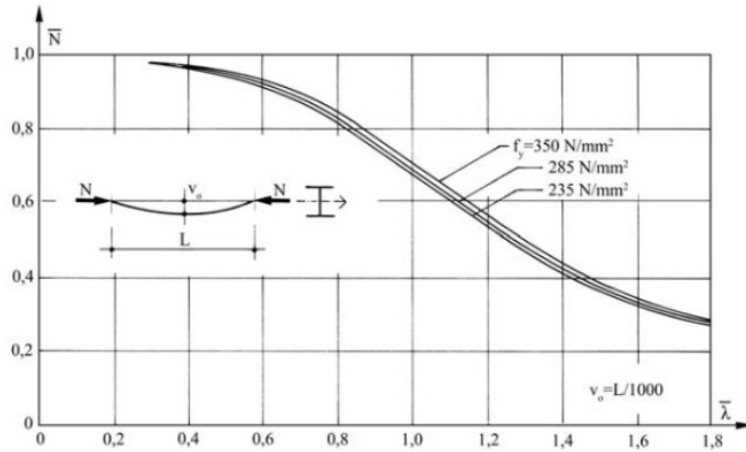


Figure 1. Influence of the variable yielding. Image taken by [2].

If we exclude the absence of mechanical imperfection, the shape of the section could be neglected. As showed in

Figure 2, there are not significant differences between the most used profiles such as HE or IPE. However, the production of steel members is the major cause in yielding structural imperfections.

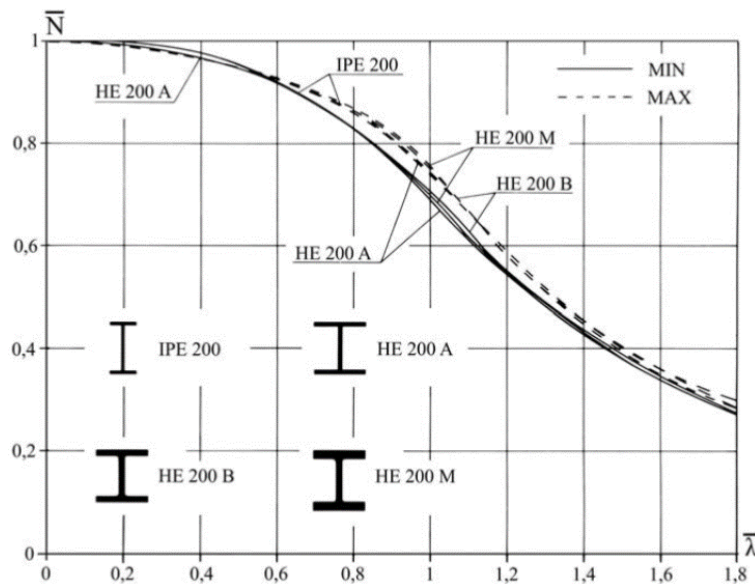


Figure 2. Stability curves about strong axis (- -) and weak axis. Image taken by [2].

Obviously, comparing the most used profiles in steel constructions based on the transversal cross-section, the differences are more evident. The structural behavior of all these members is clearly different and generally weaker with respect the expected one defined by Euler.

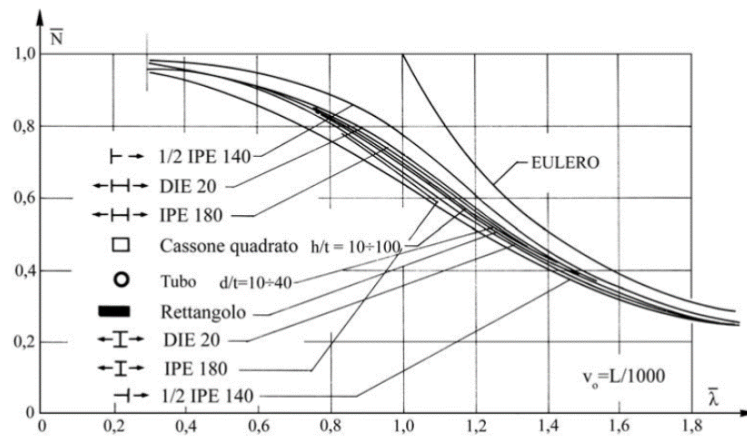


Figure 3. Influence of cross-sectional shape on stability curves. Image taken by [2].

The initial curvature of steel members always produces a non negligible effect. In addition, the presence of residual stresses inside the profile, due to the fabrication stage, e.g. cooling phase, may condition the structural behaviour. As indicated in Figure 4, initial curvature and residual stresses cause a weakening, reducing the carrying capacity.

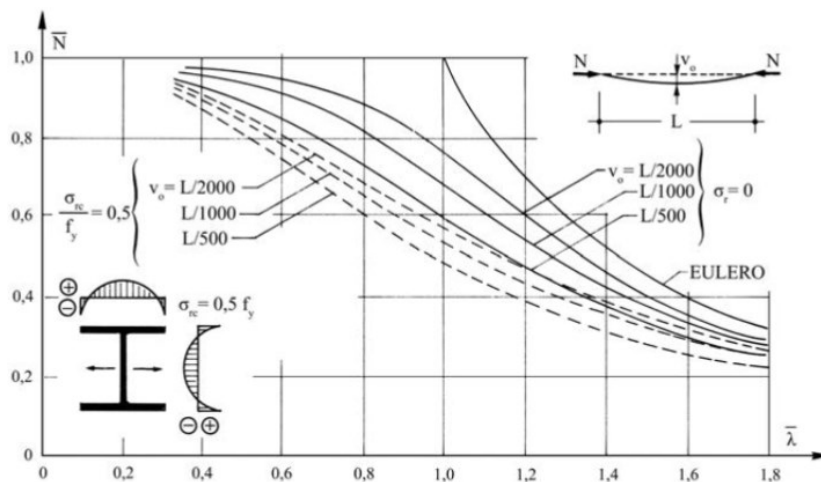


Figure 4. Influence of initial curvature and residual stresses in steel members. Image taken by [2].

Even for circular profiles it is needed to consider the initial curvature as a weakening parameter, taking into consideration that operating the ratio between diameter and thickness, no significant improvements will be achieved.

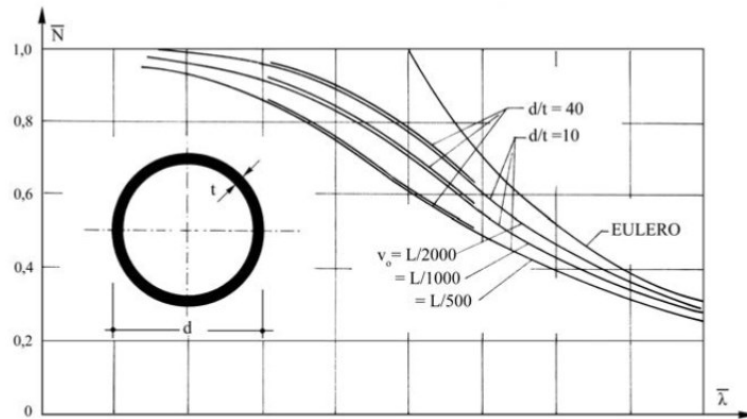


Figure 5. Influence of initial curvature in circular steel profiles. Image taken by [2].

In conclusion, the experimental data demonstrate that the variable distribution of the yielding strength plays a dominant role in structural behaviour. However, the simultaneous presence of residual stresses can mitigate the deficiency of yielding strength and be beneficial to the carrying capacity. Going a bit more in detail, we want compare the residual stresses and yielding stresses on flanges and webs of double T profiles. At the flanges there is always lower yielding stresses and residual tensile stresses compared to the web. Therefore, on the flanges we have a compensation between yielding and residual stresses that results in a compression strength reserve. At the web, the residual stresses are compressive and we have a compensable effect again. In Figure 6 is well represented the better behaviour of an IPE200 in which variable yielding and residual stresses are considered together compared to the case in which are taken singularly.

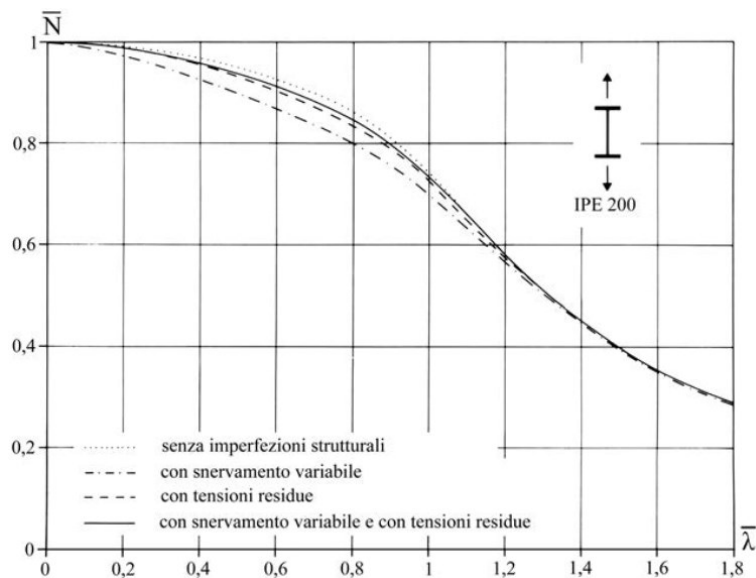


Figure 6. Influence of different imperfections on IPE profile. Image taken by [2].

Given all the experimental results and the numerical investigations according to the *European Convention for Constructional Steelwork* (CECM, English ECCS) three curves were defined for the simply compressed columns:

- “a” for circular hollow sections;
- “b” for double T sections inflected about the strong axis;
- “c” for double T sections inflected about the weak axis.
-

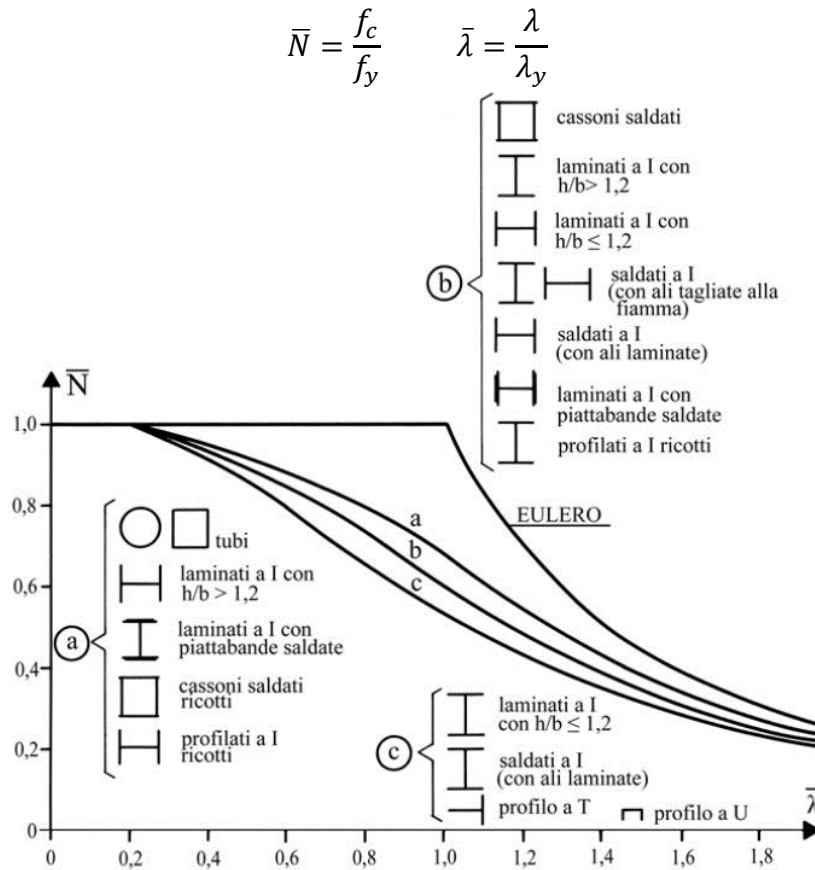


Figure 7. The first three stability curves proposed by CECM-ECCS. Image taken by [2].

For $\lambda/\lambda_y \leq 0.2$, structural members can achieve full plasticization because they are thick element and therefore, are not interest in flexural buckling. As a sequent development, was proposed to consider different yielding strength values based on thickness of the members. For usual thickness $20 \leq t \leq 30 \text{ mm}$ the yielding strength is the nominal one, for $t \leq 20 \text{ mm}$ it is accepted an increase of 6% of f_y , at the contrary, for $t \geq 20 \text{ mm}$ f_y is reduced by 6%. The increasing use of structural steel in constructions, and consequently the availability of different profiles, especially high strength ones, the “a0” and “d” curves were introduced. The quality of the steel is independent of the distribution of residual stresses, and we know that the latter has effects on the stability curves with the ratio between the maximum residual stress and

the yielding stress. Therefore, as the quality of the steel increases, and therefore of f_y , this ratio decreases, as does the consequent unfavorable effect. Hence the “a₀” curve which limits the behavior of high strength and quality steels that have undergone heat treatments aimed to reduce residual stresses and therefore this ratio. The “d” curve” has been introduced for all those sections exceeding 40 mm thickness, called “jumbo profiles” which have the residual compressive stresses like the yielding strength at the flanges. This situation is very unfavorable, especially for thick profiles, which are largely employed in this type of cross-sections.

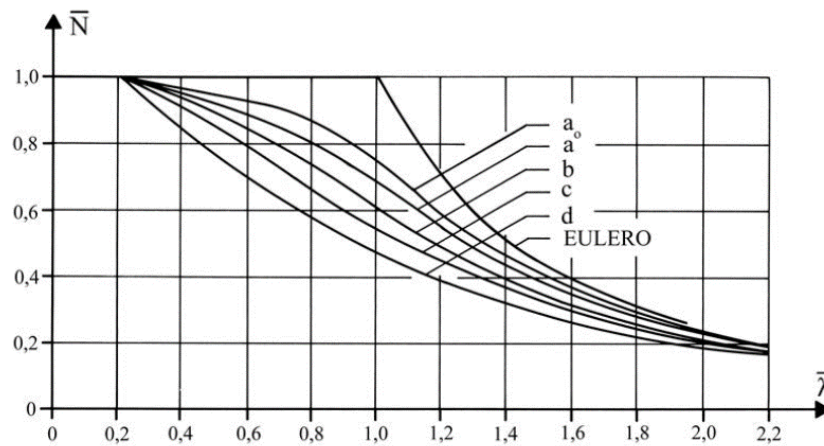


Figure 8. The five stability curves proposed by CECM-ECCS. Image taken by [2].

1.2.2 Classification of instability phenomena

The phenomena of instability can affect a single component of the structure or the entire structure itself.

The *global instability of the entire structure* occurs when the half-wavelength of the unstable deformation has the same order of magnitude as one of the main dimensions of the structure. It can have instability of frames, shells or tanks, and also cantilevered structures. There is an important deviation from the undeformed configuration, and some points in which the stresses increase significantly, causing subsequent unstable phenomena up to collapse.

The *global instability* phenomena occurs when the half-wavelength of the unstable deformation has the same order of magnitude as the structural element considered. They can be grouped into flexural, torsional, flexural-torsional instability.

- Pure flexural instability: heeling occurs in a single plane and is contrasted by the flexural stiffness EI . It can normally involve axially loaded doubly symmetrical sections in which the bending plane coincides with a main plane of inertia;



Figure 9. Pure flexural instability.

- Pure torsional instability: it is caused by a pure screwing characterized by torsional rotations of the cross section thwarted by the torsional rigidity (GJ_t ; EI_ω). Typically involves axially loaded bars with doubly symmetrical cross-section with low secondary stiffness;



Figure 10. Pure torsional instability.

- Lateral-torsional instability: this phenomenon groups the first two mentioned above, exhibiting displacements of the transversal section according to the two orthogonal planes and also torsional rotations. Consequently, this instability is opposed by all the stiffnesses, i.e. bending and torsional, involving members subjected to axial action and bending moment, or beams which are only inflected. The latter is the case of lateral instability or twisting, characterized by displacements of the beam orthogonally to the deflection plane and by torsional rotations of the cross section.



Figure 11. Lateral-torsional instability.

Local instability refers to a set of phenomena characterized by a half wavelength of the unstable deformation comparable to the dimensions of the cross section. For example it could be compressed areas that become unstable locally, or parts of steel profiles subjected to shear. In any case, we have an out-of-plane heeling contrasted by flexural stiffness. Obviously, in absence of other external actions, the element remains undeformed globally.



Figure 12. Local instability.

We may also have distortion instability, typical of thin-walled open sections, which can affect individual parts or the entire structure. It is placed in the middle between global and local instability because the half-wavelength is included between the length of the bar and the main dimensions of the cross section, considering that the deformation in the plane of the latter produces effects at the global level of the element as well.

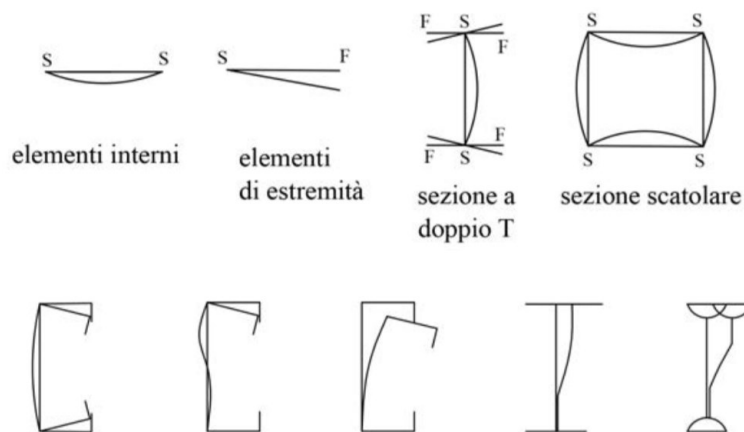


Figure 13. Typical shapes of local instability and below distortional instability. Image taken by [2].

In conclusion, it can be stated that all types of phenomena associated to the loss of stability are strictly related to the geometry of the problem, such as the type of section, the length, the constraints conditions and load conditions.

1.2.3 Design and verifications of compressed columns at Eurocodes and NTC18

It is considered the case of compressed elements in which the action is axial directed along the barycentric axis and any eccentricity can be neglected as well as the associated bending action. The case of flexural instability is treated. The critical load for a column, in pure buckling, is defined by Gere &

Timoshenko (1961) as the axial force that is sufficient to keep the bar in slightly bent form.

$$\lambda_{eq} = \frac{L}{i_{eq}}$$

$$N_{cr} = \frac{\pi^2 EI}{L^2}$$

where L , *length of free inflection*, is dependent on the constraint conditions and represents the distance between two points of inflection of the deformed configuration, or equally, between two contiguous points of zero moment.

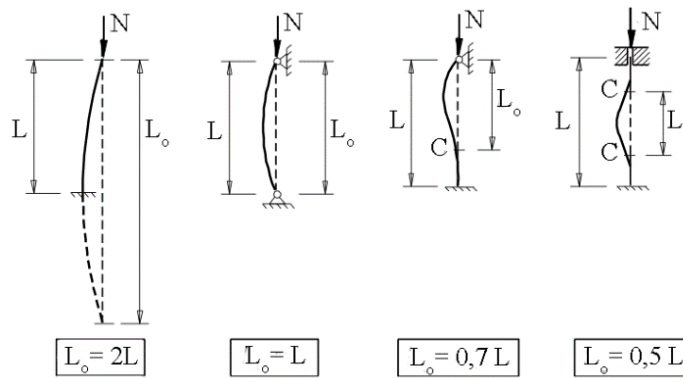


Figure 14. Typical deformed configuration for stability. Image taken by [2].

A compression member should be verified against buckling as follows:

$$\frac{N_{Ed}}{N_{b,Rd}} \leq 1$$

where N_{Ed} is the design value of the compression force and $N_{b,Rd}$ is the design buckling resistance of the compression member.

The design buckling resistance of a compression member should be taken as:

$$N_{b,Rd} = \frac{\chi A f_y}{\gamma_{M1}} \quad \text{for Class 1,2 and 3 cross - sections}$$

$$N_{b,Rd} = \frac{\chi A_{eff} f_y}{\gamma_{M1}} \quad \text{for Class 4 cross - sections}$$

Where χ is the reduction factor for the most relevant buckling mode.

$$\chi = \frac{1}{\Phi + \sqrt{\Phi^2 - \bar{\lambda}^2}} \leq 1$$

The normalized slenderness $\bar{\lambda}$ can be evaluated as follows:

$$\bar{\lambda} = \sqrt{\frac{A f_{yk}}{N_{cr}}} \quad \text{for Class 1, 2 and 3 cross – sections}$$

$$\bar{\lambda} = \sqrt{\frac{A_{eff} f_{yk}}{N_{cr}}} \quad \text{for Class 4 cross – section}$$

Then, the imperfection parameter

$$\phi = 0.5[1 + \alpha(\bar{\lambda} - 0.2) + \bar{\lambda}^2]$$

where α is the imperfection factor, evaluated following *Tab. 4.2 VIII NTC18* or *Tab 6.1,6.2 EC3*

Buckling curve	a ₀	a	b	c	d
Imperfection factor α	0.13	0.21	0.34	0.49	0.76

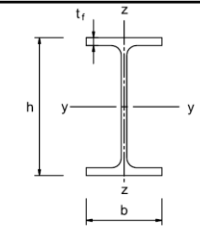
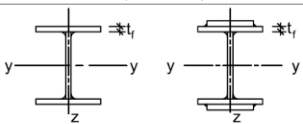
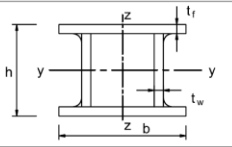
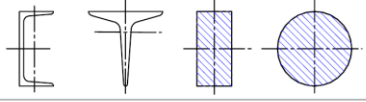
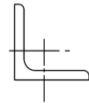
Cross section	Limits	Buckling about axis	Buckling curve	
			S 235 S 275 S 355 S 420	S 460
Rolled sections 	$h/b > 1,2$	y-y z-z	$t_f \leq 40$ mm	a a ₀
			$40 < t_f \leq 100$	b c
	$h/b \leq 1,2$	y-y z-z	$t_f \leq 100$ mm	b c
			$t_f > 100$ mm	d c
Welded I-sections 	$t_f \leq 40$ mm	y-y z-z	b c	
	$t_f > 40$ mm	y-y z-z	c d	
Hollow sections 	hot finished	any	a	
	cold formed	any	c	
Welded box sections 	generally (except as below)	any	b	
	thick welds: $a > 0,5t_f$ $b/t_f < 30$ $h/t_w < 30$	any	c	
U-, T- and solid sections 		any	c	
L-sections 		any	b	

Figure 15.

1.3 Concepts of Theory of Elastic Stability

1.3.1 Elastic buckling of bars

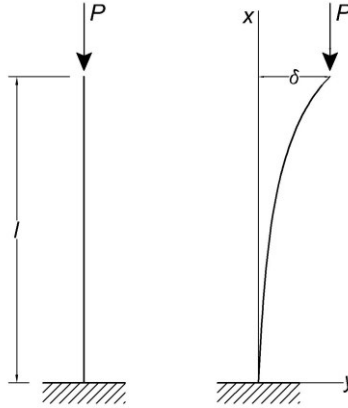


Figure 16.

Neglecting shearing deformations and shortening of the beam axis, the expression for the curvature is

$$EI \frac{d^2 y}{dx^2} = -M$$

Assuming the coordinate system as indicated in Figure 6, the bending moment at any cross section is

$$M = -P(\delta - y)$$

and the differential equation becomes

$$EI \frac{d^2 y}{dx^2} = P(\delta - y)$$

The column is free at the upper end, thus buckling occurs in the plane of minimum flexural rigidity.

Given

$$k^2 = \frac{P}{EI}$$

the previous equation can be written in the form

$$\frac{d^2 y}{dx^2} + k^2 y = k^2 \delta$$

The general solution of this equation is

$$y = A\cos(kx) + B\sin(kx) + \delta$$

where A and B are the constants of integration and they can be evaluated from the boundary condition

$$y = \frac{dy}{dx} = 0 \quad \text{at } x = 0$$

Thus

$$A = -\delta \quad B = 0$$

and then

$$y = \delta(1 - \cos(kx))$$

At the upper end of the bar the boundary condition is the following

$$y = \delta \quad \text{at } x = l$$

Thus

$$\delta \cos(kl) = 0$$

The previous relation is true when $\delta = 0$ or $\cos(kl) = 0$. The first solution is the obvious one, the second one gives

$$kl = (2n - 1) \frac{\pi}{2}$$

For $n = 1$ the corresponding value of P will be the smallest critical load

$$kl = l \sqrt{\frac{P}{EI}} = \frac{\pi}{2}$$

Finally

$$P_{cr} = \frac{\pi^2 EI}{4l^2}$$

By using $n = 2, 3, 4, \dots$ we will find larger critical loads with different deflection curves. These forms of buckling are unstable and they have little practical meaning.

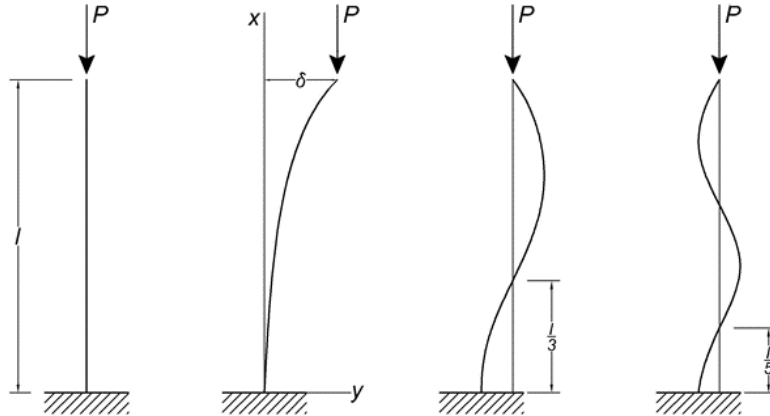


Figure 17.

The critical loads for columns having different end conditions may be obtained. In the case of a bar with hinged ends from symmetry it can be recognised that half of the bar is in the same condition as the entire bar fixed at one end. Hence the critical load is obtained by substituting $l/2$ which gives

$$P_{cr} = \frac{\pi^2 EI}{l^2}$$

Another strategy is to consider the total potential energy in the deformed configuration of a system composed by a thin beam of constant cross section, inextensible and not deformable in shear, constrained at one end by a hinge and at the other by a pinned support, loaded by an axial force N and by an orthogonal distributed load $q(z)$. [8]

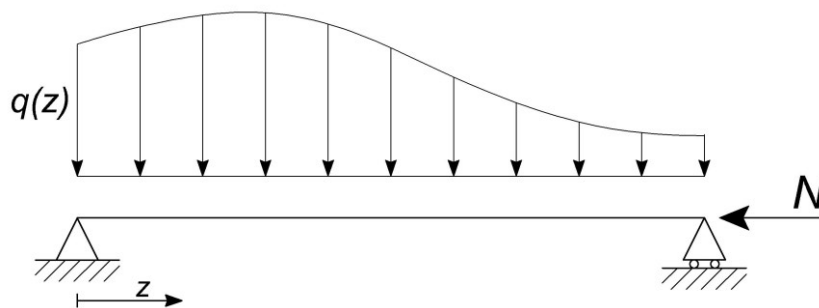


Figure 18.

$$W = \frac{1}{2} \int_0^l \frac{M^2}{EI} dz - Nw - \int_0^l q(z)v(z) dz$$

Performing Taylor expansion about zero, neglecting the shear deformation, applying the rules of Variational Calculus and finally integrating by parts, it gives elastic line with second-order effects

$$EIv^{IV} + Nv'' - q = 0$$

Supposing $q(z) = 0$, the equation of the elastic line with geometrical nonlinearities modifies as follows:

$$EIv^{IV} + Nv'' = 0$$

The solution is

$$v(z) = A\cos\alpha z + B\sin\alpha z + Cz + D$$

Implementing the boundary conditions, we obtain

$$v(0) = v(l) = EIv''(0) = EIv''(l) = 0$$

$$\begin{bmatrix} 1 & 0 & 0 & 1 \\ \cos\alpha l & \sin\alpha l & l & 1 \\ -\alpha^2 & 0 & 0 & 0 \\ -\alpha^2\cos\alpha l & -\alpha^2\sin\alpha l & 0 & 0 \end{bmatrix} \begin{bmatrix} A \\ B \\ C \\ D \end{bmatrix} = \begin{bmatrix} 0 \\ 0 \\ 0 \\ 0 \end{bmatrix}$$

The determinant of the coefficient matrix is zero when $\sin\alpha l = 0$. This is the Euler's condition, that for $\alpha l \rightarrow \pi$ gives

$$N_c = \pi^2 \frac{EI}{l^2}$$

An alternative is to verify that the destabilizing moment is equal to the stabilizing one

$$\begin{aligned} M_i &= Nv \\ M_s &= -EI \frac{d^2v}{dz^2} \end{aligned}$$

obtaining the differential equation

$$v'' + \alpha^2 v = 0$$

The solution is

$$v(z) = A\cos\alpha z + B\sin\alpha z$$

Imposing boundary conditions

$$v(0) = v(l) = 0$$

we have

$$A = 0; \quad \sin \alpha l = 0$$

By definition $\alpha^2 = N/EI$ and the eigenvalues can be evaluated knowing that $\alpha l \rightarrow \pi$. Thus $\alpha_n = n\pi/l$ and by substitution is obtained

$$N_c = n^2 \pi^2 \frac{EI}{l^2}$$

For each eigenvalue corresponds an eigenfunction in which n represents the number of sinusoidal half-waves. If there are not any other constraints, the critical load is the one for $n = 1$.

$$v_n(z) = B \sin \alpha_n z$$

$$N_{c1} = \pi^2 \frac{EI}{l^2}$$

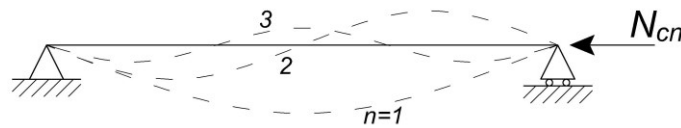


Figure 19

1.3.2 Buckling of bars with multiple intermediate supports

In this case it would be easier to think the bar as a continuous beam on rigid supports subjected to axial and lateral loads. We will call $1, 2, 3, \dots, n$, the supports; $M_1, M_2, M_3, \dots, M_n$ the bending moments; $l_1, l_2, l_3, \dots, l_n$ the length of the spans; $u_1, u_2, u_3, \dots, u_{n-1}$ the axial load factors. Moreover, the force P and the bending rigidity EI are considered constant.

Now we are focusing on a beam having two spans: because of the action of loads, angles of rotation θ_n and θ_{n-1} are generated, and they are located respectively at the intermediate, and at the edge supports. Obviously at the intermediate supports we expect to have the same tangent.

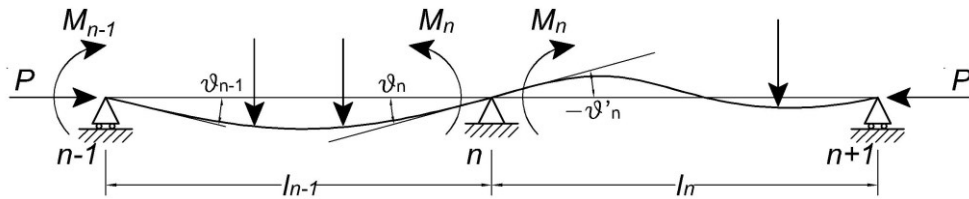


Figure 20.

The expression of θ_n , that in this paper we will not demonstrate it, it has the following expression:

$$\theta_n = \theta_{0n} + \frac{M_{n-1}l_{n-1}}{6EI_{n-1}}\Phi(u_{n-1}) + \frac{M_n l_{n-1}}{3EI_{n-1}}\psi(u_{n-1})$$

where the first term θ_{0n} is dependent on the lateral load and the second is dependent on the moments.

Knowing that at the intermediate supports $\vartheta_n = \vartheta'_n$ we obtain:

$$\begin{aligned} \theta_{0n} + \frac{M_{n-1}l_{n-1}}{6EI_{n-1}}\Phi(u_{n-1}) + \frac{M_n l_{n-1}}{3EI_{n-1}}\psi(u_{n-1}) = \\ = - \left[\theta'_{0n} + \frac{M_{n-1}l_{n-1}}{6EI_{n-1}}\Phi(u_{n-1}) + \frac{M_n l_{n-1}}{3EI_{n-1}}\psi(u_{n-1}) \right] \end{aligned}$$

Finally:

$$\begin{aligned} M_{n-1}\Phi(u_{n-1}) + 2M_n \left[\psi(u_{n-1}) + \frac{l_n}{l_{n-1}} \frac{I_{n-1}}{I_n} \psi(u_n) \right] + M_{n+1} \frac{l_n}{l_{n-1}} \frac{I_{n-1}}{I_n} \Phi(u_n) = \\ = - \frac{6EI_{n-1}}{l_{n-1}} (\theta_{0n} + \theta'_{0n}) \end{aligned}$$

This equation contains three unknowns M_{n-1} , M_n , M_{n+1} and it can be proposed for any numbers of constraints. Exploiting the known conditions at the outer sides the problem becomes statically determined with sufficient equations to evaluate the unknown moments.

Coming back to stability topic, it is important to recall the meaning of $\Phi(u)$ and $\psi(u)$. Considering a simple supported beam subjected to axial load, the equation of the deformed curve can be evaluated through the linear elastic equation, and then performing the first derivative, the rotation can be computed as well. Thus, it may recognise that these expressions are multiplied by trigonometric factors representing the influence of the axial force. Moreover, when u tends to zero (and it means that the load is decreasing), $\Phi(u)$ and $\psi(u)$ move to unity.

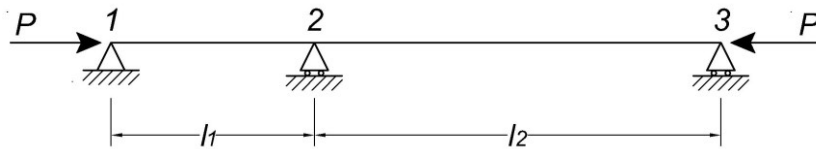


Figure 21.

By the way, given hinged ends, most part of the left-hand side of the previous equation vanish and becomes:

$$2M_2 \left[\psi(u_1) + \frac{l_2 I_1}{l_1 I_2} \psi(u_2) \right] = -\frac{6EI_1}{l_1} (\theta_{02} + \theta'_{02})$$

The critical load is that value for which the bending moment tends to infinite, therefore it is sufficient that:

$$\psi(u_1) + \frac{l_2 I_1}{l_1 I_2} \psi(u_2) = 0$$

Assuming the two spans have the same cross section, we obtain:

$$u_1 = \frac{k_1 l_1}{2} = \frac{l_1}{2} \sqrt{\frac{P}{EI}} \quad u_2 = \frac{k_2 l_2}{2} = \frac{l_2}{2} \sqrt{\frac{P}{EI}}$$

$$\frac{u_1}{u_2} = \frac{l_1}{l_2}$$

The previous equation can be written as follows:

$$\frac{\psi(u_1)}{\psi\left(\frac{u_1 l_2}{l_1}\right)} = -\frac{l_1}{l_2}$$

Taking $2l_1 = l_2$, we find:

$$\frac{\psi(u_1)}{\psi(2u_1)} = -2$$

And given the following expressions:

$$\Phi(u) = \frac{3}{u} \left(\frac{1}{\sin 2u} - \frac{1}{2u} \right)$$

$$\psi(u) = \frac{3}{2u} \left(\frac{1}{2u} - \frac{1}{\tan 2u} \right)$$

we find $2u_1 = 1.93$, thus

$$P_{cr} = \frac{4EI(u_1)^2}{l_1^2} = \frac{EI(2u_1)^2}{l_1^2} = \frac{3.72EI}{l_1^2} = \frac{14.9EI}{l_2^2}$$

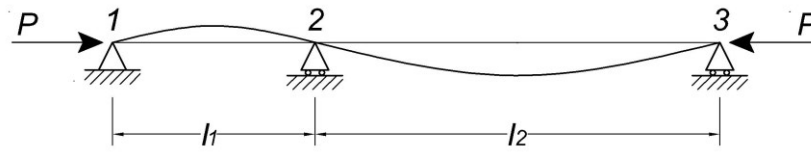


Figure 22.

In conclusion, the presence of intermediate support has the benefit to decrease the critical load. In any case we expect to have the critical value always between the critical ones evaluated as single bars:

$$\frac{\pi^2 EI}{l_2^2} \leq \frac{3.72 EI}{l_1^2} = \frac{14.9 EI}{l_2^2} \leq \frac{\pi^2 EI}{l_1^2}$$

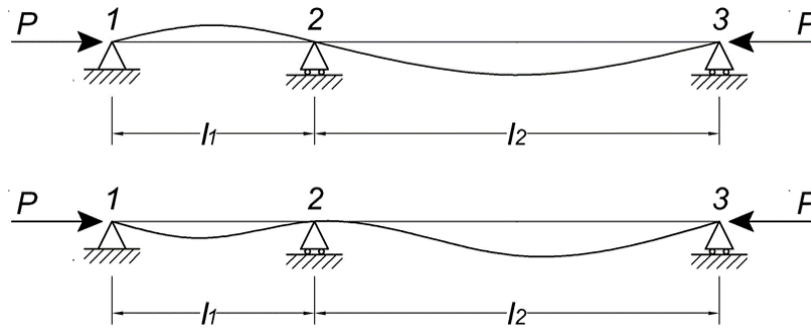


Figure 23.

In Figure 23 are showed the two forms of buckling, but only the first one has relevant significance.

1.3.3 Buckling of bars with elastic supports

In this chapter is discussed the case of a simply supported beam with an intermediate elastic support that operates as follows

$$R_2 = K_2 \delta_2$$

where R_2 is the reaction in the internal support, K_2 the spring constant and δ_2 the settlement. Considering

Figure 24, R_2 can be evaluated from a statical point of view:

$$R_2 = K_2 \delta_2 = \frac{P_1 \delta_2}{l_1} + \frac{P_2 \delta_2}{l_2} - \frac{M_2}{l_1} - \frac{M_2}{l_2}$$

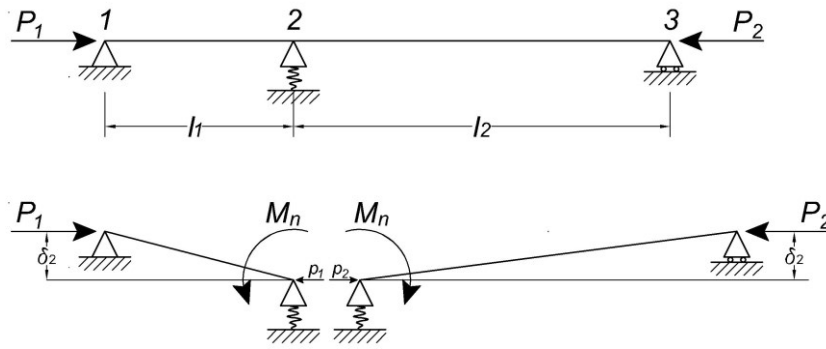


Figure 24.

In the deformed curve, the angle β_2 at the intermediate support is

$$\beta_2 = \frac{\delta_2}{l_1} + \frac{\delta_2}{l_2}$$

In this way, the equation showed previously becomes:

$$2M_2 \left[\psi(u_1) + \frac{l_2 I_1}{l_1 I_2} \psi(u_2) \right] = \frac{6EI_1}{l_1} \left(\frac{\delta_2}{l_1} + \frac{\delta_2}{l_2} \right)$$

It is possible to write a new expression, remembering that buckling can occur only when M_2 and δ_2 are different from zero.

$$2 \left[K_2 - \frac{P_1}{l_1} - \frac{P_2}{l_2} \right] \left[\psi(u_1) + \frac{l_2 I_1}{l_1 I_2} \psi(u_2) \right] = -\frac{6EI_1}{l_1} \left(\frac{\delta_2}{l_1} + \frac{\delta_2}{l_2} \right)$$

Considering $P_1 = P_2$ and $I_1 = I_2$, we find:

$$\sin 2u_1 \sin 2u_2 = 2(u_1 + u_2) \sin 2(u_1 + u_2) \left[\frac{l_1 l_2}{(l_1 l_2)^2} - \frac{P}{K_2(l_1 + l_2)} \right]$$

When $K_2 = \infty$, the support reacts rigidly, and the result is the same treated in §2.3.2. At the contrary, if K_2 goes to zero, the right side of the equation tends to infinite, and the problem can be solved only if $\sin 2(u_1 + u_2)$ goes to zero at the same time. In this last case we have:

$$\sin 2(u_1 + u_2) = \sin k(l_1 + l_2) = 0$$

where

$$k = \sqrt{\frac{P}{EI}}$$

Hence

$$P_{cr} = \frac{\pi^2 EI}{(l_1 + l_2)^2}$$

This is the same solution about the critical load for a bar with hinged and length equal to the sum of l_1 and l_2 .

Considering $l_1 = l_2 = l/2$ the equation can be written as follow:

$$\sin 2u_1 \left[-\sin 2u_1 + 8u_1 \cos 2u_1 \left(\frac{1}{4} - \frac{P}{K_2 l} \right) \right] = 0$$

In this case, when $K_2 = \infty$ corresponds $2u_1 = \pi$, obtaining:

$$P_{cr} = \frac{\pi^2 EI}{l_1^2} = \frac{4\pi^2 EI}{l^2}$$

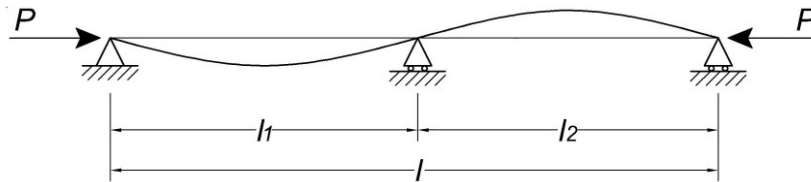


Figure 25.

Instead, when $K_2 = 0$, it means absolutely flexible support, and it corresponds $2u_1 = \pi/2$, obtaining:

$$P_{cr} = \frac{\pi^2 EI}{l^2}$$



Figure 26.

In conclusion, these two different situations represent respectively the upper and lower limit for the critical load, and in particular $\pi/2 \leq 2u_1 \leq \pi$. We find that $\sin 2u_1 \leq 0$ and $\cos 2u_1 \geq 0$. As consequence, to have the whole relation equal to zero it is necessary that $\left(\frac{1}{4} - \frac{P}{K_2 l} \right) \leq 0$. In this way we obtain:

$$P = \frac{K_2 l}{4}$$

It is interesting to show that if we substitute this last equation to the critical load, we find the minimum value of spring rigidity at which buckling occurs:

$$\frac{4\pi^2 EI}{l^2} = \frac{K_2 l}{4}$$

Finally

$$K_2 = \frac{16\pi^2 EI}{l^3}$$

All this can be summarized by considering the two opposite situations in which we have infinitely rigid supports and absolutely flexible supports. Indeed, there is a proportional response between critical load and stiffness of the support. Introducing P_e as the critical load in case of $K_2 = 0$ (simply supported beam), we can describe the trend of P_{cr} with respect the rigidity of the intermediate constraint.

$$P_e = \frac{\pi^2 EI}{l^2}$$

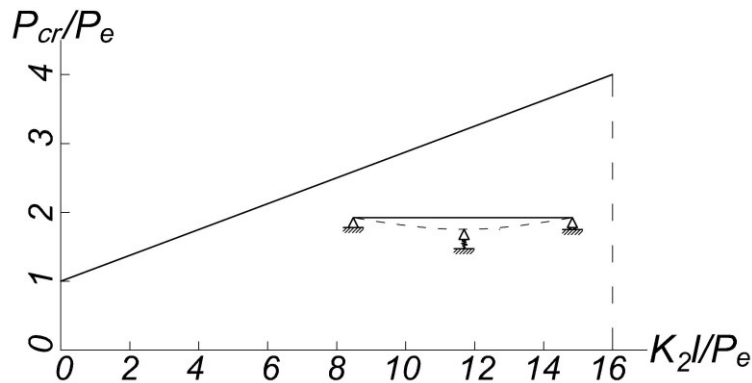


Figure 27. As the stiffness of intermediate support increases, the critical load increases as well. For $K_2 = 0$ the critical load is the same for a simply supported beam, and $P_{cr} = P_e$.

Another strategy is to reason from an energetic point of view. Supposing to have the same model as before, the total potential energy of the system is

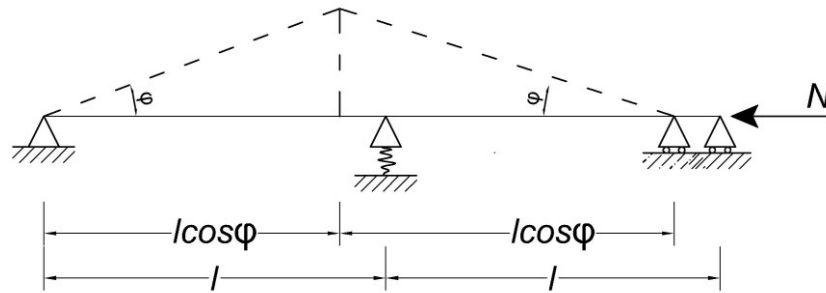


Figure 28.

$$W(\varphi) = \frac{1}{2} k (l \sin \varphi)^2 - 2Nl(1 - \cos \varphi)$$

The equilibrium can be evaluated by imposing the stationarity of W

$$W'(\varphi) = l \sin \varphi (kl \cos \varphi - 2N) = 0$$

Thus

$$N(\varphi) = \frac{kl}{2} \cos \varphi$$

$$N = \frac{kl}{2}$$

The same result can be obtained by equalling the stable and unstable bending moments:

$$M_{stb} = Nl \sin \varphi \approx Nl \varphi$$

$$M_{unst} = \frac{1}{2} kl^2 \sin \varphi \cos \varphi \approx \frac{1}{2} kl^2 \varphi$$

1.3.4 Buckling of bars with multiple elastic supports

Now we move to the case in which we have several intermediate supports without entering much in detail but taking some things for granted.

Let us consider a continuous beam AB of length l subjected to lateral and axial loads and calling the unknown reactions R_1, R_2, \dots, R_n and c_1, c_2, \dots, c_n the distances of the intermediate supports from the right end of the beam.

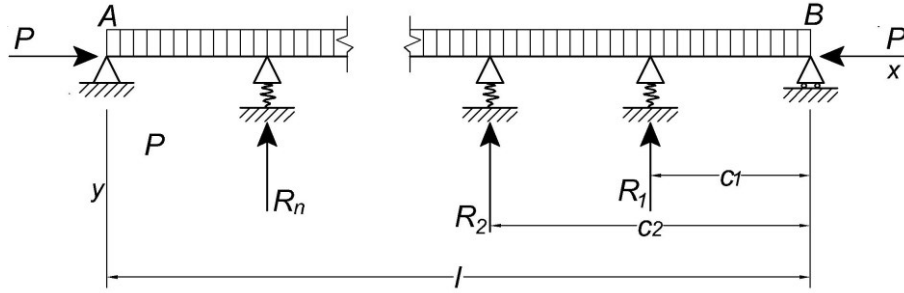


Figure 29.

To determine these unknown quantities we use two different relations: the first one related to the deflection due to concentrated loads, the second one related to the deflection due to continuous lateral load:

$$y = \frac{\text{sink}x}{Pk\text{sink}l} \sum_{i=1}^{i=m} R_i \text{sink}c_i - \frac{x}{Pl} \sum_{i=1}^{i=m} R_i c_i + \frac{\text{sink}(l-x)}{Pk\text{sink}l} \sum_{i=m+1}^{i=n} R_i \text{sink}(l-c_i) - \frac{l-x}{Pl} \sum_{i=m+1}^{i=n} R_i (l-c_i)$$

$$y = \frac{ql^4}{16EIu^4} \left[\frac{\cos(u - 2ux/l)}{\cos u} - 1 \right] - \frac{ql^2}{8EIu^2} x(l-x)$$

Imposing $x_m = l - c_m$ and combining the two previous expressions an equation for any support m is defined:

$$\frac{ql^4}{16EIu^4} \left[\frac{\cos\left(u - \frac{2ux_m}{l}\right)}{\cos u} - 1 \right] - \frac{ql^2}{8EIu^2} x_m(l-x_m) - \frac{\text{sink}x_m}{Pk\text{sink}l} \sum_{i=1}^{i=m} R_i \text{sink}c_i + \frac{x_m}{Pl} \sum_{i=1}^{i=m} R_i c_i - \frac{\text{sink}(l-x_m)}{Pk\text{sink}l} \sum_{i=m+1}^{i=n} R_i \text{sink}(l-c_i) + \frac{l-x_m}{Pl} \sum_{i=m+1}^{i=n} R_i (l-c_i) = \frac{R_m}{K_m}$$

Essentially now the problem is well-defined having as many equations as many intermediate supports, therefore it is possible to evaluate the unknowns reactions. A continuous beam having two intermediate supports equally spaced having the same spring constant K and the same cross section for the whole length l is considered. The equation becomes:

$$-\frac{\sin \frac{2kl}{3}}{Pksinkl} R_3 \sin \frac{kl}{3} + \frac{2}{3P} R_3 \frac{l}{3} - \frac{\sin \frac{kl}{3}}{Pksinkl} R_2 \sin \frac{kl}{3} + \frac{1}{3P} R_2 \frac{l}{3} = \frac{R_3}{K}$$

$$-\frac{\sin \frac{kl}{3}}{Pksinkl} R_3 \sin \frac{kl}{3} - \frac{\sin \frac{kl}{3}}{Pksinkl} R_2 \sin \frac{2kl}{3} + \frac{1}{3P} \left(R_3 \frac{l}{3} + R_2 \frac{2l}{3} \right) = \frac{R_2}{K}$$

If the supports are infinitely rigid, buckling occurs as for a bar double hinged with $l = l/3$.

Recalling $k = \sqrt{\frac{P}{EI}}$, we obtain:

$$\frac{kl}{3} = \pi$$

$$P_{cr} = \frac{9\pi^2 EI}{l^2}$$

Now we suppose the rigidities of the intermediate supports approximately next to the values at which correspond a rigid behaviour of the supports. It is introduced a small quantity Δ which allows to describe the change of the response form infinitesimal point of view:

$$\frac{kl}{3} = \pi - \Delta$$

Substituting this last equation and neglecting small quantities we find:

$$\frac{1}{9P} R_2 + \left(\frac{2l}{9P} - \frac{1}{K} \right) R_3 = 0$$

$$\left(\frac{2l}{9P} - \frac{1}{K} \right) R_2 + \frac{1}{9P} R_3 = 0$$

To find K is necessary to nullify the determinant:

$$\left(\frac{2l}{9P} - \frac{1}{K} \right)^2 + \left(\frac{1}{9P} \right)^2 = 0$$

Hence

$$K = \frac{9P}{l}$$

that represents the rigidity of the supports at the border rigid-elastic behaviour. As before, we can describe the critical load against the rigidity of the supports. When the rigidity is small, there are no inflection points and

the deflection curve is the same as a bar of length equal to l . At the contrary, when the rigidity increases one inflection point occurs at the middle. Instead, reaching absolutely rigid supports the critical load is again $9\pi^2 EI/l^2$ as for a double hinged bar of length $l/3$. Increasing more the rigidity at the supports no significant benefits will be achieved.

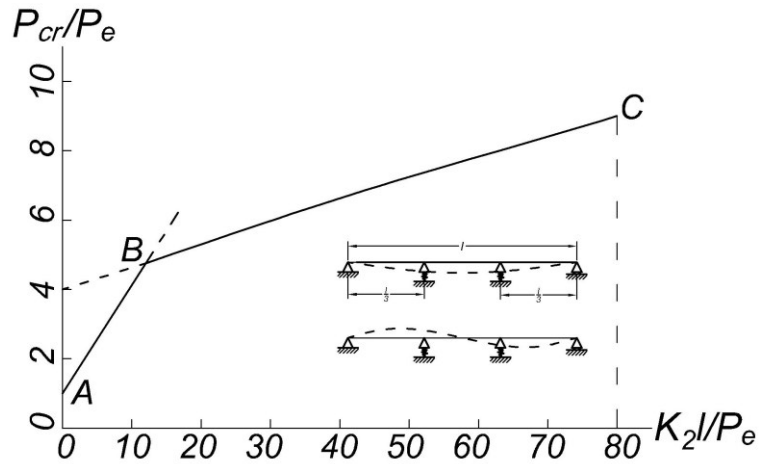


Figure 30. As the stiffness of intermediate support increases, the critical load increases as well. For $K_2 = 0$ the critical load is the same for a simply supported beam, and $P_{cr} = P_e$.

Increasing the number of spans m and keeping the same length of the bar (maintaining spans of l/m), we can evaluate the necessary rigidity of the elastic supports at which the system behaves as infinitely rigid:

$$K = \frac{mP}{\gamma l}$$

Where γ is a numerical factor that depends on the number of spans, hence:

$$P_{cr} = \frac{m^2 \pi^2 EI}{l^2}$$

m	2	3	4	5	6	7	8	9
γ	0.500	0.333	0.293	0.276	0.268	0.263	0.258	0.255

An alternative could be reasoning from an energetic point of view. In this case we are dealing with n degree of freedom systems.

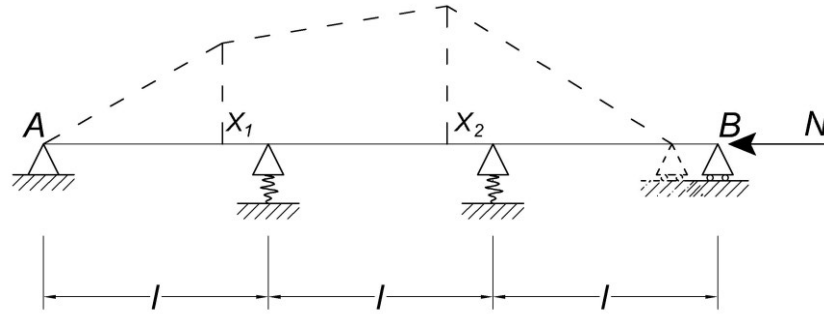


Figure 31

$$W(x_1; x_2) = \frac{1}{2}k(x_1^2 + x_2^2) - Nl \left[3 - \cos\left(\arcsin \frac{x_1}{l}\right) - \cos\left(\arcsin \frac{x_2}{l}\right) - \cos\left(\arcsin \frac{x_2 - x_1}{l}\right) \right]$$

Evaluating a Taylor expansion about the origin

$$W(x_1; x_2) \approx \frac{1}{2}k(x_1^2 + x_2^2) - \frac{N}{l}((x_1^2 + x_2^2 - x_1x_2))$$

Stationarity of W means imposing equal to zero the first derivatives

$$\frac{\partial W}{\partial x_1} = x_1 \left(k - \frac{2N}{l} \right) + \frac{N}{l} x_2 = 0$$

$$\frac{\partial W}{\partial x_2} = \frac{N}{l} x_1 + x_2 \left(k - \frac{2N}{l} \right) = 0$$

Obtaining the coefficient matrix and the characteristic equation

$$\begin{vmatrix} \left(k - \frac{2N}{l} \right) & \frac{N}{l} \\ \frac{N}{l} & \left(k - \frac{2N}{l} \right) \end{vmatrix} = 0$$

$$\frac{3}{l^2} N^2 - \frac{4k}{l} N + k^2 = 0$$

In this way, it is possible to compute two eigenvalues and two eigenvectors, giving the two buckling modes.

$$N_{c1} = \frac{1}{3}kl$$

$$N_{c2} = kl$$

$$x_1 = -x_2$$

$$x_1 = x_2$$

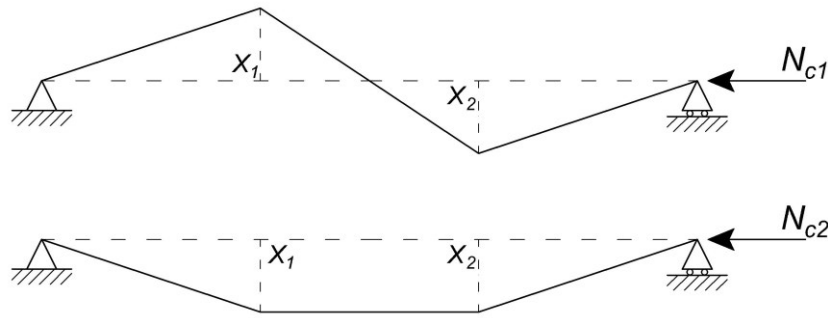


Figure 32

Obviously the first configuration (the anti-symmetric one) is more probable because the eigenvalue is lower. Once again, the same result can be demonstrated by rotational equilibrium of the two external bars with respect the intermediate hinges, the translational equilibrium along the vertical direction, the rotational equilibrium about the point A for the whole system

$$Nx_1 = V_A l$$

$$Nx_2 = V_B l$$

$$V_A + V_B = k(x_1 + x_2)$$

$$kx_1 l + 2kx_2 = 3V_B l$$

Obtaining

$$V_B = \frac{k}{3}(x_1 + 2x_2)$$

$$V_A = \frac{k}{3}(2x_1 + x_2)$$

Solving the linear system by imposing equal to zero the determinant, the characteristic equation can be written once again as before

$$\begin{vmatrix} \left(\frac{2}{3}kl - N\right) & \frac{kl}{3} \\ \frac{kl}{3} & \left(\frac{2}{3}kl - N\right) \end{vmatrix} \begin{vmatrix} x_1 \\ x_2 \end{vmatrix} = \begin{vmatrix} 0 \\ 0 \end{vmatrix}$$

$$\frac{3}{l^2}N^2 - \frac{4k}{l}N + k^2 = 0$$

For $N = 0$, the matrix obtained before corresponds to the stiffness matrix of the system. Instead, the last matrix has not any physical meaning. In

conclusion the problem related to the stability of the elastic equilibrium can be summarized as follows:

$$([K] - \lambda[K_g])\{\delta\} = \{0\}$$

where

- $[K]$ is the elastic stiffness matrix of the system;
- $[K_g]$ is the geometric stiffness matrix;
- $\{\delta\}$ is the vector of nodal displacement;
- λ is the load multiplier.

The eigenvalues of the problem are obtained by imposing equal to zero the determinant

$$\text{Det}([K] - \lambda[K_g]) = 0$$

2 Bracing of columns

2.1 Overview

In the previous chapter we have discussed about how intermediate supports influence the stability of a column, and the possibility to prevent buckling reducing the span or changing the cross-section. The length of span can be reduced by using braces (Winter, 1958). The braces can be classified as elastic or ideal. An elastic brace takes the load and reacting proportionally as its stiffness, moving from its origin. Instead, the ideal bracing with infinite rigidity remains in place. To have an effective bracing against buckling, we have to know well the required strength and the stiffness of the whole structure; moreover it is important to take into account effects of structural imperfections, and by load positions. The imperfections due to not well load positioning could create unwanted moments that may cause deflections of the column.

2.2 Bracing at the end of a bar

Let us consider a column subjected to an axial load, hinged on the ends with the assumption of adequate stiffness to the restraints; the critical load is

$$N_{cr} = \frac{\pi^2 EI}{l^2}$$

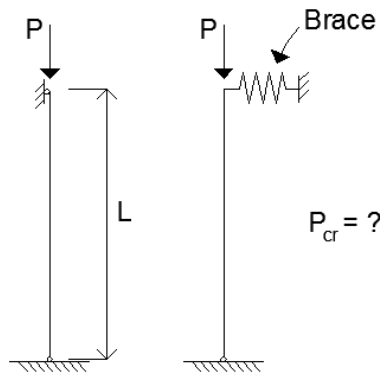


Figure 33.

Now we put at the top end of the bar an elastic support, supposing it completely inadequate. As a result, we will have deflection of the column together with the bracing.

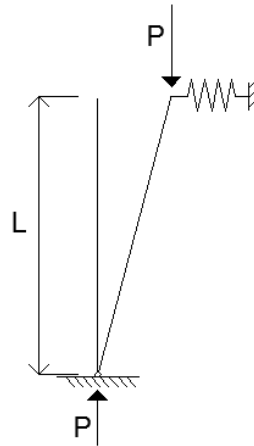


Figure 34. Inadequate stiffness gives sidesway (Helwig & Yura, 1996).

Performing the equilibrium rotation about the hinge, there is no deflection in case the moment provided by bracing is larger with respect that one produced by the load itself. F is the elastic force provided by the spring. Obviously the limit conditions, that represents also the equilibrium limit, is

$$P \cdot d = F \cdot l$$

Given

$$F = K \cdot d$$

By substitution, we find

$$P \cdot d = K \cdot d \cdot l$$

Hence

$$P = K \cdot l$$

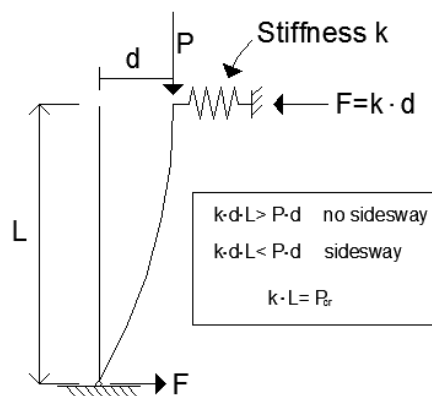


Figure 35. The equilibrium state is controlled by the equilibrium rotation (Helwig & Yura, 1996).

It can be recognized a linear relation between the first buckling load and the stiffness of the spring. The first buckling load is described as a linear relation, which is dependent on the stiffness of the spring. When the second buckling load is reached, the spring reacts more like a hinge, in this way the load can be expressed with Euler's critical load. The ideal stiffness for the bracing, according to Winter (1958), can be derived as follows

$$K_{ideal} = \frac{P_{cr}}{l} = \frac{\pi^2 EI}{l^3}$$

There is a correlation between the stiffness of the bracing and the critical buckling load. The critical load increases as the stiffness of the bracing increases. Then, when the critical one reaches the second buckling mode, there will not be any improvement for what concern load capacity if we increase more the stiffness of the bracing (Galambos & Surovek, 2008).

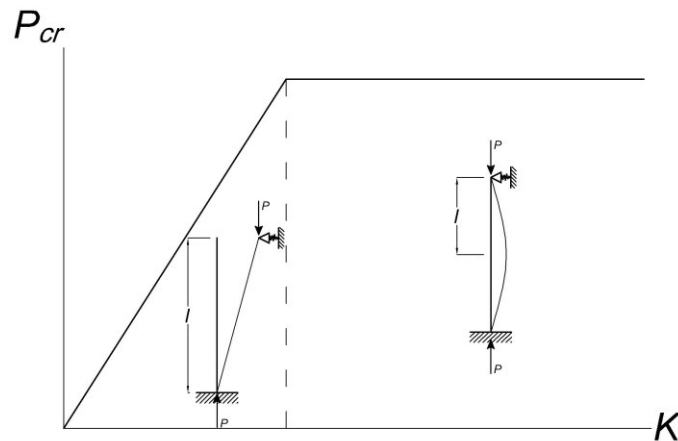


Figure 36. Relation between the stiffness and critical load when bracing at the top (Helwig & Yura, 1996).

It has been demonstrated that it is not necessary to realize too much high brace stiffness, in fact, the buckling mode can be avoided through bracing sufficiently stiff (Winter, 1958). It is only required to have enough strength and rigidity to withhold the effects from the critical load.

During previous chapters we have discussed about imperfections, how to consider them? The problem is quite easy because it is sufficient to consider an initial curvature in our calculations.

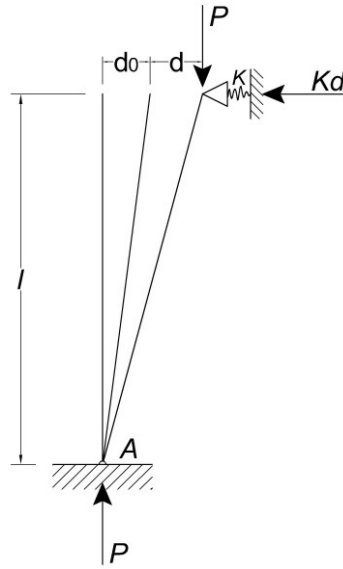


Figure 37.

Introducing d_0 as the initial curvature of the columns, we perform the equilibrium rotation at the point A, that gives $P \cdot d_0 = KL(d_{tot} - d_0)$. It is obvious that if $d_0 = 0$ we obtain the same result as before $P_{cr} = KL$, meaning that the critical load increases with the stiffness of the bracing. Imposing $K = K_{ideal} = P_{cr}/L = \pi^2 EI/L^3$, the critical load can be reached at large deflections and moreover loading a lot the bracings, since $F_{br} = K \cdot d$. Therefore, the displacements should be kept small in a practical point of view. To do that we can adopt $K > K_{ideal}$, for instance taken $K = 2 \cdot K_{ideal}$, then $d = d_0$. From Figure 38 we can recognise that larger is the brace stiffness, lower will be the brace force. The brace force is a linear function of the initial curvature. An important recommendation is to take a brace stiffness at least twice the ideal one in order to keep low sway deflection and at the same time being able to reach higher value of load.

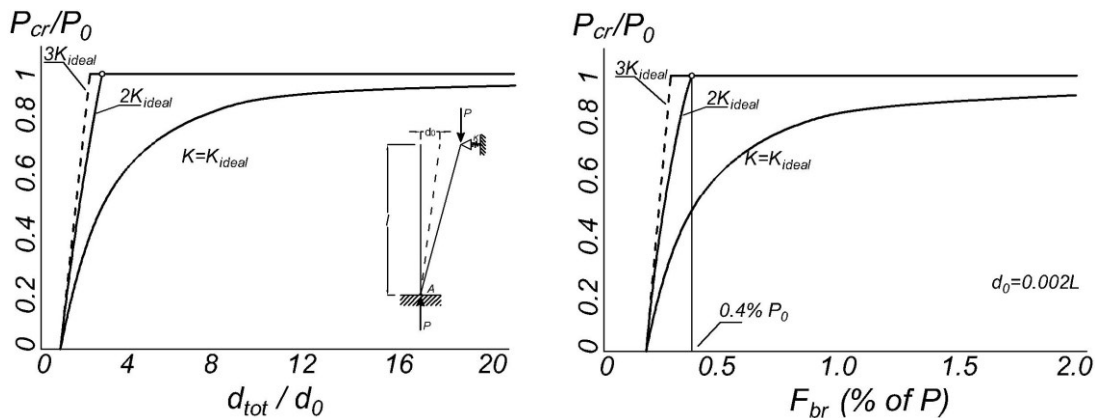


Figure 38. Effect of initial out of plumb.

2.3 Bracing at the middle of a bar

The most common strategy to stabilize a column with two hinges at each end, is to connect it to a bracing. In particular, it can be done in the middle. Based on previous calculations we could consider more than one bracing between two supports. Winkler (1958) asserts that the buckling mode follows a deformed shape two half sine waves if the bracing in the middle has adequate stiffness.



Figure 39. Column with sinusoidal shaped curvature (Helwig & Yura, 1996).

Nevertheless, if the bracings are too much elastic, the result would be a deformed shape similar to a buckling mode of a simply supported beam.

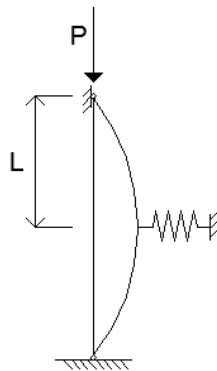


Figure 40. Inadequate stiffness (Helwig & Yura, 1996)

It is quite interesting to recognise that we have the same buckling mode if the intermediate support (bracing) is made of an unyielding support at a miniscule portion of the middle, or by a real or fictitious hinge. In fact the bar will buckle into two half sine-waves (Winter 1958).

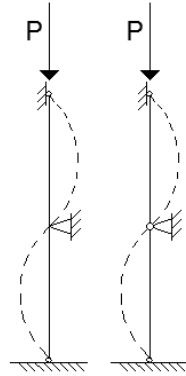


Figure 41. Illustrating column that is subjected to column buckling with a minuscule unyielding support versus a hinge in the middle (Winkler, 1958).

Performing the equilibrium, we find

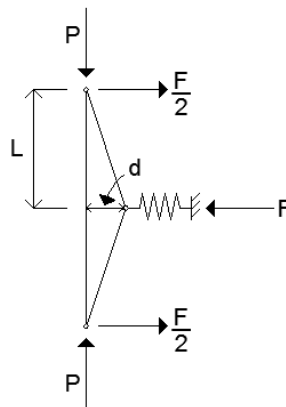


Figure 42. Moment equilibrium (Helwig & Yura, 1996).

$$P \cdot d = \frac{K \cdot d}{2} L$$

thus

$$K = 2 \frac{P_{cr}}{L}$$

hence

$$K_{ideal} = 2 \frac{\pi^2 EI}{L^3}$$

Even in this case we can describe the relationship between the critical buckling and the stiffness of the bracing. Bracings have a great importance in the critical buckling load, in which an increase of stiffness means an increase in terms of load capacity. On the other hand, when the columns reach the second buckling mode, the increase of stiffness doesn't change significantly the strength of the column.

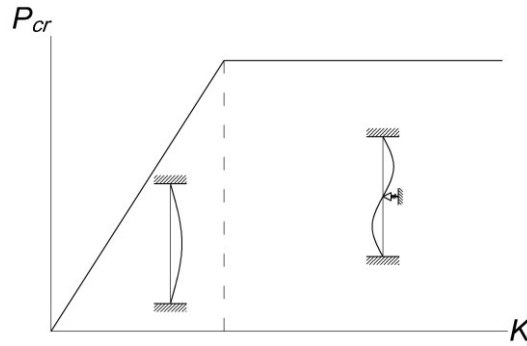


Figure 43.

2.4 Imperfections in braced columns

Now we pass through the presence of imperfections, introducing d_0 as initial curvature.

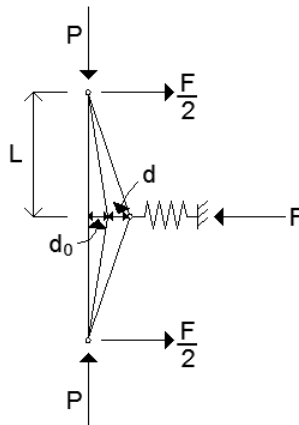


Figure 44. Equilibrium with initial curvature (Winter, 1958).

$$M = \frac{FL}{2} - P_e(d_0 + d) = 0$$

And substituting, we find

$$K_{req} = \frac{P_e}{L} \left[\left(\frac{d_0}{d} \right) + 1 \right]$$

Winter (1958) demonstrates that in case of imperfections, the stiffness of the bracing must be larger with respect the case of ideal column. As a result, given $F = K \cdot d$, according to Yura & Helwig, we can evaluate the brace force in case of imperfections

$$F_{br} = \frac{2P}{L} (d_0 + d)$$

hence

$$F_{br} = \frac{2P}{L} \left(\frac{d_0}{1 - \frac{K_{ideal}}{K}} \right)$$

An adequate brace system requires both strength and stiffness. When the brace is designed for 2% of the member compressive force, the design is addressed only for what concern the strength. About the stiffness, if the bracings are too much flexible, we may have detrimental effects.

2.5 Discrete Bracing System for columns

There are four general types of bracing system: *relative*, *discrete*, *continuous* and *lean-on*. In this chapter we will refer to the discrete system because is the object of our study. We are talking about a technique in which the brace controls the movement only at the point where it is fixed, for example a column braced by cross beam. It is called discrete system because the brace is not present at each point of the column, unlike the relative system in which wherever we perform the cut, the bracing is always intersected, for instance shear walls or truss bracing. A discrete system is a particular case of the continuous one, in which the column is constrained by finite number of bracings, such as external metal cladding for covering perimetral columns. Instead, in the lean-on system, the structural elements are connected to each other, and the stability of one of them is regulated by the others and vice versa.

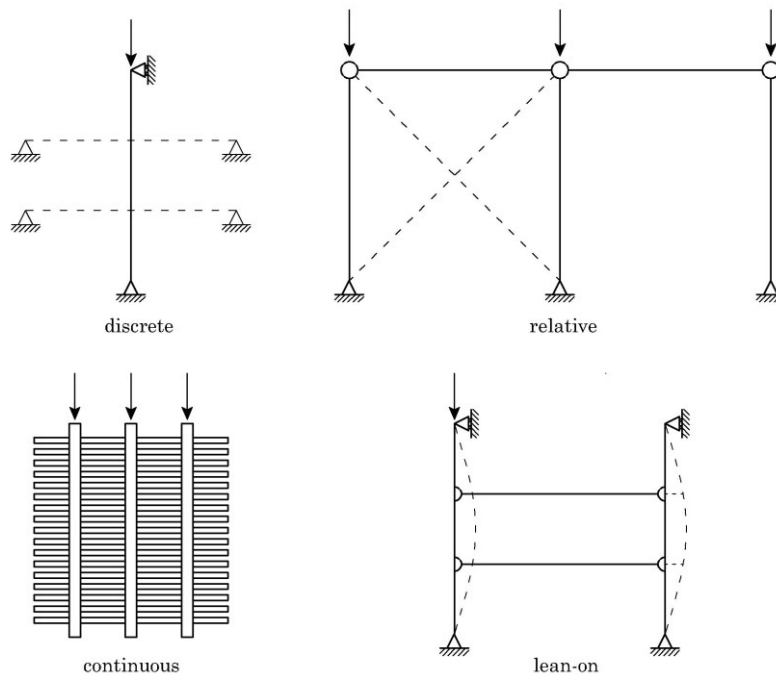


Figure 45. Different types of bracing systems.

In case of discrete bracing, the load acting on the member is usually considered as the average load above and below the brace point. As we have seen previously d_0 is a small displacement due to lateral forces, like the wind action, or due to initial curvature, well known as out-of-plumb, etc. Typically, d_0 is taken equal to $0.2\%L$, the load is factored by $\Phi = 0.75$, and for serviceability limit states a safety factor of 2 may be introduced.

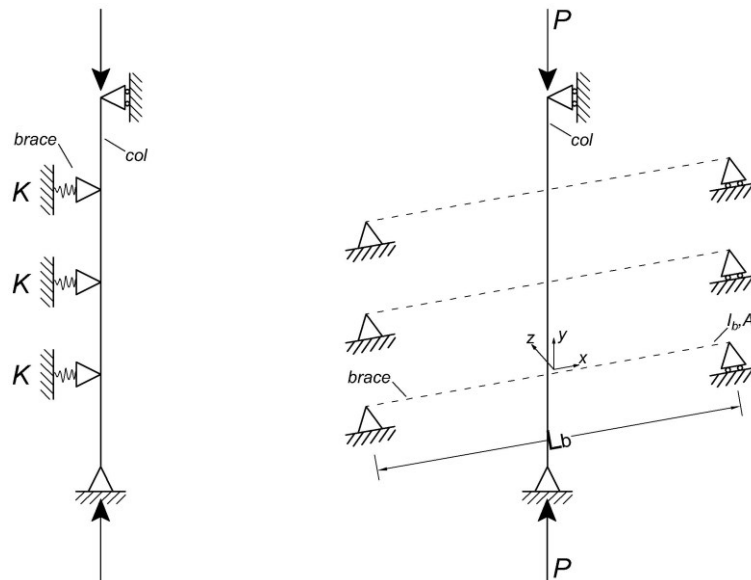


Figure 46.

Discrete bracing, also called *single point bracing system* control the deflection of the columns only at the point of junction. In the case of systems able to resist to compressive forces, the brace force can be divided by two, otherwise if the system is tensile, the bracing must resist to the entire force.

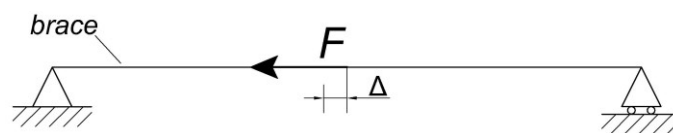


Figure 47.

Along x-direction it is possible to calculate the required stiffness of the bracing in case of compression resistant braces.



Figure 48.

$$\Delta = \frac{FL}{EA} = \frac{F}{EA} \left(\frac{L_b}{2} \right)$$

$$K_x = \frac{F}{\Delta} = \frac{4A_B E}{L_b}$$

And now, in the same manner, for tensile resistant braces.



Figure 49.

$$\Delta = \frac{FL}{EA} = \frac{F \left(\frac{L_b}{2} \right)}{EA_b}$$

$$K_x = \frac{F}{\Delta} = \frac{2A_B E}{L_b}$$

Instead, along z-direction, we consider the sag for a simply supported beam subjected to a concentrated force F

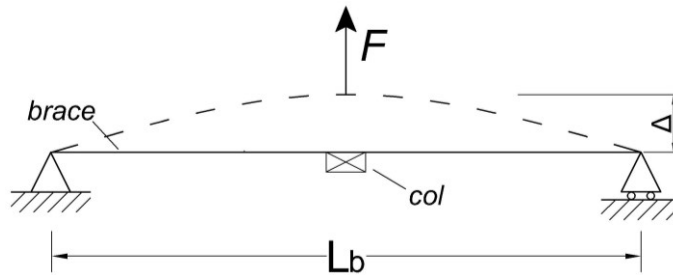


Figure 50.

$$\Delta = \frac{FL^3}{48EI_b}$$

$$K_z = \frac{F}{\Delta} = \frac{48EI_B}{L_b^3}$$

There is a relationship between the critical load and the brace stiffness, in particular at low brace rigidity the critical load approaches to the buckling load at the first mode $\pi^2 EI / (4L)^2$. Instead, increasing the braces stiffness an inflection point is created at the middle of the column, until reaching the final situation in which inflection points move to the intermediate supports (bracing points) and from here other improvement in bracings are not effective anymore.

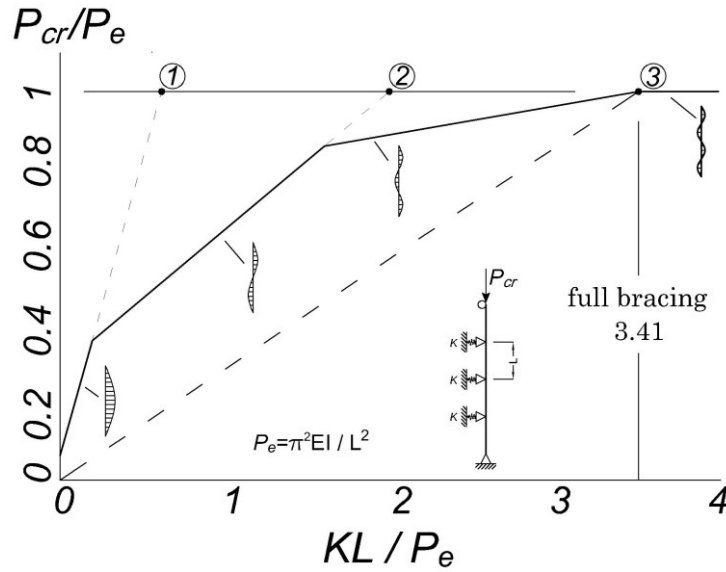


Figure 51.

The required stiffness is inversely proportional to the spacing between bracings. Typically, we recognise more brace points than necessary to support the member because many times the required stiffness could be conservatively estimated by using the permissible unbraced length rather than the actual one. As we have showed before, Timoshenko & Gere (1961) provided the required stiffnesses with respect the number of bracings, and from that we can recognise how the rigidity of the brace increases with the number of them.

# braces	1	2	3	4	5	...
KL/P_e	2	3	3.41	3.63	3.73	4.0

In order to cover uncertainties related to the initial out-of-plumb the ideal stiffness is doubled and the recommended brace force is $1\%P$.

$$\phi = 0.75$$

$$\# \cong 4 - (2/m)$$

$$K_{req,d} = \# \frac{2P}{\phi L}$$

$$F_{br} = 0.01P$$

where m is the number of bracings and L the required brace spacing.

2.6 Continuous Bracing System for Columns and Beams

In this type of system the column is entirely constrained by bracings, such as siding for columns or the joists from concrete slab.

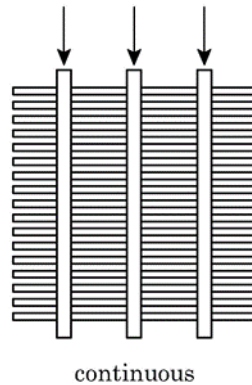


Figure 52. Continuous bracing system.

We have seen in the previous chapter that increasing the stiffness of the bracing the columns undergoes many changes in the number of waves in the buckled shape. First of all the column becomes unstable in a half-sine curve followed by a mode with two waves, three waves, and at the end reaches the maximum load capacity for $P_{cr}/P_e = 1$ between two brace points at the ideal stiffness of $3.41 P_e/L_b$. Timoshenko (1961) defined the concept of continuous bracing as a system in which the column is placed on a continuous medium and the reaction at any cross section is proportional to the deflection at that section. In other words, calling “ α ” the spring constant of the medium, and “ a ” the spacing between each spring, providing the ratio between them, the modulus of the foundations is calculated.

$$K = \frac{\alpha}{a} \quad \frac{[F]}{[L]}$$

Starting from this assumption, Timoshenko developed the elastic buckling capacity of a column with pinned ends and continuous lateral bracing as follows

$$P_{cr} = P_e \left(n^2 + \frac{KL^2}{n^2\pi^2 P_e} \right)$$

where “ n ” represents the number of half-sine waves in the buckled shape. As the brace stiffness K increases, the buckling load and the number of half-sine waves increase as well. P_e is the elastic Euler buckling capacity of the column

with no intermediate bracing $P_e = \pi^2 EI/L^2$. There is difficulty to use this formula because “ n ” is in the numerator and the denominator, therefore we should apply an iterative procedure in order to evaluate which is the expected value of “ n ” that gives the lowest buckling capacity. Consequently, Bleich (1952) introduced an approximate solution developed by Engesser previously, in which any iterative procedure is needed.

$$P_{cr} = \frac{2L}{\pi} \sqrt{\bar{K}\tau P_e}$$

where τ is an inelastic stiffness reduction factor.

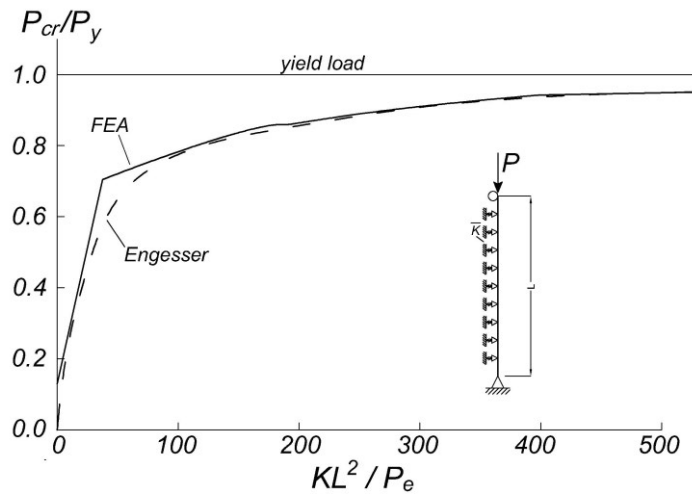


Figure 53. Continuous inelastic lateral column bracing solutions.

“Effective bracing system for columns and beams exist in many forms, including point bracing and continuous bracing. Employing continuous bracing formulations for cases with point braces provides an attractive solution that can significantly improve the efficiency and economy of the bracing design relative to current methods commonly utilized in design [6]”. To pass from discrete to continuous bracing it is necessary to convert the stiffness K to an equivalent continuous stiffness \bar{K} . Given n as the number of intermediate point braces, we sum all their contributions by $n \cdot K$ and divide by the total length of the member.

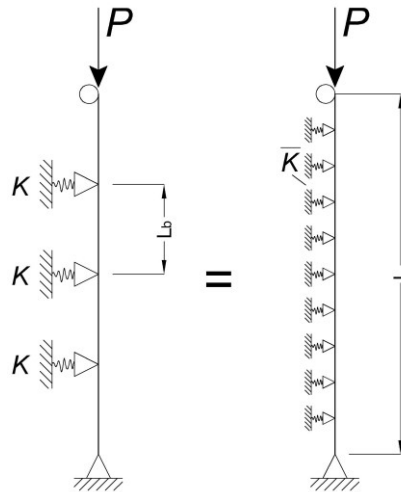


Figure 54. Modelling point bracing.

By using $\tau P_e = \tau \pi^2 EI / L^2$ we obtain

$$\bar{K} = \frac{P^2}{4\tau EI} = \frac{nK}{L}$$

If we compare the solution using finite element analysis FEA for a discrete system, in this case three-point braces, we will recognise differences with respect the solution of continuous bracing, or the Engesser’s approximation. Typically, the continuous solution gives a conservative estimation of the brace stiffness compared to the exact point brace solution for any axial force. The Engesser’s solution is 3.5% unconservative because the real unbraced length is usually smaller than the unbraced length required to support the design load.

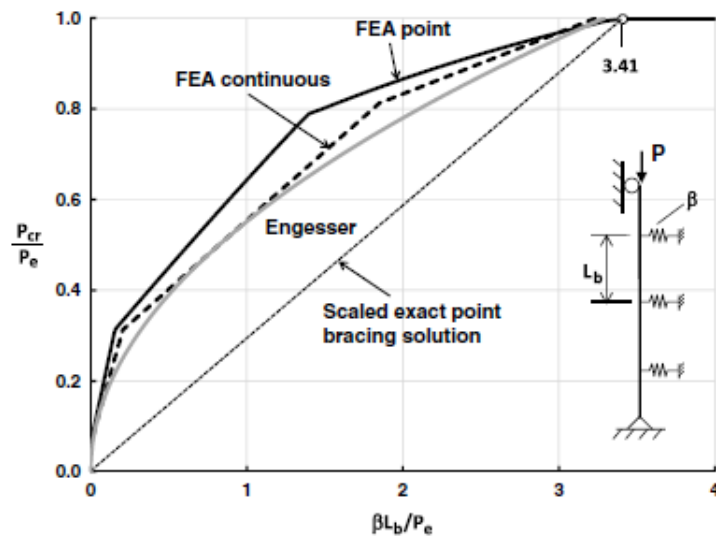


Figure 55. Point and continuous lateral column bracing-elastic.

In Figure 55 the relationship between applied load and point brace stiffness is showed. Typically, we refer to $P_{cr}/P_y = 1 - 0.25 P_y/P_e$ because the critical load cannot be reached due to inelastic limits for what concern small unbraced lengths. We can recognise that for an higher number of intermediate braces the Engesser continuous approximation fit well the exact solution at FEA. Instead for three braces the Engesser solution doesn't fit good, however, it is conservative. For many braces, the estimation of the ideal stiffness is lower with respect the exact solution (Timoshenko), while for three braces the estimation is more accurate.

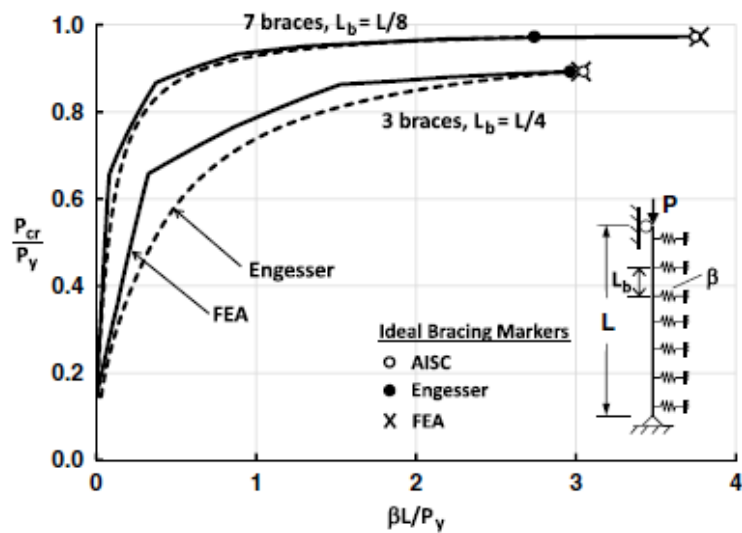


Figure 56. Point and continuous lateral column bracing-inelastic.

3 Basic of Structural Optimization

Hafka explains the optimization as a whole of techniques devoted to «achieve the best outcome of a given operation while satisfying certain restrictions» [11]. Typically, people act in such a way in order to minimize expenditure and discomfort. From a structural point of view, the idea of optimization was first developed to reduce the weight of the structures, especially in the aerospace industry, but later other parameters, such as costs and performances, began to be taken into consideration. For instance, a structure could be designed making it lighter as possible, stiffer, or insensitive to instability. Clearly, there is no limit in stiffness and other aspects, so we need to introduce some constraints. Therefore it is important to understand our priorities, recognising which parameter/s must be maximized or minimized [12].

In a structural optimization problem there is always an objective function (OF), used to evaluate the goodness of the design, its result consists simply in a number if the objective is only one. Typically OF measures weight, stress, displacement, and even costs. When more than one OF is employed, the optimization is called *Multicriteria Optimization* [11]. On the other hand, optimizing a structure presupposes the possibility to have some parameters that can be changed, included by a vector $\bar{X} = [x_1, x_2, \dots, x_n]$ that collects the so called design variables. Usually, design variables can be members sizes or other parameters that control the geometry of the problem. In addition, a function y is introduced in order to measure the response of the structure, such as strain, stress or displacement, and it is called state variable. Even in this case, we may introduce more than one [12].

Problems of structural optimization can be managed by determining the optimal cross-sectional areas of structural members keeping stresses and displacements as constraints. This type of approach is known as size optimization, and it is widely applied when the costs minimizations and the control of usage of materials are fundamental.

An alternative is to assign as design variables the nodal coordinates of the structural domain described by partial differential equations. Called shape optimization, the goal is to define the right integration domain.

There is also the possibility to optimize a structure by improving the arrangement of the elements and at the same time refining the spatial distribution of the material, providing, if needed, removal unnecessary structural members. In this case, we are referring to the so called topology optimization.

In summary, it may be said that structural optimization objectives are the cost minimization and structural performance improvement. Nowadays, it is also necessary to take into account the environmental impact, for this reason, the optimization can be developed based on this aspect, limiting the greenhouse gas emission or energy consumption [12][13].

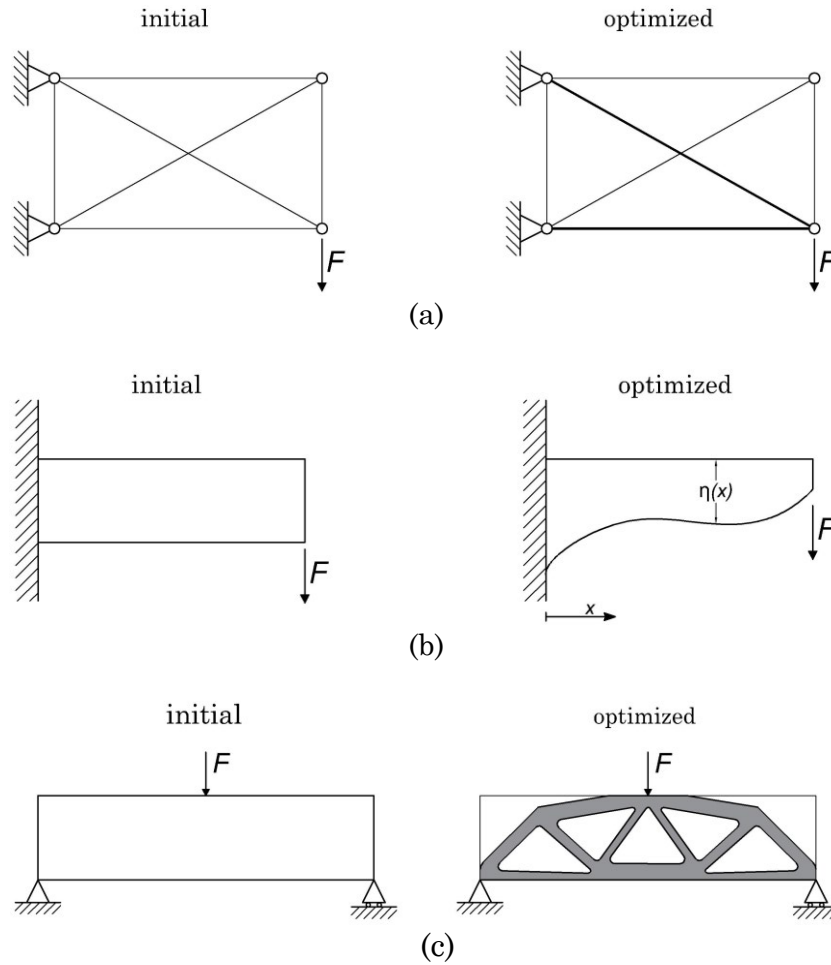


Figure 57: Images taken by [12]. Initial designs and optimized solutions are proposed. (a) Size optimization; (b) Shape optimization with the function $\eta(x)$; (c) Topology optimization saving 50% of structural material.

Typically in civil engineering applications, the structural optimization is performed with more than one objective. This is the reason why we usually refer to multi-objective optimization. For example, we may consider minimizing deflection and weight concomitantly, but clearly, the procedure is more complex and we need sophisticated computational algorithms. Obviously it is not possible to reach the best solution for both objectives because the growth of one may be incompatible with the growth of the other. For this reason the optimization procedure returns trade-off solutions. A multi-objective optimization problem can be proposed as follows:

$$f(\bar{X}) = [f_1(\bar{X}), f_2(\bar{X}), f_3(\bar{X}), \dots, f_k(\bar{X})]^T$$

$$\begin{aligned} g_i(\bar{X}) &\leq 0, & i &= 1, 2, 3, \dots, m; \\ h_j(\bar{X}) &= 0, & j &= 1, 2, 3, \dots, p; \\ \bar{X} &\in S \end{aligned}$$

where $f(\bar{X})$ are the OFs if more than one, $g_i(\bar{X})$ and $h_j(\bar{X})$ are the constraints; $\bar{X} = [x_1, x_2, \dots, x_n]$ is the vector containing the design variables, and S is the domain of the solution [13].

Optimization processes can be classified into classical deterministic methods and stochastic or heuristic methods. The reason why they are defined as classic methods is the rigorous usage of mathematically “well posed” formulation; moreover they can be further divided into direct search methods and gradient methods. Classical methods have the advantage to evaluate well the local optimum but they are not good to ensure the convergence to the global optimum in the case of multiple optima. Tuan Q. Pharn pointed out discrepancies testing two traditional approaches (Hooke and Jeeve’s method and Quasi-Newton method) and a stochastic method (Genetic Algorithms i.e. GA) for a representative engineering problem [14]. He asserts that for engineering applications, many problems must be treated by sets of non-linear equations or differential equation solved using numerical methods, committing rounding and errors. Therefore he states that heuristic methods, such as evolutionary algorithms, are better than the classical approaches “*to solve real problems in the process industries*”.

If in the classical deterministic method the solution is taken by well-defined mathematical form, in the heuristic method the problem is solved implementing artificial intelligence techniques that improve the accuracy by iterations. However, solution ambiguities may be founded, in particular in the interpretation of the local and global optimum. Nevertheless, the setting of the problem is quite easy, ensuring high computational speed [13].

To achieve a better optimization, researchers introduced an improved method, called meta-heuristic methods, in which trade-off solutions are employed in order to differentiate local and global optima. Metaheuristics are a group of approximate techniques that have become popular in structural optimization research for several years and they are widely used for multi-objective problem optimizations [15]. The term *metaheuristic* derives from two Greek words: *heuriskein* which means “find out”, and *meta* which means “beyond”. Anyway, metaheuristics were usually called *modern heuristics* [17]. Meta-heuristics algorithms consists of two main components: *exploration* and *exploitation*, or diversification and intensification. Exploration refers to investigating the search space on a global scale, while exploitation means to focusing the search in local region based on the acquired experience. The algorithm convergence should be found during the evaluation of the best solution and when a good balance between diversification and intensification [16][17][18]. Saka asserts that metaheuristics algorithms have the main disadvantage in high computational costs, especially in extensive structures [19]. The same opinion for Mahdavi [20], which refers to the so called Large Scale Global Optimization (LSGO) associated with projects with large number of decision variables, is difficult to manage because of the high complexity of the search space.

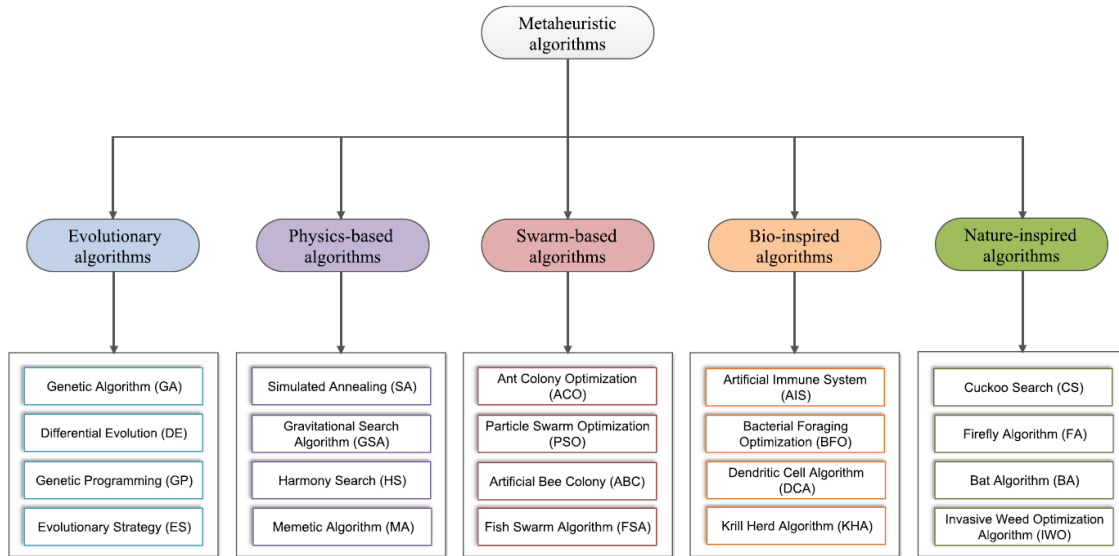


Figure 58: Classification of meta-heuristic algorithms. Image taken by [16].

Metaheuristics methods are normally based on natural or man-made phenomena, such as water flow, immune system, ensemble of musicians, and ant colony [13]. They can be classified as indicated in Figure 58.

3.1 Evolutionary Algorithms

Evolutionary algorithms (EAs) are the first metaheuristic techniques which have been employed and they take inspiration from the Darwinian Theory of Evolution. EAs collect four different procedures which are the Genetic Algorithms (GAs), Differential Evolution (DE), Genetic Programming (GP) and Evolutionary Strategy (ES). The idea is to generate a numerical procedure in which an artificial population of trial solutions must reach the global optimum. “*Each candidate solution in the population is called an individual*” [19], and they are randomly established selecting values from set of design variables, according to the reduced space by the presence of the constraints. The sequent manipulation of these data carries out new individuals called offspring and among them only those with higher fitness value are taken into a new generation. Those individuals with low fitness values (having worse OF value) are eliminated. Populations are created until one individual dominates a certain percentage of the population or a predefined number of generations is iterated. At the end of the procedure the individual with the higher fitness value is taken as the optimum solution, much like in natural selection. Therefore, we can distinguish in EAs four steps: initialization, selection, genetic operators, and termination [21].

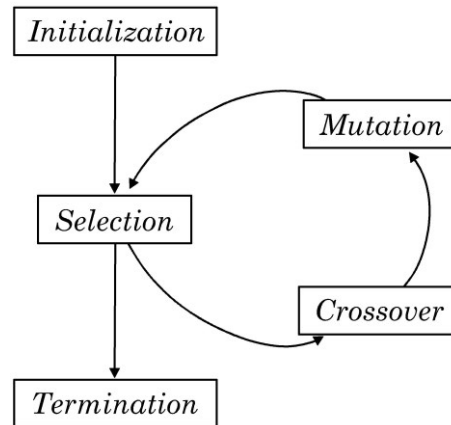


Figure 59. Image taken by [21].

As explained above, at the initialization phase, an initial population of solutions is created, and it contains a defined number of individuals. It can be generated randomly, according to the constraints, or defined a priori if there is enough knowledge of the problem. Obviously, it should be better to include a wide range of solutions in order to explore many different possibilities during the execution of the algorithm. Once a population is created, the selection phase consists of the evaluation of the individuals according to a fitness function that takes the characteristics of each of them and returns a numerical representation of the goodness of the solution. The fitness of all individuals is computed, and then, the top-scoring ones can be selected.

It is important to differentiate the fitness function $F(\bar{X})$ and the objective function $f(\bar{X})$: the fitness function is used to guide the optimization process, while OF is the function being optimized. Essentially, they represent the same concept, even if they may be stated with different mathematical formulations, as in the case of a Genetic Algorithm, in which for a minimization problem it is better to have $F(x)$ positive [32]

$$F(\bar{X}) = \frac{1}{1 + f(\bar{X})}$$

In the case of MOFs, the process is more complicated because there is a need to identify more than one optimal point, and for this reason, we have to find out a set of optimal points. The set is called Pareto Frontier, and collects members equally optimal; in other words, there is no solution that dominates other solutions in the frontier. However, a *decider* may be used in order to narrow the field of the solutions, finding out a single one based on the context of the problem or other empirical evaluations [21].

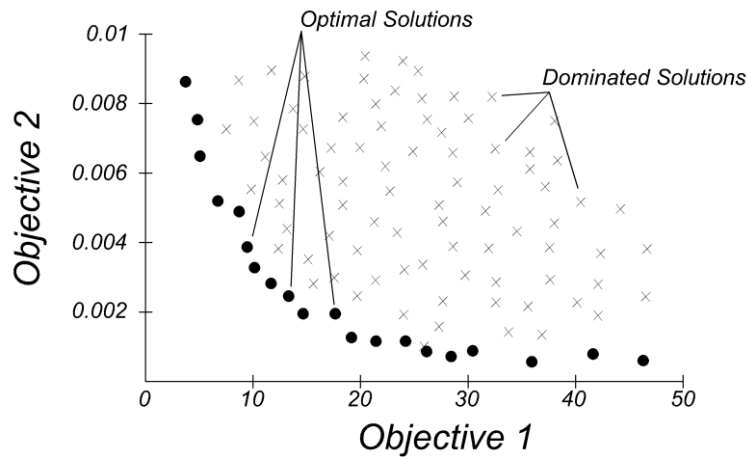


Figure 60.

Usually, two individuals are selected, and they are now used to create the next generation. Employing some characteristics of them (crossover), new individuals, called offspring are generated, and other new properties must be introduced in order to do not perfectly reflect the “old” generation anymore (mutation). The mutation is made in a probabilistic manner, in fact, the probability that offspring receive a mutation and its severity, is governed by a probability distribution. Termination occurs when the algorithm ends, i.e. when the algorithm has reached maximum runtime or the threshold of performance.

3.1.1 Genetic Algorithm (GA)

Genetic algorithms (GAs) are probably the most popular evolutionary algorithms with a wide range of applications [18], and they were developed by John Holland in the 1960s and 1970s, based on Darwin’s Theory of natural selection [23]. Each individual is encoded in binary strings forming arrays of bits (chromosomes) in which each bit is an allele [32]. The population may be initialized randomly if further information are not present. The dimension of the population should be at least $2n$ to $4n$, if n is the number of the design variable [31]. Genetic algorithm and evolutionary algorithm are usually intended as the same thing, this is the reason why the previous explanation about the EAs will be substantially the same for GAs, adding a simple example.

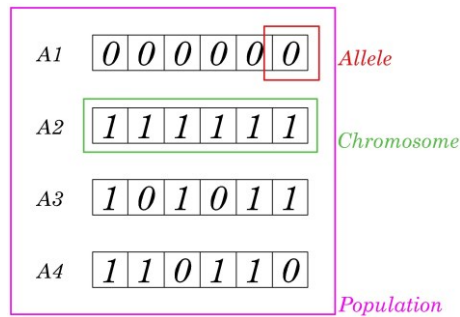


Figure 61. Population, Chromosome and Alleles (genes). Image taken by [24].

The fitness function gives a score to each individual, from that it depends on probability to an individual to be selected for reproduction. Once two pairs of strings are taken with a high score, a cross-point is chosen randomly.

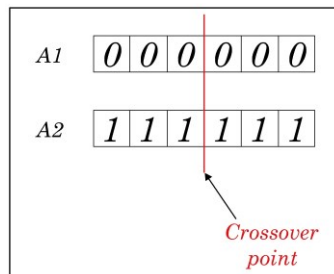


Figure 62. Crossover point. Image taken by [24].

New members are generated (offspring) by exchanging the alleles until the crossover point is reached.

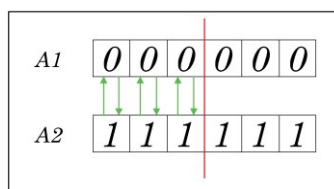


Figure 63. Exchanging alleles. Image taken by [24].

The new offspring are now part of the population.

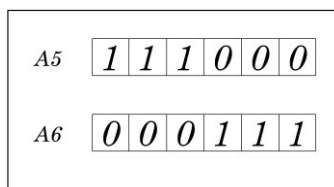


Figure 64. New offspring. Image taken by [24].

Some genes may be randomly changed in order to have much diversity with parents and to avoid premature convergence of the algorithm (mutation).

<i>before mutation</i>						
A5	1	1	1	0	0	0
<i>after mutation</i>						
A5	1	1	0	1	1	0

Figure 65. Mutation: Before and After. Image taken by [24].

Obviously, every time a new generation is created, members with the least fitness score are canceled, providing space for new offspring. The goal is to produce generations having more quality than the previous ones; the sequence get stops when the algorithm returns a set of solutions which are not significantly better.

3.1.2 Differential Evolution (DE)

The Differential Evolution (DE) is a population-based metaheuristic algorithm and it can be considered as a development of genetic algorithms. DE was proposed by R. Storn and K. Price in 1996 and 1997 and nowadays it is one of the most stochastic optimization methods widely used in the field of structural engineering [18]. Unlike the genetic algorithm, in DE the mutation phase occurs before the crossover operation, moreover, the mutation operator is not created by a probability distribution but by creating a unit vector. Therefore, DE Algorithm consists of five steps: initialization, mutation, crossover, selection and termination . We have a population of n solution vectors $X_i (i = 1, 2, \dots, n)$, and for each generation t , a generic chromosome can be indicated by a vector $X_i^t = (x_{1,i}^t, x_{2,i}^t, \dots, x_{D,i}^t)$, where D is the dimension of the optimization problem.

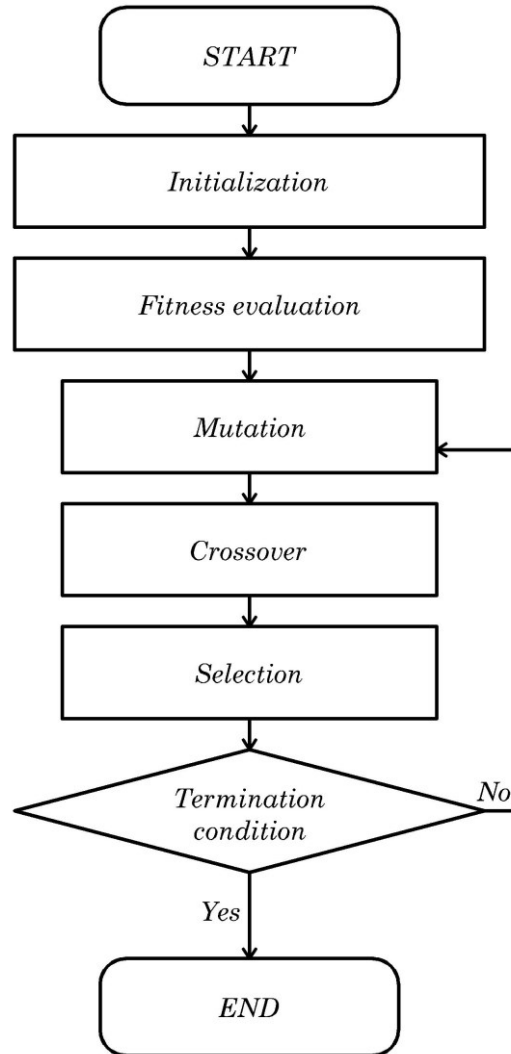


Figure 66. Differential Evolution flow chart. Image taken by [25].

As a first stage, the population is initialized by defining upper and lower bounds for each parameter $x_j^L \leq x_{j,i}^1 \leq x_j^U$, and randomly selecting the initial values on the intervals $[x_j^L, x_j^U]$. Each parameter vector is subjected to mutation, crossover (recombination) and selection. During the mutation process, an individual can be generated as follows

$$v_i^{t+1} = x_{r_1}^t + F(x_{r_2}^t - x_{r_3}^t)$$

where r_1, r_2, r_3 are random values generated within the interval $[1, n]$, F is the mutation factor within $[0, 2]$. The result is the so-called *donor vector*. Mutation allows expanding the search space. Crossover procedure provides an exchange of information between old and new individuals in order to generate a new member [25]. The new one is called trial vector, and it contains some elements of the donor vector with probability CR (crossover probability); trial vector may be represented as follows

$$X_i^{t+1} = (x_{1i}^{t+1}, x_{2i}^{t+1}, \dots, x_{Di}^{t+1})$$

where

$$x_{ji}^{t+1} = \begin{cases} v_{j,i}^{t+1} & \text{if } rand_{j,i} \leq CR \text{ or } j = mbr(i) \\ x_{j,i}^t & \text{if } rand_{j,i} > CR \text{ and } j \neq mbr(i) \end{cases}$$

where $rand_{j,i}$ is the uniformly distributed probability in $[0,1]$ and $mbr(i)$ is the random integer matrix in $[0, D]$. At the selection phase, the vector obtained during mutation (target vector) and the trial vector (from crossover operation) are compared, and the one with the lowest fitness value is admitted to the next generation.

$$x_i^{t+1} = \begin{cases} x_i^{t+1} & \text{if } f(x_i^{t+1}) \leq f(x_i^t) \\ x_i^t & \text{otherwise} \end{cases}$$

The algorithm gets stops when one of these criteria is reached. DE algorithm is able to adapt well during the process because the differences decrease if the population converges toward the optima. Furthermore, it is important to take into account the population size: a too-small population means a premature convergence, while too large size would lead to inconclusions and high computational times [32].

3.1.3 Genetic Programming (GP)

Genetic Programming is a special type of Evolution Algorithm, and it can be considered as an extension of Genetic Algorithm. In fact the procedure begins with the initialization of the population that progressively is refined through crossover and mutation processes until reaching an optimum solution. GP adopts trees as genotypes to represent the problems, and each individual has the ability to change itself by adding terminal and other commands [23]. In other words, individuals can operate individually by function and transition rules.

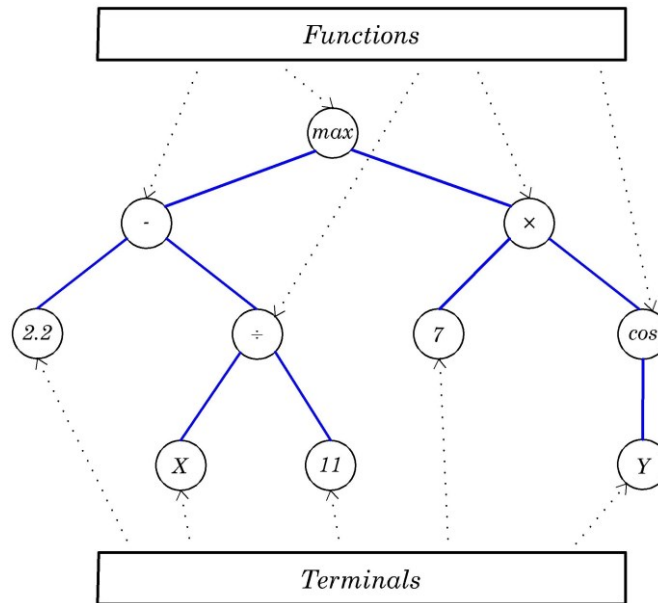


Figure 67. An example of Genetic Programming flow chart. Image taken by [28].

As for all EAs, the first stage is the initialization of the population and the design of the fitness function. For standard GE the population is created uniformly randomly among the domain, instead for GP we need to define well the syntax of the problem, setting a minimum and maximum depth for each tree. It means that each individual must be inside *min* and *max* depth layers. Crossover operation occurs by selecting (randomly) a subtree in each parent and matching it with the subtree of the other parent, creating offspring.

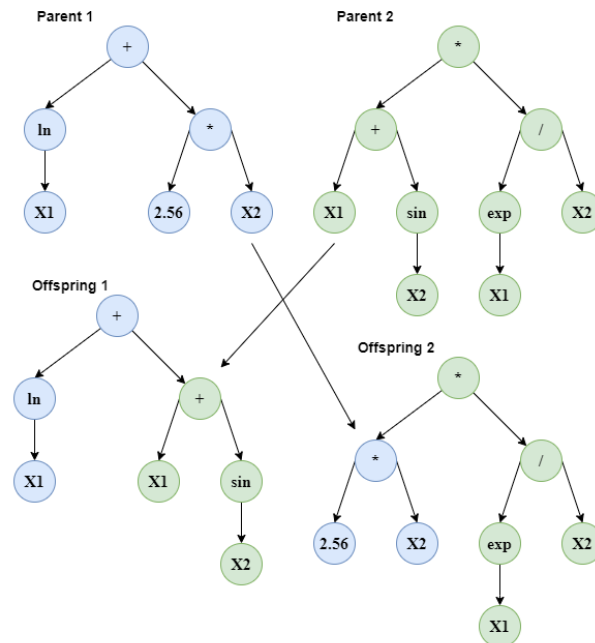


Figure 68. Crossover. Image taken by [28].

For what concerns the mutation, this process may be performed in many ways. We could change the function node or the terminal node. Another strategy could be swapping two terminal nodes, or truncating (deleting) a single function node. Finally, we could add other functions devoted to growing trees.

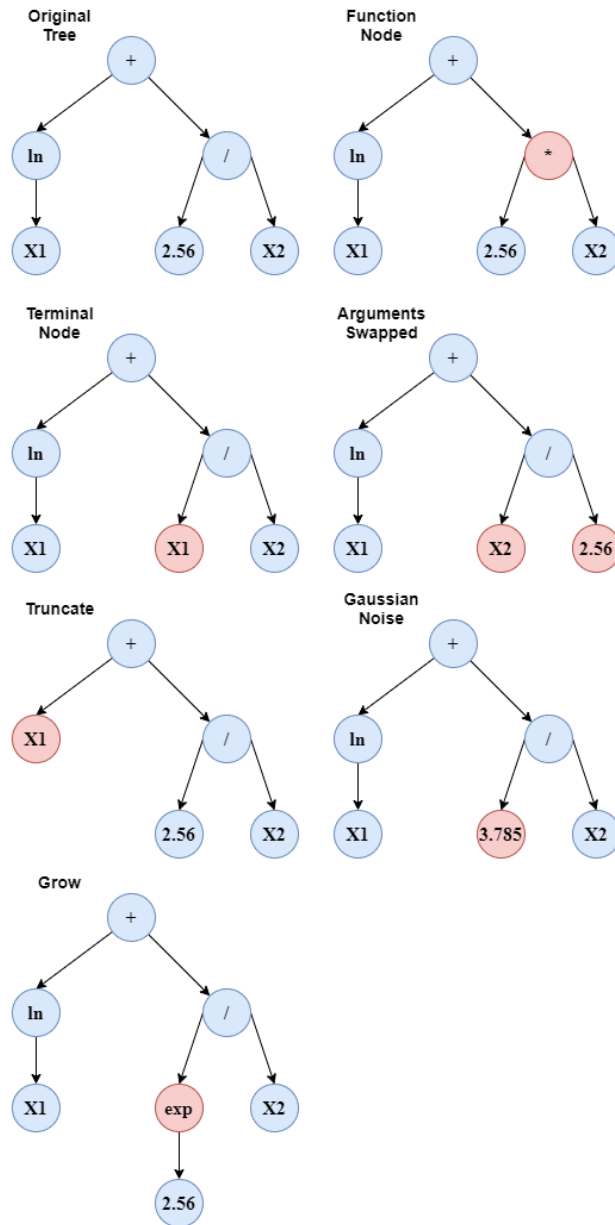


Figure 69. Mutation. Image taken by [28].

The substantial difference between *GAs* and *GP* is that in Genetic Programming individuals can grow and shrink by adding new terminal nodes and functions.

3.1.4 Evolutionary Strategy (ES)

Evolution Strategies (ES) are evolutionary algorithms developed in 1960s by Rechenberg and Schwefel at the Technical University of Berlin [32]. They are inspired by biological evolution and operates applying mutation, recombination and selection processes [29]. Substantially, the algorithm evaluates stochastically new candidate solutions by using a probability distribution, typically a multivariate normal one. Once again, at each iteration, new candidates (offspring) are generated, fitness scores are evaluated, and the better ones are employed for the next generation.

We can have two different versions of ES: the first one is the $(\mu + \lambda) - ES$ in which more than one offspring is created for each iteration, however, it is needed to keep constant the population size, so the worst individuals λ out of $\mu + \lambda$ are rejected [30]; the other version, known as $(\mu, \lambda) - ES$, selection occurs among the λ offspring only, and there is no comparison between old and new generation. Clearly, we have an offspring surplus $\mu > \lambda$, according to Darwin's Theory of Natural Selection.

In ES an individual is characterized by n -tuple of values for design variables $[x_1, x_2, \dots, x_n]^T$ for establishing the candidate solution, a tuple of strategy parameters, and the fitness value that usually is linked to OF value [26]. Typically, strategy parameters are collected in a vector $\sigma = [\sigma_1, \sigma_2, \dots, \sigma_n]$ which represent the standard deviations, they are continuously adjusted by the algorithm in order to control the optimization process according to the design space. This skill of "self-adaptation" is an important advantage that allows obtaining success and efficiency.

The recombination occurs by an operator, called *Recombine*, that starts from μ individuals, it generates λ offspring. The scope is to exchange design characteristics in terms of design variables and strategy parameters. Therefore, we need to introduce a vector $s \in (x, \sigma)$ that contains both of them, then in order to recombine an individual, we must introduce a temporary vector that operates as follows

$$s'_i = \begin{cases} s_{a,i} \\ s_{a,i} \text{ OR } s_{b,i} \\ s_{a,i} \text{ OR } s_{bj,i} \\ s_{a,i} + \frac{(s_{b,i} - s_{a,i})}{2} \\ s_{a,i} + \frac{(s_{bj,i} - s_{a,i})}{2} \end{cases}$$

In case of respectively: no recombination, discrete, global discrete, intermediate, and global intermediate. Where s_a and s_b are the components of the two parent individuals which are randomly taken from the population. In the first case, recombination does not occur because the new element has been pasted by the same family. In the second case the element is taken with equal probability from one of the two parents. In the third, the first parent s_a is

chosen and kept unaltered while a new second parent s_{bj} is chosen randomly from the parent population for each element. The last two cases are like the second and third cases respectively, the only difference is the calculus of the arithmetic means of the elements. These new individuals are then mutated by another operator, called *Mutate*. At each iteration the best solution (x_i^{best}, f_i^{best}) is updated and the next generation is established by selecting μ best solutions from λ offspring in case of $(\mu, \lambda) - ES$, or from μ parents and λ offspring in case of $(\mu + \lambda) - ES$. The algorithm gets stops until the termination condition is not met, and the best attained solution is the output. However, the procedure could be stopped when the algorithm converges to a certain number of iterations, beyond which there is no significant improvement.

4 Optimization Strategy

4.1 Interaction Matlab® - SAP2000® and integration of the Genetic Algorithm (GA)

The structural optimization has been performed by using Matlab® as controller, instead FEM structural analysis is conducted with SAP2000®. The communication between the two software is established by the so-called “*API Functions*”, or “*Application Programming Interfaces*”. If we think Matlab® and Sap2000® as the actors of the procedure, the first is the “*Client*”, or the user which performs the call in order to obtain the return of the results, the second is the “*Server*”, or the entity that supplies data requested and fix rules about API operation. The Client does not need to know the software operations, but just the rules needed to perform the call. The communication between them is standardized through *API Documentation*, that is a technical report consisting of instructions about how API functions work, and it is edited by the Server [33].

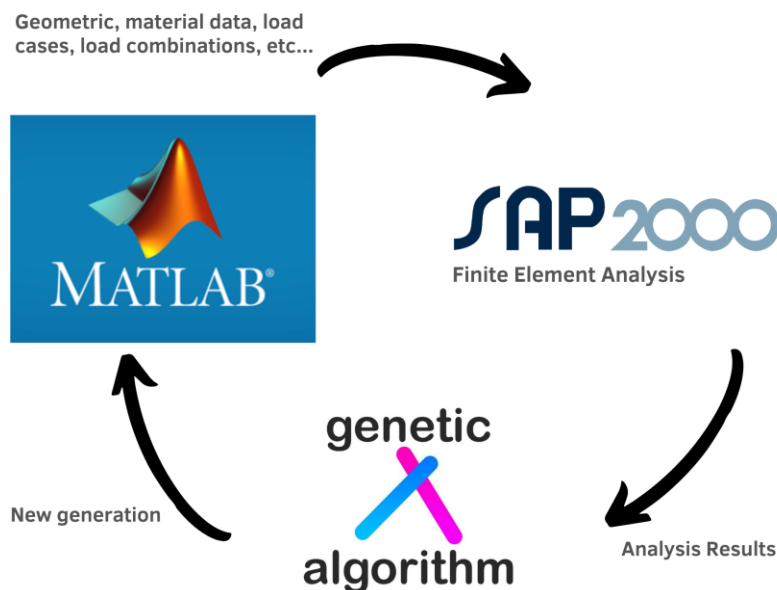


Figure 70. Workflow adopted for the case study.

4.2 Optimization Problem

Since the structure investigated cannot be modified because of fixed geometry, size optimization is the strategy that fits very well to achieve the optimal solution. In Chapter 3, a wide discussion about optimization procedures has been done, anyway, at this stage it is important to highlight which are the characters involved.

Typically, the objective of a size-optimization is the control of usage of material, that essentially reflects in economic consequences.

It does not exist a well-posed engineering problem when it has been conceived without a scheme that provides exactly how much material must be used according to technical standards, or to structural mechanics teachings. The tendency to concentrate resources where they are strictly required is a common practice, but this can be done in a more accurate and conscious manner.

A Genetic Algorithm is implemented in our calculations in order to perform the structural optimization of the case study. *GA* basically consists of three main quantities, which are:

- Design vector \mathbf{x} ;
- Objective function $f(\mathbf{x})$;
- Constraint function $g(\mathbf{x})$;

The objective function (OF) $f(\mathbf{x})$ is related to searching the minimum mass of the structure, that it can be defined as

$$f(\mathbf{x}) = W(\mathbf{x}) = \sum_{i=1}^{N_{el}} \rho_i V_i(\mathbf{x})$$

in which \mathbf{x} represents the external diameter of the tubular cross-section Φ_i , ρ_i is the steel density (7850 kg/m^3), $V_i(\mathbf{x})$ is the volume of each steel member and N_{el} is the total number of segments [32][37]. If prismatic members with constant area $A_i(x)$ along their length L_i are used, it is possible to define OF as:

$$f(\mathbf{x}) = W(\mathbf{x}) = \rho \cdot \sum_{i=1}^{N_{el}} A_i L_i$$

A generic *constrained optimization problem* is defined as:

$$\begin{aligned} & \min_{\mathbf{x} \in \Omega} \{f(\mathbf{x})\} \\ & g_q(\mathbf{x}) \leq 0 \quad \forall q = 1, \dots, n_q \\ & h_r(\mathbf{x}) \leq 0 \quad \forall r = 1, \dots, n_r \end{aligned}$$

where $\mathbf{x} = \{x_1, \dots, x_j, \dots, x_n\}^T$ is the design vector of the variables to be optimized. ‘Omega’ Ω is the search domain characterized by a multidimensional space defined by admissible intervals for each j -th variable. These intervals are defined by lower and upper bounds $[x_j^l, x_j^u]$. This describes a *box-type hyper-rectangular search space* Ω typically defined as a Cartesian Product [39]:

$$\Omega = [x_1^l, x_1^u] \times \dots \times [x_j^l, x_j^u] \times \dots \times [x_n^l, x_n^u]$$

The constraint functions $g_q(\mathbf{x}), h_r(\mathbf{x})$ are called respectively *inequality and equality constraints*.

Different approaches can be adopted in order to minimize OF ; there are methods in which OF and *constraints* are taken into consideration separately, or others in which constraints are transformed in *Penalty-functions*. The latter can be grouped into a category, called *Penalty-functions-based methods*, in which the constrained optimization problem can be converted into an equivalent unconstrained version:

$$\min_{\mathbf{x} \in \Omega} \{\phi(\mathbf{x})\} = \min_{\mathbf{x} \in \Omega} \{f(\mathbf{x}) + H(\mathbf{x})\}$$

where $H(\mathbf{x})$ is the penalty function. If the penalty functions doesn't change at each iteration, it is a *static penalty function* $H_S(\mathbf{x})$, otherwise it is addressed as *dynamic penalty function*. $H_S(\mathbf{x})$ can be expressed as follows:

$$H_S(\mathbf{x}) = \omega_1 H_{NVC}(\mathbf{x}) + \omega_2 H_{SVC}(\mathbf{x})$$

where H_{NVC} is the number of violated constraints, H_{SVC} is the sum of all constraints that are violated, and ω_1, ω_2 are static control parameters of the penalty scheme [39]:

$$H_{SVC}(\mathbf{x}) = \sum_{p=1}^{n_p} \max\{0, g_p(\mathbf{x})\}$$

The choice of $\omega_1 = \omega_2 = 100$ is suggested by Parsopoulos and Vrahatis [38].

4.3 Optimization problem for the case study

At the end of the optimization procedure what we want to obtain is a tapered pole, with $\Phi_{top} \leq \Phi_{bottom}$. A linear function with two design variables is adopted: $x(1)$ is the diameter of the pole at the bottom, $x(2)$ is the diameter at the top for $z = L$, where L is the total length of the pole. Being the entire length covered by five segments, it is supposed to have constant cross-section for each segment. Figure 71 illustrates this assumption.

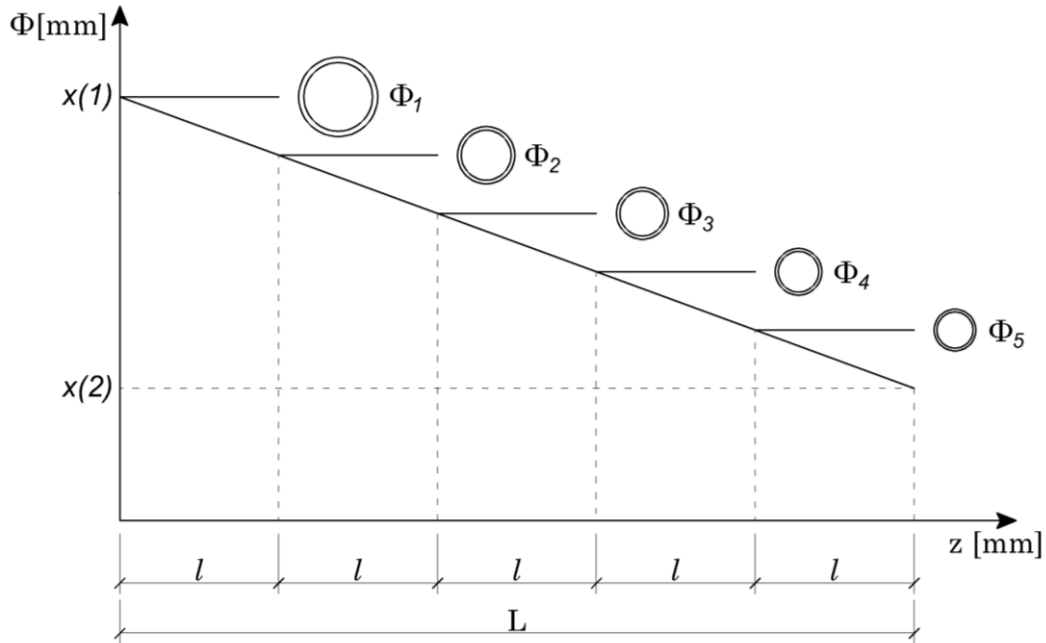


Figure 71. Linear interpolation used to determine pole-diameter.

The linear function takes the following expression:

$$\Phi = x(1) - \left| \frac{x(1) - x(2)}{L} \right| \cdot z$$

The slope coefficient is proposed in absolute value because algorithm may generate couples of values in which $x(2) > x(1)$, that means an increasing function that returns $\Phi_5 > \Phi_1$

Thus, steel members take the following relations:

$$\Phi_1 = x(1) - \left| \frac{x(1) - x(2)}{L} \right| \cdot 0 = x(1)$$

$$\Phi_2 = x(1) - \left| \frac{x(1) - x(2)}{L} \right| \cdot l$$

$$\Phi_3 = x(1) - \left| \frac{x(1) - x(2)}{L} \right| \cdot 2l$$

$$\Phi_4 = x(1) - \left| \frac{x(1) - x(2)}{L} \right| \cdot 3l$$

$$\Phi_5 = x(1) - \left| \frac{x(1) - x(2)}{L} \right| \cdot 4l$$

The *design vector* \mathbf{x} can be proposed as follows:

$$\mathbf{x} = (\Phi(1), \Phi(2), F, t, \dots)$$

where F is the prestressing at the cables, t the thickness of the main pole.

At this moment, just to ease the understanding, four variables fill the design vector, and three different scenarios will be proposed and discussed.

The *Objective Function* $f(\mathbf{x})$ is evaluated once a populations has been created and the *FEM Analysis* has been performed. It takes the following relation:

$$f(\mathbf{x}) = W(\Phi) = \sum_1^5 \rho \cdot \{\pi \cdot t \cdot [\Phi_i - t] \cdot l\}$$

To be exact, after the population creation and the FEA, constraints assessment occurs, and in this phase are imposed some criteria that must be respected during the optimization process. In other words, the objective function is not free in the solution space, but it is constrained by some variables pre-defined by the user. In *Errore. L'origine riferimento non è stata trovata.* is proposed the flowchart of the optimization process using GA. In the case of interest, these criteria are the performance ratios, also called efficiency indexes EI , evaluated at Ultimate Limit State, and the displacements, evaluated at Serviceability Limit State. EI are computed by SAP2000® according to *Italian Standards NTC2018*, with reference to buckling, tensile, and other specific requirements. The displacement at the top Δ_{SLE} is computed, and it is compared to the deflection limit according to Italian Standards as well.

$$\bigcup_{i=1}^{N_{tot}} EI_i \leq 1$$

$$\Delta_{SLE}(z = L) \leq \Delta_{LIM}$$

where N_{tot} is the total number of steel members.

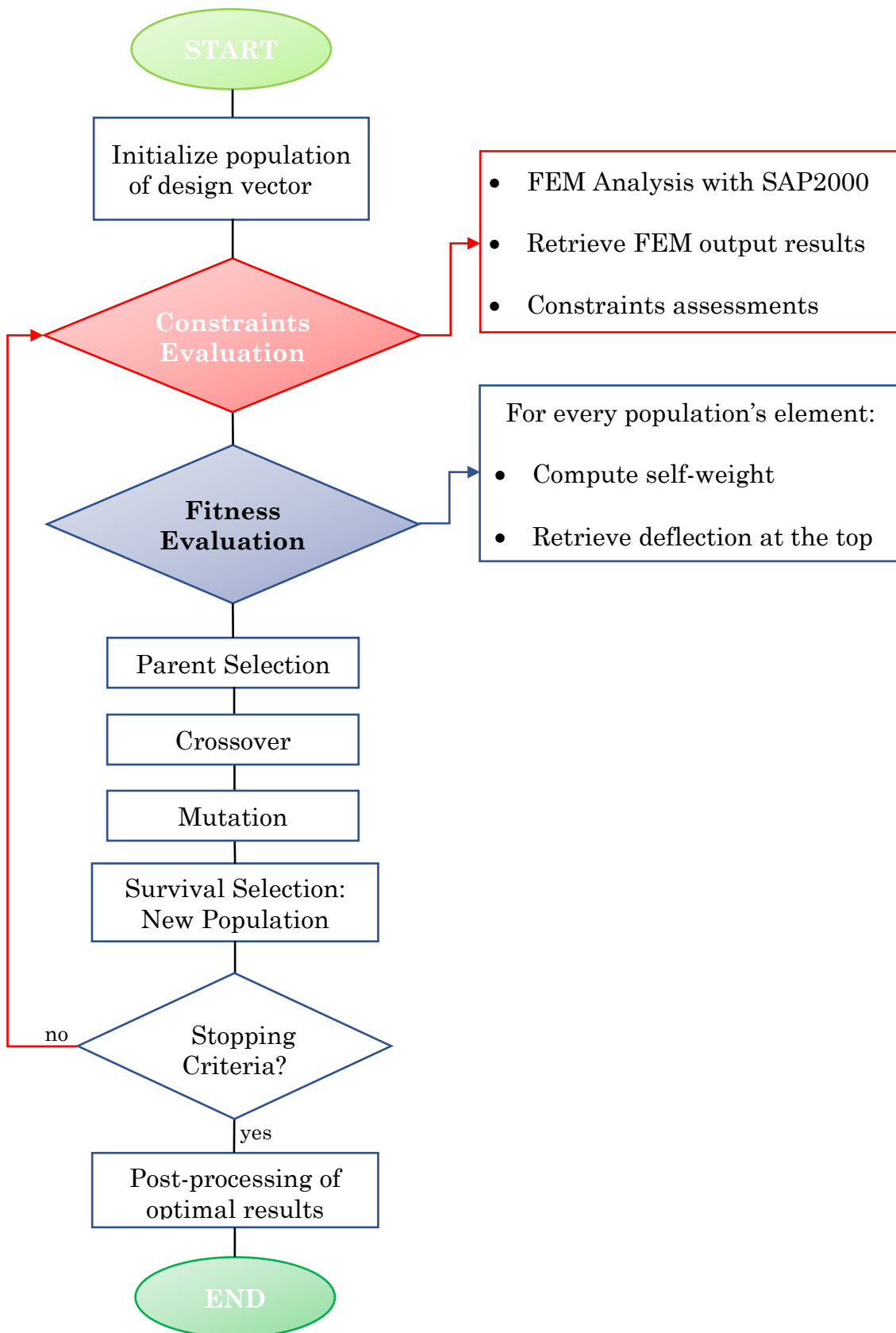


Figure 72. Flowchart of the optimization procedure using GA.

4.4 Investigated Scenarios

In this chapter i investigate differents scenarios by introducing more design variables in order to looking for different situations and responses.

4.4.1 Scenario A

In scenario A, the objective is to minimize as more as possible the usage of material acting on the diameter of the main pole, as indicated in the Chapter 4. The design vector \mathbf{x} is the following:

$$\mathbf{x} = [\phi]$$

where ϕ is the diameter.

The objective function $f(\mathbf{x})$ is the mass of the pole, expressed in kg. The lower and upper bounds (L_B, U_B) define the search space of the objective function and they are set by the user.

$$\begin{aligned} L_B &= [\phi^L] \\ U_B &= [\phi^U] \end{aligned}$$

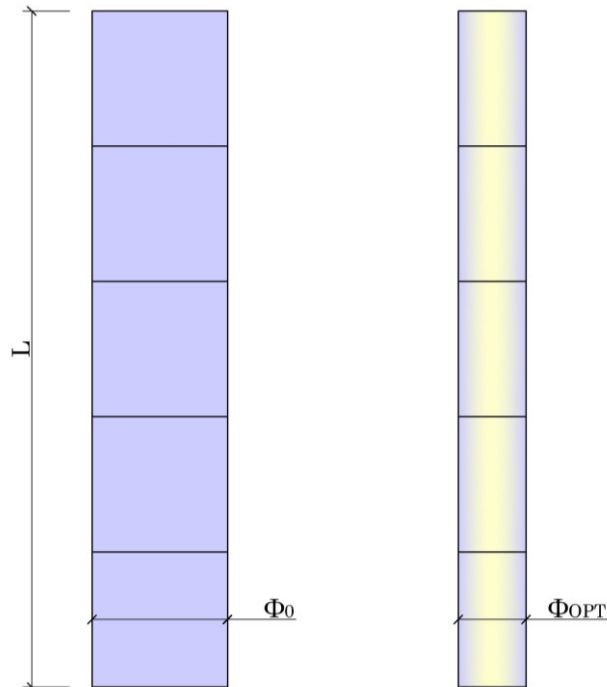


Figure 73. Conceptual scheme of Scenario A.

4.4.2 Scenario B

In scenario *B*, a “pure” size-optimization is performed. The objective is to minimize as more as possible the usage of material acting on the diameter of the main pole, as indicated in the Chapter 4. The design vector \mathbf{x} is the following:

$$\mathbf{x} = [\phi_i, \phi_f]$$

where ϕ_i, ϕ_f are respectively the bottom and top diameters.

The objective function $f(\mathbf{x})$ is once again the mass of the pole, expressed in kg. The lower and upper bounds (L_B, U_B) define the search space of the objective function and they are set by the user. Substantially GA works in that domain looking at the best couple ϕ_i, ϕ_f according to the constraints.

$$L_B = [\phi_i^L, \phi_f^L]$$

$$U_B = [\phi_i^U, \phi_f^U]$$

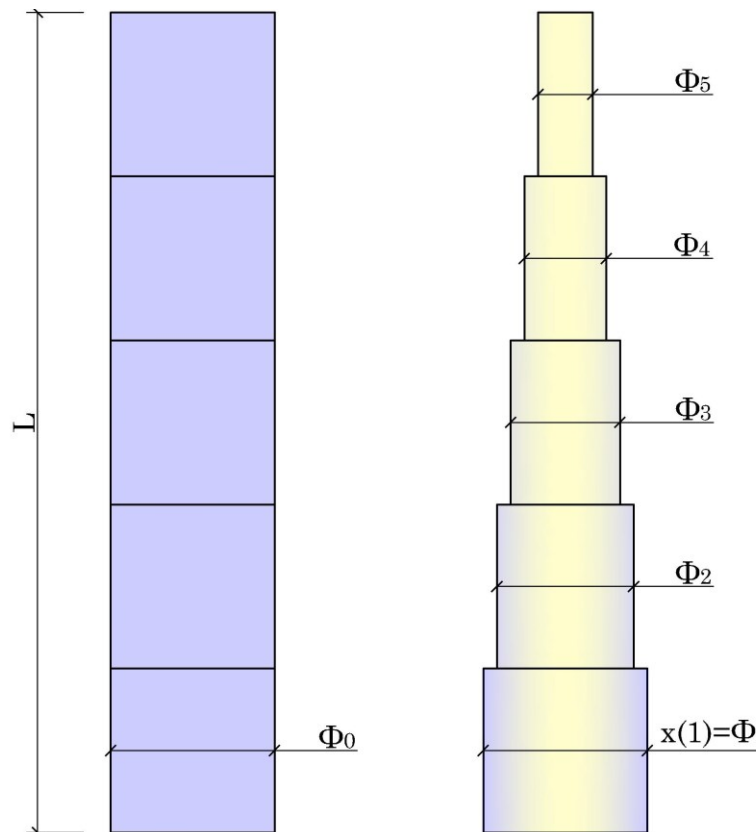


Figure 74. From initial to optimized solution. A conceptual scheme.

4.4.3 Scenario C

Scenarios ‘A’ and ‘B’ are now condensed in a unique situation, *scenario ‘C’*, in which the design vector \mathbf{x} is proposed as follows:

$$\mathbf{x} = [\phi_i, \phi_f, F]$$

At this scenario we want to investigate a hybrid solution in which both section properties and pre-tensioning can be managed. Exactly as in the two scenarios, the tapering of the main pole is governed by linear law, while the cable preload is a value that ‘moves’ within a user-defined range

$$L_B = [\phi_i^L, \phi_f^L, F^L]$$

$$U_B = [\phi_i^U, \phi_f^U, F^U]$$

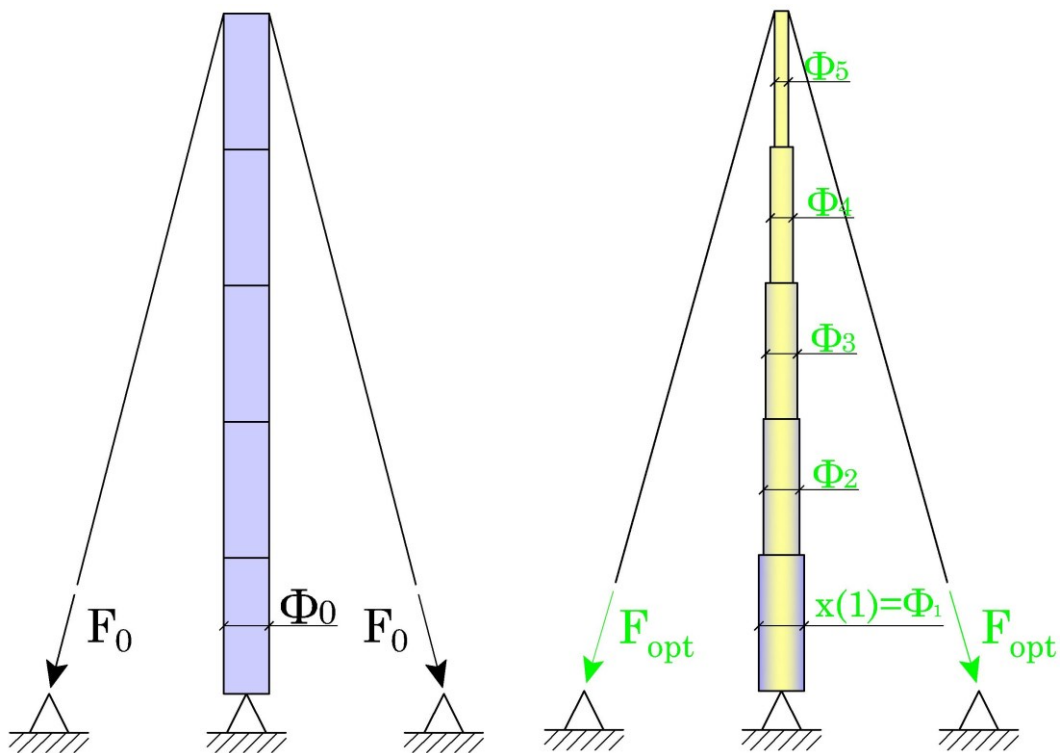


Figure 75. Scenario C.

4.4.4 Scenario D

Scenarios 'A' and 'B' condensed once again in a unique situation, *scenario 'D'*, in which the design vector \mathbf{x} is proposed as follows:

$$\mathbf{x} = [\phi_i, \phi_f, t]$$

At this scenario we want to investigate a hybrid solution in which both tapering and thickness of the main pole are considered. Exactly as in the two scenarios, the tapering of the main pole is governed by linear law, while the thickness can varies between 3 and 12.5 mm.

$$L_B = [\phi_i^L, \phi_f^L, t^L]$$

$$U_B = [\phi_i^U, \phi_f^U, t^U]$$

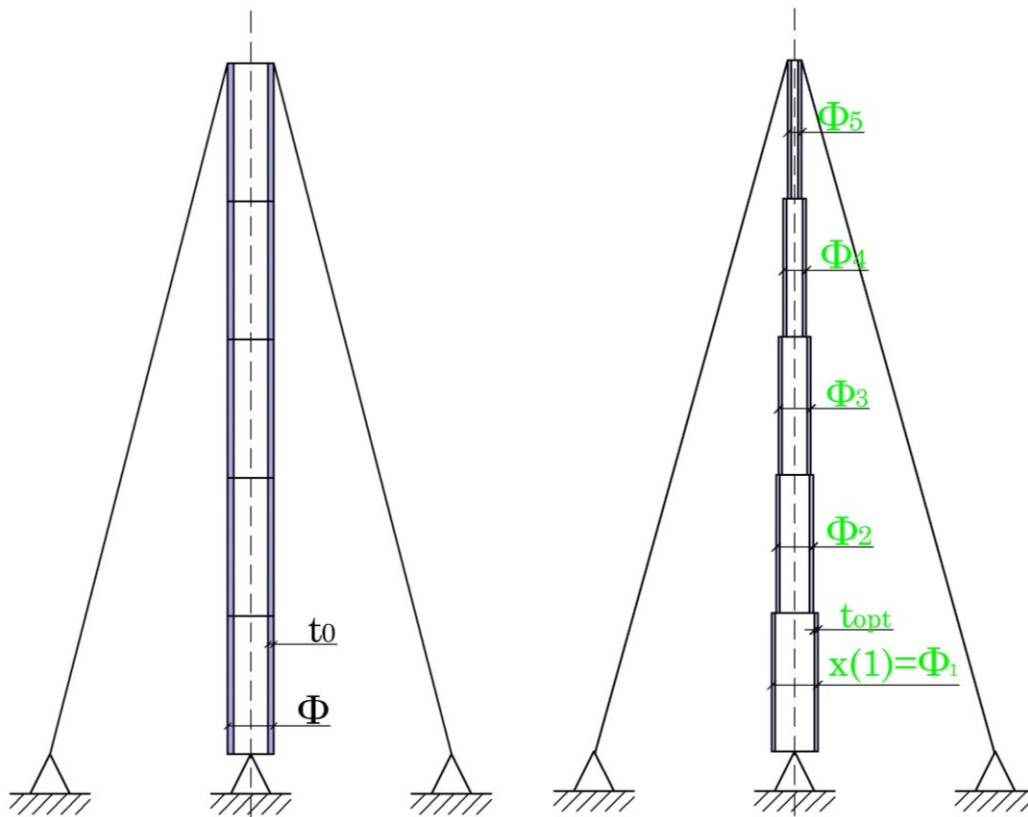


Figure 76. Scenario D.

4.4.5 Scenario E

In this scenario is introduced a new design variable t , that is the thickness of the pole, considered constant along the entire length. Once again, the diameter changes by linear law.

$$\mathbf{x} = [\phi_i, \phi_f, t, F]$$

$$L_B = [\phi_i^L, \phi_f^L, t^L, F^L]$$

$$U_B = [\phi_i^U, \phi_f^U, t^U, F^U]$$

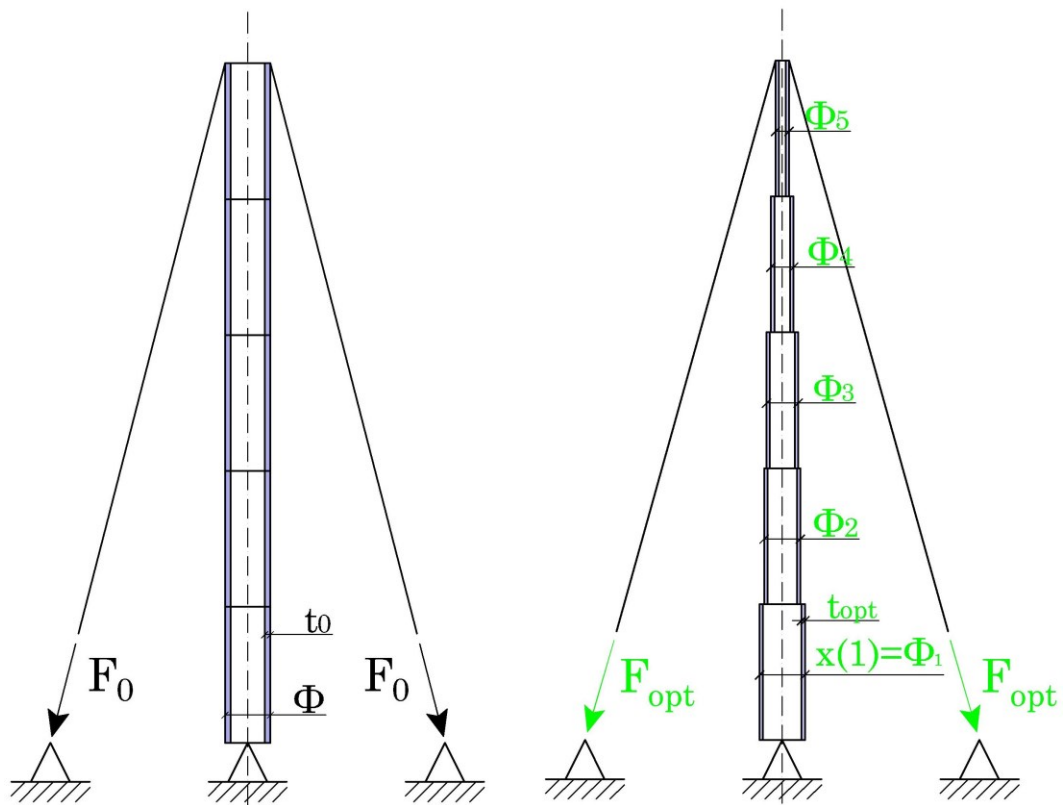


Figure 77. Scenario E.

4.4.6 Scenario F

The tapering of the main pole governed by the linear law could be not well effective due to intermediate segments that could be more stressed with respect those at the ends. Consequently, a linear tapering too much translated until covering these area results in an overall suboptimal solution.

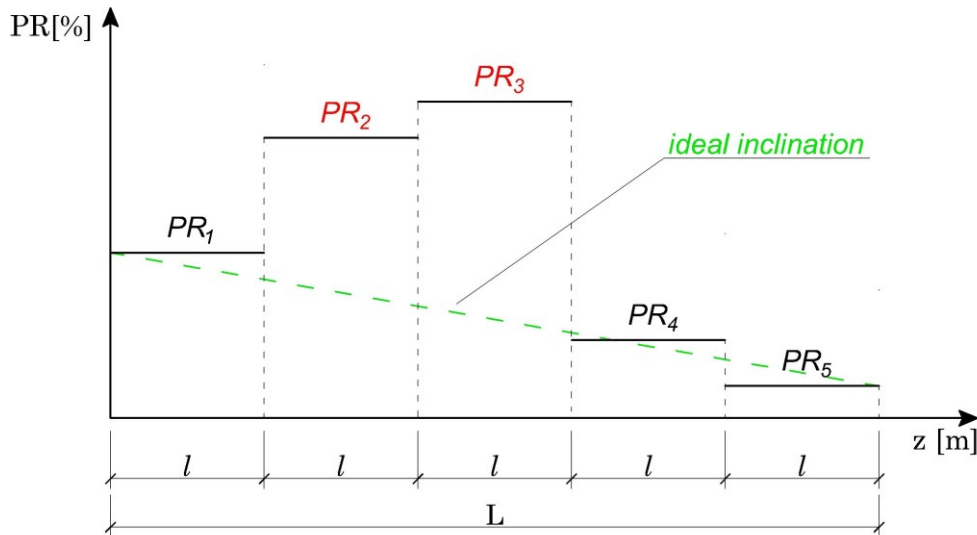


Figure 78. Performance ratios. Adapting segments 2 and 3 means performing a poor optimization of the elements at the ends.

The linear law forces to use larger sections where it is not necessary in order to optimize intermediate areas where there is a smaller solution space. To improve the solution, two additional variables are introduced, t_{2-3} which is the thickness of the intermediate sections, t_{ends} which is the thickness of segments at the ends of the main pole. The design vector \mathbf{x} is proposed as follows:

$$\mathbf{x} = [\phi_i, \phi_f, t_{2-3}, t_{ends}, F]$$

$$L_B = [\phi_i^L, \phi_f^L, t_{2-3}^L, t_{ends}^L, F^L]$$

$$U_B = [\phi_i^U, \phi_f^U, t_{2-3}^U, t_{ends}^U, F^U]$$

4.4.7 Scenario G

In scenario ‘G’ the only design variable is the thickness of the main pole, that in this case may takes different values for each segment:

$$\mathbf{x} = [t_1, t_2, t_3, t_4, t_5]$$

$$L_B = [t_1^L, t_2^L, t_3^L, t_4^L, t_5^L]$$

$$U_B = [t_1^U, t_2^U, t_3^U, t_4^U, t_5^U]$$

This situation is interesting because it could highlight what the structure really needs, and in particular what is the origin of the cause, if flexural, axial or something else. As shown in Chapter **Errore. L'origine riferimento non è stata trovata.**, we will see that the axial components will condition the structural behaviour. For this reason we want to understand if it is preferable to move the masses away from the centre of gravity in order to increase the flexural performances.

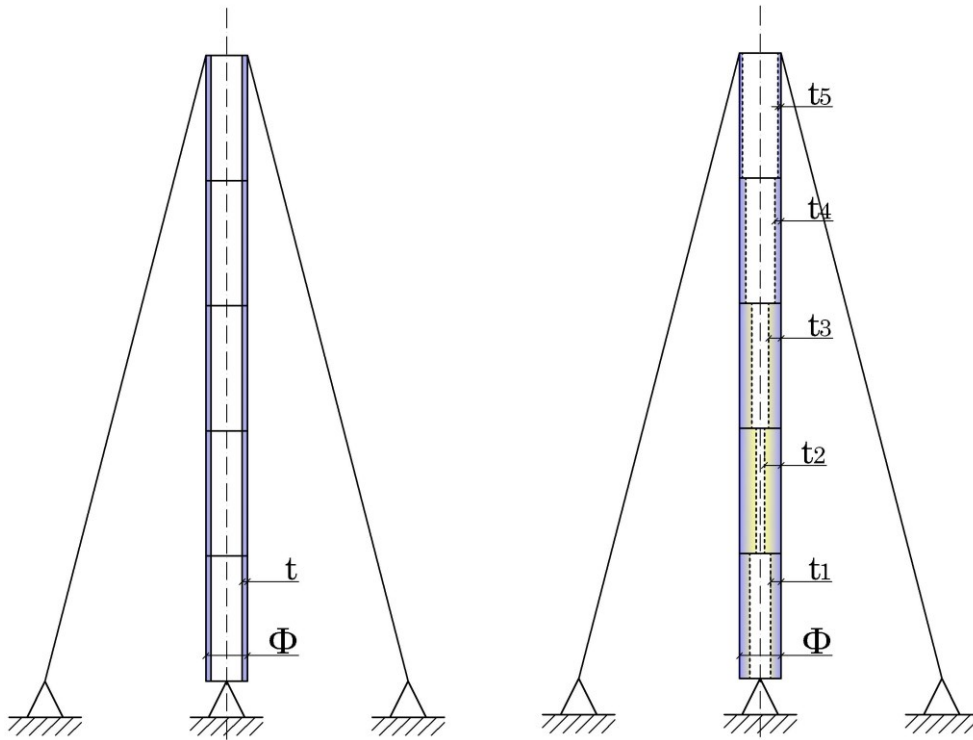


Figure 79. Scenario G.

4.4.8 Scenario H

In this scenario, many variables are introduced to find a solution that fits well in all its parts. For each segment a design variable representing the thickness of the cross section is set.

$$\mathbf{x} = [\phi_i, \phi_f, t_1, t_2, t_3, t_4, t_5, F]$$

$$L_B = [\phi_i^L, \phi_f^L, t_1^L, t_2^L, t_3^L, t_4^L, t_5^L, F^L]$$

$$U_B = [\phi_i^U, \phi_f^U, t_1^U, t_2^U, t_3^U, t_4^U, t_5^U, F^U]$$

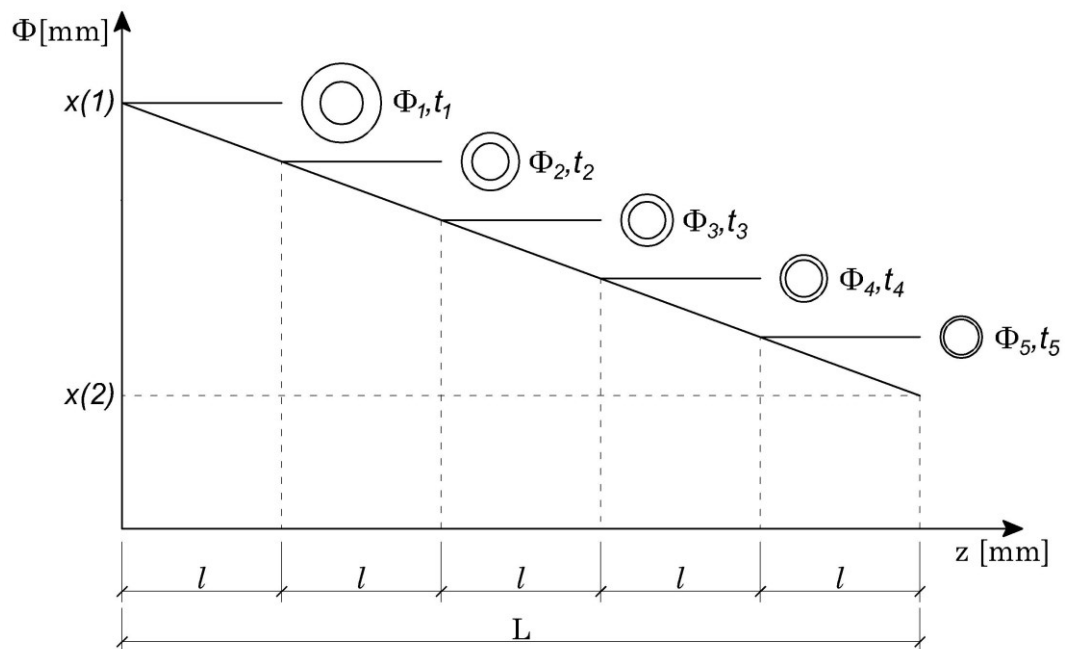


Figure 80. Scenario H.

5 Case Study: Structural Analysis of a Guyed Radio Mast

5.1 General description of the structure

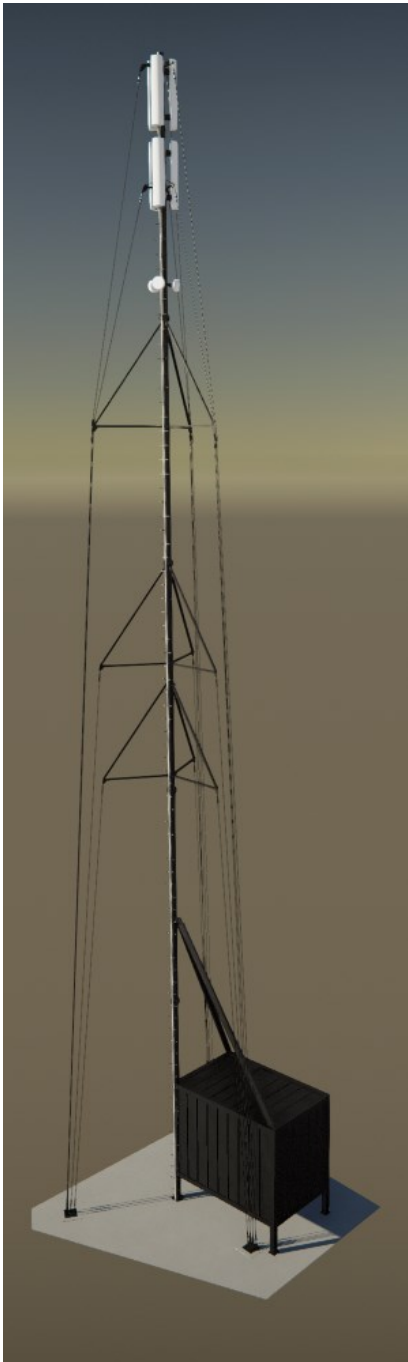


Figure 81. Render model realized using Tekla Structures.

The main pole consists of n°5 pipe steel members

The structure investigated is a guyed radio mast, also called cable-stayed tower. It is a thin and slender vertical structure sustained by tensioned cables fixed to the ground, typically arranged at 120° to each other. The main body is a single central column, made of tube profiles, or truss systems when high elevation structures occur. The employment of this type of structure in a high urbanized context is quite discouraged because cables require large space at the base. To prevent buckling, more than one set of cables is placed at different elevations. A guyed tower is usually built for meteorological purposes or to support radio antennas. The latter represents the case study of this thesis. In particular, this kind of structure may be used for limited time related to its scope, that could be an event or to guarantee the service continuity in case of maintenance to primary towers. For these reasons we will talk about *Temporary Base Transceiver Station, (BTS)*, as structures typically adopted to supply immediate service. Sporting events, concerts, motor racing, military camps, but also emergency events, are typical example of Temporary BTS applications. The BTS is usually mounted on a moveable platform, also called *shelter*, able to move itself wherever is needed, or to be towed by a tractor unit [34].

The structure investigated is located in *Bassano Del Grappa*, in the north of Italy, at 129 m elevation. The surrounded area is essentially low urbanized, with little forest, without relevant obstacles. The height of the structure is 30.00 m, it is centrally sustained by a pole in which 21 cables are fixed. Other elements, having rectangular cross-section, are placed in order to create a truss systems that connect cables and the central pole.

jointed through “flanged joints” having the same length (6.00 m). Joints are realized by bolted connections, even for cable connections.



Figure 82. Other points of view. Tekla Structures.

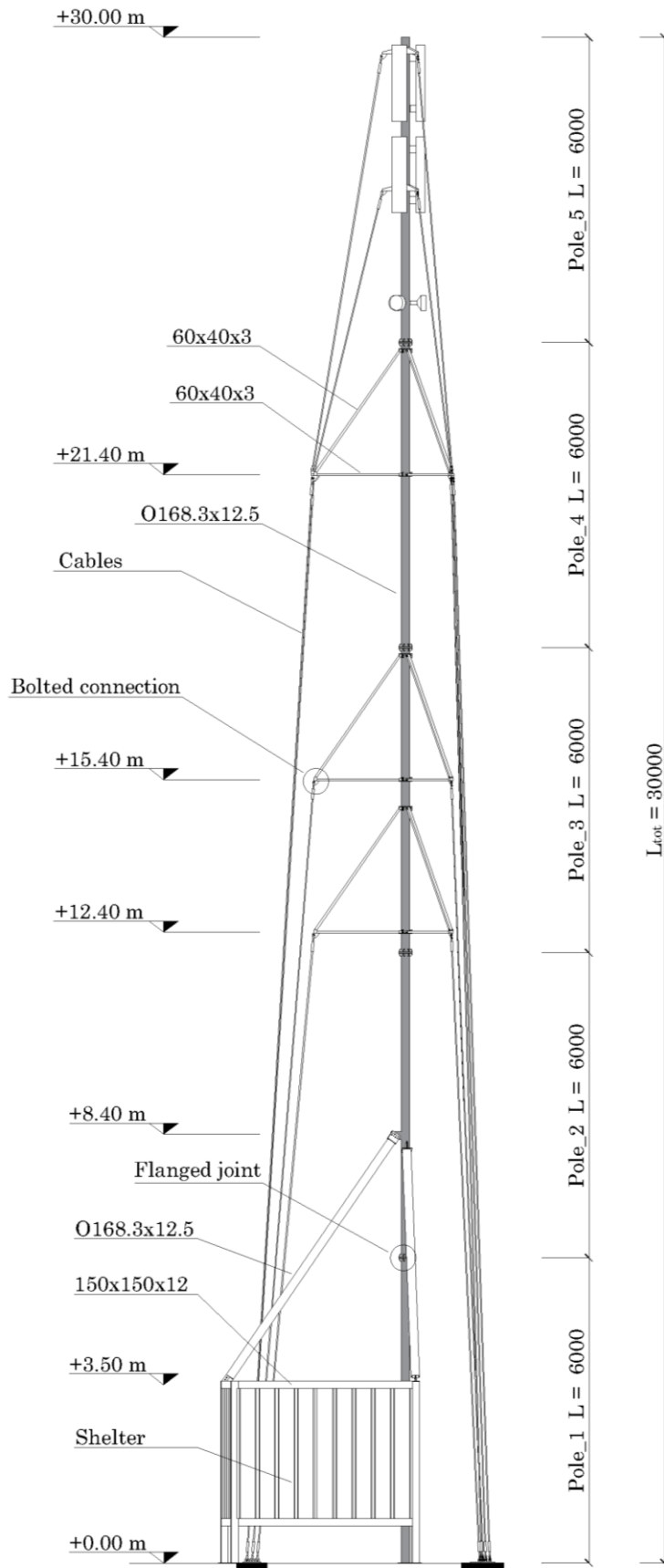


Figure 83. Technical drawing of the structure investigated [mm].

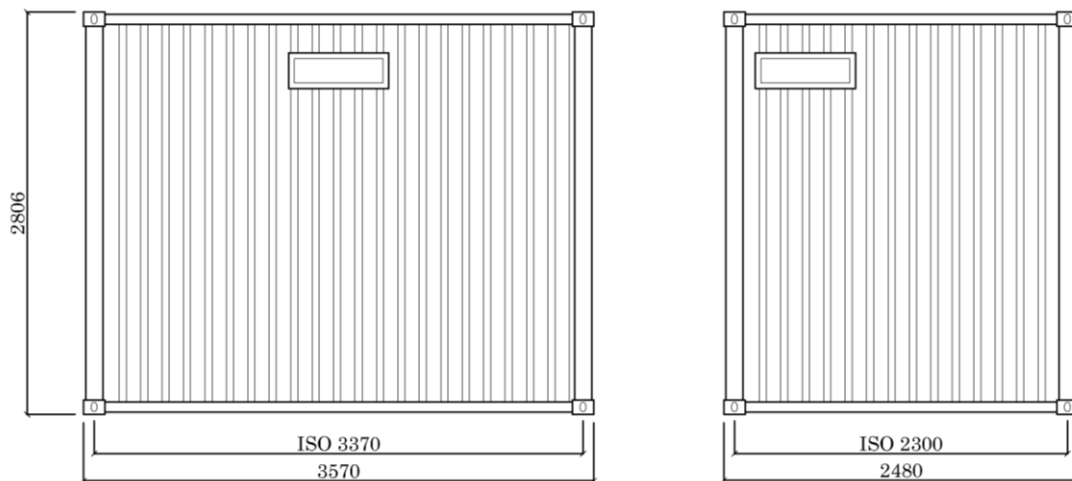


Figure 84. Technical drawing of the Shelter.

The shelter is a steel box which is devoted to partially sustain the structure and to host electronic equipment, as electrical wires and other components. It is usually mounted on a moveable platform.



Figure 85. Photographic material of the site

5.2 Load Analysis

5.2.1 Permanent loads (Dead) G1

The structure is realized of *structural steel S355* with the following characteristics:

$$\begin{aligned} f_{u,k} &= 510 \text{ MPa} \\ f_{y,k} &= 355 \text{ MPa} \\ E_s &= 210000 \text{ MPa} \end{aligned}$$

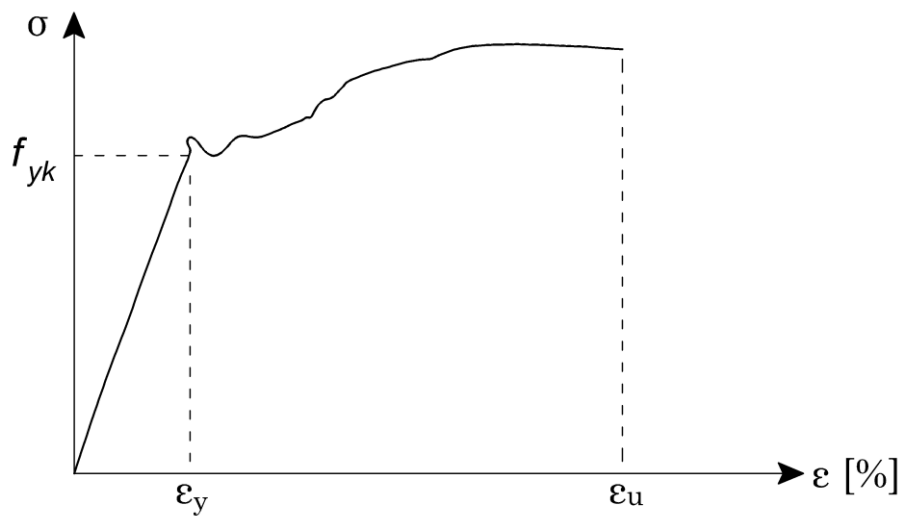


Figure 86. Constitutive law stress-strain

Steel Category	$t < 40 \text{ mm}$		$40 \text{ mm} \leq t \leq 80 \text{ mm}$	
	$f_y \text{ (N/mm}^2\text{)}$	$f_u \text{ (N/mm}^2\text{)}$	$f_y \text{ (N/mm}^2\text{)}$	$f_u \text{ (N/mm}^2\text{)}$
S235	235	360	215	360
S275	275	430	255	410
S355	355	510	335	550

Table 1.

The strength of the steel is almost the same in tension and in compression. Despite that, compressed steel members are not able to reach their maximum strength due to instability phenomena. Moreover, the structural response is strictly influenced by rotational capacity of the section, that affects the ultimate load resistance, evaluated according to plastic or elastic properties. From here, the need to define which types of section are able to fully bear the loads with the entire cross-section area, and the other ones which sustain loads with the *effective-cross section area*. For this reason, steel members are

classified in CLASS I-II-III-IV, based on rotation capacity, as briefly illustrated in Figure 87.

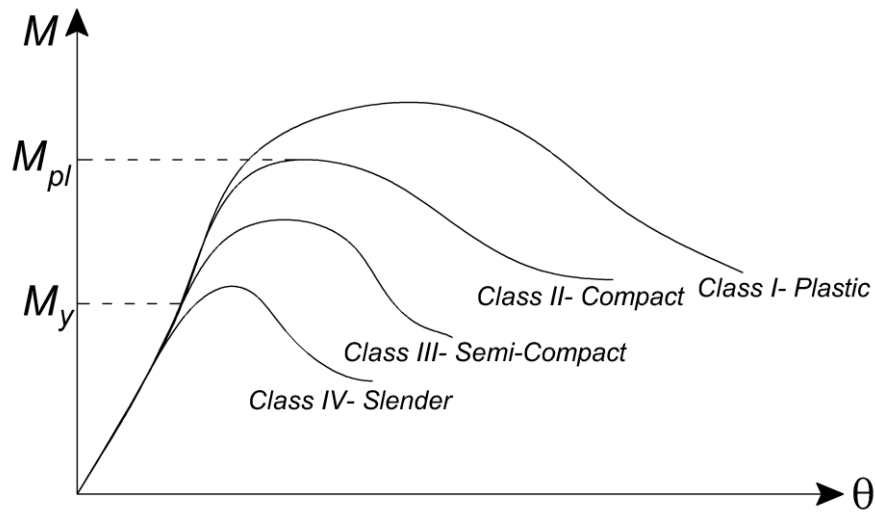


Figure 87. Rotation capacity of steel members.

The material employed for cables is the galvanized steel consisting of 6 strands (216 wires) with an independent metal core (49 wires). The main characteristics are taken from TECNOFUNI®, as illustrated in Table 2.

Steel Ropes (Cables)				
Model		6x36WS + IWRC/265 wires		
Construction pattern		6 · (14+(7+7)+7+1)+(7 · 7)		
Winding direction		right cross		
Material		galvanized steel		
Resistance		1170 N/mm ² – 180 kg/mm ²		
Cable diameter	Weight	Area	Wire diameter	Load to failure
[mm]	[kg/m]	[mm ²]	[mm]	[kN]
16	1.36	173.25	0.91	161
18	1.67	212.74	1.03	204
20	2.02	257.32	1.14	252
22	2.41	307.01	1.26	305

Table 2. Technical specifications of steel ropes. Tecnofuni®

Basically, the structure investigated consists of few type of elements, as indicated in Table 3. Dead loads are simply evaluated by know the weight per unit length of each member.

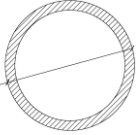
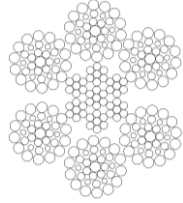
Computation of DEAD Loads					
Profile [mm]	w [kg/m]	Length[m]	n°	W _{tot} [kg]	
	D168.3x12.5	48.0	6	5	1440
	D168.3x12.5	48.0	5.65	2	543
	60x40x3	4.35	3.16	9	124
	60x40x3	4.35	1.80	9	71
	100x40x3	6.13	0.45	6	17
	D16	1.36	12.45	3	51
	D16	1.36	15.44	3	63
	D16	1.36	24.43	9	300
	D16	1.36	5.76	3	24
	D16	1.36	8.46	3	35
			$\sum W_i = 2651 \text{ kg}$		

Table 3. Computation of Dead Loads.

5.2.2 Non-structural permanent loads G2

The non-structural permanent loads are represented by the weight of the wiring and the steel ladder that allows inspection and maintenance. This load is estimated to 30 kg/m. The weight of the equipment is represented by antennas and parabolas. Two groups of three antennas are located at 26,00 m and 29.25 m height, spaced 120° apart from each other. The first one is the model *AOC4518R7v06* produced by Huawei®, as showed in Figure 88.

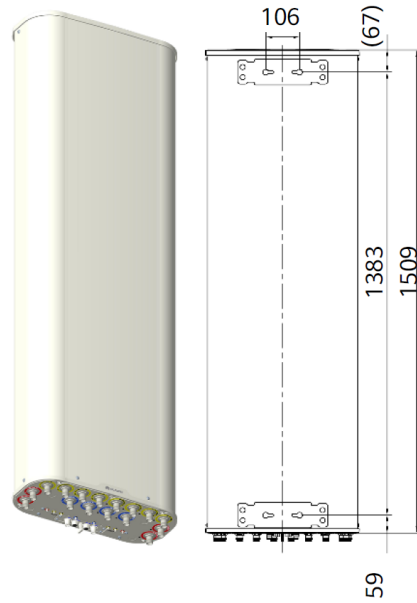


Figure 88. Huawei antenna.

The second one is the model 6888670N manufactured by Amphenol®, as showed in Figure 89.

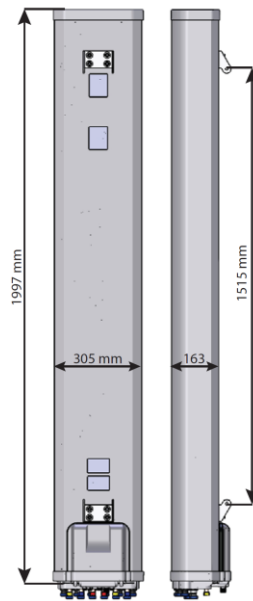


Figure 89. Amphenol antenna.

Finally, there are three parabolas located at 23,15 m height, spaced 120° apart from each other, having 30 cm as diameter.

Equipment							
Typology	Model	n°	elevation	H x W x D	self- weight	clamps weight	Overall weight
			[m]	[mm]	[kg]	[kg]	[kg]
Ant.	AOC4518R7v06	3	29.25	1509x4 69x206	39.3	2 x 5.8	152.7
Ant.	6888670N	3	26.00	1997x3 05x163	32	2 x 3.9	119.4
Parab.	n.d	3	23.15	D = 300	15	2.2	51.6

Table 4. Weight of equipment.

Non-structural permanent loads G2		
ITEM	q _k [kN/m]	Q _k [kN]
Steel ladder, other	0.30	-
Antenna	-	1.53
Antenna	-	1.19
Parabolas	-	0.52

Table 5. G2 loads.

5.2.3 Variable loads

5.2.3.1 Wind load

Wind action has been evaluated according to §3.3.4-NTC2018 and in “Istruzioni per la valutazione delle azioni e degli effetti del vento sulle costruzioni” CNR-DT 207 R1/2018.

Wind pressure is given by the following expression:

$$p = q_r \cdot c_e \cdot c_p \cdot c_d$$

where:

- q_r is the reference kinetic pressure;
- c_e is the exposure coefficient;
- c_p is the shape coefficient;
- c_d is the dynamic coefficient.

The reference kinetic pressure q_r is equal to:

$$q_r = \frac{1}{2} \rho v_r^2$$

where:

- ρ is the air density (1.25 kg/m³)
- v_r is the reference wind velocity:

$$v_r = v_b \cdot c_r$$

where v_b is the *basic wind velocity* and c_r is the *return period coefficient* that is function of the *design return period* T_R . Imposing $T_R = 10$ years, we referring to temporary structures. In this case the return period coefficient can be computed as follows:

$$c_r = 0.75 \cdot \sqrt{1 - 0.2 \cdot \log(-\log(1 - 1/T_R))} = 0.9031$$

The basic wind velocity v_b is function of the location of the structure, and it is evaluated as follows:

$$v_b = v_{b,0} \cdot c_a$$

where $v_{b,0}$ is the *basic wind velocity at sea level*, given into Tab.3.3.I-NTC2018; c_a is the *altitude coefficient*.

As showed in §3.3.I-NT2018, the structure under investigation is located in “Zona 1”.

Zona	$v_{b,0}$ [m/s]	a_0 [m]	k_s [1/s]
1	25	1000	0,040

Table 6.

The *exposure coefficient* c_e depends upon:

- the elevation z of the structure from the ground;
- the roughness and topography of the terrain;

c_e is defined as

$$c_e(z) = k_r^2 \cdot c_t \cdot \ln\left(\frac{z}{z_0}\right) \cdot \left[7 + c_t \cdot \ln\left(\frac{z}{z_0}\right)\right] \quad \text{for } z \geq z_{min}$$

$$c_e(z) = c_e(z_{min}) \quad \text{for } z < z_{min}$$

k_r , z_0 , e z_{min} are defined according to fig.3.3.2-NTC2018 based on

- *Roughness Class* of soil ‘B’ (urban area, industrial and wooded areas);
- distance from the sea coast equal to 400 km;

These assumptions set the “*categoria di esposizione III*”, that gives the following values:

CATEGORIA DI ESPOSIZIONE	k_r	z_0 [m]	z_{min} [m]
IV	0,20	0,10	5

Table 7.

The topography coefficient c_t takes into account the topographical and orographical characteristics of the site, and in the absence of more detailed evaluations the topography coefficient is set equal to 1.

The *peak wind kinetic pressure* q_p is the expected value of the maximum wind kinetic pressure over the time interval $T = 10$ minutes. In the absence of specific analyses the peak kinetic pressure is given by the relation:

$$q_p(z) = \frac{1}{2} \cdot \rho \cdot v_r^2 \cdot c_e(z)$$

For constructions or elements with curved surfaces, aerodynamic actions are characterized by the Reynolds number (§3.3.7- CNR-DT 207 R1/2018) and the roughness of the surface. *Peak aerodynamic actions* q_p on the construction are defined as the expected values of the maximum wind actions, over an interval $T = 10$ min, evaluated neglecting the reductive effects due to the non-contemporaneity of the maximum local pressures and the amplifying effects produced by structural vibrations. They are proportional to the peak wind kinetic pressure q_p , and in the case of slender structures these actions are represented by forces and moments per unit length acting along the axis of the structure. The peak aerodynamic actions are represented by a pair of drag and lift forces, f_D and f_L , respectively parallel and orthogonal to the wind direction, and a torque $m = m_z$, per unit length, applied along the longitudinal axis. They are evaluated by the relations:

$$\begin{aligned} f_D(z) &= q_p(z) \cdot l \cdot c_D \\ f_L(z) &= q_p(z) \cdot l \cdot c_L \\ m_z(z) &= q_p(z) \cdot l^2 \cdot c_M \end{aligned}$$

c_D, c_L, c_M are the coefficients of resistance, lift and torque. l is the reference dimension of the element.

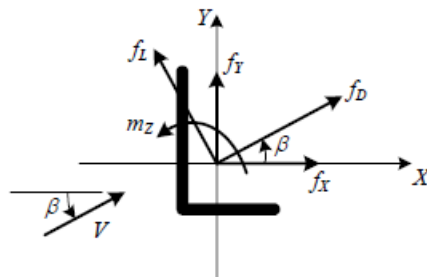


Figure 90. Actions per unit length on slender structures [36].

Reynolds number Re is a dimensionless number that expresses the relationship between inertia forces and viscous forces, i.e., between a characteristic dimension of the structure and a characteristic dimension of the flow. It plays a crucial role in the aerodynamic behavior of bodies with rounded surfaces. At height z above the ground it is given by the relation:

$$Re(z) = \frac{l \cdot v_m(z)}{\nu}$$

where:

- l is a characteristic dimension of the construction or element considered [L];
- v_m is the average wind speed [m/s];
- ν is the kinematic viscosity of air [$\nu = 15 \cdot 10^{-6} \text{ m}^2/\text{s}$]

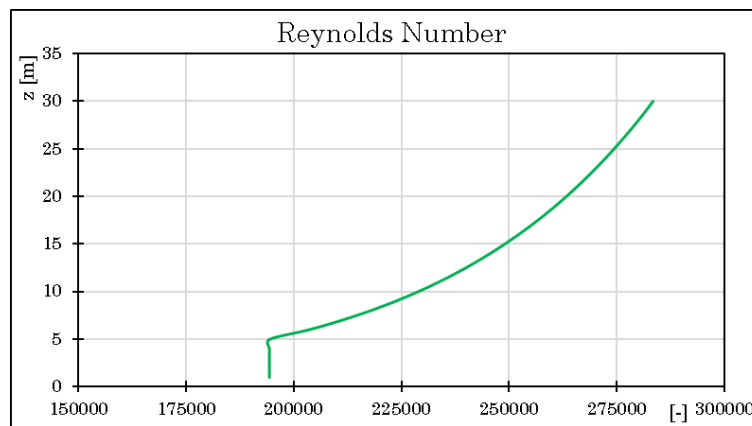


Figure 91. Reynolds number.

The non-contemporaneity of the peak actions reduces the global aerodynamic actions, if the body object of study is large. On the other hand, the amplification of the dynamic response gives rise to large displacements and stresses if the structure is flexible and it has small damping.

The actions and effects associated with wind-structure interaction are known as aeroelastic phenomena and they can cause very dangerous situations.

The wind action can be represented by equivalent load distributions that are applied statically to the structure and give rise to displacements and stresses equal to the maximums induced by the dynamic action of the wind. They may be evaluated as follows:

$$\text{Equivalent static actions} = \text{Peak aerodynamic actions} \cdot c_d$$

in which c_d is a dimensionless parameter called *dynamic coefficient*. In particular, it is defined as *longitudinal dynamic coefficient*, c_{dL} , *transverse dynamic coefficient*, c_{dL} , and *torsional dynamic coefficient*, c_{dM} , depending on

the wind action applied parallel to the wind direction itself, in the transverse direction or in the torsional direction.

For slender or flexible structures or elements with small damping, the amplification of the longitudinal dynamic response prevails, and c_{dL} is usually greater than 1.

To evaluate the aerodynamic actions per unit length on one-dimensional structures, the force and moment coefficients per unit length are given by the relations:

$$\begin{aligned} c_{fX} &= c_{fx0} \cdot \psi_\lambda \\ c_{fY} &= c_{fy0} \cdot \psi_\lambda \\ c_{fZ} &= c_{mz0} \cdot \psi_\lambda \end{aligned}$$

where:

- c_{fx0} , c_{fy0} , c_{mz0} are the force and moment coefficients per unit length related to structures and elements of ideal infinite length;
- ψ_λ is the slenderness coefficient, which takes into account reductive edge effects.

Figure 92 shows the force coefficients c_{fx0} of the circular sections as a function of Reynolds number Re and the ratio k/b , being k the surface roughness and b the diameter of the section. The curves A and B shown in Figure 92 are given by the expressions:

$$c_{fx0} = \frac{0.11}{(Re/10^6)^{1.4}} \leq 1.2 \quad \text{curve A}$$

$$c_{fx0} = 1.2 + \frac{0.18 \cdot \log_{10}(10 \cdot k/b)}{1 + 0.4 \cdot \log_{10}(Re/10^6)} \leq 1.2 \quad (k/b \geq 10^{-5}) \quad \text{curve B}$$

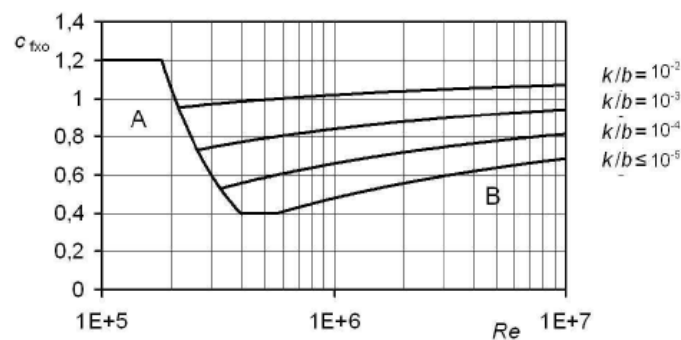


Figure 92. Force coefficients c_{fx0} for circular elements.

Roughness	
Surface	k [mm]
Glass	0.0015
Polished steel	0.05
Cast iron	0.2
Galvanized steel	
Smoothed concrete	
Rough concrete	1.0
Rusty surfaces	2
Masonry	3

Table 8. Most common surface roughness.

The *transverse force coefficient*, c_{fy0} , and the *torque coefficient*, c_{mz0} , can take on values different from zero for little imperfections in the shape of the circular section. Moreover structural elements that have finite elongation, give rising a reduction in the aerodynamic forces that would act on an infinitely long structure. This reduction can be neglected for safety, or evaluated by the slenderness coefficient ψ_λ .

The slenderness coefficient ψ_λ is given by the following relations and indicated in Figure 93

$$\begin{aligned} \psi_\lambda &= 0.6 + 0.1 \cdot \log_{10}(\lambda) && \text{for } 1 \leq \lambda \leq 10 \\ \psi_\lambda &= 0.45 + 0.25 \cdot \log_{10}(\lambda) && \text{for } 10 \leq \lambda \leq 100 \\ \psi_\lambda &= 0.61 + 0.17 \cdot \log_{10}(\lambda) \leq 1 && \text{for } 100 \leq \lambda \leq 1000 \end{aligned}$$

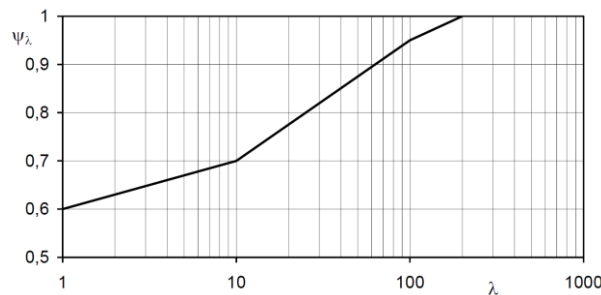


Figure 93. Slenderness coefficient ψ_λ .

where λ is a dimensionless parameter called effective slenderness.

Lenght L [m]	Effective Slenderness		Confined flow at both ends
	Free flow at least at one end Sharp-edged section	Circular section	
$L \leq 20 \text{ m}$	$\lambda = 2 \cdot L/l$	$\lambda = L/l$	$\lambda = L/l \geq 70$
$20 \leq L \leq 50$	$\lambda = (2.4 - 0.02L) \cdot L/l$	$\lambda = (1.2 - 0.01L) \cdot L/l$	$\lambda = (1.2 - 0.01L) \cdot L/l$ $\lambda \geq 70$
$50 \text{ m} \leq L$	$\lambda = 1.4 \cdot L/l$	$\lambda = 0.7 \cdot L/l$	$\lambda = 0.7 \cdot L/l \geq 70$

Table 9. Effective slenderness λ [36].

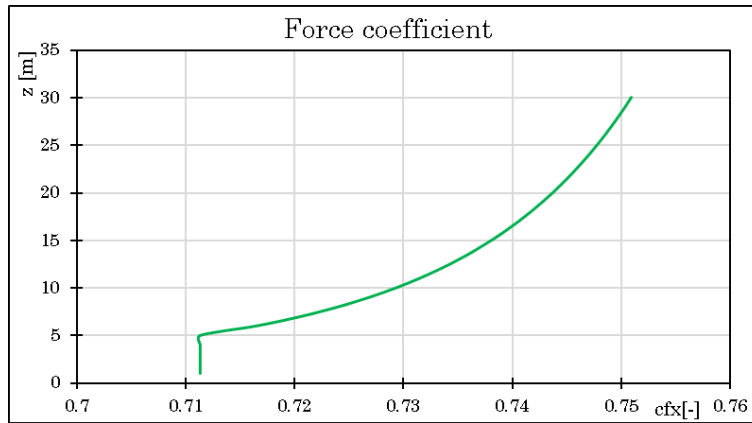


Figure 94. Force coefficients.

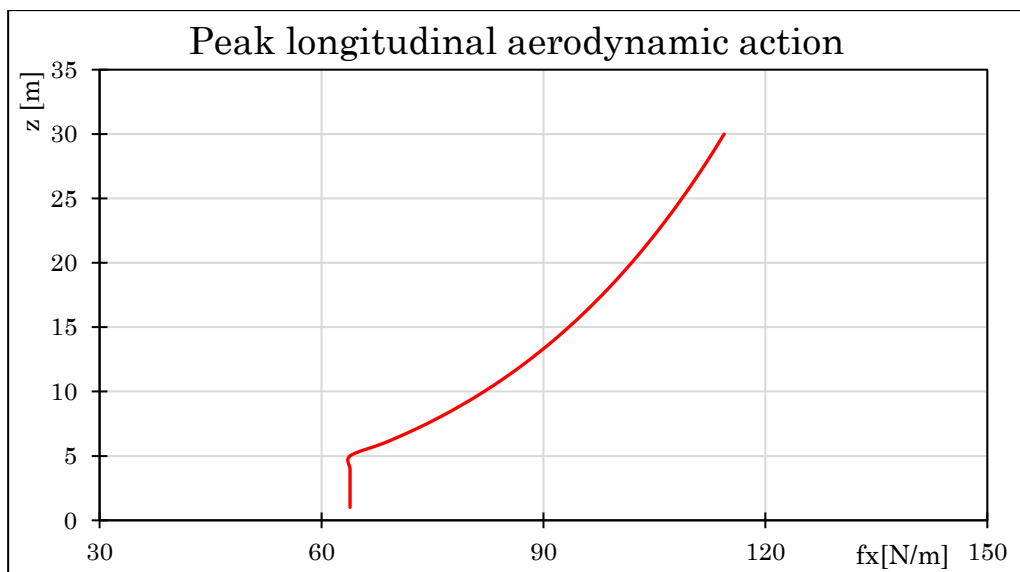


Figure 95. Peak longitudinal aerodynamic actions.

<i>Entity</i>	<i>Symbol</i>	<i>Value</i>	<i>Unit</i>
Altitude above s.l	a_s	129	m
Base wind velocity above s.l	$v_{b,0}$	25	m/s
Zoning parameter (1)	a_0	1000	m
Zoning parameter (2)	k_s	0,4	-
Reference base wind velocity	v_b	25	m/s
Return period	T_R	10	y
Return coefficient	c_r	0,903	-
Reference wind velocity	v_r	22,58	m/s
Roughness Class	-	C	-
Exposure Site Category	-	III	-
Exposure parameter (1)	k_r	0,2	-
Exposure parameter (2)	z_0	0,1	m
Exposure parameter (3)	z_{min}	5	m
Topographic coefficient	c_t	1	-
Air density	ρ_{air}	1,25	kg/m ³
Air viscosity	μ_{air}	$15 \cdot 10^{-6}$	m ² /s
Characteristic element size	l	165	mm
Steel roughness	k	0,2	mm
Total structure height	L	30	m
Slenderness	λ	168,75	-
Slenderness coefficient	ψ_λ	0,9886	-
Average wind profile coefficient	$c_m(z \leq z_{min})$	0,7824	-
Average wind velocity	$v_m(z \leq z_{min})$	17,67	m/s
Reynolds number	$Re(z \leq z_{min})$	$1.94 \cdot 10^5$	-
Force coefficient	$c_{fx,0}(z \leq z_{min})$	0.7212	-
Corrected force coefficient	$c_{fx}(z \leq z_{min})$	0.7113	-
Peak longitudinal aerodynamic action	$f_x(z \leq z_{min})$	68.45	N/m
Average wind profile coefficient	$c_m(z = L)$	141	-
Average wind velocity	$v_m(z = L)$	26	m/s
Reynolds number	$Re(z = L)$	$2,83 \cdot 10^5$	-
Force coefficient	$c_{fx,0}(z = L)$	0.7613	-
Corrected force coefficient	$c_{fx}(z = L)$	0.7510	-
Peak longitudinal aerodynamic action	$f_x(z = L)$	114.43	N/m

Table 10. Main quantities calculated for this case study.

Equivalent longitudinal static actions (*D*, or ‘drag’) are defined as the equivalent static actions in the wind direction. They take the form:

$$\begin{aligned} & \text{Equivalent longitudinal static actions} \\ & = \text{Peak longitudinal aerodynamic actions} \cdot c_{dD} \end{aligned}$$

where peak aerodynamic actions are defined as the longitudinal force per unit length on one-dimensional elements. The longitudinal dynamic coefficient c_{dD}

is a dimensionless quantity that modifies the peak aero-dynamic actions, taking into account the partial correlation of wind actions and the resonant amplification of the structure. Generally $c_{dD} > 1$ for flexible, slender e poorly damped structures.

The longitudinal dynamic coefficient c_{dD} is provided by the relations:

$$c_{dD} = \frac{G_D}{1 + 7 \cdot I_v(z_e)}$$

$$G_D = 1 + 2 \cdot g_D \cdot I_v(z_e) \cdot \sqrt{B_D^2 R_D^2}$$

where:

- G_D is the longitudinal gust factor;
- z_e is the reference height
- $I_v(z_e)$ is the turbulence intensity calculated at height $z = z_e$;
- g_D is the longitudinal peak factor, defined as the ratio of the maximum value of the fluctuating part of the response to its standard deviation;
- B_D is the quasi-static response factor, which takes into account the imperfect correlation of the pressure acting on the structure;
- R_D is the resonant response factor, which takes into account the resonance between the turbo-slow excitation and the first vibration mode of the structure.

The quasi-static response factor B_D is provided by the relation

$$B_D^2 = \frac{1}{1 + 0.9 \cdot \left(\frac{b+h}{L_v(z_e)}\right)^{0.63}}$$

where:

- b is the width of the structure;
- h is the height of the structure;
- $L_v(z_e)$ is the integral scale of turbulence calculated at height $z = z_e$.

It is conservative to assume $B_D = 1$.

The resonant response factor R_D is given by the relations:

$$R_D^2 = \frac{\pi}{4\xi_D} \cdot S_D \cdot R_h \cdot R_b$$

$$S_D = \frac{6.868 \cdot n_D \cdot L_v(z_e)/v_m(z_e)}{[1 + 10.302 \cdot n_D \cdot L_v(z_e)/v_m(z_e)]^{5/3}}$$

$$R_h = \begin{cases} 1 & \text{for } \eta_h = 0 \\ \frac{1}{\eta_h} - \frac{1}{2 \cdot \eta_h^2} (1 - e^{-2\eta_h}) & \text{for } \eta_h > 0 \end{cases}$$

$$R_b = \begin{cases} 1 & \text{for } \eta_b = 0 \\ \frac{1}{\eta_b} - \frac{1}{2 \cdot \eta_b^2} (1 - e^{-2\eta_b}) & \text{for } \eta_b > 0 \end{cases}$$

$$\eta_h = 4 \cdot \frac{n_D \cdot h}{v_m(z_e)}, \quad \eta_b = 4 \cdot \frac{n_D \cdot b}{v_m(z_e)}$$

where:

- ξ_D is the damping ratio relative to the critical for the first vibration mode of the structure in the wind direction;
- n_D is the frequency of the first vibration mode in the wind direction (
- $v_m(z_e)$ is the average wind speed, calculated at height $z = z_e$;
- $L_v(z_e)$ is the turbulence integral scale, calculated at height $z = z_e$;
- S_D is a dimensionless parameter that takes into account the spectral content of the longitudinal turbulence;
- R_h e R_b are two dimensionless parameters that account for the partial coherence (i.e., lack of correlation) of the longitudinal turbulence

The peak factor in the longitudinal direction is provided by the relations:

$$g_D = \sqrt{2 \cdot \ln(v_D \cdot T)} + \frac{0.8772}{\sqrt{2 \cdot \ln(v_D \cdot T)}} \geq 3$$

$$v_D = n_D \cdot \sqrt{\frac{R_D^2}{B_D^2 + R_D^2}} \geq 0.08 \text{ Hz}$$

where:

- v_D is the expected frequency of the longitudinal response;
- T is the time interval over which the average wind speed is evaluated, $T = 600 \text{ s}$.

Equivalent longitudinal static actions evaluation D (drag)			
<i>Entity</i>	<i>Symbol</i>	<i>Value</i>	<i>Unit</i>
Turbulence intensity	$I_v(z_e = 15m)$	0,1996	-
Turbulence integral scale	L_v	72,18	-
Structural damping	ξ_s	0,0060	-
1 st vibration mode frequency	n_D	1,7100	Hz
Equivalent mass	$m_{e,D}$	80,00	kg/m
Aerodynamic damping ratio	ξ_a	0,0020	-
Aerodynamic damping	ξ_d	0,0080	-
Quasi-static resonant response factor	B_D^2	0,6581	-
Spectral longitudinal turbulence parameter (1)	S_D	0,0441	-
	η_h	9.0690	-
	η_b	0,0499	-
Longitudinal turbulence parameter (1)	R_h	0,1042	-
Longitudinal turbulence parameter (2)	R_b	0,9676	-
Resonant response factor	R_D^2	0,4365	-
Expected frequency longitudinal response	v_D	1.0798	Hz
Longitudinal peak factor	g_D	3.7587	-
Longitudinal gust factor	G_D	2.5696	-
Longitudinal dynamic coefficient	$c_{d,D}$	1.0720	-

Table 11. Evaluation of the longitudinal dynamic coefficient for the case study.

Equivalent transverse static force per unit length is given by the relation:

$$f_{dL} = q_p(z) \cdot c_D \cdot b \cdot c_{dL}$$

where:

- $q_p(z)$ is the peak kinetic pressure evaluated at height z ;
- c_D is the aerodynamic drag coefficient;
- b is the reference transverse dimension of the section;
- c_{dL} is the transverse dynamic coefficient, provided by the relations:

$$G_L = |\mu_L| + 2 \cdot g_L \cdot I_v(z_e) \cdot \sqrt{B_L^2 + R_L^2}$$

where:

- G_L is the transverse gust factor;
- μ_L is the static response factor in the transverse direction;
- $I_v(z_e)$ is the turbulence intensity evaluated at the equivalent height z_e , equal to $0.6L$, assuming the vertical model proposed by CNR2018, which also specifies $\Phi=0^\circ$ and $h=0$;

- B_L is the quasi-static response factor in the transverse direction; it takes into account the partial correlation of the actions acting on the structure along its axis;
- R_L is the resonant response factor in the transverse direction; it takes into account the resonance between the turbulent excitation and the first mode of vibration of the structure in the transverse direction;
- g_L is the peak factor in the transverse direction, defined as the ratio between the maximum value of the fluctuating part of the response and its standard deviation. It is given by the relation:

$$g_L = \sqrt{2 \cdot \ln(v_L \cdot T)} + \frac{0.5772}{\sqrt{2 \cdot \ln(v_L \cdot T)}} \geq 3 \quad \text{per } \mu_L = 0$$

$$g_L = \sqrt{2 \cdot \ln(v_L \cdot T)} + \frac{0.5772}{\sqrt{2 \cdot \ln(v_L \cdot T)}} \geq 3 \quad \text{per } \mu_L \neq 0$$

where:

- v_L is the expected frequency of the transverse response. It is given by the relation:

$$v_L = n_L \cdot \sqrt{\frac{R_L^2}{B_L^2 + R_L^2}} \geq 0.08 \text{ Hz}$$

where n_L is the frequency of the first transverse vibration mode.

Static, quasi-static, and resonant response factors are provided by the relations:

$$\mu_L = \frac{c_L}{c_D}$$

$$B_L^2 = \left(\frac{c_L}{c_D}\right)^2 \cdot B_{L1}^2 + \left(\frac{c_D + c'_L}{c_D}\right)^2 \cdot B_{L2}^2$$

$$B_L^2 = \frac{\pi}{4 \cdot \xi_L} \cdot \left[\left(\frac{c_L}{c_D}\right)^2 \cdot S_{L1} \cdot R_{L1} + \left(\frac{c_D + c'_L}{c_D}\right)^2 \cdot S_{L2} \cdot R_{L2} \right]$$

where:

- c_L is the lift coefficient (paragraph O.5);
- c'_L is the first derivative of the lift coefficient (paragraph O.5); L_c
- ξ_L is the damping ratio relative to the critical for the first transverse vibration mode ;

Moreover:

$$B_{L1}^2 = \frac{1}{1 + 1.280 \cdot \left(\frac{k_L \cdot l}{L_v(z_e)}\right)^{0.63}}$$

$$B_{L2} = \frac{0.141 \cdot \cos^2 \Phi}{1 + 1.913 \cdot \left(\frac{k_L \cdot l}{L_v(z_e)}\right)^{0.63}} + \frac{0.0625 \cdot \sin^2 \Phi}{1 + 3.407 \cdot \left(\frac{k_L \cdot l}{L_v(z_e)}\right)^{0.63}}$$

$$S_{L1} = \frac{6.868 \cdot n_L \cdot L_v(z_e)/v_m(z_e)}{[1 + 10.302 \cdot n_L \cdot L_v(z_e)/v_m(z_e)]^{5/3}}$$

$$S_{L2} = \frac{0.332 \cdot n_L \cdot L_v(z_e)/v_m(z_e) \cdot \cos^2 \Phi}{[1 + 3.544 \cdot n_L \cdot L_v(z_e)/v_m(z_e)]^{5/3}} + \frac{0.0588 \cdot n_L \cdot L_v(z_e)/v_m(z_e) \cdot \sin^2 \Phi}{[1 + 1.411 \cdot n_L \cdot L_v(z_e)/v_m(z_e)]^{5/3}}$$

$$R_{L1} = \begin{cases} 1 & \text{for } \eta_{L1} = 0 \\ \frac{1}{\eta_{L1}} - \frac{1}{2 \cdot \eta_{L1}^2} (1 - e^{-2\eta_{L1}}) & \text{for } \eta_{L1} > 0 \end{cases}$$

$$R_{L2} = \begin{cases} 1 & \text{for } \eta_{L2} = 0 \\ \frac{1}{\eta_{L2}} - \frac{1}{2 \cdot \eta_{L2}^2} (1 - e^{-2\eta_{L2}}) & \text{for } \eta_{L2} > 0 \end{cases}$$

$$\eta_{L1} = 10 \cdot \frac{k_L \cdot n_L \cdot l}{v_m(z_e)}, \quad \eta_{L2} = 6.5 \cdot \frac{k_L \cdot n_L \cdot l}{v_m(z_e)}$$

where:

- B_{L1} , B_{L2} are dimensionless parameters that take into account the effects of the partial correlation of the lateral and vertical turbulence with respect to the quasi-static part of the response;
- S_{L1} , S_{L2} are dimensionless parameters that account for the spectral content of the lateral and vertical turbulence;
- R_{L1} , R_{L2} are dimensionless parameters taking into account the effects of the partial correlation of the lateral and vertical turbulence on the resonant part of the response.

Equivalent transverse static actions evaluation L (lift)			
Entity	Symbol	Value	Unit
Turbulence intensity	$I_v(z_e = 0.6 \cdot L)$	0,1926	-
Turbulence integral scale	L_v	79.79	-
	η_{L1}	0.0600	-
	η_{L2}	0.0390	-
Transverse turbulence parameter (1)	R_{L1}	0.9612	-
Transverse turbulence parameter (2)	R_{L2}	0.9745	-
Transverse turbulence parameter (3)	B_{L1}^2	0.9835	-
Transverse turbulence parameter (4)	B_{L2}^2	0.1375	-
Spectral transverse turbulence parameter (1)	S_{L1}	0.2124	-
Spectral transverse turbulence parameter (2)	S_{L2}	0.0232	-
Resonant response factor	R_L^2	2.2783	-
Quasi-static resonant response factor	B_L^2	0.1414	-
Expected frequency transverse response	v_L	1.6593	Hz
Transverse peak factor	g_L	4.0459	-
Transverse gust factor	G_L	2.4239	-
Transverse dynamic coefficient	$c_{d,L}$	1.0323	-

Table 12. Evaluation of the transverse dynamic coefficient for the case study.

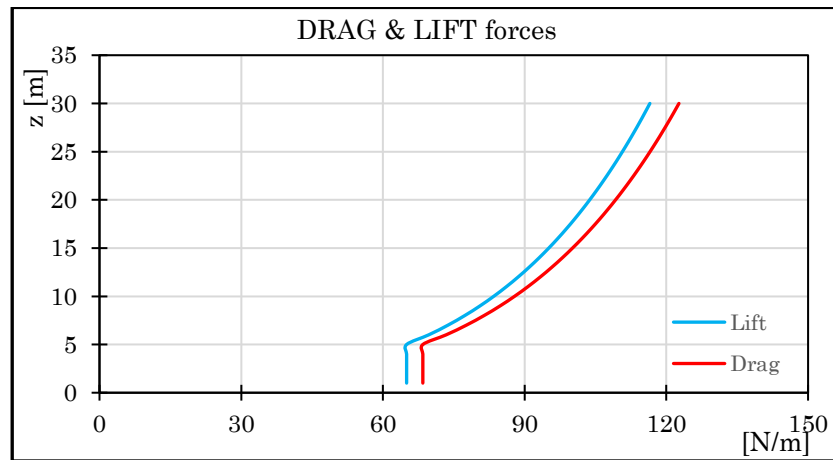


Figure 96. Drag and Lift forces

Transverse actions must be properly combined with longitudinal actions. It is recommended to apply three combination rules shown in Table 13. Combinations according to [36].

Combination	Longitudinal Action	Transverse Action
1	$0.7 \cdot f_{Dm}(z) + 0.3 \cdot f_D$	f_L
2	$0.2 \cdot f_{Dm}(z) + 0.8 \cdot f_D$	$0.2 \cdot \mu_L \cdot f_{Dm}(z) + 0.8 \cdot f_L$
3	f_D	$0.7 \cdot \mu_L \cdot f_{Dm}(z) + 0.3 \cdot f_L$

Table 13. Combinations according to [36].

f_D and f_{Dm} are the *equivalent static resisting force* per unit length in the longitudinal direction and the average value of the resisting force per unit length in the longitudinal direction, respectively. They are given by the relations:

$$f_D(z) = q_p(z) \cdot c_D \cdot b \cdot c_{dD}$$

$$f_{Dm}(z) = \frac{q_p(z)}{1 + 7 \cdot I_v(z_e)} \cdot c_D \cdot b$$

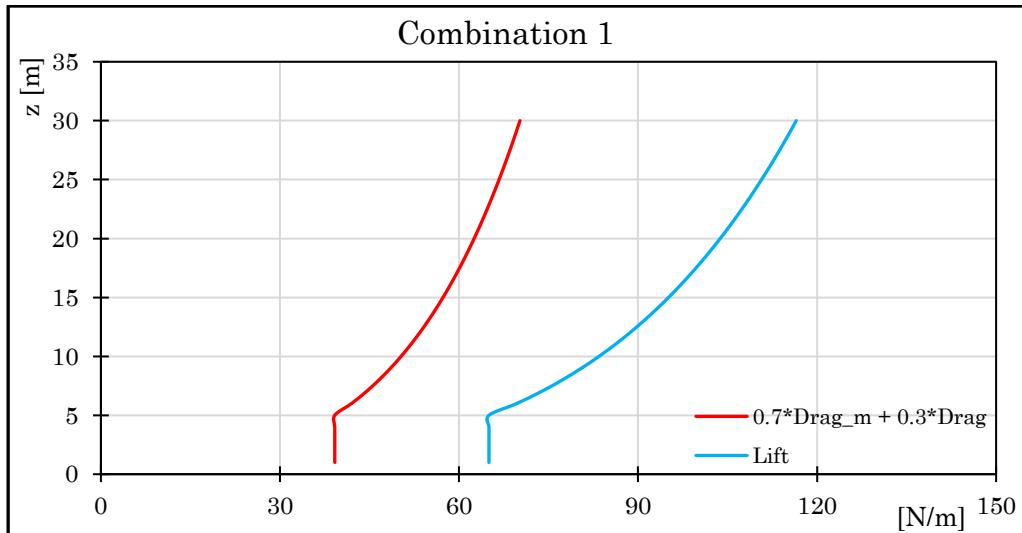


Figure 97. Drag and Lift forces. Combo 1.

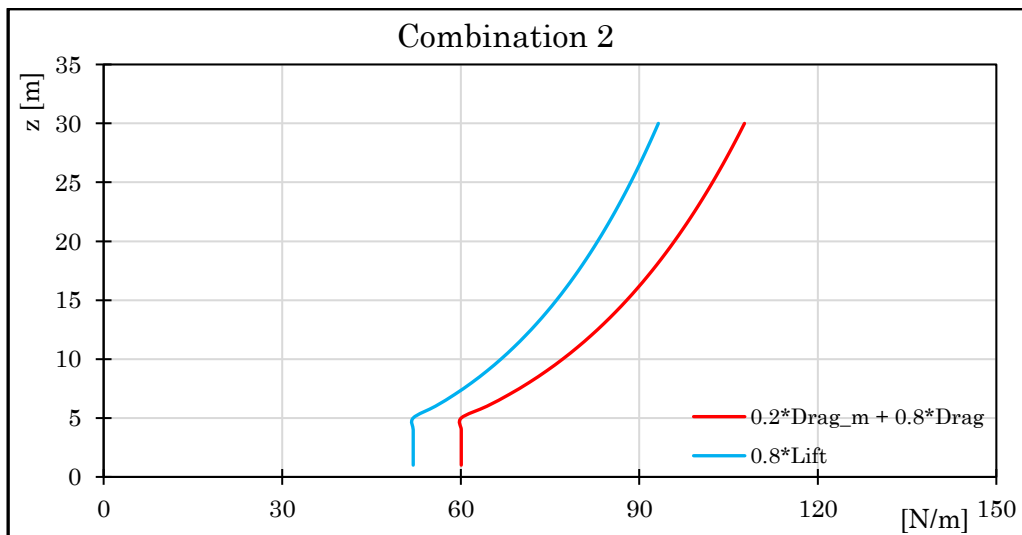


Figure 98. Drag and Lift forces. Combo 2.

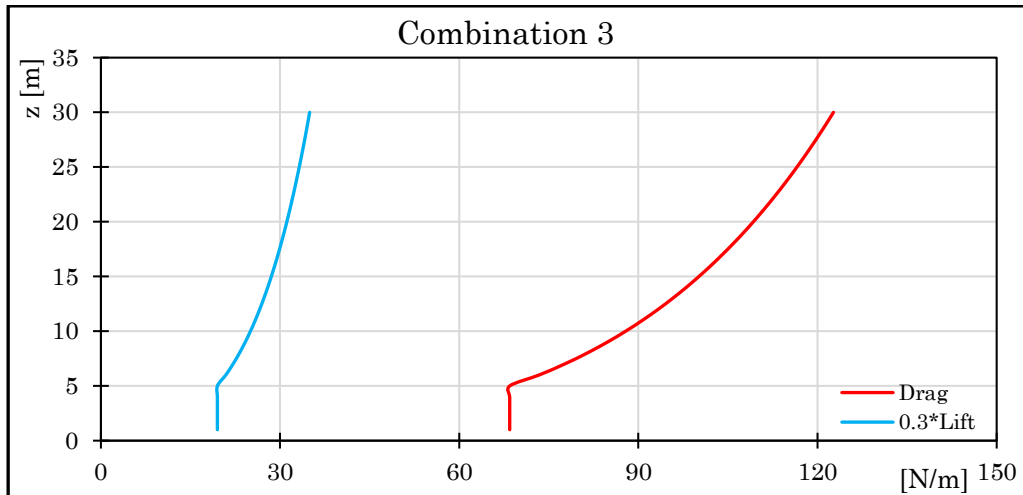


Figure 99. Drag and Lift forces. Combo 3.

For what concern antennas and parabolas, any *quality certificate* provide the exact force coefficients, but they provide the wind load evaluated for 150 km/h. This simplification is much conservative, and it is assumed in the structural model by applying concentrated forces at the centre of the antennas.

Wind action on equipment					
Typology	Model	n°	elevation [m]	frontal wind load [daN]	lateral wind load [daN]
Antenna	AOC4518R7v06	3	29.25	44.5	26.5
Antenna	6888670N	3	26.00	79.49	36.09

Table 14. Equipment

Given this conservative aspect, the wind is acting along one direction hitting frontally one antenna, and the other two laterally.

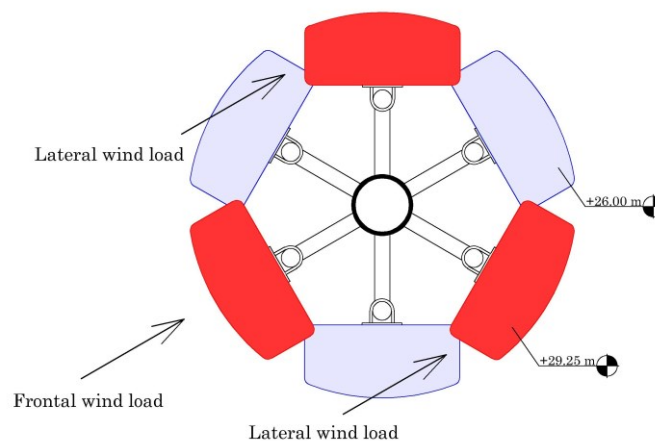


Figure 100. Wind action on electronic equipment.

5.2.3.2 Maintenance load

According to §3.3.4-NTC2018 Tab.3.1.II, we refer to “Category H, accessible roofs for repair and maintenance only”. It is supposed a typical situation of inspection or maintenance performed by an operator which work along the steel ladder. A concentrated load of 120 kg is applied at the top of the tower. Despite that, it is reasonable believed that the operator could work by using a basket elevator, without loading the structure.

Category	Typology	Q_k [kN]
H	accessible roofs for repair and maintenance	1.20

Table 15. Maintenance Load.

5.2.3.3 Ice Load

In slender and lighter structures, the presence of *ice* and snow attached to structural surface may cause dangerous situations. In particular, the radio mast is very sensitive to changes in wind surface exposed: the new ice layer can increase the volume and the surface of the single component than twice due to the thin thickness of the main pole. §G.9.6-CNR-DT-2018 provides several scenarios which explain how Ice may covers the structural members, as indicated in Figure 101.

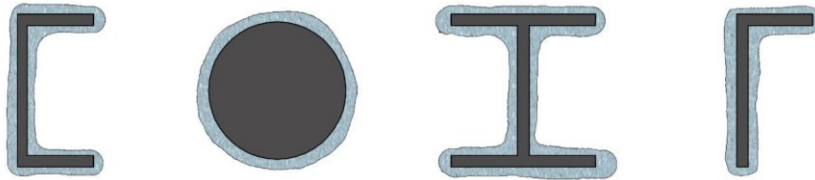


Figure 101. Example of ice formation on different shape section [36].

In absence of more detailed evaluations, it is usual to suppose ice sleeves formation of 12.5 mm.

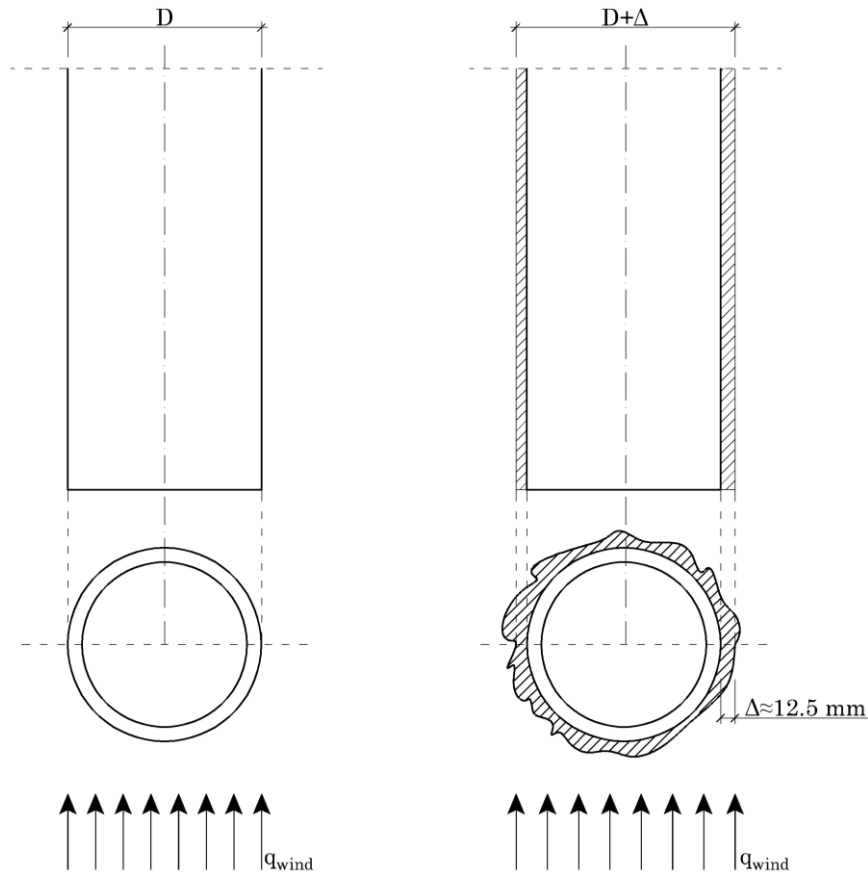


Figure 102. Influence of ice formation.

Once wind actions have been evaluated according to chapter Wind load 5.2.3.1, the influence of ice sleeve-formation on the structure is taken into consideration by considering an additional exposed surface equal to 15% of the original one.

Element [mm]	Exposed wind area A_w [m^2/m]	Ice area exposed to wind A_{ice} [m^2/m]	(A_w / A_{ice}) [-]	Wind pressure due to ice_sleeve formation q_{ice} [kN/m]
D168.3	0.1683	0.025	$0.148 \cong 0.15$	$0.15 \cdot q_w$

Table 16. Computation of wind action on ice-sleeves.

5.2.4 Seismic action

Seismic action is evaluated according to §5.1.3.12 and §3.2-NTC2018. In particular a modal analysis with response spectrum is conducted. Specifically, seismic actions are analysed as acting independently in X, Y directions. Then, an envelope of the actions was provided as follow:

$$\begin{aligned} E_1 &= \pm 1.00 \cdot E_x \pm 0.30 \cdot E_y \\ E_2 &= \pm 0.30 \cdot E_x \pm 1.00 \cdot E_y \end{aligned}$$

Due to the geometrical symmetry of the structure, the effect of two combinations investigated must provide the same result.

5.2.4.1 Geotechnical information of the site

For the evaluation of site-dependent parameters, we refer to the location of the structure, that is Bassano Del Grappa (VI).

Following assumptions are done:

- Nominal Life: 10 years;
- Class of use: II ($C_U=0.5$);
- Topography category T1;
- Soil category B;

The design life is $V_R = 35 \text{ years}$

Structural analysis will be performed according to the Life Safety Limit State SLV, in which there is a level of probability of 10% to exceed it in the reference period V_R .

5.2.4.2 Design Response Spectrum

According to 3.2.3.5 D.M. 17/01/2018, for ULS the design spectrum can be obtained by replacing $1/q$ to η in elastic spectrum formulations, where q it the structure factor defined at chapter 7 of NTC2018.

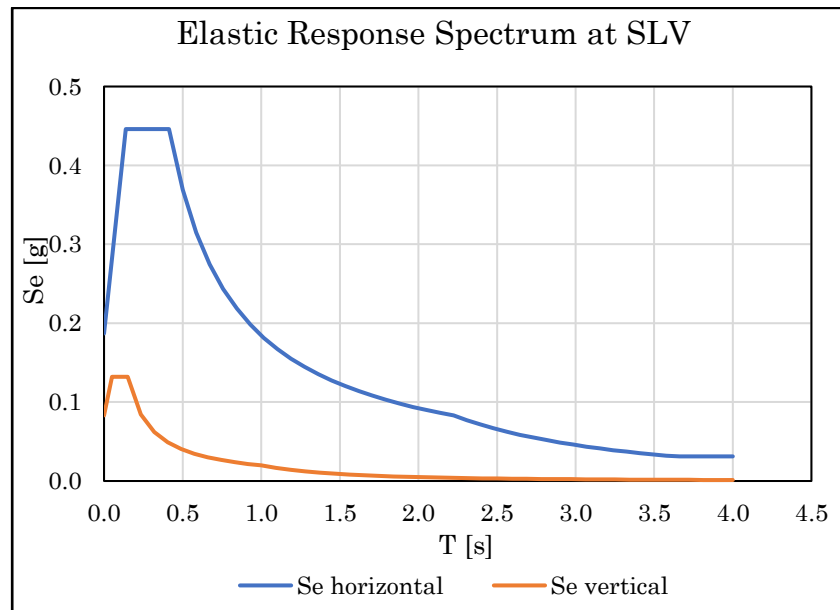


Figure 103. Elastic Response Spectrum Acceleration at SLV

5.2.4.3 Vibration Modes

Deformed shapes with significant participant mass are reported in the following figures:

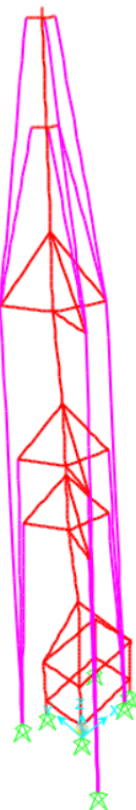


Figure 104. Mode 10 - $T_s = 0.437s$ - Mass Participant $X = 9.6\%$ $Y = 26.2\%$

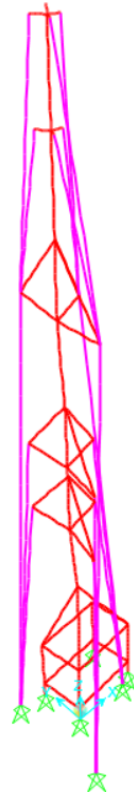


Figure 105. Mode 11 - $T_s = 0.434s$ - Mass Participant $X = 26.4\%$ $Y = 9.2\%$

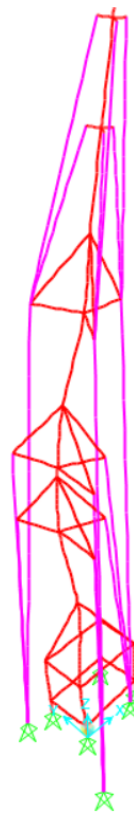


Figure 106. Mode 12 - $T_s = 0.206s$ - Mass Participant $X = 7.2\%$ $Y = 4.4\%$

5.2.5 Combinations of actions

The combinations of loads are performed with respect the Italian Standards NCT2018. It has been chosen the *fundamental combination* for *ULS*, the *characteristic combination* for *SLS*, and a *seismic combination* typically used for both *ULS* and *SLS*.

$$\gamma_{G1} \cdot G_1 + \gamma_{G2} \cdot G_2 + \gamma_P \cdot P + \gamma_{Q1} \cdot Q_{k1} + \gamma_{Q1} \cdot \psi_{02} \cdot Q_{k2} + \dots \quad \text{ULS fundamental}$$

$$G_1 + G_2 + P + Q_{k1} + \psi_{02} \cdot Q_{k2} + \psi_{03} \cdot Q_{k3} + \dots \quad \text{SLS characteristic}$$

$$E + G_1 + G_2 + P + \psi_{21} \cdot Q_{k01} + \psi_{22} \cdot Q_{k2} + \dots \quad \text{Seismic combination}$$

It is quite reasonable believed that wind action is the main one, and probably there would not be significant results by considering the maintenance load as main action and the wind as secondary one. In the same way, permanent loads set as favourable actions ($\gamma_{G1} = 1, \gamma_{G2} = 0.8$) do not produce the most critical configuration because the main problem is related to buckling. In particular the pole is subjected to axial force, due to G and wind, bending moments M_x, M_y , due to wind action mainly, and torsion. Overall, each section is checked by biaxial bending verification. Wind action is considered as the principal one because it causes tensile forces at guyes, and consequently, reactive forces are totally concentrated at the pole as compressive stresses. In addition, horizontal distributed forces along the structure produce bending moments in both directions (x,y). Being the pole thin, and extremely slender, flexural instability occurs in many parts of that. Each combination must be repeated three times in order to take into account the three combinations of wind evaluated previously and explained in Table 13. Combination coefficients and partial factor are taken from §2.5.3-NTC2018 Tab.2.5.I, Tab.2.6.I.

Category - Variable action	$\psi_{0,j}$	$\psi_{1,j}$	$\psi_{2,j}$
H-accessible roofs for repair and maintenance	0.0	0.0	0.0
Wind	0.6	0.2	0.0
Snow ($\leq 1000 \text{ m a. s. l}$)	0.5	0.2	0.0

Table 17. Combination coefficients.

Load type		Coefficient γ_F	EQU	A1	A2
G_1	Favorable	γ_{G1}	0.9	1.0	1.0
	Unfavorable		1.41	1.3	1.0
G_2	Favorable	γ_{G2}	0.8	0.8	0.8
	Unfavorable		1.5	1.5	1.3
Q	Favorable	γ_{Qi}	0.0	0.0	0.0
	Unfavorable		1.5	1.5	1.3

Table 18. Partial factor for the actions at ULS

Combinations of actions	
ULS Max_1	$1.3 \cdot G_1 + 1.5 \cdot G_2 + 1.5 \cdot Wind_1 + 1.5 \cdot 0.5 \cdot Wind_{Ice_1} + 1.5 \cdot 0 \cdot Maintenance$
ULS Max2_1	$1.3 \cdot G_1 + 1.5 \cdot G_2 + 1.5 \cdot Maintenance + 1.5 \cdot 0.6 \cdot Wind_1 + 1.5 \cdot 0.2 \cdot Wind_{Ice_1}$
ULS Min_1	$1 \cdot G_1 + 0.8 \cdot G_2 + 1.5 \cdot Wind_1 + 1.5 \cdot 0.5 \cdot Wind_{Ice_1} + 1.5 \cdot 0 \cdot Maintenance$
SLS Char_1	$1 \cdot G_1 + 1 \cdot G_2 + Wind_1 + 0.5 \cdot Wind_{Ice_1} + 0 \cdot Maintenance$
Quake_1	$E + G_1 + G_2 + 0 \cdot Wind_1 + 0 \cdot Wind_{Ice_1} + 0 \cdot Maintenance$
ULS Max_2	$1.3 \cdot G_1 + 1.5 \cdot G_2 + 1.5 \cdot Wind_2 + 1.5 \cdot 0.5 \cdot Wind_{Ice_2} + 1.5 \cdot 0 \cdot Maintenance$
ULS Max2_2	$1.3 \cdot G_1 + 1.5 \cdot G_2 + 1.5 \cdot Maintenance + 1.5 \cdot 0.6 \cdot Wind_2 + 1.5 \cdot 0.2 \cdot Wind_{Ice_2}$
ULS Min_2	$1 \cdot G_1 + 0.8 \cdot G_2 + 1.5 \cdot Wind_2 + 1.5 \cdot 0.5 \cdot Wind_{Ice_2} + 1.5 \cdot 0 \cdot Maintenance$
SLS Char_2	$1 \cdot G_1 + 1 \cdot G_2 + Wind_2 + 0.5 \cdot Wind_{Ice_2} + 0 \cdot Maintenance$
Quake_2	$E + G_1 + G_2 + 0 \cdot Wind_2 + 0 \cdot Wind_{Ice_2} + 0 \cdot Maintenance$
ULS Max_3	$1.3 \cdot G_1 + 1.5 \cdot G_2 + 1.5 \cdot Wind_3 + 1.5 \cdot 0.5 \cdot Wind_{Ice_3} + 1.5 \cdot 0 \cdot Maintenance$
ULS Max2_3	$1.3 \cdot G_1 + 1.5 \cdot G_2 + 1.5 \cdot Maintenance + 1.5 \cdot 0.6 \cdot Wind_3 + 1.5 \cdot 0.2 \cdot Wind_{Ice_3}$
ULS Min_3	$1 \cdot G_1 + 0.8 \cdot G_2 + 1.5 \cdot Wind_3 + 1.5 \cdot 0.5 \cdot Wind_{Ice_3} + 1.5 \cdot 0 \cdot Maintenance$
SLS Char_3	$1 \cdot G_1 + 1 \cdot G_2 + Wind_3 + 0.5 \cdot Wind_{Ice_3} + 0 \cdot Maintenance$
Quake_3	$E + G_1 + G_2 + 0 \cdot Wind_3 + 0 \cdot Wind_{Ice_3} + 0 \cdot Maintenance$

Table 19. Combinations of actions.

5.2.6 Verification Criteria

SAP2000® performs checking of structural members according to *Italian Standards NTC2018*.

First of all, it evaluates the section compactness, if Class I,II,III,IV. In our case all the elements are in *Class I* (ductile section) and they are able to exhibit completely plastic behaviour. Then, the *section compression capacity* $N_{c,Rd}$, the *section shear capacity* $V_{c,y,Rd}$, the *section bending capacity* $M_{c,Rd}$ are evaluated:

$$N_{c,Rd} = N_{pl,Rd} = \frac{A \cdot f_y}{\gamma_{M0}}$$

$$V_{c,Rd} = \frac{f_y \cdot A_v}{\gamma_{M0} \cdot \sqrt{3}}$$

$$M_{c,Rd} = \frac{W_{pl} \cdot f_y}{\gamma_{M0}}$$

Other specific verifications are done in case of shear action is so relevant that may cause a reduction in terms of bending performance. Therefore, for specific details i suggest consulting the specifications of *CSi Computers & Structure Inc*.

For what concern buckling resistance, *member compression* and *member bending capacities* are evaluated as follows:

$$N_{b,Rd} = \frac{\chi \cdot A \cdot f_y}{\gamma_{M1}}$$

$$M_{b,Rd} = \frac{\chi_{LT} \cdot W_{pl} \cdot f_y}{\gamma_{M1}}$$

When compression and bending are present, interaction capacity is computed as follows, according to *formula NTC 4.2.39*:

$$\frac{D}{C} = \left[\frac{M_{y,Ed}}{M_{N,y,Rd}} \right]^2 + \left[\frac{M_{z,Ed}}{M_{N,z,Rd}} \right]^{5n} \leq 1$$

SAP2000® uses also the so called “*Method B*” according to *Annex B Eurocode 3*, in which a couple of non-dimensional assessments are proposed:

$$\frac{D}{C} = \frac{N_{Ed}}{\frac{\chi_y \cdot A \cdot f_{yk}}{\gamma_{M1}}} + k_{yy} \frac{M_{y,Ed}}{\chi_{LT} \frac{W_{pl,y} \cdot f_{yk}}{\gamma_{M1}}} + k_{yz} \frac{M_{z,Ed}}{\frac{W_{pl,z} \cdot f_{yk}}{\gamma_{M1}}} \leq 1$$

$$\frac{D}{C} = \frac{N_{Ed}}{\frac{\chi_z \cdot A \cdot f_{yk}}{\gamma_{M1}}} + k_{zy} \frac{M_{y,Ed}}{\chi_{LT} \frac{W_{pl,y} \cdot f_{yk}}{\gamma_{M1}}} + k_{zz} \frac{M_{z,Ed}}{\frac{W_{pl,z} \cdot f_{yk}}{\gamma_{M1}}} \leq 1$$

A	Cross-section area	$[mm^2]$
A_v	Cross-section shear area	$[mm^2]$
W_{pl}	Plastic Section Modulus	$[mm^3]$
f_y	Yielding strength	$[MPa]$
γ_{M0}	Partial factor	$[-]$
γ_{M1}	Partial factor for buckling	$[-]$
χ	Reduction factor for flexural instability	$[-]$
χ_{LT}	Reduction factor for lateral instability	$[-]$
k	Interaction factors	$[-]$
$N_{c,Rd}=N_{pl,Rd}$	Compression Capacity	$[N]$
N_{Ed}	Acting Axial Load	$[N]$
$V_{c,Rd}$	Acting Shear	$[N]$
V_{Ed}	Acting Bending Moment	$[N]$
M_{Ed}	Shear Capacity	$[N]$
$M_{c,Rd}$	Compression Capacity	$[N]$
$N_{b,Rd}$	Flexural Buckling Resistance	$[N]$
$M_{b,Rd}$	Torsional-Flexural Buckling Resistance	$[N]$

Table 20. Input parameters for verifications.

5.3 Structural Analysis

5.3.1 Modelling solution

The structural model has been implemented by using two different types of elements: beams and cables. Beam elements (also called *'frame'*) take into account geometric and material properties and return 6 static quantities (axial force (F_x), torsion (M_x), 2 bending moments (M_y , M_z)), 2 shear forces (F_y , F_z) and 6 DOF (u_x , u_y , u_z , r_x , r_y , r_z). They are used to model the main pole and secondary elements. Moreover, except for the main pole, rotation releases are applied at the ends in order to consider no flexural rigidity, as for trussed structures.

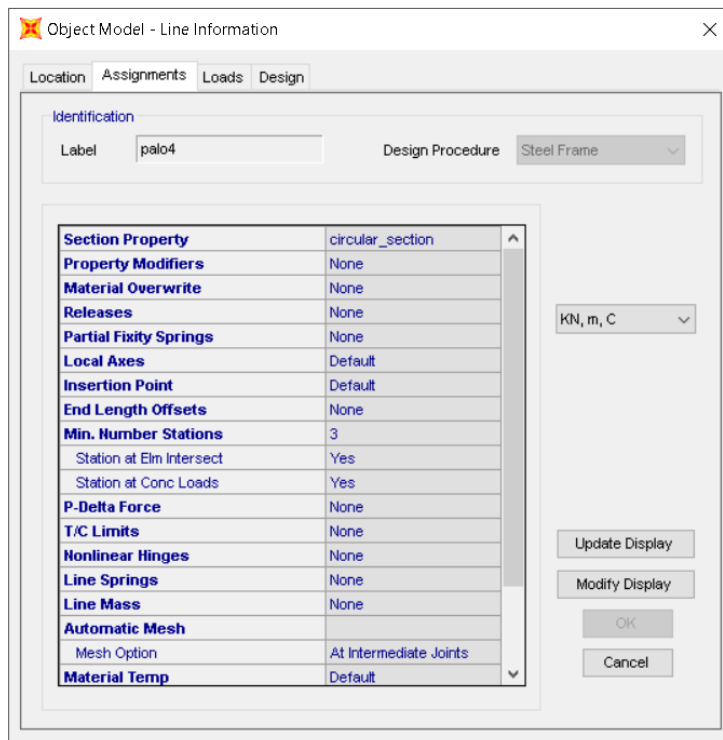


Figure 107. Example of beam element in SAP2000.

Cable elements are used to simulate steel ropes, and SAP2000 permits to model them by acting on the tension applied to one end, or controlling the geometry in the deformed or not-deformed configuration.

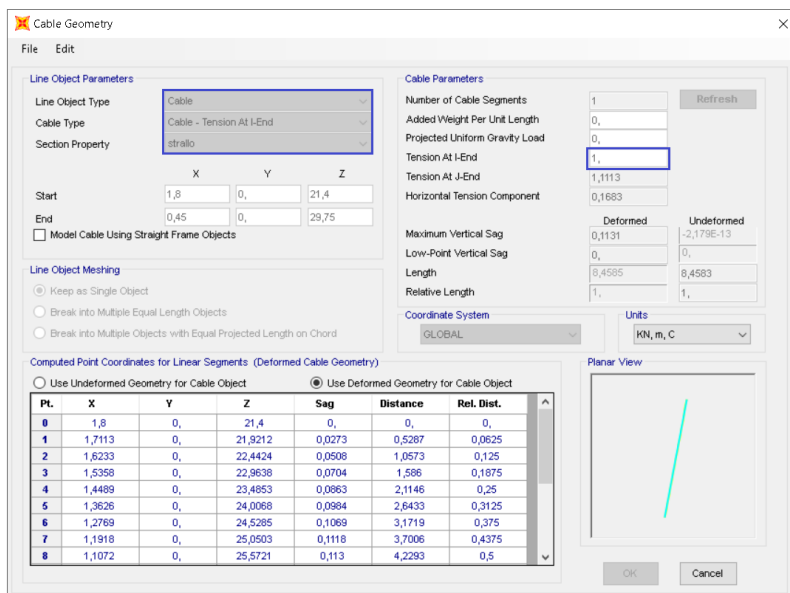


Figure 108. Example of cable modelling in SAP2000.

Cables are subjected to large displacements that give rise to geometric nonlinearities, which is one of the reasons why is mandatory to perform a non-linear analysis. The structural behaviour of guyed towers is very complicated, especially for low pre-tensioning forces at the cables, which exhibit larger displacements. At the contrary, by increasing the pre-tension, the nonlinearities becomes less obvious, resulting in high compression levels and probability of buckling on the mast [35].

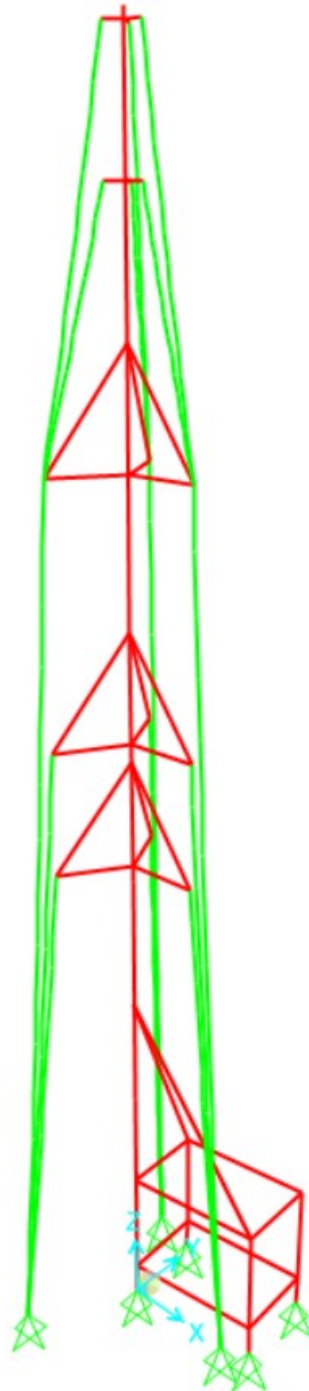


Figure 109. 3D model in SAP2000.

5.3.2 G2 loads

Non-structural permanent loads G2		
ITEM	q_k [kN/m]	Q_k [kN]
Steel ladder, other	0.30	-
Antenna	-	1.53
Antenna	-	1.19
Parabolas	-	0.52

Table 21. G2 loads.

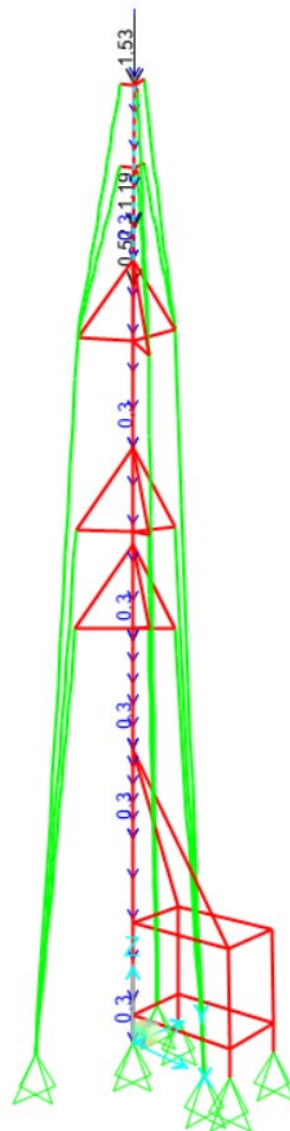


Figure 110. G2 loads.

5.3.3 Maintenance load

Category	Typology	Q_k [kN]
H	accessible roofs for repair and maintenance	1.20

Table 22. Maintenance load.

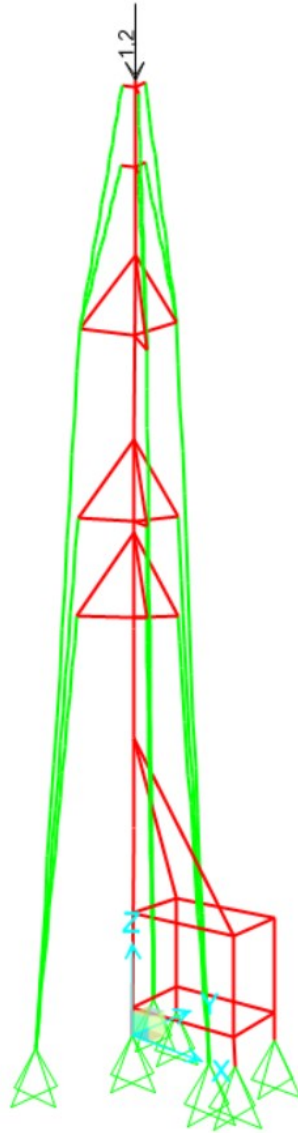


Figure 111. Maintenance load.

5.3.4 Wind action

As widely discussed in previous chapter, wind action has been evaluated according to CNR-DT 207 R1/2018. Just to summarize, Italian Standards consider three different combinations, as showed in Table 13. *Drag D* and *Lift L* forces are reported in

Table 23.

Wind action (<i>Drag D</i> , <i>Lift L</i>) at ULS						
z	Drag_1	Lift_1	Drag_2	Lift_2	Drag_2	Lift_3
[m]	[kg/m]	[kg/m]	[kg/m]	[kg/m]	[kg/m]	[kg/m]
1	3.92	6.50	6.01	5.20	6.85	1.95
2	3.92	6.50	6.01	5.20	6.85	1.95
3	3.92	6.50	6.01	5.20	6.85	1.95
4	3.92	6.50	6.01	5.20	6.85	1.95
5	3.92	6.50	6.01	5.20	6.85	1.95
6	4.20	6.97	6.44	5.58	7.34	2.09
7	4.44	7.37	6.81	5.90	7.76	2.21
8	4.66	7.73	7.15	6.19	8.14	2.32
9	4.85	8.05	7.44	6.44	8.48	2.42
10	5.03	8.35	7.71	6.68	8.79	2.50
11	5.19	8.61	7.96	6.89	9.07	2.58
12	5.34	8.86	8.19	7.09	9.33	2.66
13	5.48	9.09	8.40	7.27	9.57	2.73
14	5.61	9.31	8.60	7.45	9.80	2.79
15	5.73	9.51	8.79	7.61	10.01	2.85
16	5.85	9.70	8.97	7.76	10.22	2.91
17	5.96	9.88	9.13	7.91	10.41	2.97
18	6.06	10.06	9.29	8.04	10.59	3.02
19	6.16	10.22	9.45	8.18	10.76	3.07
20	6.25	10.38	9.59	8.30	10.92	3.11
21	6.34	10.53	9.73	8.42	11.08	3.16
22	6.43	10.67	9.86	8.54	11.23	3.20
23	6.51	10.81	9.99	8.65	11.38	3.24
24	6.59	10.94	10.11	8.75	11.52	3.28
25	6.67	11.07	10.23	8.86	11.66	3.32
26	6.75	11.19	10.35	8.96	11.79	3.36
27	6.82	11.31	10.46	9.05	11.91	3.39
28	6.89	11.43	10.56	9.14	12.03	3.43
29	6.96	11.54	10.67	9.23	12.15	3.46
30	7.02	11.65	10.77	9.32	12.27	3.50

Table 23. Drag and Lift forces according to[36] at ULS.

Wind action (<i>Drag D, Lift L</i>) at SLS						
z	Drag_1	Lift_1	Drag_2	Lift_2	Drag_2	Lift_3
[m]	[kg/m]	[kg/m]	[kg/m]	[kg/m]	[kg/m]	[kg/m]
1	2.29	3.81	3.52	3.05	4.01	1.14
2	2.29	3.81	3.52	3.05	4.01	1.14
3	2.29	3.81	3.52	3.05	4.01	1.14
4	2.29	3.81	3.52	3.05	4.01	1.14
5	2.29	3.81	3.52	3.05	4.01	1.14
6	2.31	3.84	3.54	3.07	4.04	1.15
7	2.32	3.86	3.57	3.09	4.06	1.16
8	2.34	3.88	3.58	3.10	4.08	1.16
9	2.34	3.89	3.60	3.11	4.10	1.17
10	2.35	3.90	3.61	3.12	4.11	1.17
11	2.36	3.92	3.62	3.13	4.12	1.17
12	2.37	3.93	3.63	3.14	4.13	1.18
13	2.37	3.94	3.64	3.15	4.14	1.18
14	2.38	3.94	3.64	3.15	4.15	1.18
15	2.38	3.95	3.65	3.16	4.16	1.19
16	2.39	3.96	3.66	3.17	4.17	1.19
17	2.39	3.96	3.66	3.17	4.17	1.19
18	2.39	3.97	3.67	3.18	4.18	1.19
19	2.40	3.98	3.67	3.18	4.19	1.19
20	2.40	3.98	3.68	3.19	4.19	1.19
21	2.40	3.99	3.68	3.19	4.20	1.20
22	2.40	3.99	3.69	3.19	4.20	1.20
23	2.41	4.00	3.69	3.20	4.21	1.20
24	2.41	4.00	3.70	3.20	4.21	1.20
25	2.41	4.00	3.70	3.20	4.21	1.20
26	2.41	4.01	3.70	3.21	4.22	1.20
27	2.42	4.01	3.71	3.21	4.22	1.20
28	2.42	4.01	3.71	3.21	4.23	1.20
29	2.42	4.02	3.71	3.21	4.23	1.21
30	2.42	4.02	3.72	3.22	4.23	1.21

Table 24. Drag and Lift forces according to [36] at SLS.

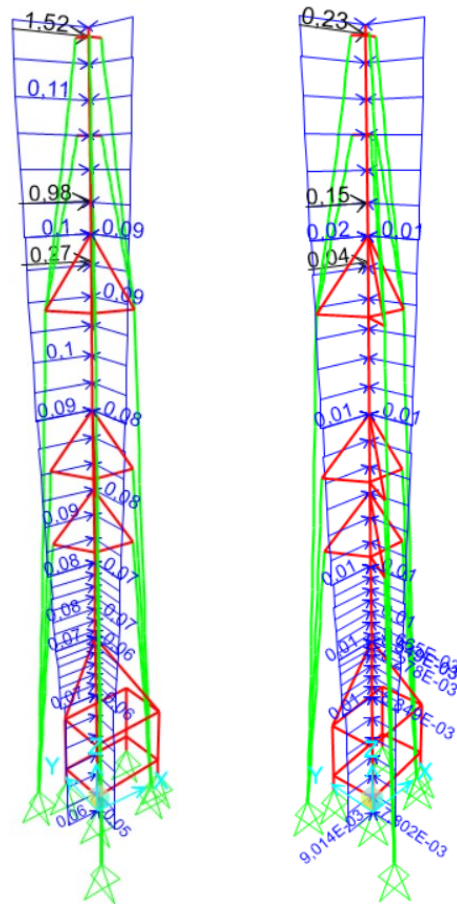


Figure 112. On the left, the distribution of wind load, on the right, the distribution of wind action due to presence of ice sleeves at ULS.

5.3.5 Results

After launching the analysis it is possible to collect all the results. In particular, we are interested to the *ENVELOPE Combination*, that is the configuration that combines all the load cases and returns maximum and minimum values.

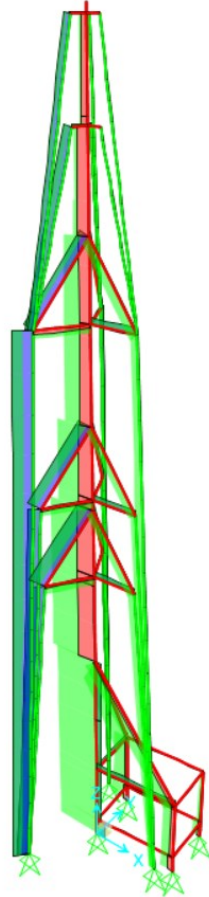


Figure 113. Axial forces diagram.

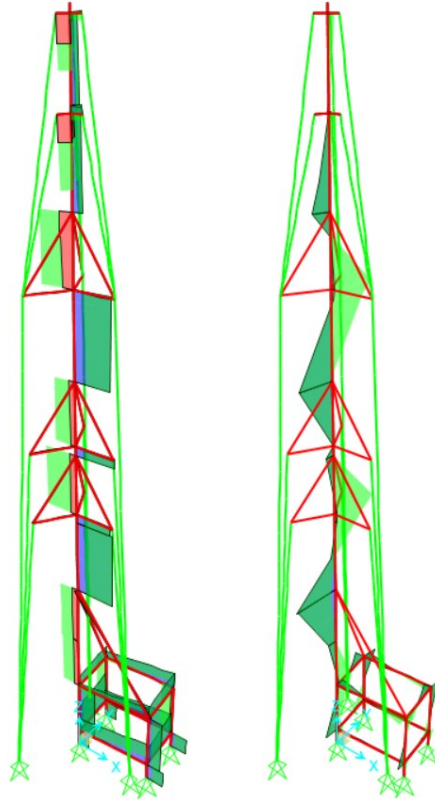


Figure 114. On the left the shear force V_2 , On the right the bending moment M_2 .

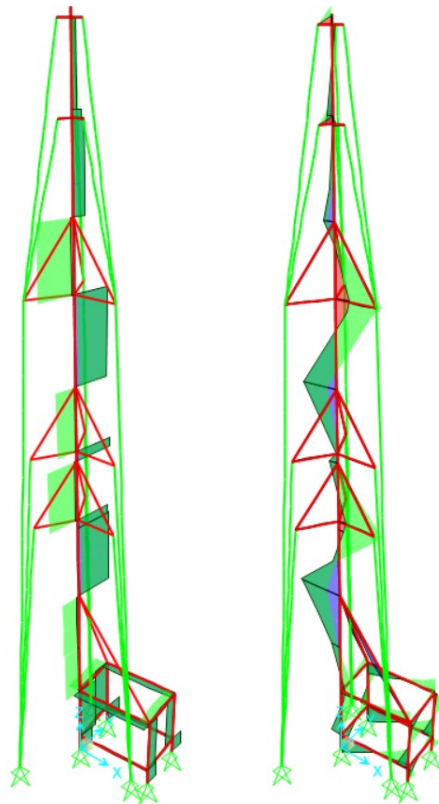


Figure 115. On the left the shear force V_3 , On the right the bending moment M_3 .

ENVELOPE: Element Forces - Frames									
Frame	Station	Combo	Step	P	V2	V3	T	M2	M3
Text	[m]	Text	Text	[kN]	[kN]	[kN]	[kNm]	[kNm]	[kNm]
pole1	0	ENV	Max	19.28	2.58	3.72	0.00	0.00	0.00
pole1	0.8	ENV	Max	20.01	2.58	3.72	0.00	-0.07	-0.08
pole1	0.8	ENV	Max	8.80	5.54	6.12	0.08	6.77	5.59
pole1	3	ENV	Max	10.81	5.54	6.12	0.08	-0.52	-0.79
pole1	3.5	ENV	Max	11.26	5.54	6.12	0.08	-0.71	-1.07
pole1	3.5	ENV	Max	8.04	-0.76	-0.44	0.11	-0.93	-1.48
pole1	6	ENV	Max	10.32	-0.86	-0.52	0.11	3.79	3.74
pole1	0	ENV	Min	-93.96	0.11	0.10	0.00	0.00	0.00
pole1	0.8	ENV	Min	-93.11	0.08	0.07	0.00	-2.98	-2.07
pole1	0.8	ENV	Min	-94.53	0.66	0.45	-0.04	0.39	0.56
pole1	3	ENV	Min	-92.20	0.57	0.38	-0.04	-6.70	-6.59
pole1	3.5	ENV	Min	-91.67	0.55	0.36	-0.04	-9.76	-9.36
pole1	3.5	ENV	Min	-90.99	-4.93	-4.76	-0.02	-8.10	-8.58
pole1	6	ENV	Min	-88.33	-4.93	-4.76	-0.02	0.28	0.53
pole2a	0	ENV	Max	10.32	-0.86	-0.52	0.11	3.79	3.74
pole2a	1.35	ENV	Max	11.55	-0.91	-0.57	0.11	10.83	11.02
pole2a	2.7	ENV	Max	12.78	-0.96	-0.61	0.11	17.88	18.30
pole2a	0	ENV	Min	-88.33	-5.39	-5.22	-0.02	0.28	0.53
pole2a	1.35	ENV	Min	-86.90	-5.39	-5.22	-0.02	1.02	1.72
pole2a	2.7	ENV	Min	-85.46	-5.39	-5.22	-0.02	1.81	2.98
pole2b	0	ENV	Max	-38.39	10.21	10.20	0.01	18.68	18.69
pole2b	1.65	ENV	Max	-36.88	10.21	10.20	0.01	1.84	2.31
pole 2b	3.3	ENV	Max	-35.37	10.21	10.20	0.01	-1.23	-2.21
pole 2b	0	ENV	Min	-100.48	1.65	1.00	0.00	1.88	3.03
pole 2b	1.65	ENV	Min	-98.73	1.59	0.94	0.00	0.28	0.35
pole 2b	3.3	ENV	Min	-96.97	1.52	0.89	0.00	-14.99	-14.99
pole 3	0	ENV	Max	-35.37	9.55	9.55	0.01	-1.23	-2.21
pole 3	0.4	ENV	Max	-35.01	9.55	9.55	0.01	-1.58	-2.82
pole3	0.4	ENV	Max	-34.85	-1.29	-0.71	0.01	-1.58	-2.82
pole3	3	ENV	Max	-32.48	-1.40	-0.80	0.01	3.49	3.47
pole3	3	ENV	Max	-29.73	10.42	10.42	0.01	3.49	3.47
pole3	3.4	ENV	Max	-29.36	10.42	10.42	0.01	-0.03	0.01
pole3	3.4	ENV	Max	-29.21	-1.13	-0.63	0.01	-0.03	0.01
pole3	6	ENV	Max	-26.84	-1.23	-0.72	0.01	13.85	14.05
pole3	0	ENV	Min	-96.97	1.52	0.89	0.00	-14.99	-14.99
pole3	0.4	ENV	Min	-96.55	1.51	0.87	0.00	-18.81	-18.81
pole3	0.4	ENV	Min	-96.40	-8.57	-8.58	0.00	-18.81	-18.81
pole3	3	ENV	Min	-93.63	-8.57	-8.58	0.00	0.38	0.68
Pole3	3	ENV	Min	-73.69	1.83	1.02	0.00	0.38	0.68
pole3	3.4	ENV	Min	-73.26	1.81	1.01	0.00	-0.67	-0.70
pole3	3.4	ENV	Min	-73.11	-5.67	-5.59	0.00	-0.67	-0.70

pole3	6	ENV	Min	-70.35	-5.67	-5.59	0.00	1.74	3.03
pole4	0	ENV	Max	-23.92	9.26	9.24	0.01	13.85	14.05
pole4	3	ENV	Max	-21.18	9.26	9.24	0.01	-1.45	-2.96
pole4	3.4	ENV	Max	-20.82	9.26	9.24	0.01	-1.85	-3.73
pole4	3.4	ENV	Max	-20.66	-1.85	-1.00	0.01	-1.85	-3.73
pole4	5.16	ENV	Max	-19.06	-1.92	-1.06	0.01	0.53	-0.42
pole4	5.16	ENV	Max	-18.54	-2.20	-1.06	0.01	0.53	-0.42
pole4	6	ENV	Max	-17.77	-2.23	-1.09	0.01	6.93	4.17
pole4	0	ENV	Min	-50.73	2.06	1.11	0.00	1.74	3.03
pole4	3	ENV	Min	-47.55	1.94	1.01	0.00	-13.88	-13.72
pole4	3.4	ENV	Min	-47.12	1.92	1.00	0.00	-17.57	-17.42
pole4	3.4	ENV	Min	-46.97	-8.30	-9.42	0.00	-17.57	-17.42
pole4	5.16	ENV	Min	-45.10	-8.30	-9.42	0.00	-0.99	-2.80
pole4	6	ENV	Min	-44.32	-8.30	-9.42	0.00	-0.99	-2.80
pole5	0	ENV	Max	-43.43	-8.30	-9.42	0.00	0.87	0.65
pole5	1.02	ENV	Max	-14.77	2.67	2.97	0.01	6.93	4.17
pole5	1.02	ENV	Max	-13.84	2.50	2.97	0.01	3.90	1.87
pole5	3	ENV	Max	-12.65	2.25	2.97	0.01	3.90	1.87
pole5	3	ENV	Max	-10.84	2.25	2.97	0.01	0.49	-0.25
pole5	3.25	ENV	Max	-7.66	2.49	2.25	0.00	2.15	1.90
pole5	3.25	ENV	Max	-7.44	2.49	2.25	0.00	1.78	1.28
pole5	5.75	ENV	Max	-7.44	1.38	1.46	0.00	1.78	1.28
pole5	5.75	ENV	Max	-5.15	1.38	1.15	0.00	-1.02	-0.08
pole5	5.76	ENV	Max	-1.76	0.11	1.61	0.00	0.03	0.03
pole5	5.76	ENV	Max	-1.75	0.11	1.61	0.00	0.03	0.03
pole5	6	ENV	Max	-0.22	0.11	0.11	0.00	0.03	0.03
pole5	0	ENV	Min	0.00	0.11	0.11	0.00	0.00	0.00
pole5	1.02	ENV	Min	-34.32	1.70	0.35	0.00	0.87	0.65
pole5	1.02	ENV	Min	-33.39	1.66	0.31	0.00	0.54	-1.99
pole5	3	ENV	Min	-32.20	0.03	0.31	0.00	0.54	-1.99
pole5	3	ENV	Min	-30.40	-0.28	0.24	0.00	-1.97	-2.59
pole5	3.25	ENV	Min	-13.68	0.09	0.78	0.00	0.65	-0.81
pole5	5.75	ENV	Min	-13.45	0.08	0.77	0.00	0.09	-0.86
pole5	5.75	ENV	Min	-13.45	0.08	0.77	0.00	0.09	-0.86
pole5	6	ENV	Min	-11.17	-0.24	0.68	0.00	-2.78	-2.18

Table 25. Static quantities at Envelope Combination.

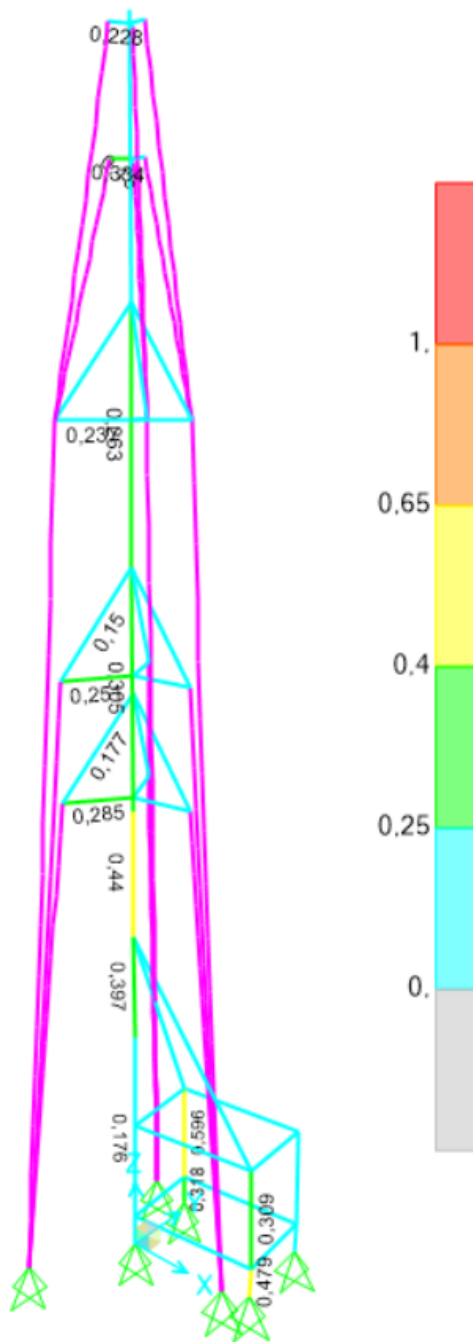


Figure 116. Performance Ratios.

ENVELOPE: Steel Design - Summary Data - Italian NTC 2018				
Frame	DesignSect	Combo	Ratio	Ratio
Text	Text	Text	[-]	[%]
pole1	D168,3x12,5	ENVELOPE	0.1758	17.6
pole2a	D168,3x12,5	ENVELOPE	0.3979	39.8
pole2b	D168,3x12,5	ENVELOPE	0.4413	44.1
pole 3	D168,3x12,5	ENVELOPE	0.3054	30.5
pole 4	D168,3x12,5	ENVELOPE	0.2635	26.4
pole 5	D168,3x12,5	ENVELOPE	0.0952	9.5
conn_oriz1_1	60x40x3	ENVELOPE	0.0558	5.6
conn_diag1_1	60x40x3	ENVELOPE	0.0141	1.4
conn_oriz1_2	60x40x3	ENVELOPE	0.2849	28.5
conn_diag1_2	60x40x3	ENVELOPE	0.1775	17.7
conn_oriz1_3	60x40x3	ENVELOPE	0.0649	6.5
conn_diag1_3	60x40x3	ENVELOPE	0.0376	3.8
conn_oriz2_1	60x40x3	ENVELOPE	0.0483	4.8
conn_diag2_1	60x40x3	ENVELOPE	0.0141	1.4
conn_oriz2_2	60x40x3	ENVELOPE	0.2507	25.1
conn_diag2_2	60x40x3	ENVELOPE	0.1503	15.0
conn_oriz2_3	60x40x3	ENVELOPE	0.0666	6.7
conn_diag2_3	60x40x3	ENVELOPE	0.0377	3.8
conn_oriz3_1	60x40x3	ENVELOPE	0.0581	5.8
conn_diag3_1	60x40x3	ENVELOPE	0.0141	1.4
conn_oriz3_2	60x40x3	ENVELOPE	0.2369	23.7
conn_diag3_2	60x40x3	ENVELOPE	0.0966	9.7
conn_oriz3_3	60x40x3	ENVELOPE	0.0761	7.6
conn_diag3_3	60x40x3	ENVELOPE	0.0396	4.0
conn_oriz4_1	150-60x40x3	ENVELOPE	0.0277	2.8
conn_oriz4_2	150-60x40x3	ENVELOPE	0.3343	33.4
conn_oriz4_3	150-60x40x3	ENVELOPE	0.1499	15.0
conn_oriz5_1	150-60x40x3	ENVELOPE	0.0282	2.8
conn_oriz5_2	150-60x40x3	ENVELOPE	0.2284	22.8
conn_oriz5_3	150-60x40x3	ENVELOPE	0.0345	3.5
conn_oriz_shelter1_1	150x150x12,5	ENVELOPE	0.0499	5.0
diag_shelter1_1	D168,3x12,5	ENVELOPE	0.0716	7.2
conn_oriz_shelter1_2	150x150x12,5	ENVELOPE	0.0481	4.8
diag_shelter1_2	D168,3x12,5	ENVELOPE	0.0645	6.4
conn_oriz_shelter1_3	150x150x12,5	ENVELOPE	0.0390	3.9
conn_oriz_shelter1_4	150x150x12,5	ENVELOPE	0.0582	5.8
conn_oriz_shelter1_5	150x150x12,5	ENVELOPE	0.0555	5.5
conn_oriz_shelter1_6	150x150x12,5	ENVELOPE	0.0888	8.9
conn_oriz_shelter1_7	150x150x12,5	ENVELOPE	0.0824	8.2
conn_oriz_shelter1_8	150x150x12,5	ENVELOPE	0.0912	9.1
conn_vert_shelter1_1	150x150x12,5	ENVELOPE	0.3090	30.9

conn_vert_shelter1_2	150x150x12,5	ENVELOPE	0.0521	5.2
conn_vert_shelter1_3	150x150x12,5	ENVELOPE	0.5960	59.6

Table 26. Performance Ratios (Efficiency indexes) at Envelope Combination.

To evaluate the deformability of the structure, it has been used a combination in which wind load is applied with a constant velocity $v = 100$ km/h and exposure coefficient $c_e = 1.00$. For Serviceability Limit State SLS, Italian Standards impose deformability limits, as showed in

Table 27.

Structure Typology	Maximum horizontal displacement allowed
	$\frac{\Delta}{H}$
Industrial building	/
Other single-storey buildings	/
Multi-storey buildings	$1/500$

Table 27. Deformability limits for structures subjected to horizontal actions.

Where Δ is the horizontal displacement at the top, H is the height of the structure.

Deformability (U_x, U_y) at SLS						
Joint	Output case	Case Type	z	U_1	U_2	U_{TOT}
Text	Text	Text	[mm]	[mm]	[mm]	[mm]
1	CHAR_SLE_2	Combination	0	0.0	0.0	0.0
q	CHAR_SLE_2	Combination	0.8	0.2	0.1	0.2
7	CHAR_SLE_2	Combination	3.5	0.7	0.3	0.8
2	CHAR_SLE_2	Combination	6	0.1	-0.3	0.3
10	CHAR_SLE_2	Combination	8.7	0.5	-0.3	0.5
3	CHAR_SLE_2	Combination	12	5.2	2.4	5.7
11	CHAR_SLE_2	Combination	12.4	5.6	2.6	6.2
15	CHAR_SLE_2	Combination	15	6.6	3.2	7.3
16	CHAR_SLE_2	Combination	15.4	6.7	3.3	7.5
4	CHAR_SLE_2	Combination	18	8.2	4.1	9.2
20	CHAR_SLE_2	Combination	21.4	13.4	7.3	15.3
5	CHAR_SLE_2	Combination	24	13.9	8.1	16.1
24	CHAR_SLE_2	Combination	27	14.3	9.6	17.3
32	CHAR_SLE_2	Combination	27.25	14.4	9.8	17.4
28	CHAR_SLE_2	Combination	29.75	14.5	11.6	18.6
6	CHAR_SLE_2	Combination	30	14.5	11.7	18.7

Table 28. Displacements of the structure along the main pole. From base to top.

The maximum displacement is located at the top of the tower, in particular at joint 6 ($z = 30.00$ m), $U_{TOT} = 18.7$ mm

$$18.6 \text{ mm} \leq \frac{H}{500} = 60.0 \text{ mm} \text{ verification is satisfied}$$

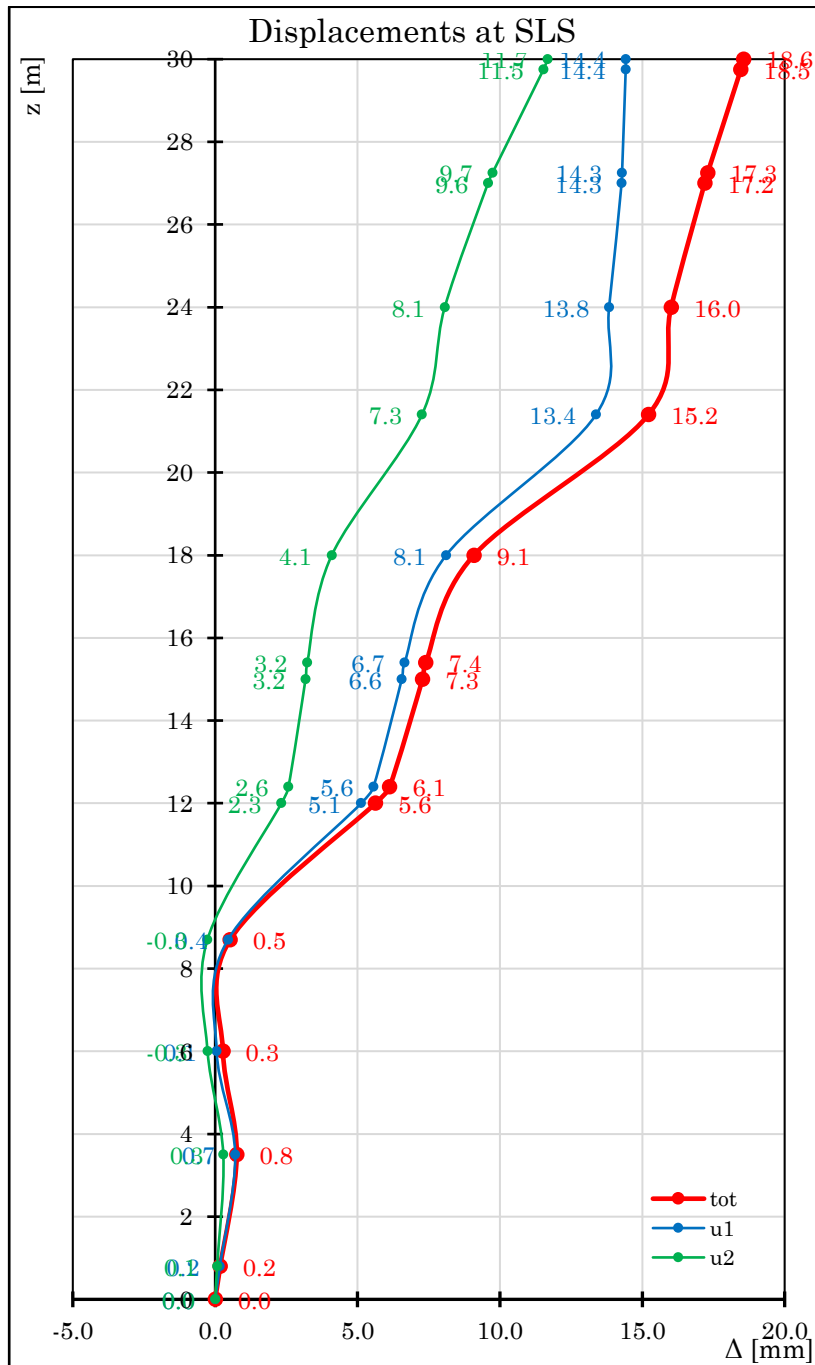


Figure 117. Displacements vs elevation at SLS.

6 How API operates

A brief discussion about managing SAP2000® using OAPI is proposed.

- You can choose to open SAP2000® using an existing instance, or to start a new one. In this phase is important to define the right version and installation path of the software. For our purposes, we prefer to perform the analysis with SAP2000® already launched to avoid multiple openings at each iteration. If *false* is selected, a new instance will be opened.

```
AttachToInstance = false(); %true()
SpecifyPath = true(); %false()
ProgramPath = 'C:\Program Files\Computers and Structures\SAP2000 21\SAP2000.exe';
APIDLLPath = 'C:\Program Files\Computers and Structures\SAP2000 21\SAP2000v1.dll';
ModelDirectory = 'C:\CSiAPIexample';
```

·
·
·

- SAP2000 can be opened, and a new model is initialized

```
%% start Sap2000 application
SapObject.ApplicationStart;
end
helper = 0;
SapModel = NET.explicitCast(SapObject.SapModel, 'SAP2000v1.cSapModel');
ret = SapModel.InitializeNewModel;
File = NET.explicitCast(SapModel.File, 'SAP2000v1.cFile');
ret = File.NewBlank;
```

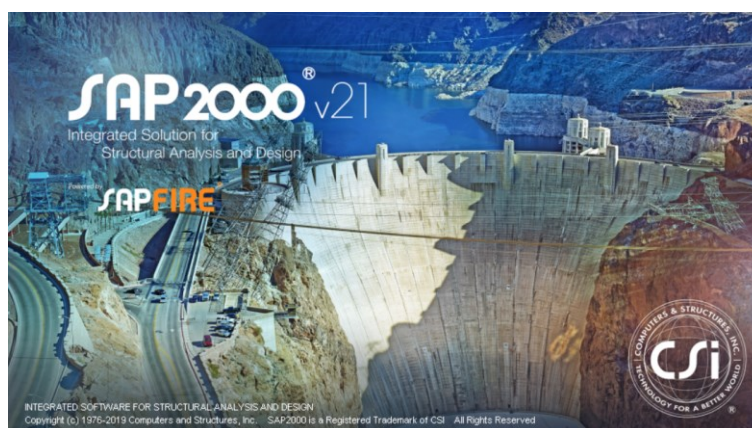


Figure 118. SAP2000 opening.

- Hide *Graphic Unit Interface*. This operation is established once we are ready to perform the optimization procedure and we need to repeat several times the algorithm. The computational speed represents a weakness point of the entire procedure. Therefore, we reduce the processing time by hiding the *GUI*, to let SAP2000® working in background mode.

```
%% mostra/nascondi GUI
%ret = SapObject.Unhide;
ret = SapObject.Hide;
```

- Once SAP2000 is open, material and section properties can be set. We can import them using libraries already present in SAP2000, or setting new ones.

```
%% define material property
PropMaterial = NET.explicitCast(SapModel.PropMaterial, 'SAP2000v1.cPropMaterial');
ret = PropMaterial.AddMaterial('S355', SAP2000v1.eMatType.Steel, 'Italy', 'NTC2008', 'S355')
```

```
%% define frame section property (diameter, thickness)
PropFrame = NET.explicitCast(SapModel.PropFrame, 'SAP2000v1.cPropFrame');
ret = PropFrame.SetPipe('circular_section', 'S355', 168.3, 12.5);
```

Figure 119. Define material properties in SAP2000.

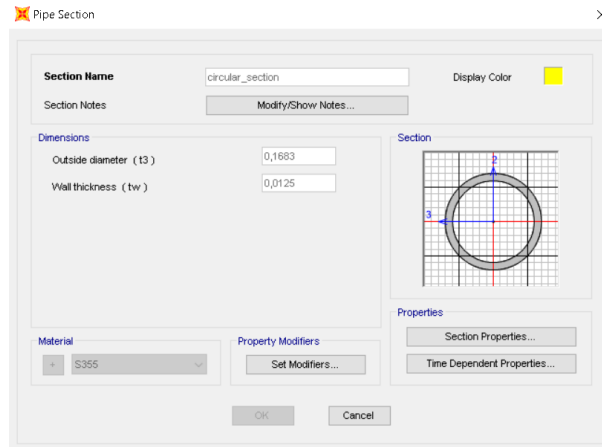


Figure 120. Define section properties in SAP2000.

- The model is created by adding points and joining them by elements.

%% add points (x,y,z,name,name)

PointObj = NET.explicitCast(SapModel.PointObj, 'SAP2000v1.cPointObj');

ret = PointObj.AddCartesian(-1.46, -2.53, 0, 'A', 'A');

.
.
.

%% join points by frame elements (pointname1,pointname2,section,frame,frame)

FrameObj = NET.explicitCast(SapModel.FrameObj, 'SAP2000v1.cFrameObj');

ret= FrameObj.AddByPoint('1', '2', 'circular_section', 'palo1', 'palo1');

.
.
.

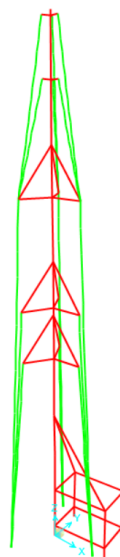


Figure 121. 3D model in SAP2000.

- Introduction of constraints. The displacements are collected in a vector of 6 components ($u_x, u_y, u_z, \Phi_x, \Phi_y, \Phi_z$). To set constraints, a Boolean System is used, where “true()” means to lock movements, “false()” means to allow movements. An example of hinge-support creation is proposed below.

```
PointObj = NET.explicitCast(SapModel.PointObj, 'SAP2000v1.cPointObj');
Restraint = NET.createArray('System.Boolean', 6);
for i = 1 : 3
    Restraint(i) = true();
end
for i = 4 : 6
    Restraint(i) = false();
end
ret = PointObj.SetRestraint('1', Restraint);
```

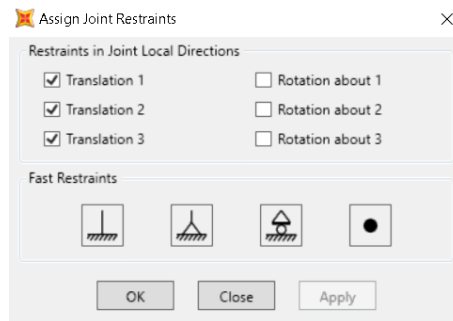


Figure 122. Define constraints in SAP2000.

- The creation of the model is completed. Load patterns, mass source, load combinations can be set.

%% add load patterns

```
LoadPatterns = NET.explicitCast(SapModel.LoadPatterns, 'SAP2000v1.cLoadPatterns');
ret = LoadPatterns.Add('DEAD', SAP2000v1.eLoadPatternType.Dead, 1, true());
```

- .
- .
- .

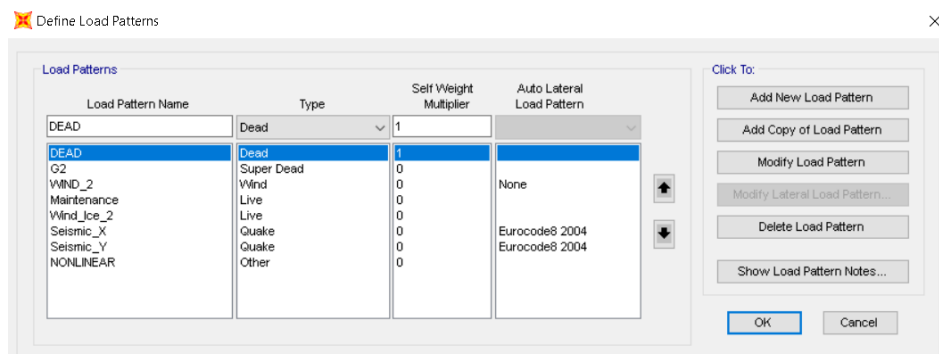


Figure 123. Define load patterns in SAP2000.

%define Seismic Combination with EUROCODE

```
AutoSeismic = NET.explicitCast(LoadPatterns.AutoSeismic, 'SAP2000v1.cAutoSeismic');
AutoSeismic.SetEurocode82004_1('Seismic_X', 1, 0.1, 2, 0.075, 0, false(), 0, 0, 1, 1, 2, 0.4, 1, 1,
1, 1, 0.2, 2, 1);
AutoSeismic.SetEurocode82004_1('Seismic_Y', 2, 0.1, 2, 0.075, 0, false(), 0, 0, 1, 1, 2, 0.4, 1, 1,
1, 1, 0.2, 2, 1);
```

%% define mass source

```
SourceMass = NET.explicitCast(SapModel.SourceMass, 'SAP2000v1.cMassSource');
LoadPat = {'DEAD'};
SF= [1];
SourceMass.SetMassSource('MSSSRC1', false(), true(), true(), true(), 1, LoadPat, SF);
```

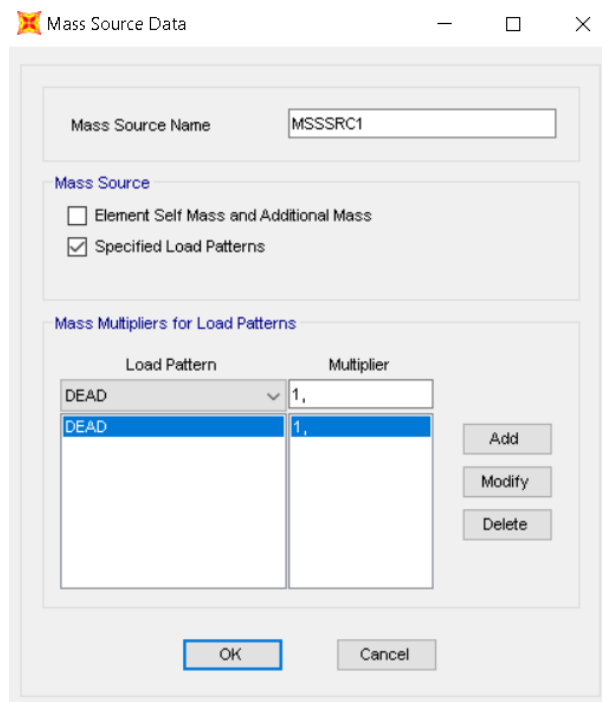


Figure 124. Define mass-source in SAP2000.

%% define NON-LINEAR CASES

```
LoadCases = NET.explicitCast(SapModel.LoadCases, 'SAP2000v1.cLoadCases');
StaticNonlinear =
NET.explicitCast(LoadCases.StaticNonlinear, 'SAP2000v1.cCaseStaticNonlinear');
StaticNonlinear.SetCase('NONLINEAR');
```

```
NumberLoads = 1;
LoadType = {'Load'};
LoadName = {'DEAD'};
SF = [1.3];
```

```
StaticNonlinear.SetLoads('NONLINEAR', 1, LoadType, LoadName, SF);
```

```
.
.
.
```

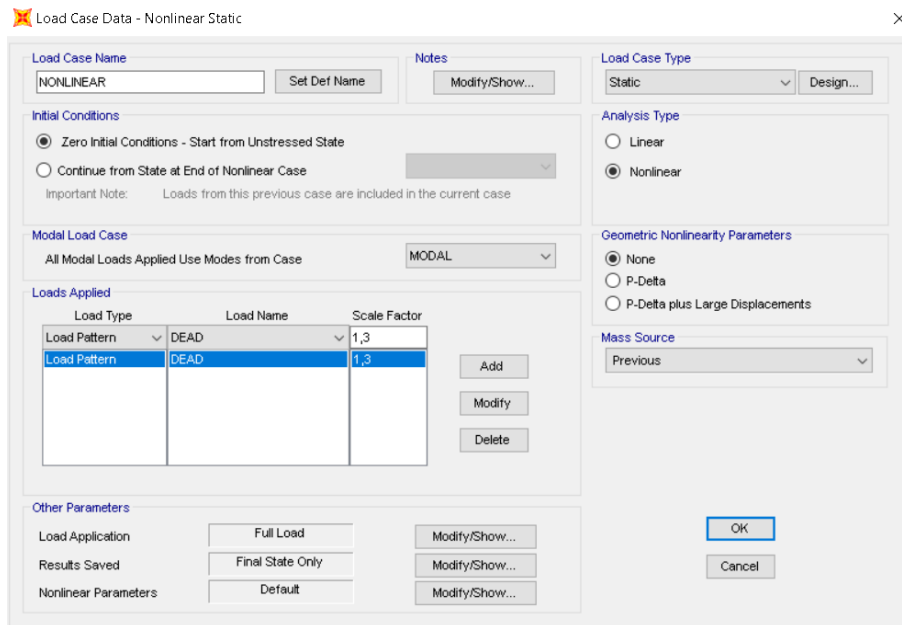


Figure 125. Set a non-linear case in SAP2000.

%% add load combinations

```
RespCombo = NET.explicitCast(SapModel.RespCombo, 'SAP2000v1.cCombo');
ret = RespCombo.Add('SLU_MAX_1', 0);
ret = RespCombo.Add('SLU_Min_1', 0);
ret = RespCombo.Add('CHAR_SLE_1', 0);
ret = RespCombo.Add('QUAKE_1', 0);
```

.
.
.

%% assing load patterns to load combinations

```
% ret = RespCombo.SetCaseList('SLU_MAX_1', SAP2000v1.eCNameType, 'DEAD', 1.3);
% ret = RespCombo.SetCaseList('SLU_MAX_1', SAP2000v1.eCNameType, 'G2', 1.5);
% ret = RespCombo.SetCaseList('SLU_MAX_1', SAP2000v1.eCNameType, 'WIND_1', 1.5);
% ret = RespCombo.SetCaseList('SLU_MAX_1', SAP2000v1.eCNameType, 'Maintenance', 0);
% ret = RespCombo.SetCaseList('SLU_MAX_1', SAP2000v1.eCNameType, 'Wind_Ice_1', 0.75);
% ret = RespCombo.SetCaseList('SLU_MAX_1', SAP2000v1.eCNameType, 'TARGET', 1);
```

.
.
.

Load Combination Data

Load Combination Name (User-Generated)

Notes

Load Combination Type

Options

Define Combination of Load Case Results

Load Case Name	Load Case Type	Scale Factor
G2	Linear Static	1,5
WIND_2	Nonlinear Static	1,5
Maintenance	Linear Static	0,
Wind_Ice_2	Linear Static	0,75
NONLINEAR	Nonlinear Static	1,

Figure 126. Add load combinations and assign load pattern in SAP2000.

- Assign loading for load patterns. Wind actions and permanent loads are applied as *distributed loads*, wind action on equipment and maintenance load as *concentrated ones*.

%%wind load

```
ret = FrameObj.SetLoadDistributed('framename', 'loadcase', 1, 2, ii, 1/6+ii, WIND2(j+jjj(i), 1), WIND2(1+jj+jjj(i), 1), 'local', true(), false());
```

.
.
.

%%vento su parabole

```
ret = FrameObj.SetLoadPoint('palo4', 'WIND_2', 1, 2, 0.86, 0.265, 'local', true(), false());
```

.
.
.

% assign loading for load pattern G2

```
ret = FrameObj.SetLoadDistributed('palo1', 'G2', 1, 10, 0, 1, 0.3, 0.3, 'global', true(), false());
```

.
.
.

% assign loading for maintenance

```
ret = FrameObj.SetLoadPoint('palo5', 'Maintenance', 1, 10, 1, 1, 'global', true(), false());
```

- The entire model is complete, the analysis can be launched:

%% save model

```
ret = File.Save(ModelPath);
```

%% run model (this will create the analysis model)

```
Analyze = NET.explicitCast(SapModel.Analyze, 'SAP2000v1.cAnalyze');
ret = Analyze.RunAnalysis();
```

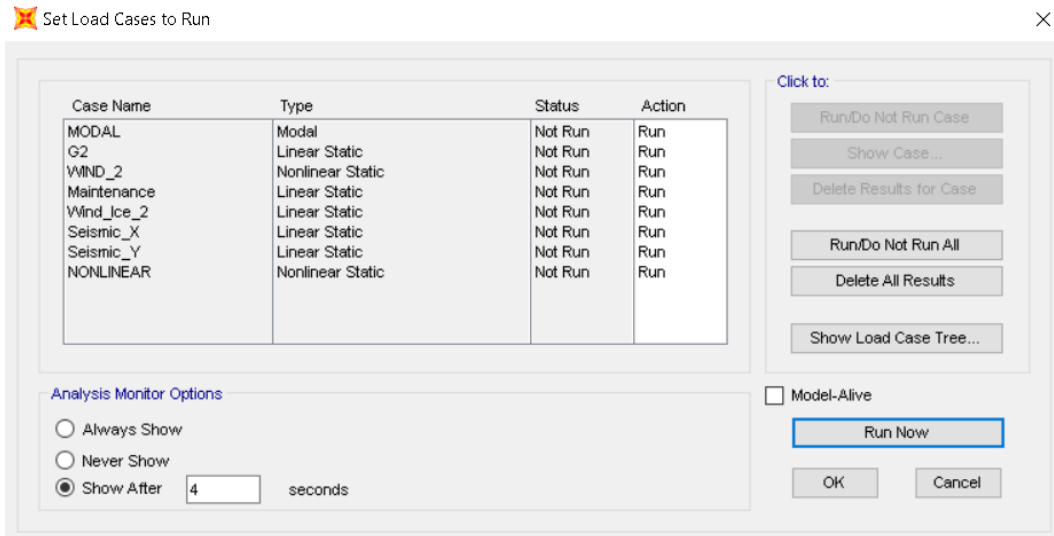


Figure 127. Define which load cases must be run in SAP2000.

- The results provided by the analysis can be collected. First of all, we need to initialize many variables. SAP2000 generates tables with all the results we want, in particular we have: the element considered, the location, the load case, the displacements U_1 , U_2 , U_3 , R_1 , R_2 , R_3 , the static quantities P , V_2 , V_3 , T , M_2 , M_3 . To extract all data, variable must be declared with the right typology, basically they could be string or numerical arrays. Thus, all the data are imported and storage in Matlab.

```
%% get Sap2000 results for load cases
```

```
AnalysisResults = NET.explicitCast(SapModel.Results, 'SAP2000v1.cAnalysisResults');
AnalysisResultsSetup =
NET.explicitCast(AnalysisResults.Setup, 'SAP2000v1.cAnalysisResultsSetup');
```

```
Number Results = 0;
Obj = NET.createArray('System.String', 2);
Elm = NET.createArray('System.String', 2);
ACase = NET.createArray('System.String', 2);
StepType = NET.createArray('System.String', 2);
StepNum = NET.createArray('System.Double', 2);
PointElm = NET.createArray('System.String', 2);
U1 = NET.createArray('System.Double', 2);
U2 = NET.createArray('System.Double', 2);
U3 = NET.createArray('System.Double', 2);
R1 = NET.createArray('System.Double', 2);
R2 = NET.createArray('System.Double', 2);
R3 = NET.createArray('System.Double', 2);
F1 = NET.createArray('System.Double', 2);
F2 = NET.createArray('System.Double', 2);
F3 = NET.createArray('System.Double', 2);
```

```

M1 = NET.createArray('System.Double',2);
M2 = NET.createArray('System.Double',2);
M3 = NET.createArray('System.Double',2);
P = NET.createArray('System.Double',2);
V2 = NET.createArray('System.Double',2);
V3 = NET.createArray('System.Double',2);
T = NET.createArray('System.Double',2);
ElmSta = NET.createArray('System.Double',2);
ObjSta = NET.createArray('System.Double',2);

ret = AnalysisResultsSetup.DeselectAllCasesAndCombosForOutput;
ret = AnalysisResultsSetup.SetCaseSelectedForOutput(ENVELOPE);

```

%%SAP2000 retrieves the values of each variable indicated in brackets.

```

[ret, NumberResults, Obj, ObjSta, Elm, ElmSta, ACase, StepType, StepNum, P, V2, V3, T, M2,
M3] = AnalysisResults.FrameForce('palo1', SAP2000v1.eltemTypeElm.ObjectElm,
NumberResults, Obj, ObjSta, Elm, ElmSta, ACase, StepType, StepNum, P, V2, V3, T, M2, M3);

```

.
.
.

- All the sections must be checked by using the *Steel Frame Design* tool provided by SAP2000. To do that, it is needed to set the desired Design Code, in our case the *Italian Standards, NTC2018*. Moreover, SAP2000 allows to modify other parameters, but that is not the case. It is important to establish which combination must be included in the assessment procedure, in our case we are interested to investigate the envelope of stresses. Even now, we are extracting data from an external routine (Sap2000), so we need to initialize new variables as well. Despite that, for our applications, we want to extract only the performance ratios from SAP2000, and store results in Matlab. When this process is over, all the performance ratios “*Ratio*” are collected in Matlab and they will be used as *constraints* during optimization procedures.

```

DesignSteel = NET.explicitCast(SapModel.DesignSteel, 'SAP2000v1.cDesignSteel');
ret = DesignSteel.SetCode('Italian NTC 2018');
ret = DesignSteel.SetComboStrength('Envelope', true());
ret = DesignSteel.SetComboAutoGenerate(false());
ret = DesignSteel.StartDesign;

```

```

FrameName = NET.createArray('System.String',2);
ComboName = NET.createArray('System.String',2);
ErrorSummary = NET.createArray('System.String',2);
WarningSummary = NET.createArray('System.String',2);
Ratio = NET.createArray('System.Double',2);
Location = NET.createArray('System.Double',2);
NumberItems = int32(0);
RatioType= int32(0);
n1=int32(0);

```

```
n2=int32(0);  
NumberNotPassed = int32(0);  
NameNotPassed=NET.createArray('System.String',2);
```

```
[ret, NumberItems, FrameName, Ratio, RatioType, Location, ComboName, ErrorSummary,  
WarningSummary] = DesignSteel.GetSummaryResults('palo1', NumberItems, FrameName,  
Ratio, RatioType, Location, ComboName, ErrorSummary, WarningSummary,  
SAP2000v1.eltmType.Objects);
```

- The analysis is complete. We can choose to close SAP2000 application, or to start a new procedure. In this last case we need to unlock the model because otherwise all the commands are blocked and it would be impossible to go on.

```
%% unlock model  
ret = SapModel.SetModelIsLocked(false());
```

```
%% close sap2000  
ret = SapObject.ApplicationExit(true());
```

7 Case Study: Structural Optimization

In this chapter will be exposed the results provided by the optimization analysis in different scenarios explained in detail in the chapter 4.4. We will refer only to the performance ratios PR of the main pole of the guyed radio mast, being the pole the most stressed element. It consists in 5 segments of 6.00 m length with the same cross-section. Starting from the ground level we have:

1. Pole_1 (0.00 to 6.00 m);
2. Pole_2 (6.00 to 12.00 m);
3. Pole_3 (12.00 to 18.00 m);
4. Pole_4 (18.00 to 24.00 m);
5. Pole_5 (24.00 to 30.00 m).

CASE STUDY- Circular Hollow Section (d,t)		
Φ_0	[mm]	168.3
t_0	[mm]	12.5
L	[mm]	6000
Mass	[kg]	288
n° elements	[-]	5
<i>Total Mass Σ</i>	<i>[kg]</i>	<i>1440</i>

Table 29. Total Mass of the main pole.
The main goal of our study is controlling the geometric and materic features..

In the following subchapters many scenarios will be investigated in which different design variables will be considered. In each of them there will be performed a comparison between the original structure, the solution obtained from the optimization procedure, and finally, a design strategy according to the product list. GA has been set as follows:

- Population Size = 10;
- Max Generation = 50;
- Cross-over Probability = 1%;
- Mutation Probability = 0.01%;
- N_{trials} = 5;

where N_{trials} is the number of time the GA has been fully execute; it provides a statistical worth to the proposed solutions.

For scenarios with many design variables n , the population size has been changed according to [31]:

$$2n \leq Pop.Size \leq 4n$$

Once defined x_{opt} , a structural analysis is performed by using the solution proposed by GA. Then, another structural analysis is conducted by fitting with profiles present in the product list, given that not all diameters are in series manufactured. Our goal is to find an economically viable solution. This is the reason why it is not possible to realize the specific diameter suggested to the GA. The design strategy is to use the least number of different profiles, trying to obtain a solution like the optimized one. In the Figure 129, the Performance Ratios PRs of the original, optimized, and design-proposed solution are compared. Obviously, the PRs of the optimized solution are higher with respect the original one, while for those of the design-proposed are typically slightly larger or lower, depending on the number of different profiles in the product list. In the Figure 130, the maximum axial load, bending moment, shear force, and the maximum deflection at the top of the pole are compared with respect the three situations as well. What expect to have in the optimized and design-proposed solutions is an increment in terms of deflection due to the employment of thinner elements, or better, due to higher performance ratios adoption. Figure 1

7.1 Scenario ‘A’

As introduced in the chapter 4.4.1, the design vector is the following:

$$\mathbf{x} = [\phi]$$

where ϕ is the diameter of the main pole and it is maintained unique along its entire length.

In this case the optimization procedure consists of 5 iterations N_{trial} , and it has been chosen the solution which have the lowest value of Fitness Function.

Ntrial = 5	
Φ_{opt}	OF
[mm]	[kN]
121	40.758
122	40.849

Table 30. Scenario ‘A’, best solutions.

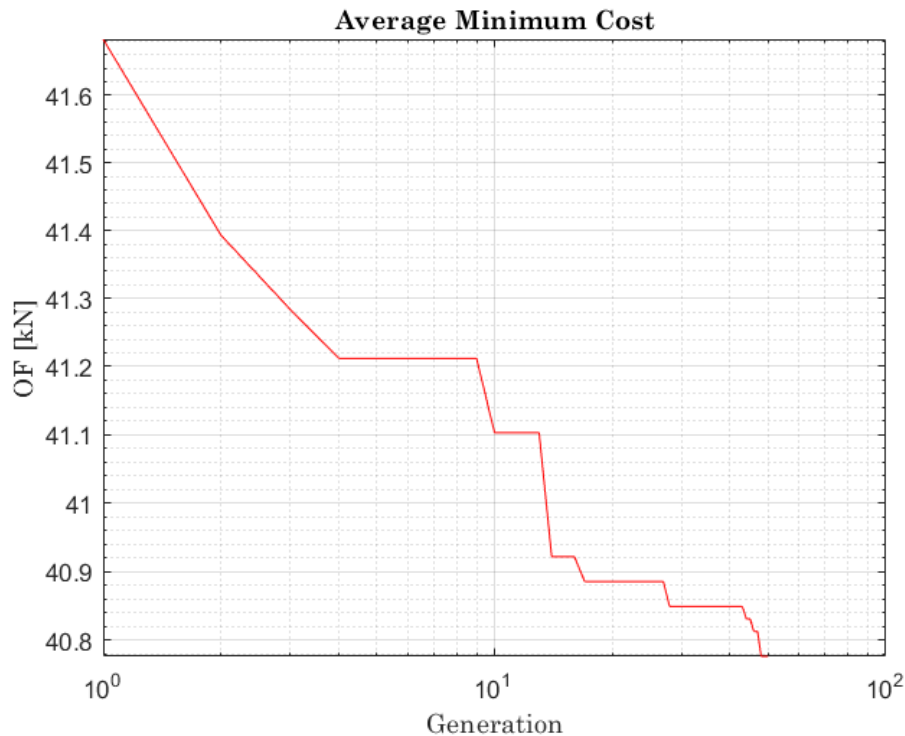


Figure 128. Scenario ‘A’. Decay of the Objective Function OF.

The total weight is computed and compared to the original structure. In this case we have a reduction of 437 kg, or 30.36% by weight with respect the initial configuration.

SCENARIO A - Optimized Solution				
Element	d [mm]	t [mm]	L [mm]	Mass [Kg]
Pole 1 (0-6 m)	121	12.5	6000	201
Pole 2 (6-12 m)	121	12.5	6000	201
Pole 3 (12-18 m)	121	12.5	6000	201
Pole 4 (18-24 m)	121	12.5	6000	201
Pole 5 (24-30 m)	121	12.5	6000	201
Total Mass [kg]			Σ	1003
Mass variation [kg]	-437	Mass variation [%]		-30.36

Table 31. Scenario 'A', Optimized solution. The optimization suggests to reduce D to 121 mm that causes a reduction of 437 kg.

In Table 32 is illustrated a possible design strategy according to a product list. In this case the mass variation is similar to the optimized solution (-18.36%).

SCENARIO A - Design proposed according to product list				
Element	d [mm]	t [mm]	L [mm]	Mass [Kg]
Pole 1 (0-6 m)	139.7	12.5	6000	235
Pole 2 (6-12 m)	139.7	12.5	6000	235
Pole 3 (12-18 m)	139.7	12.5	6000	235
Pole 4 (18-24 m)	139.7	12.5	6000	235
Pole 5 (24-30 m)	139.7	12.5	6000	235
Total Mass [kg]			Σ	1176
Mass variation [kg]	-264	Mass variation [%]		-18.36

Table 32. Scenario 'A', Design solution. In this case, industrial product list has available just D=139.7 that is quite similar to 121 mm, suggested by optimizer. For this reason the mass reduction is lower, 264 kg.

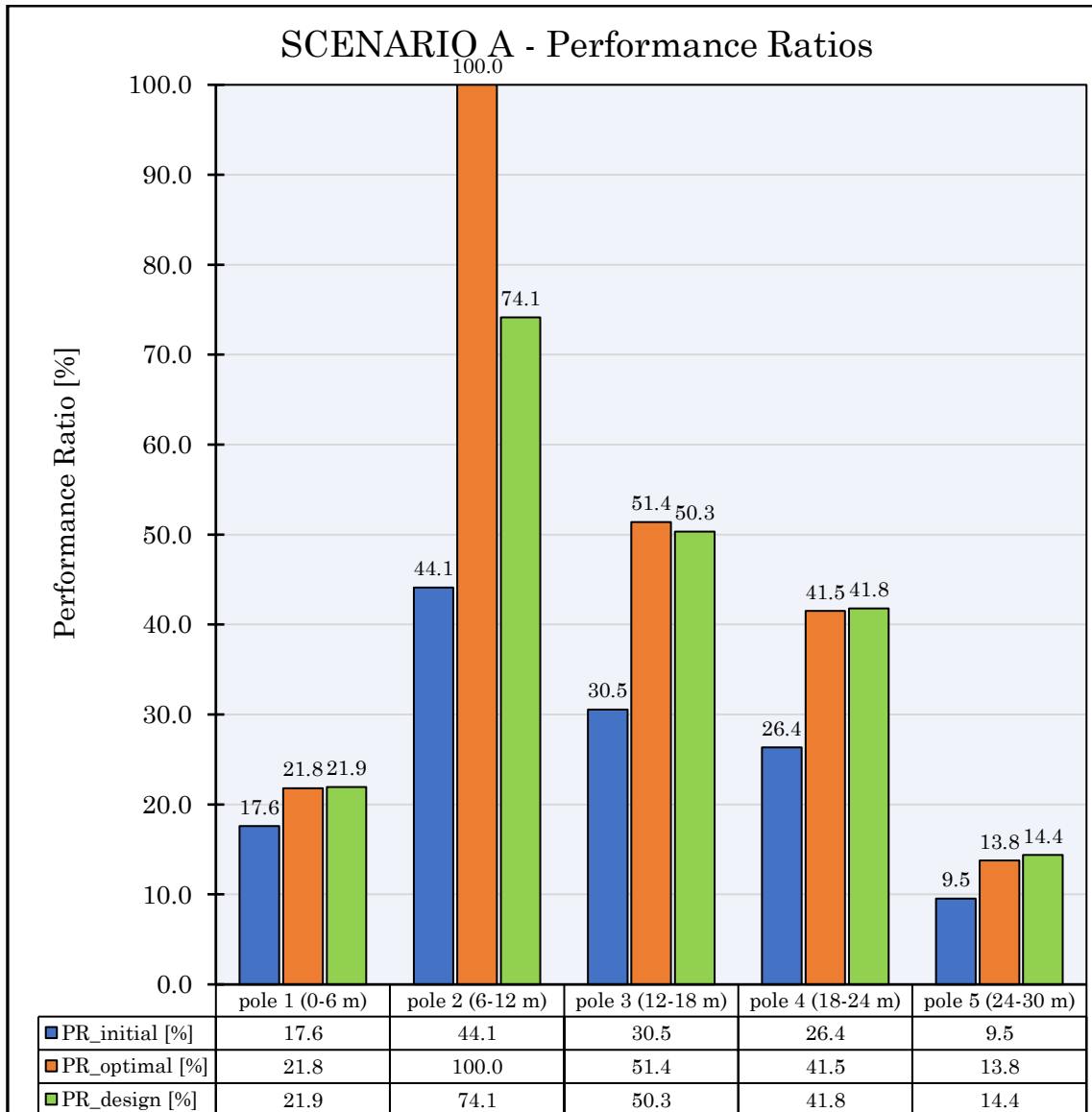


Figure 129. Scenario 'A' - PRs-trend. In blue are illustrated the Performance Ratios of each pole at the initial situation, in orange at the optimized solution. In green are represented PRs at a design configuration according to the product list.

Being the second pole the most stressed, the optimization finds the optimal diameter for that segment. As a consequence, the others, that are much less stressed, will result in overestimated solution.

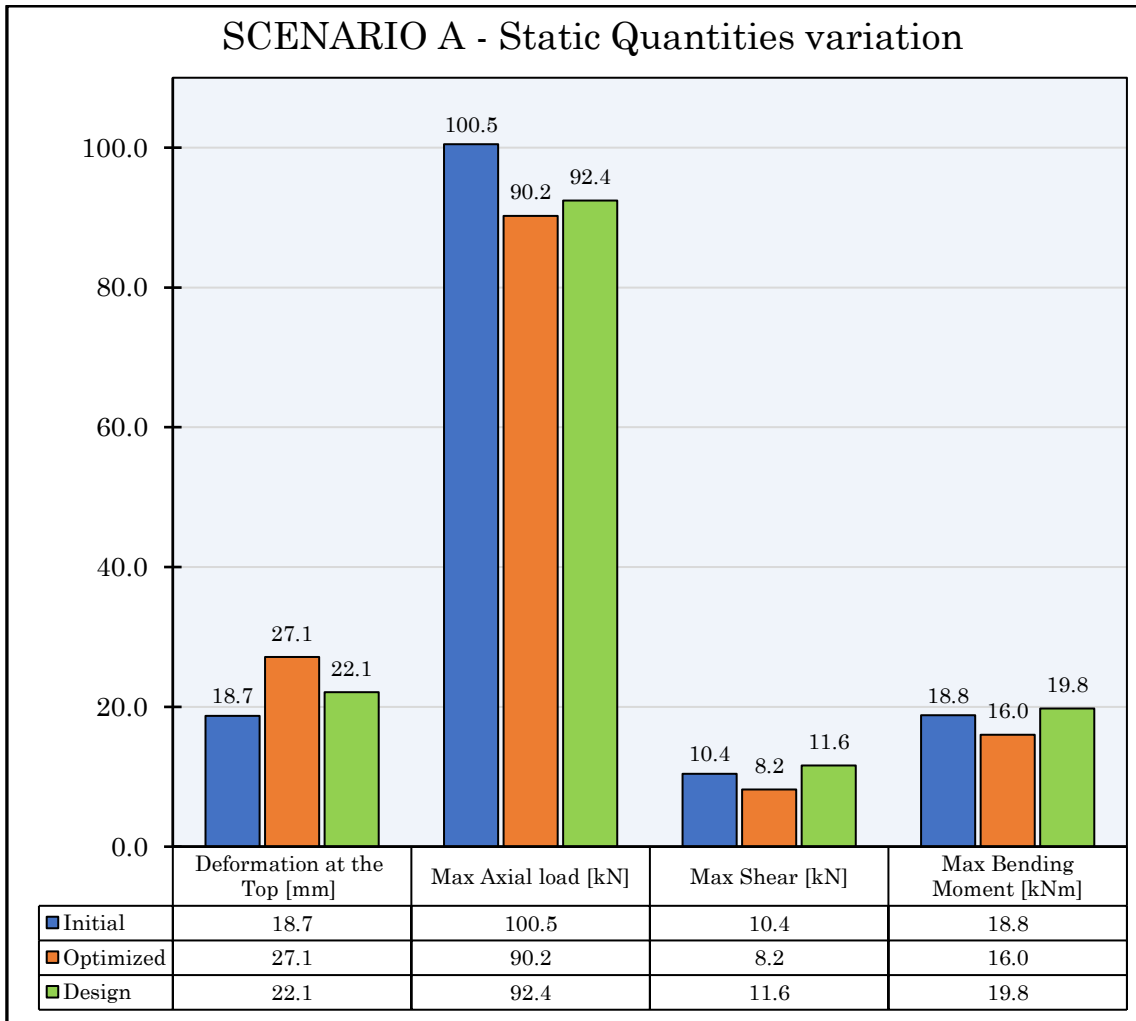


Figure 130. Scenario 'A'. In blue are illustrated the maximum values of Axial, Shear forces and Bending Moment at the initial situation, in orange at the optimized solution. In green they are represented at a design configuration according to the product list. Moreover they are reported the maximum deformation at the top of the structure.

Typically reducing the weight means have a structure lighter and flexible. This usually results in higher deformations and lower static quantities with respect the initial situation.

7.2 Scenario ‘B’

As introduced in the chapter 4.4.2 the design vector is the following:

$$\mathbf{x} = [\phi_i, \phi_f]$$

where ϕ_i, ϕ_f are respectively the diameter at the base and at the top of the structure. It is imposed a tapered solution.

In this case the optimization procedure consists of 5 iterations N_{trial} , and it has been chosen the solution which has the lowest value of Fitness Function.

Ntrial = 5		
Φ_i	Φ_f	OF
[mm]	[mm]	[kN]
148	94	41.248
146	103	41.466
148	94	41.248
146	103	41.466
149	92	41.230

Table 33. Scenario ‘B’, best solutions.

$$\mathbf{x}_{opt} = [149, 92]$$

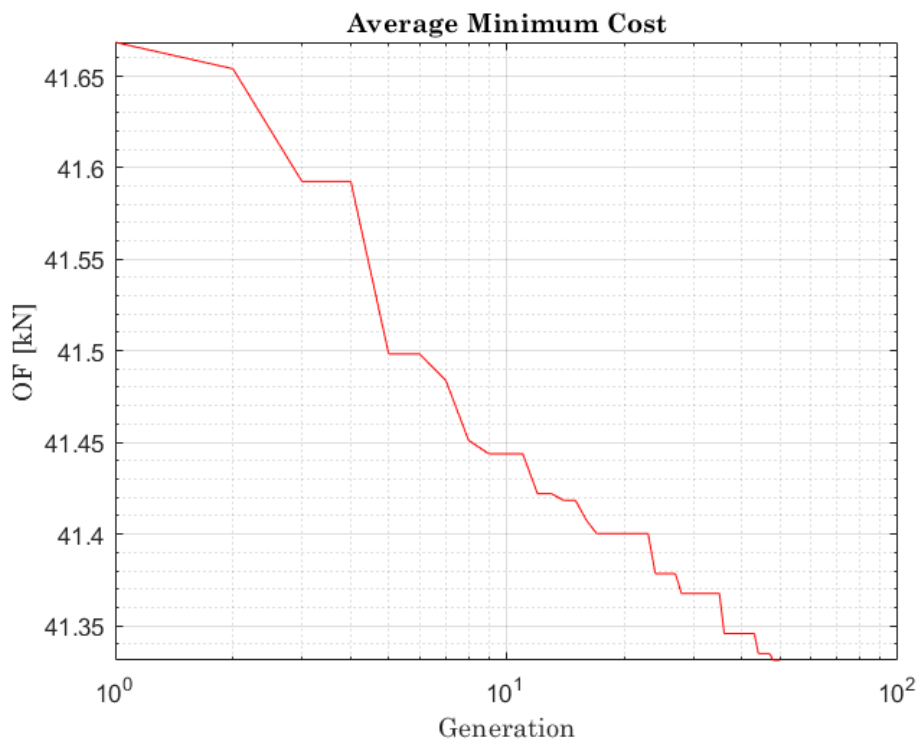


Figure 131. Scenario ‘B’. Decay of the Objective Function OF.

The total weight is computed and compared to the original structure. In this case we have a reduction of 389 kg, or 27.02% by weight with respect the initial configuration.

SCENARIO B – Optimized Solution				
Element	d [mm]	t [mm]	L [mm]	Mass [Kg]
Pole 1 (0-6 m)	149	12.5	6000	252
Pole 2 (6-12 m)	138	12.5	6000	231
Pole 3 (12-18 m)	126	12.5	6000	210
Pole 4 (18-24 m)	115	12.5	6000	189
Pole 5 (24-30 m)	103	12.5	6000	168
Total Mass [kg]			Σ	1051
Mass variation [kg]	-389	Mass variation [%]		-27.02

Table 34. Scenario 'B', Optimized solution. At the base $D=149$ mm, progressively the tapering produces a reduction of D until 103 mm, achieving a mass reduction equal to 389 kg.

In Table 35 is illustrated a possible design strategy according to a product list. In this case the mass variation is similar to the optimized solution (-22.84%).

SCENARIO B – Design proposed according to product list				
Element	d [mm]	t [mm]	L [mm]	Mass [Kg]
Pole 1 (0-6 m)	168.3	12.5	6000	288
Pole 2 (6-12 m)	139.7	12.5	6000	235
Pole 3 (12-18 m)	139.7	12.5	6000	235
Pole 4 (18-24 m)	114.3	12.5	6000	188
Pole 5 (24-30 m)	101.6	12.5	6000	165
Total Mass [kg]			Σ	1111
Mass variation [kg]	-329	Mass variation [%]		-22.84

Table 35. Scenario 'B', Design solution. In this case, industrial product list fit quite well the solution proposed by the optimizer, infact the mass reducaiton is similar (329 kg).

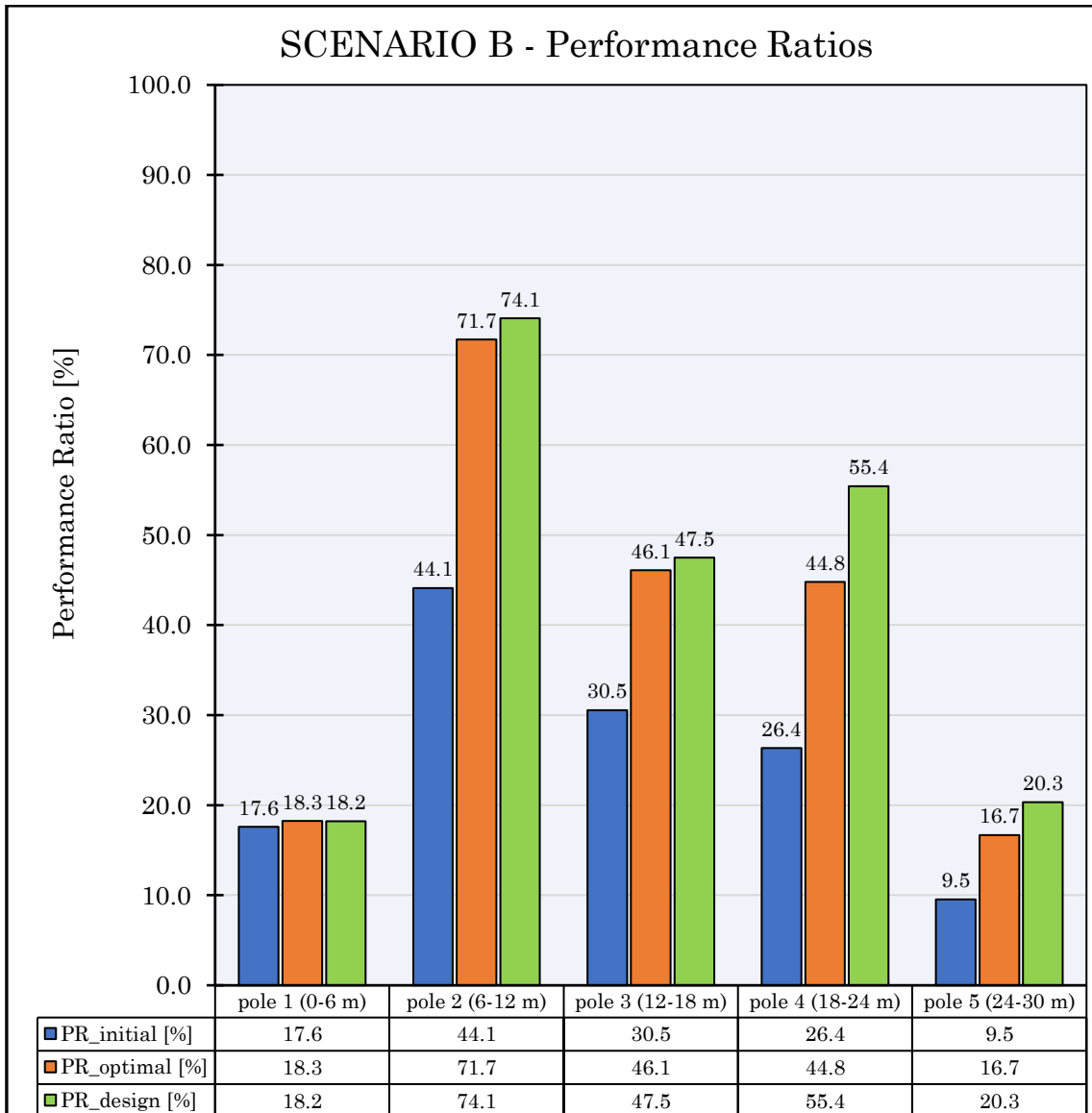


Figure 132. Scenario 'B' - PRs-trend. In blue are illustrated the Performance Ratios of each pole at the initial situation, in orange at the optimized solution. In green are represented PRs at a design configuration according to the product list.

Being the optimization constrained by the interpolation function and by a minimum diameter fixed at 100.0 mm, it is not able to even search an optimal diameter at the second pole, which is the most stressed. This reflects into overestimations to other segments.

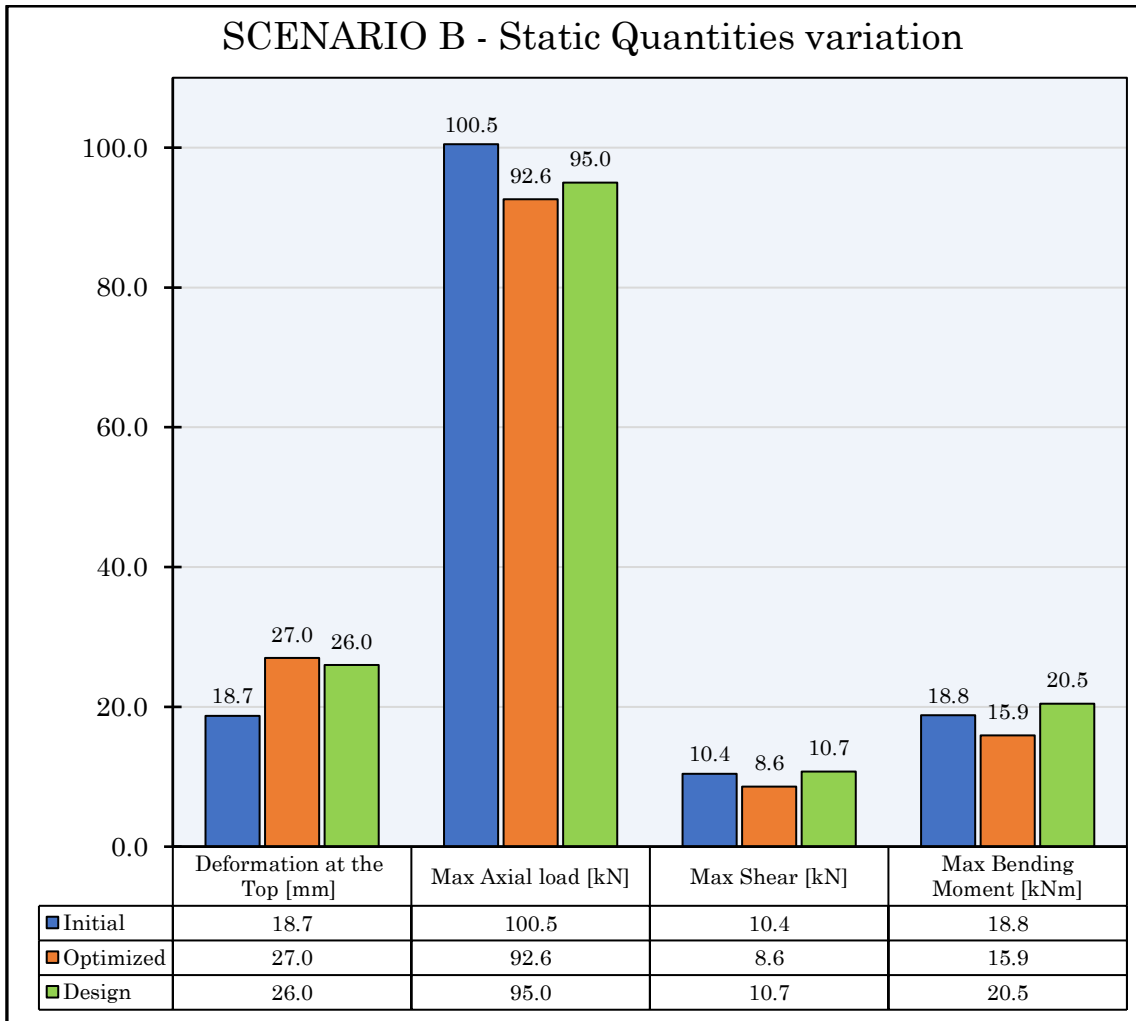


Figure 133. Scenario 'B'. In blue are illustrated the maximum values of Axial, Shear forces and Bending Moment at the initial situation, in orange at the optimized solution. In green they are represented at a design configuration according to the product list. Moreover they are reported the maximum deformation at the top of the structure.

Typically reducing the weight means have a structure lighter and flexible. This usually results in higher deformations and lower static quantities with respect the initial situation.

7.3 Scenario ‘C’

As introduced in the chapter 4.4.3. The design vector is the following:

$$\mathbf{x} = [\phi_i, \phi_f, F]$$

It is added the pre-tensioning force F at the cables together with the tapering solution proposed in the previously scenario.

In this case the optimization procedure consists of 5 iterations N_{trial} , and it has been chosen the solution which have the lowest value of Fitness Function.

Ntrial = 5			
Φ_i	Φ_f	F	OF
[mm]	[mm]	[kN]	[kN]
152	92	1.8	41.393
151	92	1.4	41.339
149	92	1	41.230
156	92	2.4	41.610
147	92	0.8	41.121

Table 36. Scenario ‘C’, best solutions.

$$\mathbf{x}_{opt} = [147, 92, 0.8]$$

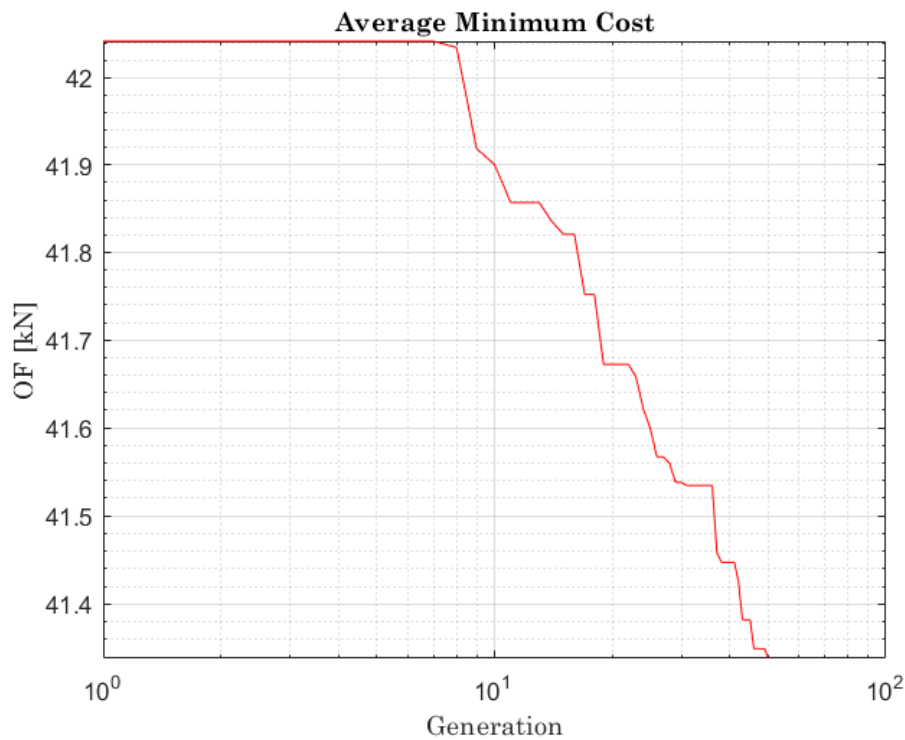


Figure 134. Scenario ‘C’. Decay of the Objective Function OF.

The total weight is computed and compared to the original structure. In this case we have a reduction of 400 kg, or 27.79% by weight with respect the initial configuration.

SCENARIO C- <i>Optimized solution</i>				
Element	d [mm]	t [mm]	L [mm]	Mass [Kg]
Pole 1 (0-6 m)	147	12.5	6000	249
Pole 2 (6-12 m)	136	12.5	6000	228
Pole 3 (12-18 m)	125	12.5	6000	208
Pole 4 (18-24 m)	114	12.5	6000	188
Pole 5 (24-30 m)	103	12.5	6000	167
Total Mass [kg]			Σ	1040
Mass variation [kg]	-400	Mass variation [%]		-27.79

Table 37. Scenario 'C', Optimized solution. At the base $D=147$ mm, progressively the tapering produces a reduction of D until 103 mm, achieving a mass reduction equal to 400 kg.

In

Table 38 is illustrated a possible design strategy according to a product list. In this case the mass variation is similar to the optimized solution (-27.22%).

SCENARIO C – <i>Design proposed according to product list</i>				
Element	d [mm]	t [mm]	L [mm]	Mass [Kg]
Pole 1 (0-6 m)	168.3	12.5	6000	288
Pole 2 (6-12 m)	139.7	12.5	6000	235
Pole 3 (12-18 m)	139.7	12.5	6000	235
Pole 4 (18-24 m)	114.3	10	6000	154
Pole 5 (24-30 m)	101.6	10	6000	135
Total Mass [kg]			Σ	1048
Mass variation [kg]	-392	Mass variation [%]		-27.22

Table 38. Scenario 'C', Design solution. In this case, industrial product list fit quite well the solution proposed by the optimizer, infact the mass reducaiton is similar (392 kg).

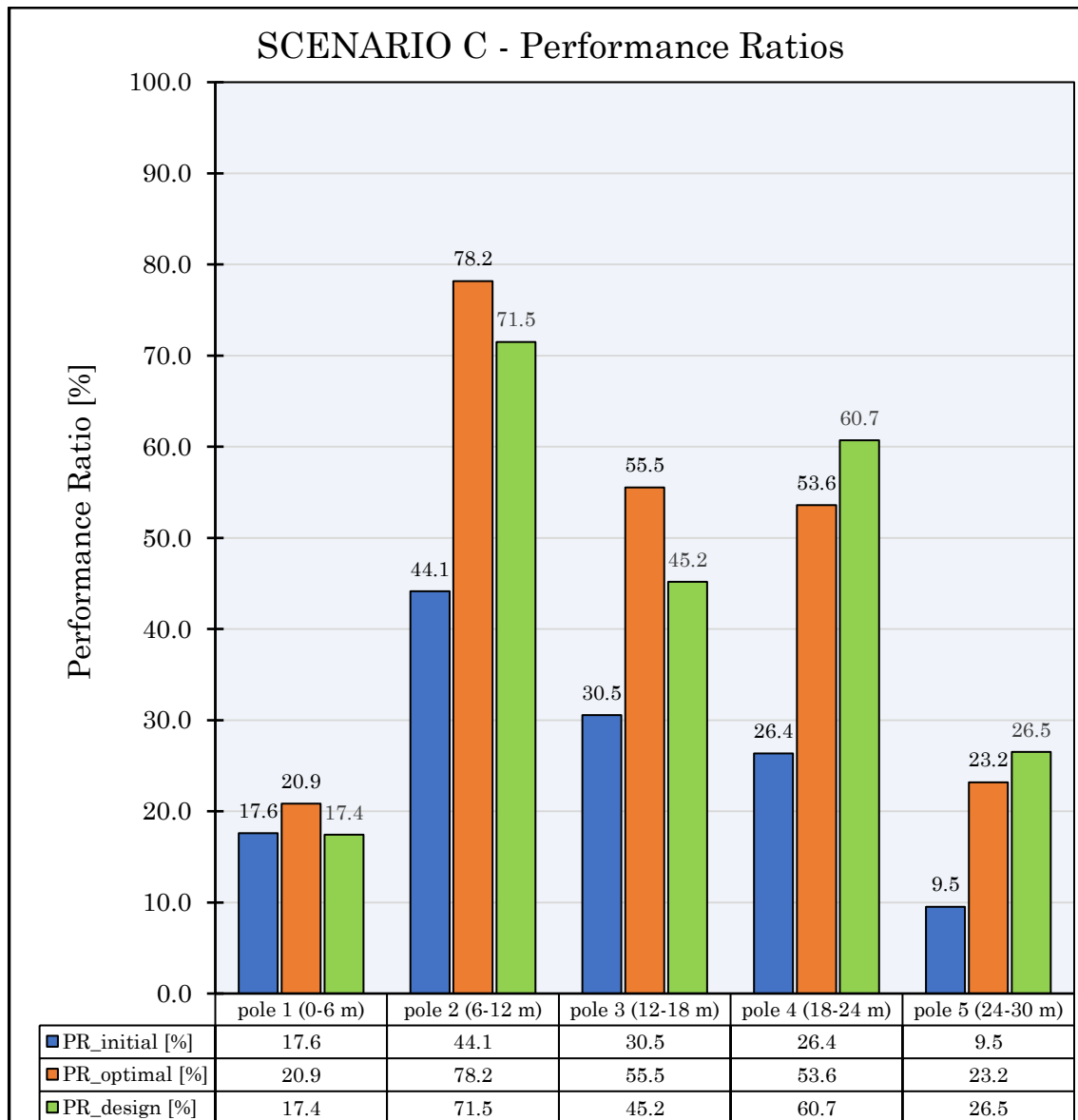


Figure 135. Scenario 'C' - PRs-trend. In blue are illustrated the Performance Ratios of each pole at the initial situation, in orange at the optimized solution. In green are represented PRs at a design configuration according to the product list.

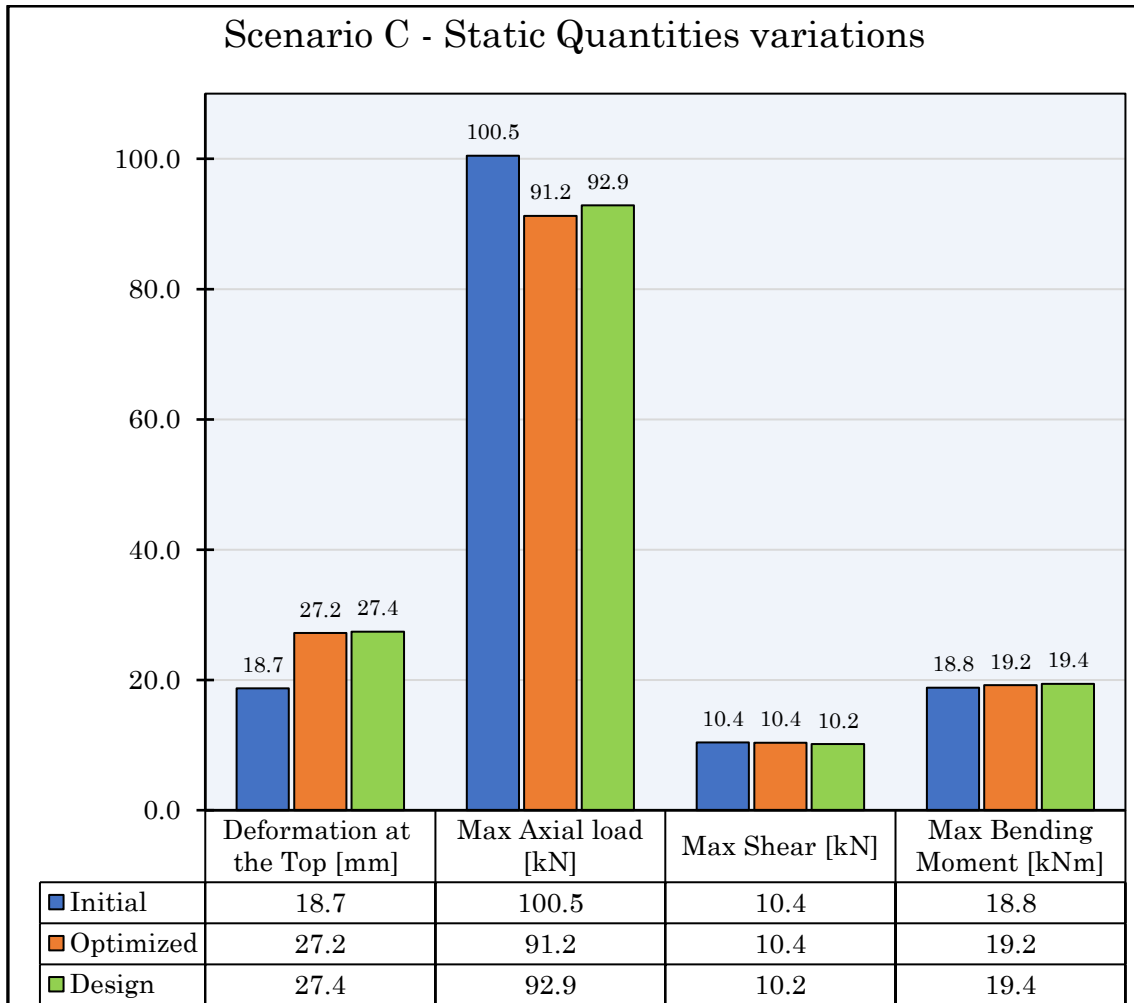


Figure 136. Scenario 'C'. In blue are illustrated the maximum values of Axial, Shear forces and Bending Moment at the initial situation, in orange at the optimized solution. In green they are represented at a design configuration according to the product list.

In this scenario, the introduction of the pre-tensioning force at the cable does not produce significant effects. This it can be detectable by compare to the previous scenario (B). Practically speaking, the pre-tensioning force allows to control the deformation of the structure which is a positive feature. On the other hand, this aspect reflects in higher compression levels at the main pole, which means sending GA into confusion. In fact, GA would like to approach $PR \sim \leq 1$ and at the same time reduce weight. The latter is obviously impossible by just managing on F . Given that pre-tensioning force does not produce negative results, but it controls deformation limits, we will continue to consider it in the subsequent scenarios.

7.4 Scenario ‘D’

As introduced in the chapter 4.4.4 the design vector is the following:

$$\mathbf{x} = [\phi_i, \phi_f, t]$$

where t is the thickness of the circular hollow section of the main pole. In this case the optimization procedure consists of 5 iterations N_{trial} , and it has been chosen the solution which have the lowest value of Fitness Function.

Ntrial = 5			
Φ_i	Φ_f	t	OF
[mm]	[mm]	[mm]	[kN]
161	92	6	36.465
146	117	7	37.389
162	92	6	36.491
162	92	6	36.491
163	92	6	36.517

Table 39

$$\mathbf{x}_{opt} = [161, 92, 6]$$

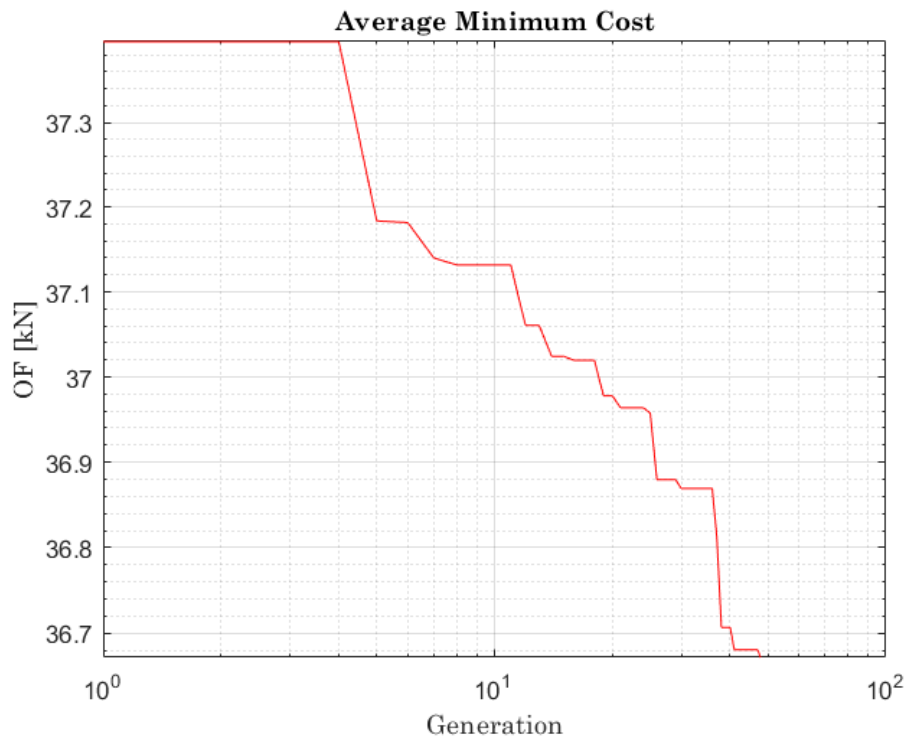


Figure 137. Scenario ‘D’. Decay of the Objective Function OF.

The total weight is computed and compared to the original structure. In this case we have a reduction of 875 kg, or 60.75% by weight with respect the initial configuration.

SCENARIO D- <i>Optimized solution</i>				
Element	d [mm]	t [mm]	L [mm]	Mass [Kg]
Pole 1 (0-6 m)	161	6	6000	138
Pole 2 (6-12 m)	147	6	6000	125
Pole 3 (12-18 m)	133	6	6000	113
Pole 4 (18-24 m)	120	6	6000	101
Pole 5 (24-30 m)	106	6	6000	89
Total Mass [kg]			Σ	565
Mass variation [kg]	-875	Mass variation [%]		-60.75

Table 40. *Optimized solution. At the base D=161 mm, progressively the tapering produces a reduction of D until 106 mm, achieving a mass reduction equal to 875 kg. The thickness is set to 6 mm.*

In the Table 41 is illustrated a possible design strategy according to a product list. In this case the mass variation is similar to the optimized solution (-27.22%).

SCENARIO D - <i>Design proposed according to product list</i>				
Element	d [mm]	t [mm]	L [mm]	Mass [Kg]
Pole 1 (0-6 m)	168.3	6	6000	144
Pole 2 (6-12 m)	168.3	6	6000	144
Pole 3 (12-18 m)	139.7	6	6000	119
Pole 4 (18-24 m)	114.3	6	6000	96
Pole 5 (24-30 m)	101.6	6	6000	85
Total Mass [kg]			Σ	588
Mass variation [kg]	-853	Mass variation [%]		-59.20

Table 41. *Design solution. Industrial product list fit well the optimize solution, in fact the mass reduction is 853kg.*

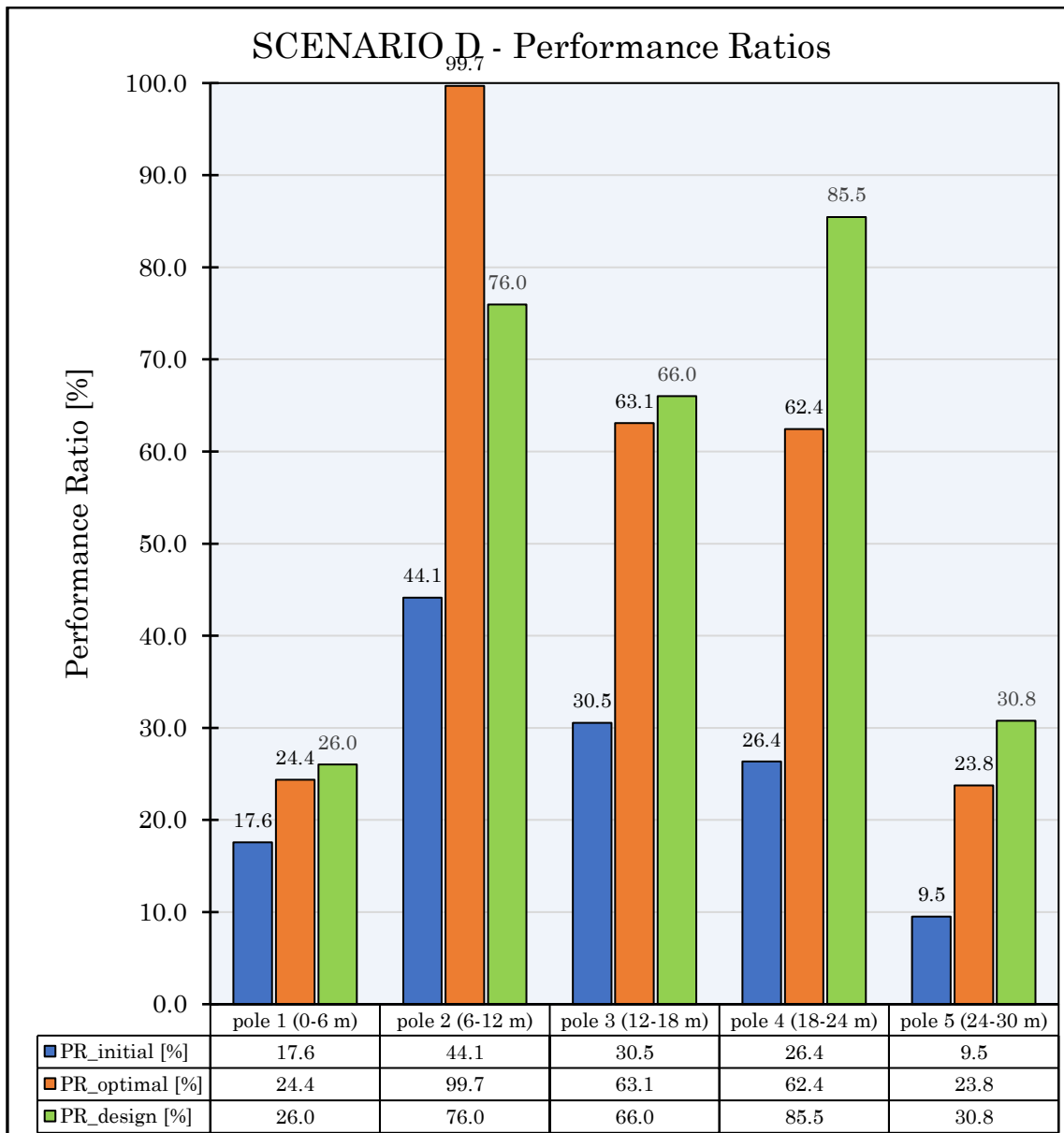


Figure 138. Scenario 'D' - PRs-trend. In blue are illustrated the Performance Ratios of each pole at the initial situation, in orange at the optimized solution. In green are represented PRs at a design configuration according to the product list.

The introduction of thickness in the design vector decreases the degrees of freedom of the problem, and starting from this scenario, the performance ratios become larger.

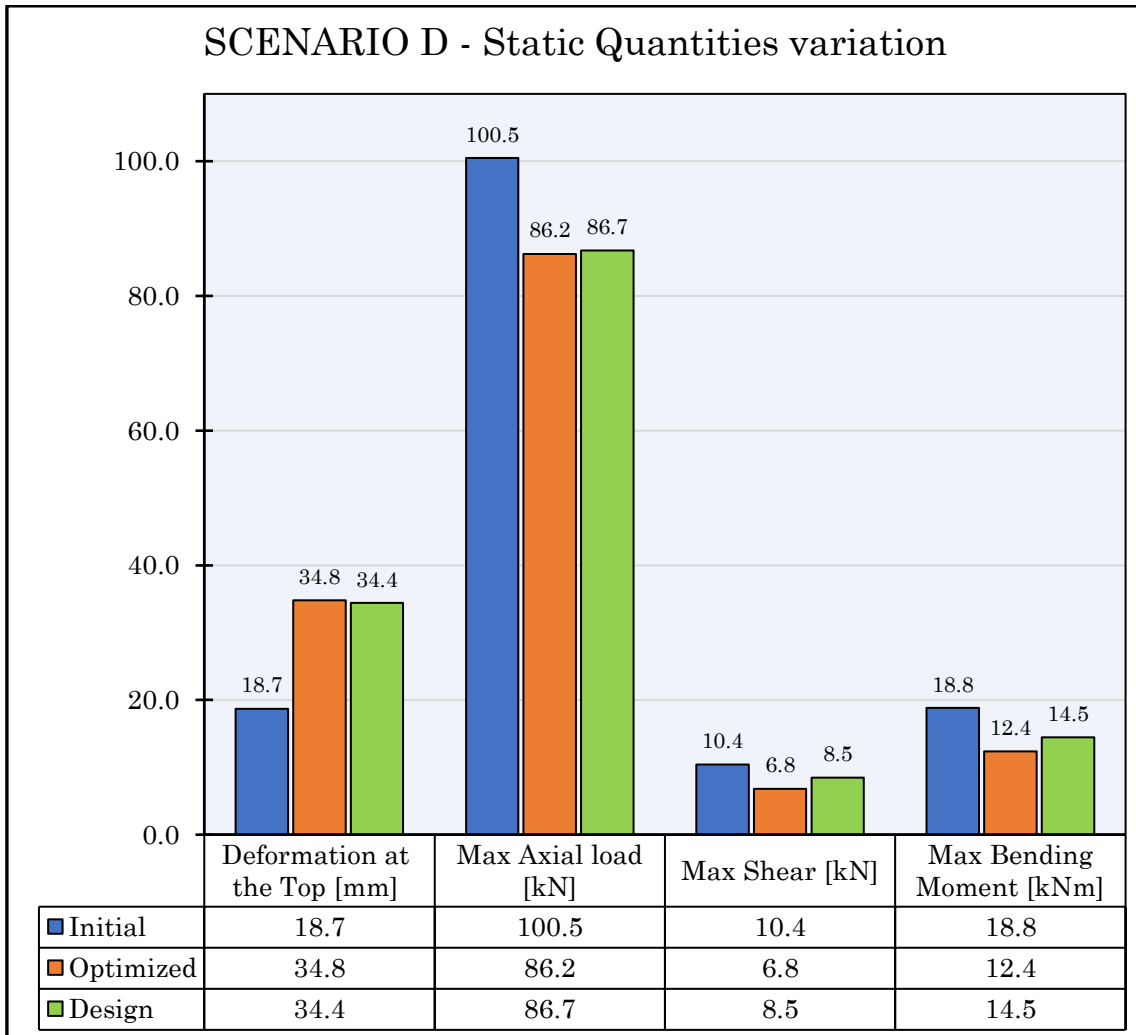


Figure 139. Scenario 'D'. In blue are illustrated the maximum values of Axial, Shear forces and Bending Moment at the initial situation, in orange at the optimized solution. In green they are represented at a design configuration according to the product list.

Also in this case, the deformations become larger after the optimization process. At the contrary, we have a lowering of the static quantities with respect the initial configuration.

7.5 Scenario ‘E’

As introduced in the chapter 4.4.5 the design vector is the following:

$$\mathbf{x} = [\phi_i, \phi_f, t, F]$$

In this case the optimization procedure consists of 5 iterations N_{trial} , and it has been chosen the solution which have the lowest value of Fitness Function.

Ntrial = 5				
Φ_i	Φ_f	t	F	OF
[mm]	[mm]	[mm]	[kN]	[kN]
150	97	7.8	1.3	37.766
153	112	6.4	1.6	36.964
165	91	6	2.3	36.552
160	91	7	1.3	37.287
139	104	8.8	1.3	38.337

Table 42. Scenario ‘E’, best solutions.

$$\mathbf{x}_{opt} = [165, 91, 6, 2.3]$$

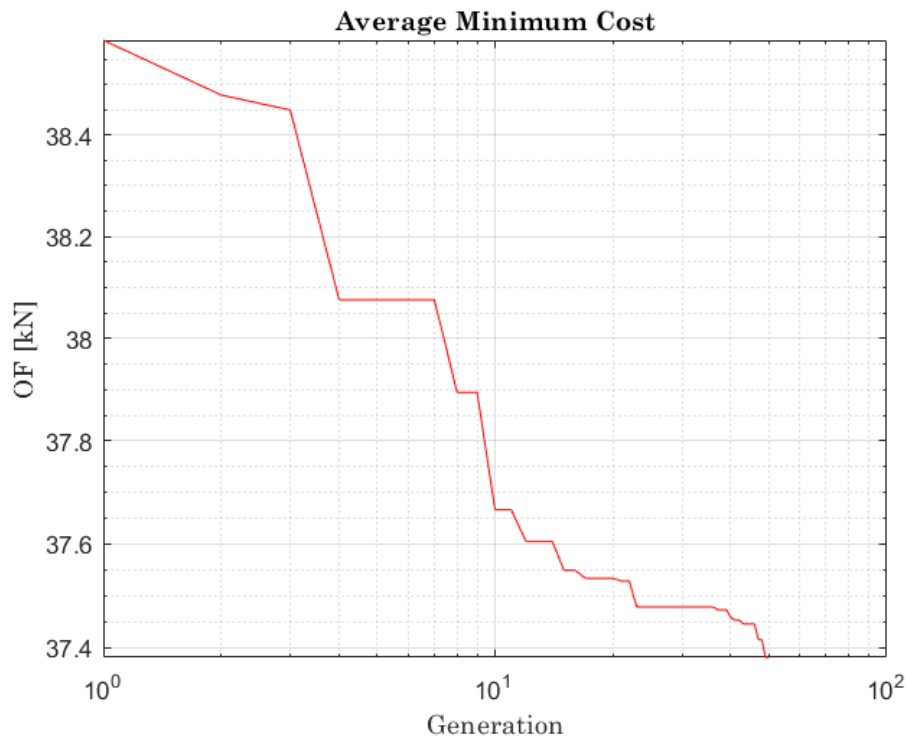


Figure 140. Scenario ‘E’. Decay of the Objective Function OF.

The total weight is computed and compared to the original structure. In this case we have a reduction of 866 kg, or 60.13% by weight with respect the initial configuration.

SCENARIO E – Optimized Solution				
Element	d [mm]	t [mm]	L [mm]	Mass [Kg]
Pole 1 (0-6 m)	165	6	6000	141
Pole 2 (6-12 m)	150	6	6000	128
Pole 3 (12-18 m)	135	6	6000	115
Pole 4 (18-24 m)	121	6	6000	102
Pole 5 (24-30 m)	106	6	6000	89
Total Mass [kg]			Σ	574
Mass variation [kg]	-866	Mass variation [%]		-60.13

Table 43. Scenario 'E', Optimized solution.

In

Table 44 is illustrated a possible design strategy according to a product list. In this case the mass variation is similar to the optimized solution (-59.20%).

SCENARIO E – Design proposed according to product list				
Element	d [mm]	t [mm]	L [mm]	Mass [Kg]
Pole 1 (0-6 m)	168.3	6	6000	144
Pole 2 (6-12 m)	168.3	6	6000	144
Pole 3 (12-18 m)	139.7	6	6000	119
Pole 4 (18-24 m)	114.3	6	6000	96
Pole 5 (24-30 m)	101.6	6	6000	85
Total Mass [kg]			Σ	588
Mass variation [kg]	-853	Mass variation [%]		-59.20

Table 44. Scenario 'D', Design solution.

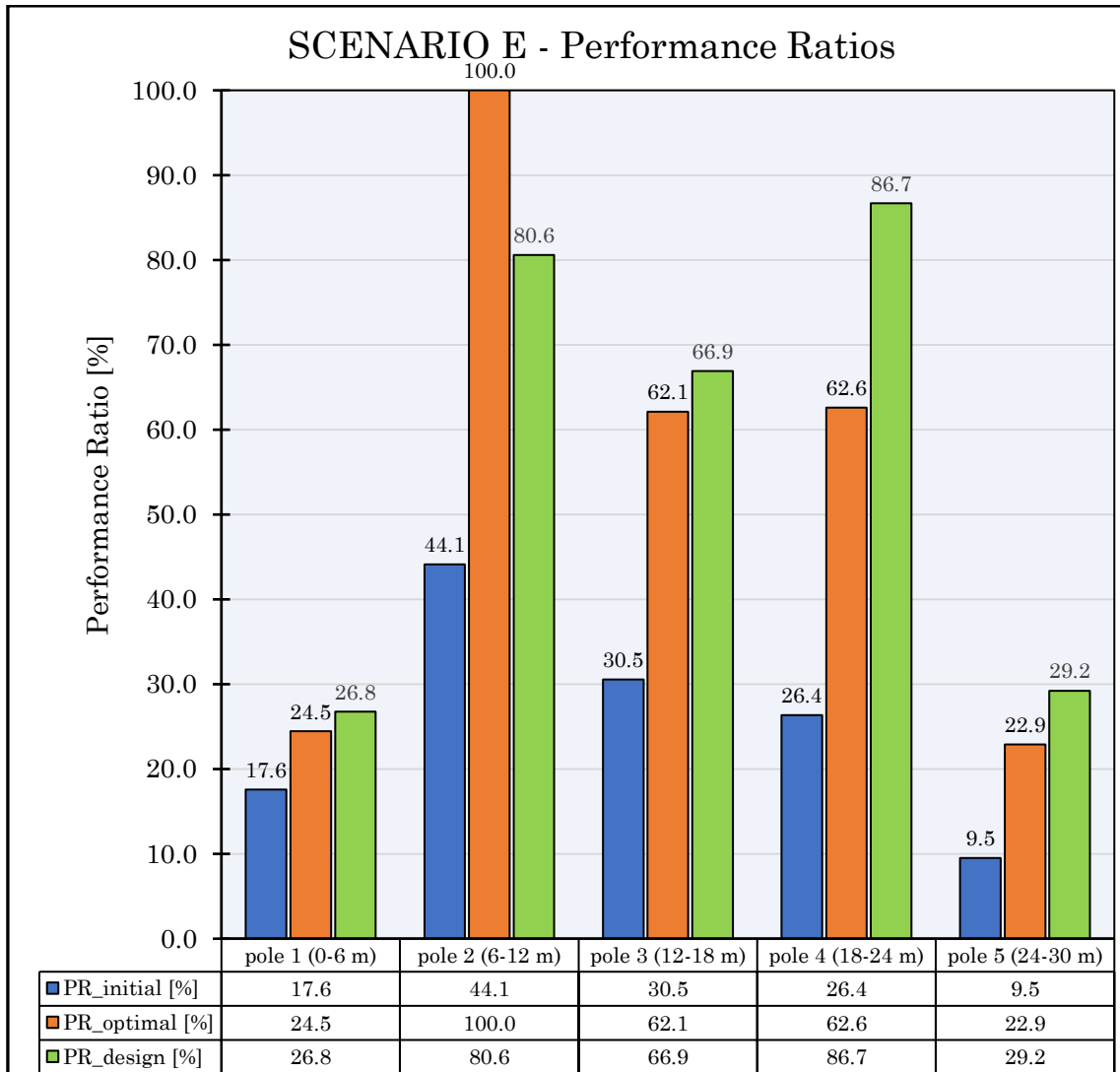


Figure 141. Scenario 'E' - PRs-trend. In blue are illustrated the Performance Ratios of each pole at the initial situation, in orange at the optimized solution. In green are represented PRs at a design configuration according to the product list.

As we expected, there are not significant differences with the previous scenario (D) because just *F* is introduced.

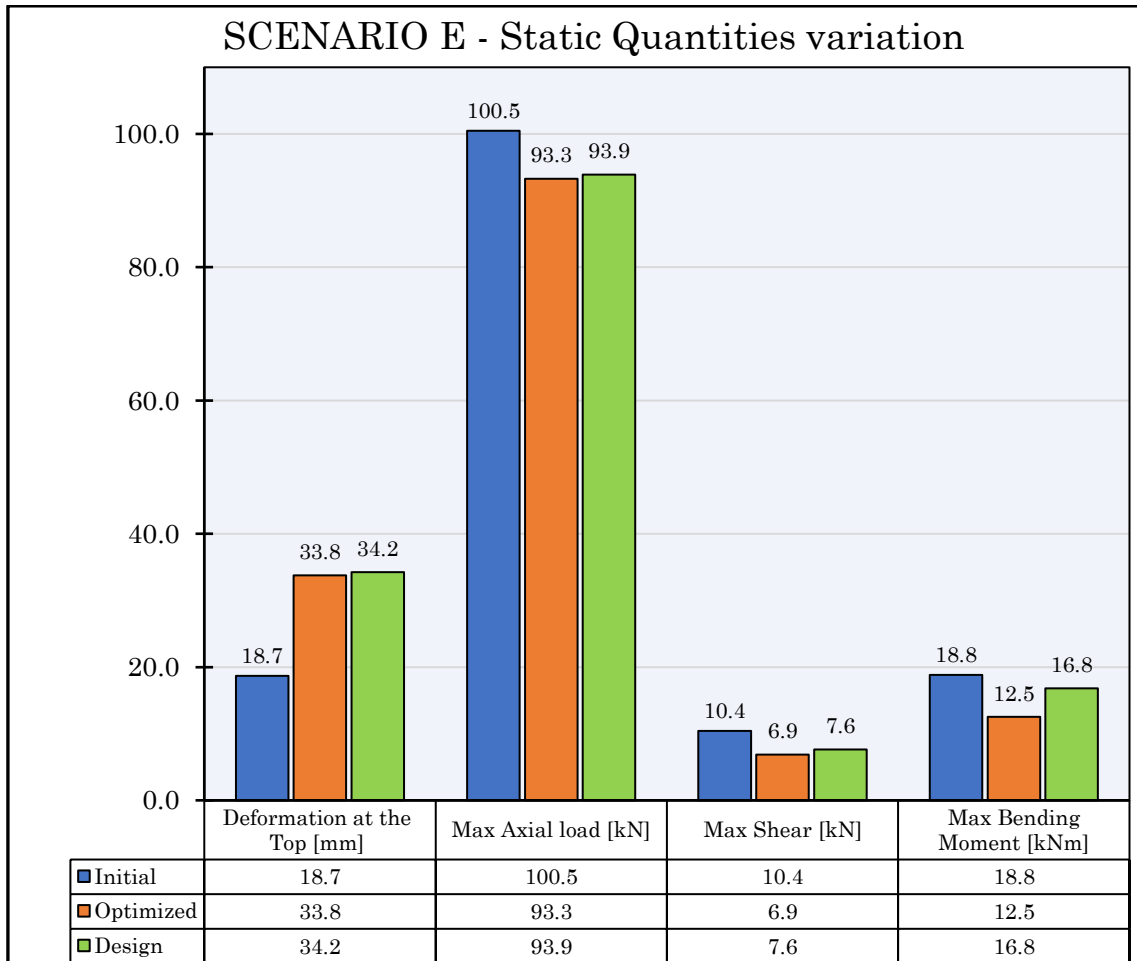


Figure 142. Scenario 'E'. In blue are illustrated the maximum values of Axial, Shear forces and Bending Moment at the initial situation, in orange at the optimized solution. In green they are represented at a design configuration according to the product list.

About deformations and static quantities the discussion is interesting. In this scenario $F_E = 2.3 \text{ kN}$ while in the previous one (D) is $F_D = 1 \text{ kN}$. As a consequence the mass reduction is quite similar (in particular, in E is a little bit lower $\sim 9 \text{ kg}$) at the expense of higher compression level ($\sim +7 \text{ kN}$) at gain of only 1 mm less as deformation at the top.

7.6 Scenario ‘F’

As introduced in the chapter 4.4.6. The design vector is the following:

$$\mathbf{x} = [\phi_i, \phi_f, t_{ends}, t_{inter}, F]$$

In this scenario two different thickness are considered in order to fit better the main pole at correspondence of the most stressed segment, and at the ends, where the stress is lower.

In this case the optimization procedure consists of 3 iterations N_{trial} , and it has been chosen the solution which have the lowest value of Fitness Function. The population-size is set to 20 according to [31], being $n = 5$.

Ntrial = 3					
Φ_i	Φ_f	t_{ends}	t_{inter}	F	OF
[mm]	[mm]	[mm]	[mm]	[kN]	[kN]
155	92	4	7	3.2	35.141
157	92	4	6	0.9	34.993
151	92	4	7	1.3	35.058

Table 45. Scenario ‘F’, best solutions.

$$\mathbf{x}_{opt} = [157, 92, 4, 6, 0.9]$$

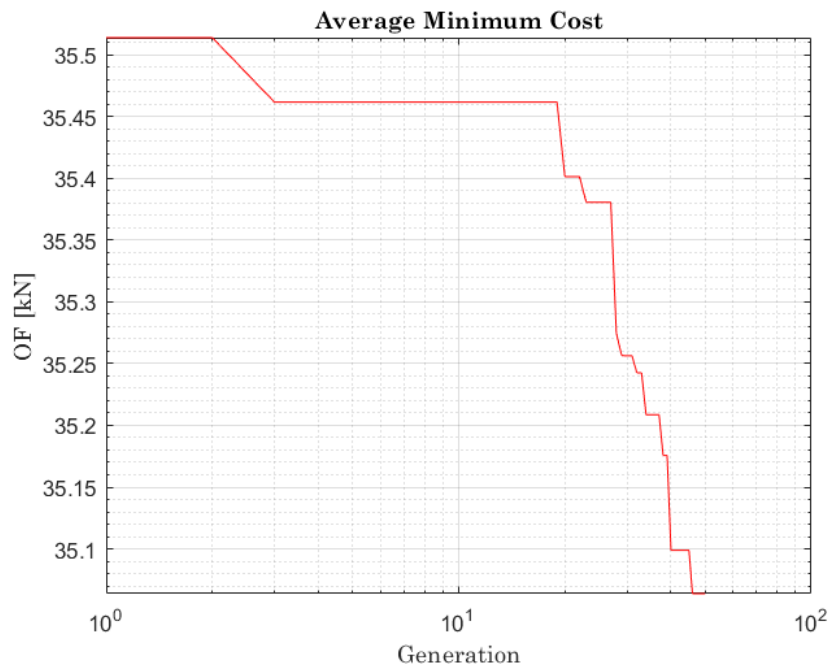


Figure 143. Scenario ‘F’. Decay of the Objective Function OF.

The total weight is computed and compared to the original structure. In this case we have a reduction of 1025 kg, or 71.16% by weight with respect the initial configuration.

SCENARIO F – <i>Optimized Solution</i>				
Element	d [mm]	t [mm]	L [mm]	Mass [Kg]
Pole 1 (0-6 m)	157	4	6000	91
Pole 2 (6-12 m)	144	6	6000	122
Pole 3 (12-18 m)	131	4	6000	75
Pole 4 (18-24 m)	118	4	6000	67
Pole 5 (24-30 m)	105	4	6000	60
Total Mass [kg]			Σ	415
Mass variation [kg]	-1025	Mass variation [%]		-71.16

Table 46. Scenario 'E', Optimized solution. It is evident how introducing two different thickness means adapting better to the problem of interest (-1025kg).

In

Table 47 is illustrated a possible design strategy according to a product list. In this case the mass variation is like the optimized solution (-70.75%).

SCENARIO F – <i>Design proposed according to product list</i>				
Element	d [mm]	t [mm]	L [mm]	Mass [Kg]
Pole 1 (0-6 m)	168.3	4	6000	97
Pole 2 (6-12 m)	168.3	5	6000	121
Pole 3 (12-18 m)	139.7	4	6000	80
Pole 4 (18-24 m)	114.3	4	6000	65
Pole 5 (24-30 m)	101.6	4	6000	58
Total Mass [kg]			Σ	421
Mass variation [kg]	-1019	Mass variation [%]		-70.75

Table 47. Scenario 'F', Design solution.

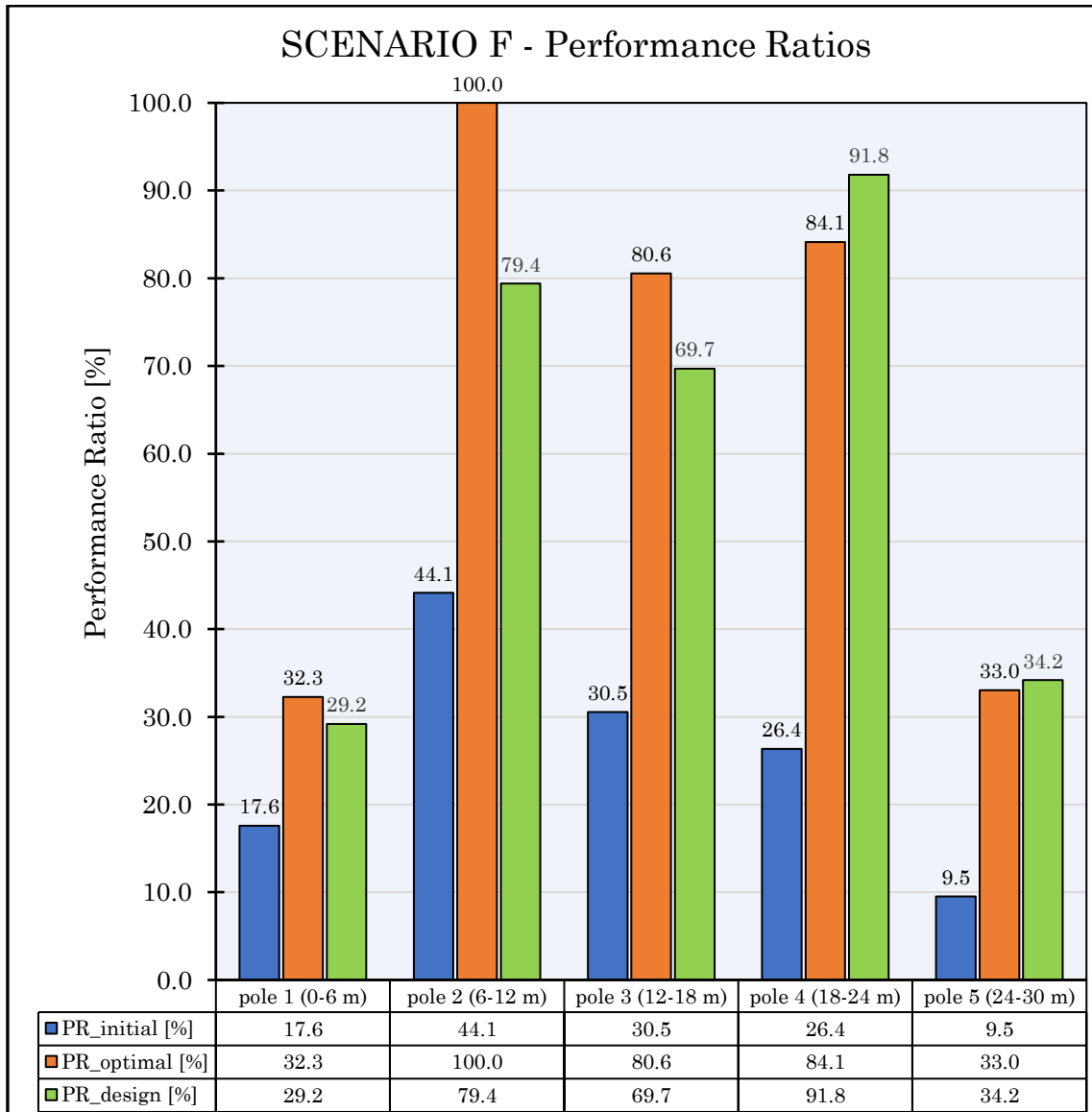


Figure 144. Scenario 'F' - PRs-trend. In blue are illustrated the Performance Ratios of each pole at the initial situation, in orange at the optimized solution. In green are represented PRs at a design configuration according to the product list.

In this scenario we have an overall improvement in the performance ratios because another thickness variable is added. Especially 2 additional thickness are introduced because the intermediate segments are more stressed and for this reason the only tapering is not sufficient to optimize well the main pole.

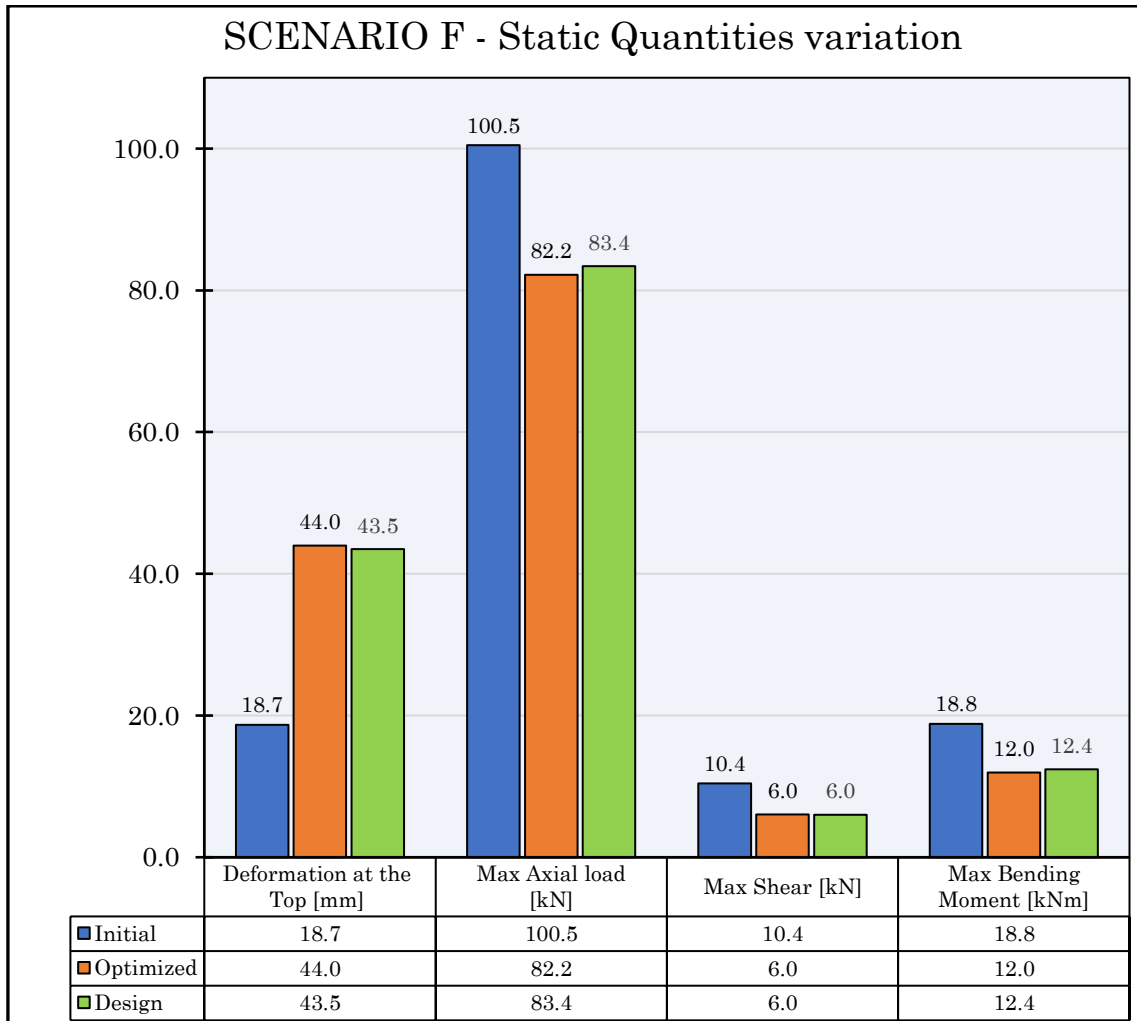


Figure 145. Scenario 'F'. In blue are illustrated the maximum values of Axial, Shear forces and Bending Moment at the initial situation, in orange at the optimized solution. In green they are represented at a design configuration according to the product list.

As more the structure becomes lighter and structurally efficient, the deformation at the top increases. For what concern the static quantities, the trend is always the same, in fact we have an overall decay in Axial load, Shear actions and bending moments.

7.7 Scenario ‘G’

As introduced in the chapter 4.4.7 the design vector is the following:

$$\mathbf{x} = [t_1, t_2, t_3, t_4, t_5]$$

Five different thickness are introduced in order to optimize as better as possible each segment. In this case the optimization procedure consists of 3 iterations N_{trial} , and it has been chosen the solution which have the lowest value of Fitness Function. The population-size is set to 20 according to [31], being $n = 5$. Because of increase of the population size, it has been decided to reduce N_{trial} in order to reduce computational time as well

Ntrial = 3					
t ₁	t ₂	t ₃	t ₄	t ₅	OF
[mm]	[mm]	[mm]	[mm]	[mm]	[kN]
3	4	4	3	3	34.985
3	4	3	3	3	34.751
3	4	3	4	3	34.985

Table 48. Scenario ‘G’, best solutions.

$$\mathbf{x}_{opt} = [3, 4, 3, 3, 3]$$

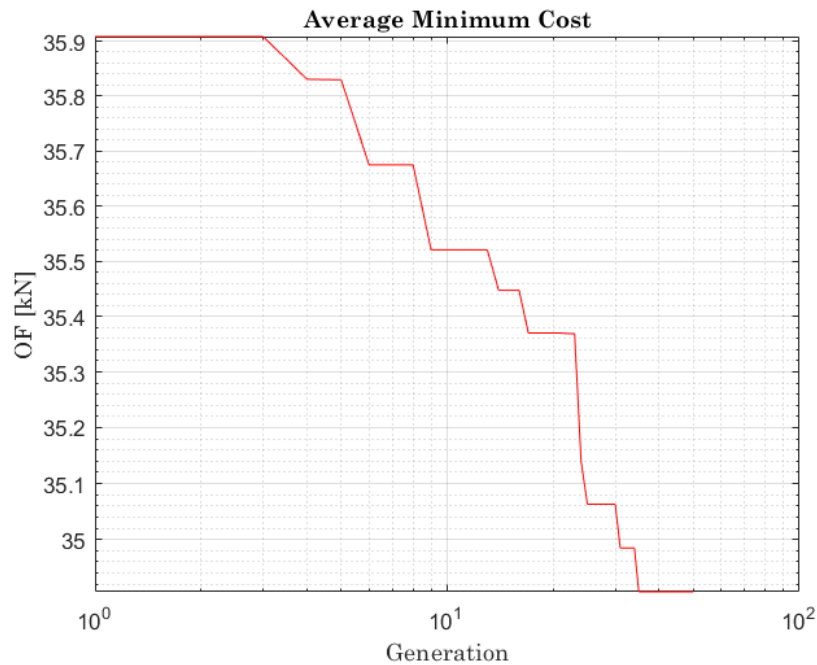


Figure 146. Scenario ‘G’. Decay of the Objective Function OF.

The total weight is computed and compared to the original structure. In this case we have a reduction of 1050 kg, or 72.88% by weight with respect the initial configuration.

SCENARIO G – <i>Optimized Solution</i>				
Element	d [mm]	t [mm]	L [mm]	Mass [Kg]
Pole 1 (0-6 m)	168.3	3	6000	73
Pole 2 (6-12 m)	168.3	4	6000	97
Pole 3 (12-18 m)	168.3	3	6000	73
Pole 4 (18-24 m)	168.3	3	6000	73
Pole 5 (24-30 m)	168.3	3	6000	73
Total Mass [kg]			Σ	391
Mass variation [kg]	-1050	Mass variation [%]		-72.88

Table 49. Scenario 'G'. Optimized solution. Keeping the same diameter at each segment and just managing the thickness of each segments the mass reduction is equal to 1050kg.

In

Table 50 is illustrated a possible design strategy according to a product list. In this case the mass variation is similar to the optimized solution (-71.22%).

SCENARIO G - <i>Design proposed according to product list</i>				
Element	d [mm]	t [mm]	L [mm]	Mass [Kg]
Pole 1 (0-6 m)	168.3	4	6000	97
Pole 2 (6-12 m)	168.3	4	6000	97
Pole 3 (12-18 m)	168.3	3	6000	73
Pole 4 (18-24 m)	168.3	3	6000	73
Pole 5 (24-30 m)	168.3	3	6000	73
Total Mass [kg]			Σ	414
Mass variation [kg]	-1026	Mass variation [%]		-71.22

Table 50. Scenario 'G'. Design solution. Industrial product list has available for a specific diameter, a large number of different thickness. This is reflected in this table, where the mass variation is similar to the optimized solution (-1026kg).

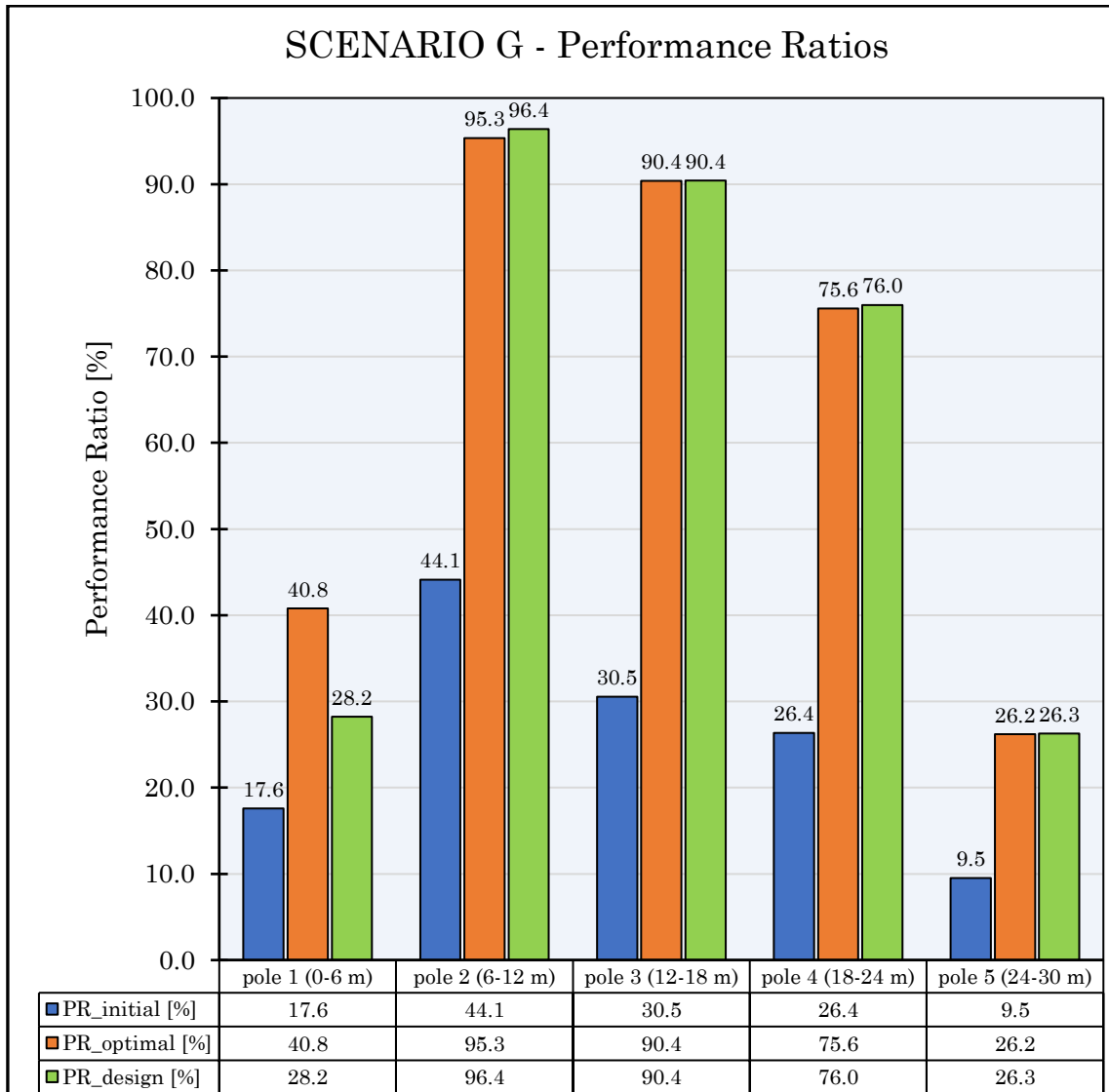


Figure 147. Scenario 'G' - PRs-trend. In blue are illustrated the Performance Ratios of each pole at the initial situation, in orange at the optimized solution. In green are represented PRs at a design configuration according to the product list.

By controlling the thickness at each segments we are able to achieve a good results in terms of Performance Ratio. Being the first and last segment low stressed, higher PRs are not reached because of the imposition of minimum thickness $t \geq 3m$.

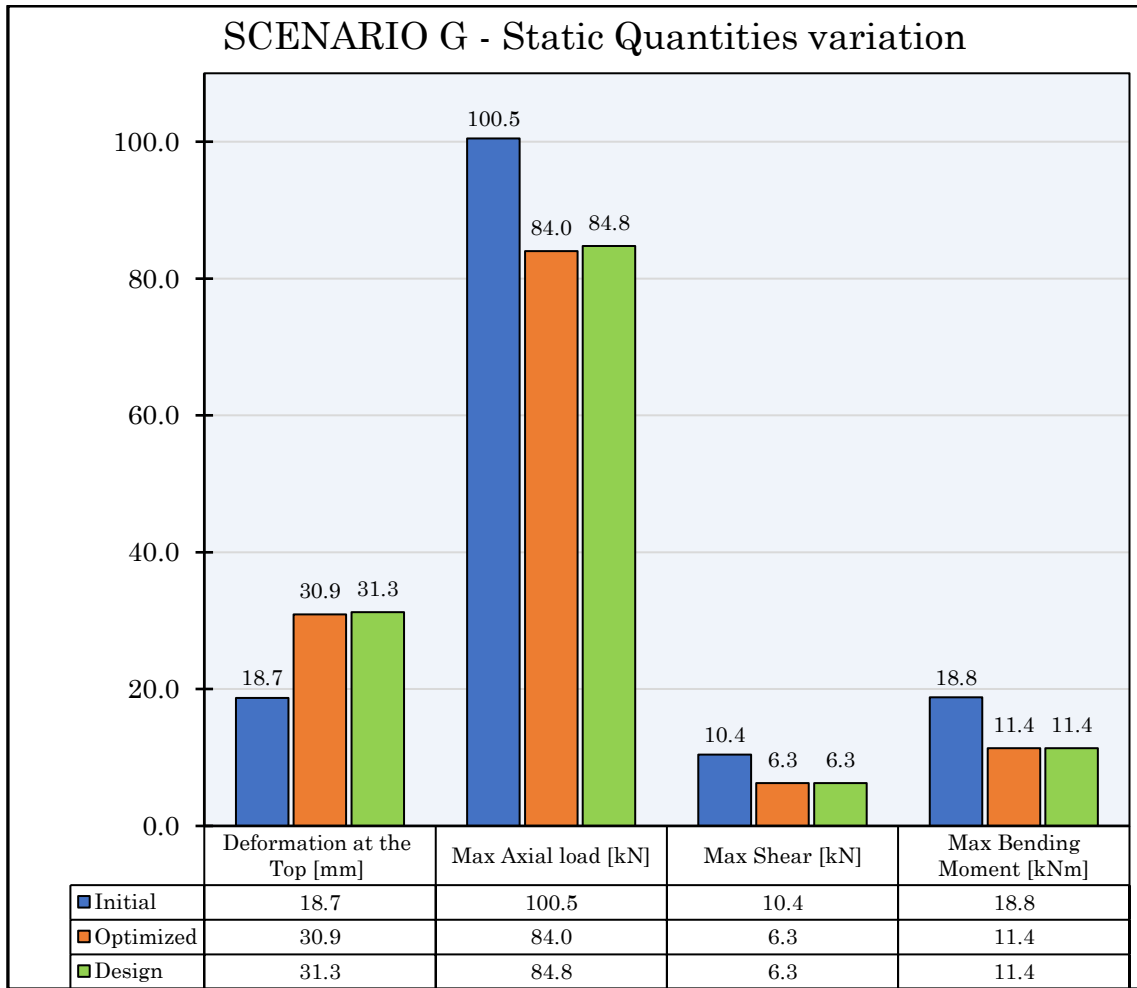


Figure 148. Scenario 'G'. In blue are illustrated the maximum values of Axial, Shear forces and Bending Moment at the initial situation, in orange at the optimized solution. In green they are represented at a design configuration according to the product list.

Compared with other scenarios, the deformation at the top is a little bit lower because in this case the diameter does not change, maintaining a certain level of stiffness.

7.8 Scenario ‘H’

As introduced in the chapter 4.4.8 the design vector is the following:

$$\mathbf{x} = [\Phi_i, \Phi_f, t_1, t_2, t_3, t_4, t_5, F]$$

In this case the optimization procedure consists of 3 iterations N_{trial} , and it has been chosen the solution which have the lowest value of Fitness Function. The population-size is set to 32 according to $2n \leq Pop.Size \leq 4n$, being $n = 8$.

Ntrial = 3								
Φ_i	Φ_f	t_1	t_2	t_3	t_4	t_5	F	OF
[mm]	[mm]	[mm]	[mm]	[mm]	[mm]	[mm]	[kN]	[kN]
164	109	4	5	4	3	3	0.9	34.789
167	111	3	6	4	3	3	2	34.839
158	96	3	6	4	4	3	2	34.695

Table 51. Scenario ‘H’, best solutions

$$\mathbf{x}_{pt} = [158, 96, 3, 6, 4, 4, 3, 2]$$

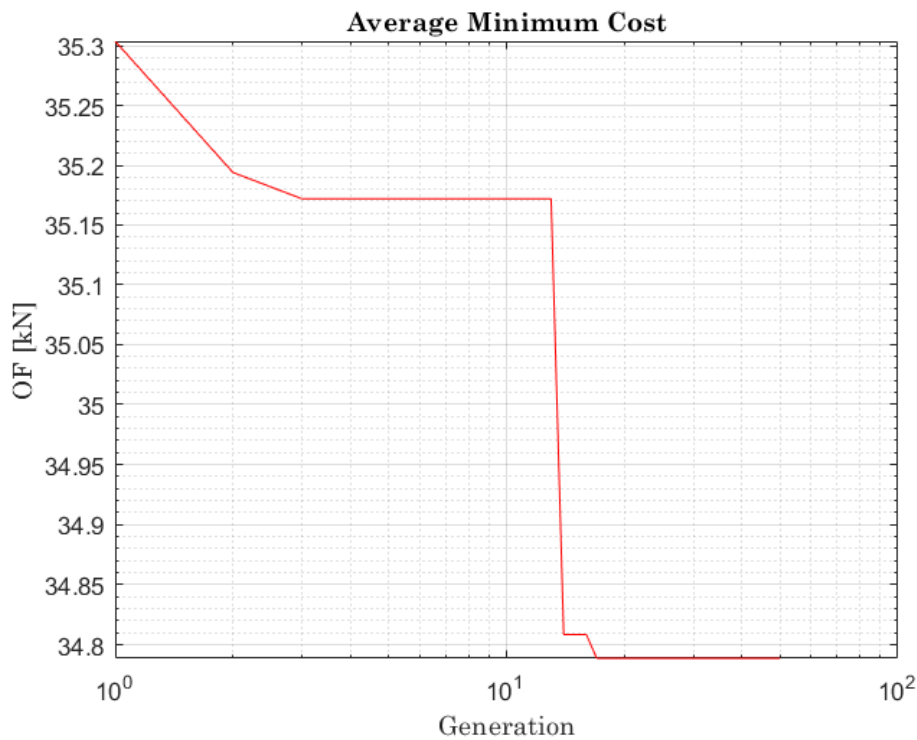


Figure 149. Scenario ‘H’. Decay of the Objective Function OF.

The total weight is computed and compared to the original structure. In this case we have a reduction of 1055 kg, or 73.27% by weight with respect the initial configuration.

SCENARIO H - <i>Optimized Solution</i>				
Element	d [mm]	t [mm]	L [mm]	Mass [Kg]
Pole 1 (0-6 m)	158	3	6000	69
Pole 2 (6-12 m)	146	6	6000	124
Pole 3 (12-18 m)	133	4	6000	76
Pole 4 (18-24 m)	121	4	6000	69
Pole 5 (24-30 m)	108	3	6000	47
Total Mass [kg]			Σ	385
Mass variation [kg]	-1055	Mass variation [%]		-73.27

Table 52. Scenario 'H', Optimized solution. Coupling tapering and 5 different thickness we obtain an hybrid solution that results in a reduction of 1055 kg.

In Table 53 is illustrated a possible design strategy according to a product list. In this case the mass variation is similar to the optimized solution (-71.65%).

SCENARIO H - <i>Design proposed according to product list</i>				
Element	d [mm]	t [mm]	L [mm]	Mass [Kg]
Pole 1 (0-6 m)	168.3	5	6000	121
Pole 2 (6-12 m)	168.3	4	6000	97
Pole 3 (12-18 m)	139.7	4	6000	80
Pole 4 (18-24 m)	139.7	3	6000	61
Pole 5 (24-30 m)	114.3	3	6000	49
Total Mass [kg]			Σ	408
Mass variation [kg]	-1032	Mass variation [%]		-71.65

Table 53. Scenario 'H'. Design solution.

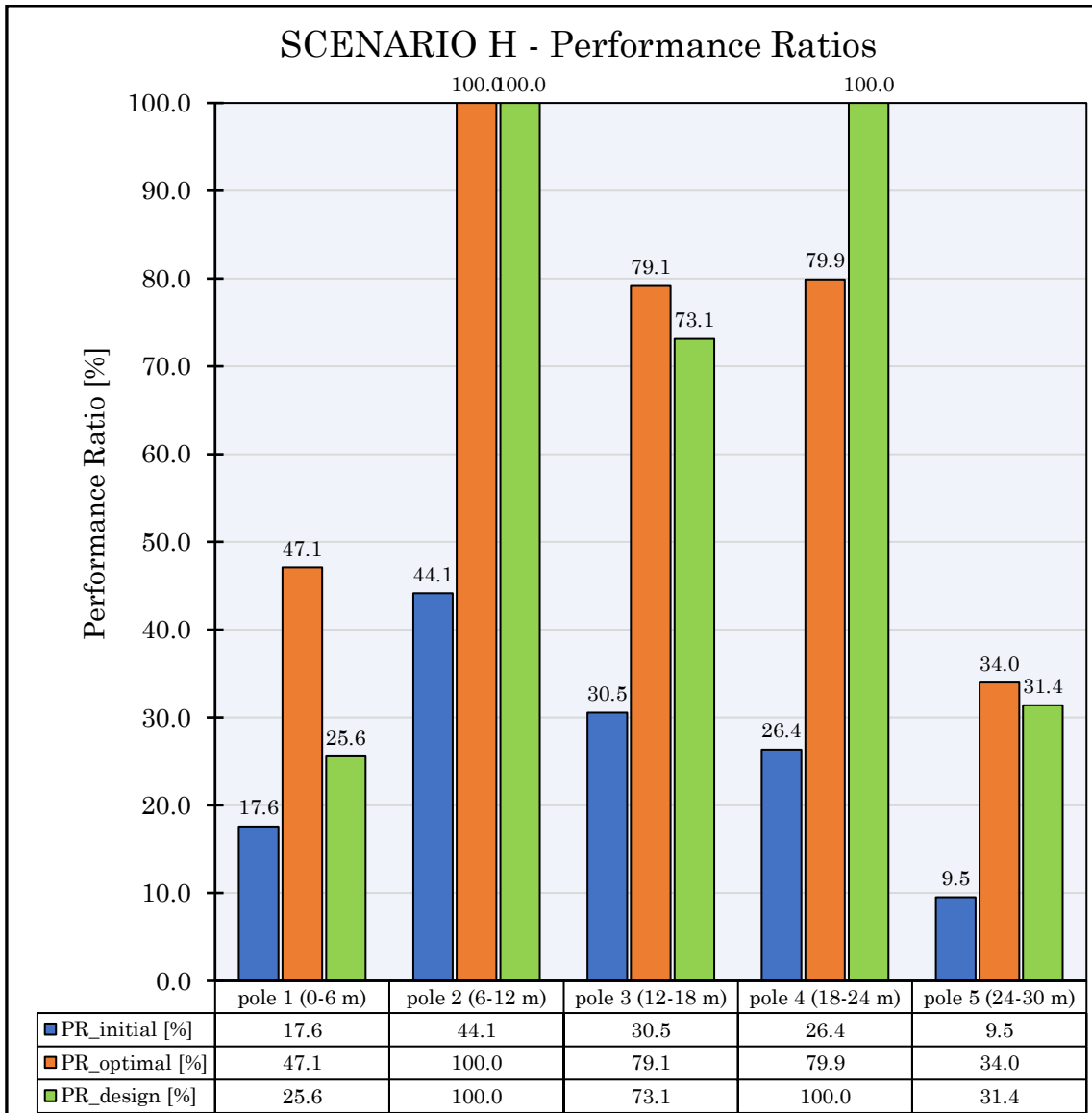


Figure 150. Scenario ‘H’ - PRs-trend. In blue are illustrated the Performance Ratios of each pole at the initial situation, in orange at the optimized solution. In green are represented PRs at a design configuration according to the product list.

In this scenario tapering and thickness are coupled. The result is overall better with respect scenarios *F* and *G*. In scenario *G* I had limitation regarding minimum thickness. Now I can proceed to reduce mass by decreasing the diameter.

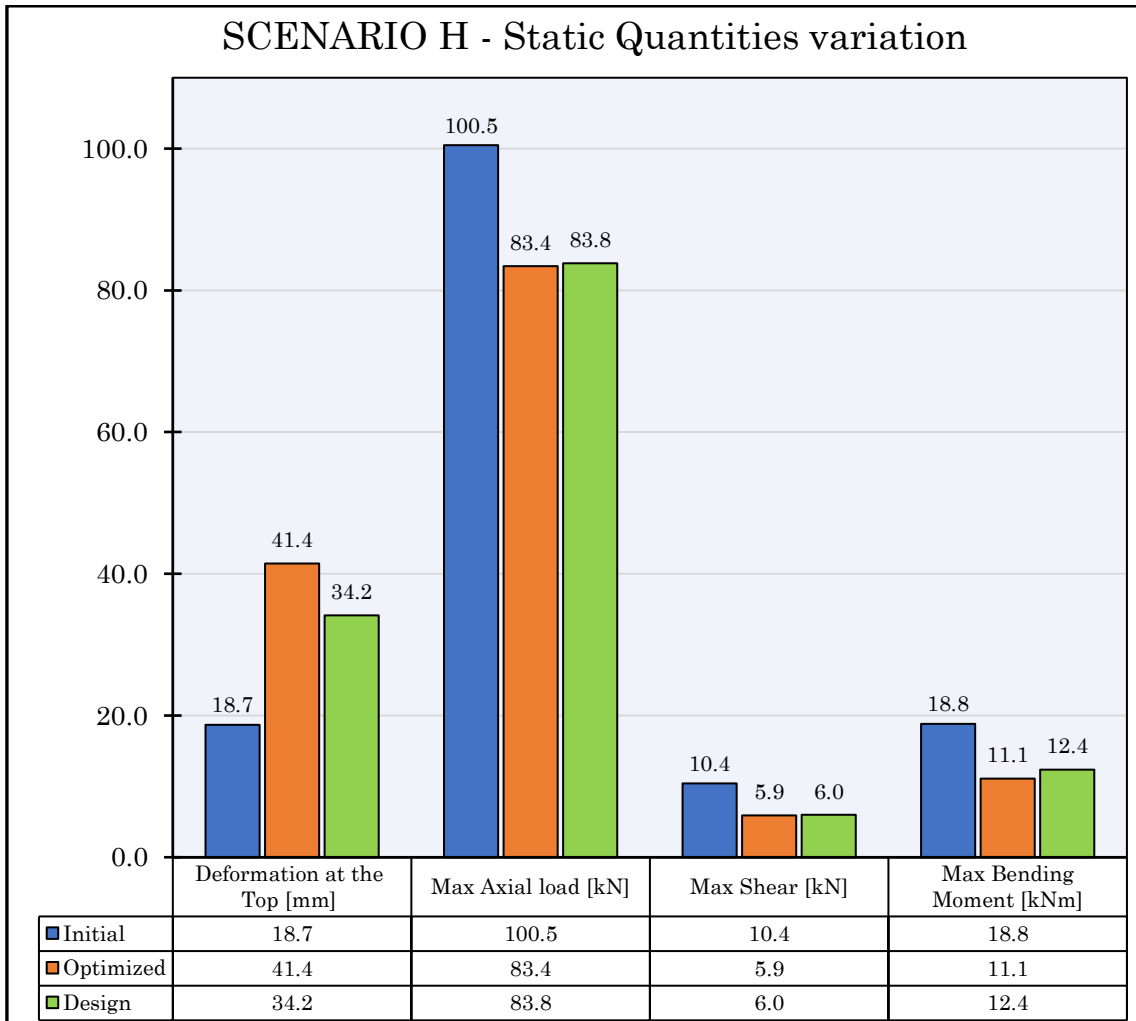


Figure 151. Scenario 'H'. In blue are illustrated the maximum values of Axial, Shear forces and Bending Moment at the initial situation, in orange at the optimized solution. In green they are represented at a design configuration according to the product lists.

In this scenario, we have higher deformation at the top with respect the previous scenario because we are managing the diameters as well.

8 Discussions and Results

It is important to notice how the *number of design variables* affect the results of the optimization procedure. The dimension of the search-space is obviously connected to the number of parameters, and clearly by using few variables, the final solution could be good, but not the best one. In our case, as discussed in *Scenario 'A'*, just managing the diameter Φ is not sufficient to find out an optimal solution. Moreover, to fit the scenario with industrial profiles, product lists do not contain infinite dimensions. Improvements are achieved when the search-space get larger by increasing the number of design variables.

First, in *Scenario 'B'*, the tapering of the main pole has been introduced using the linear law, as referred in the chapter 4.2. In this case the optimal solution is conditioned by intermediate areas which are more stressed, and consequently at the ends we have over-estimated elements. In response to that, *Scenario 'F'* has been introduced by adding t_{ends}, t_{inter} to fit better the problem. In *Scenario 'G'*, five different thickness are adopted ($t_1, t_2, t_3, t_4, t_5,$), and the results are like the previous case *'F'*. It means that the thickness of members is a good optimization parameter, while the diameter alone is not able to return interesting solutions, due to the fact that a linear interpolation trend is used. In addition, lower and upper limits were imposed for d and t . In particular, for this kind of structure it has been imposed a minimum diameter $d_{min} \geq 100 \text{ mm}$ and minimum thickness $t_{min} \geq 3 \text{ mm}$. Therefore, we ask how much d and t can affect the optimization. Given a circular hollow section, the cross-section area is:

$$A = \pi \cdot t \cdot (d + t)$$

The cross-sectional area goes with the square of t , and even if only small changes are made, the results will be consistent. In contrast, given a thin search space of d , and the linearly varying cross-sectional area, even significant modifications may not produce notable improvements.

If the increment of design variables involved in the structural optimization typically affects positively the results, the computational efforts is directly proportional to that number. The average time of each iteration is about 18 seconds. Given $Pop.Size = 10$, $Max.Gen = 50$, $Ntrial = 5$ the total time is almost 12.5 hours. Clearly for Scenarios with more than 3 design variables, according to $2n \leq Pop.Size \leq 4n$, the total time may reach much higher costs. Therefore, in some cases $Ntrial$ could be reduced to 2 or 3, because we are not interested in statistical analysis of the results. In our context the meaning of $Ntrial$ is make sure that numbers are coherent results and trial solutions are similar themselves; thereafter the solution with the lowest fitness function is chosen.

To summarize, the scenarios contain the following number of variables:

SCENARIO	n° design variables (parameters)
A (Φ)	1
B (Φ_i, Φ_f)	2
C (Φ_i, Φ_f, F)	3
D (Φ_i, Φ_f, t)	3
E (Φ_i, Φ_f, t, F)	4
F ($\Phi_i, \Phi_f, t_{ends}, t_{inter}, F$)	5
G (t_1, t_2, t_3, t_4, t_5)	5
G ($\Phi_i, \Phi_f, t_1, t_2, t_3, t_4, t_5$)	8

Table 54. Summary of the different scenarios.

In Table 55, the average values of *Performance Ratio* are illustrated. We want to demonstrate that increasing the number of design variable it may obtain better results. For our purposes the target is to exploit as more as possible the structural material, in this case the marker is the performance ratio.

n° parameters	PR_avg_initial	PR_avg_optimized	PR_avg_design
[-]	[%]	[%]	[%]
1	28.0	45.7	40.5
2		39.5	43.1
3		50.5	50.6
4		54.4	58.0
5		65.8	60.2
8		68.0	66.0

Table 55. How the number of design variables employed in the structural optimization affects the performance ratios of structural members.

As a second equally important goal, is the weight reduction. Essentially related to *PR*, mass reduction gives an idea about how much lighter (or heavier) the structure becomes as a result of the optimization process. It directly provides an estimate of cost savings.

n° parameters	Initial Mass	Optimized Mass	Design Mass
[-]	[kg]	[kg]	[kg]
1	1440	1003	1176
2		1051	1111
3		803	818
4		574	588
5		403	453
8		385	408

Table 56. How the number of design variables employed in the structural optimization affects the performance ratios of structural members.

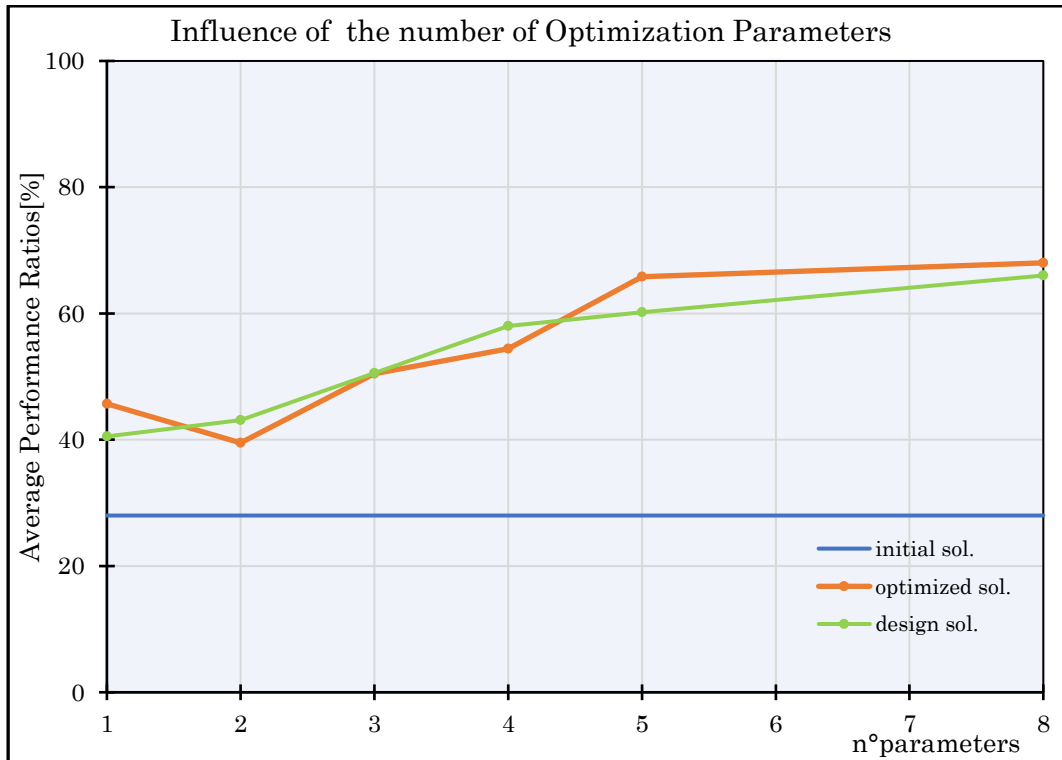


Figure 152. Influence of the number of Optimization Parameters. Average Performance Ratios.

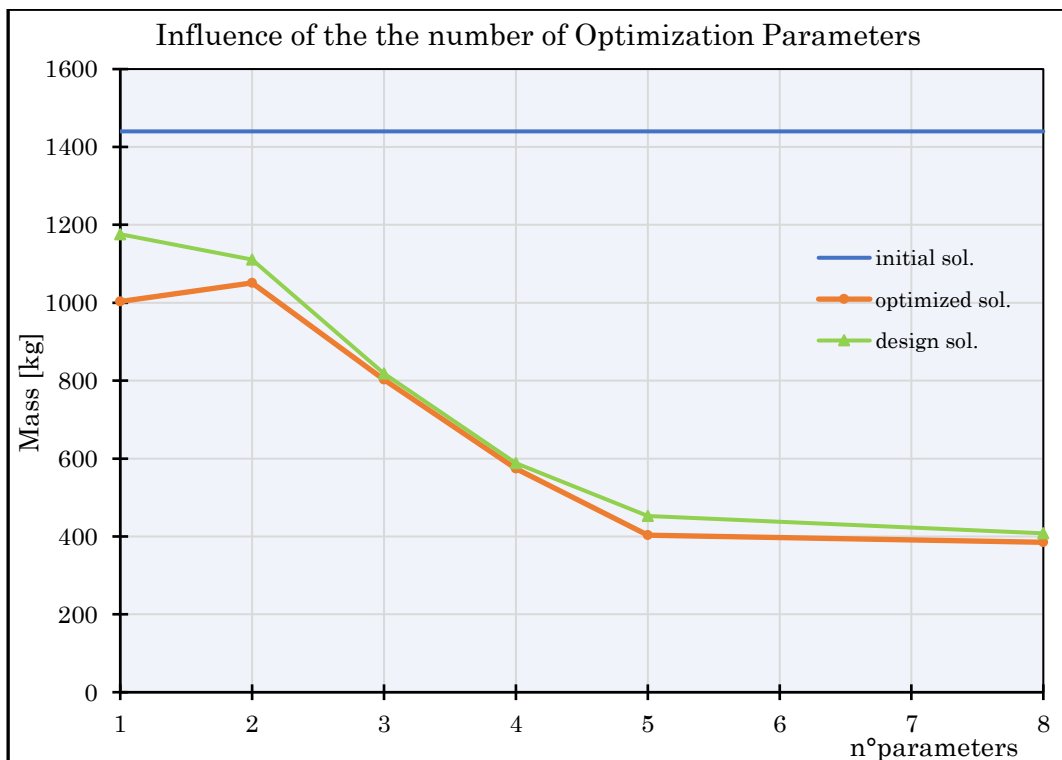


Figure 153. Influence of the number of Optimization Parameters. Mass of the main pole.

In Figure 152 is highlighted an increasing quasi-monotone behaviour of Performance Ratios with respect the number of design variables. In particular for $n \geq 5$ no significant improvements are achieved. In Figure 153 is emphasized an important reduction of structural mass as the design variables increase. Once again, $n = 5$ represents a good number of parameters. At the end of this work we need to know which is the scenario that exhibit the best value of OF in terms of Reduction weight and Performance Ratio. In Figure 154 a comparison between each scenario has been done, highlighting the difference with the initial state which has an average performance ratio $PR_0 = 25.6\%$. Once more, it is noticeable that an appreciate income is achieved for scenarios that take into consideration the thickness t as design variable.

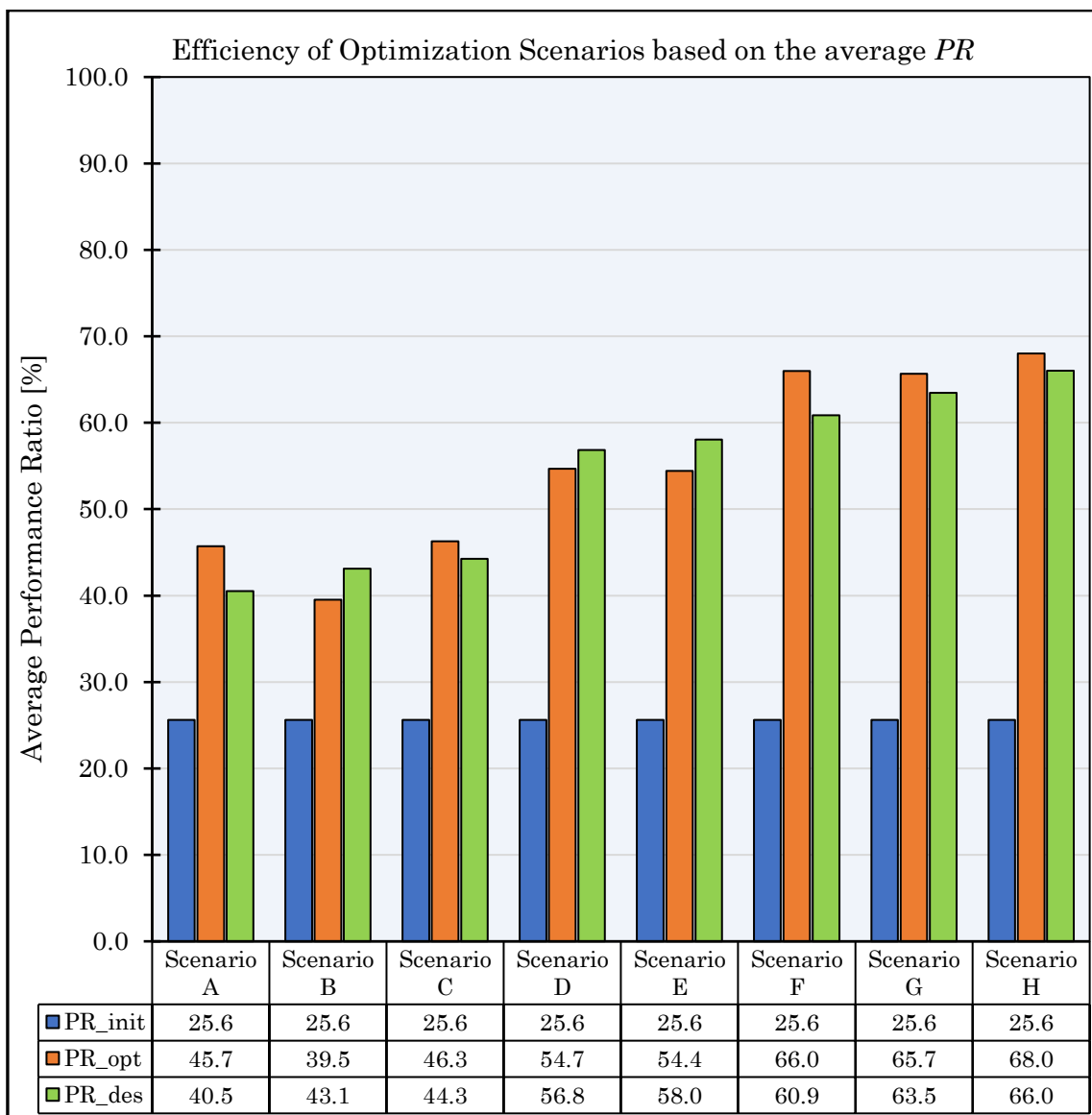


Figure 154. In blue, orange and green, the average PRs respectively at initial condition, after optimization, and design solution.

In particular, from *Scenarios D, E, F, G, H*, the average Performance Ratios exceed 50%, resulting in a potential differential equal to +40% with respect the initial state.

In every chart and table shown so far, a parallel study of a possible design strategy has been done, trying to fit the solution proposed by optimization. Looking at Figure 155 it can be recognized that the profiles provided by product list are sufficient to accommodate the optimized solution. An exception is noticeable in *Scenario ‘A’* because the optimization is performed using just one diameter Φ which is optimal for few parts of the structure, while others are “over-fitted” resulting in decrease of the performance ratios ($\cong -5\%$) and increase of structural mass (+173 kg), as showed in Figure 155.

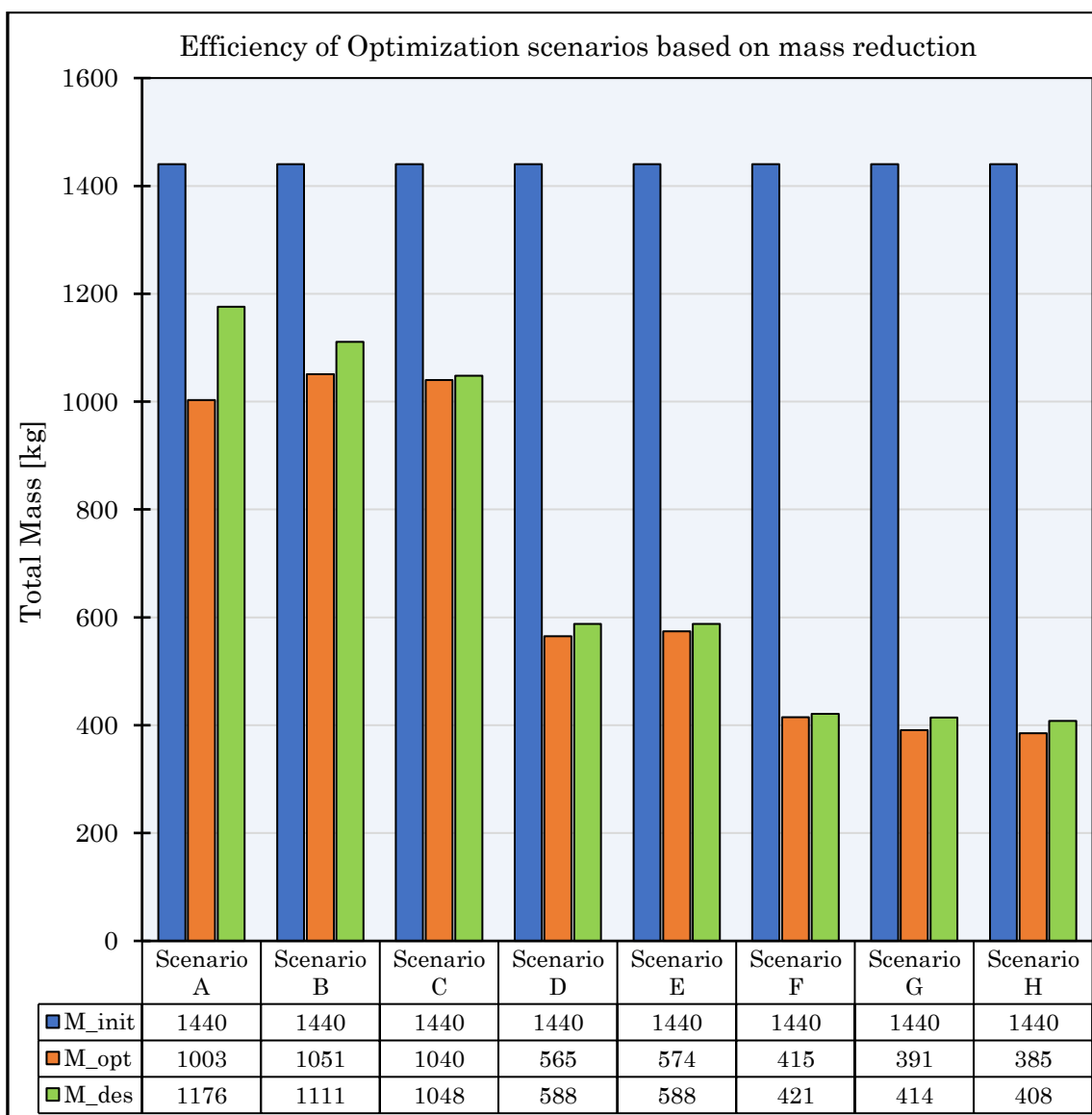


Figure 155. Increasing the number of design variables the final mass becomes gradually smaller until 385 kg (scenario H).

Until now we have discussed about the trend of PRs with respect the number of design variables, and consequently, the different scenarios. Similarly, it is once again appreciable a monotonic trend of the structural mass at the end of the optimization process. In this case, the tonnage decreases with the number of parameters. As indicated in Figure 155, from scenario D to H we have an overall decay of mass about $\cong -67.5\%$ ($\cong -972\text{ kg}$). Once more, in scenarios A, B, C, the thickness t of structural members is not taken into consideration and the mass-dropping is not satisfactory, about $\cong -28.4\%$ ($\cong -409\text{ kg}$).

The choice of the best scenario, it should be dependent from one of the five situations described above (from D to H) because of better *PRs-gain* and *mass-drop*. It could be a valid reasoning if we are studying only one single structure and clearly, we may choose whatever scenario, depending on design criteria. For example, 'G', if the thickness (t_1, t_2, t_3, t_4, t_5) is the only one variable that changes along the pole, or 'H', if also tapering (Φ_i, Φ_f) participates in the optimization. Otherwise, the discussion becomes more complicated if the optimization procedure is implemented in an *industrial supply chain project*. In this case, the time required to perform the optimization evolves into something that should not be neglected. The computational effort above-mentioned equal to 12.5 hours could change based on the number of design variables. Most scenarios that return best results are now discouraged because they require more time to provide solutions. At this point we are asked to determine which is the best option with regard computational cost as well. The main difficulty is to give the right weights to *Computational Costs T* and *Mass-Dropping ΔM* , or *PRs-gain*. Adopting a scenario which operates with high computational speed, it means to receive a low optimization degree. At the contrary, using scenarios characterized by high computational efforts, it would maximize material savings.

Scenario	N _{var}	Pop.Size	Max.Gen	N _{Trial}	t [s]	T [h]
A	1	4	50	5	~18	~5
B	2	10	50	5	~18	~12.5
C	3	10	50	5	~18	~12.5
D	3	10	50	5	~18	~12.5
E	4	10	50	5	~18	~12.5
F	5	20	50	3	~18	~15
G	5	20	50	3	~18	~15
H	8	32	50	3	~18	~24

Table 57. Computational Time $T = \text{Pop.Size} \cdot \text{Max.Generations} \cdot \text{Ntrial} \cdot t$.

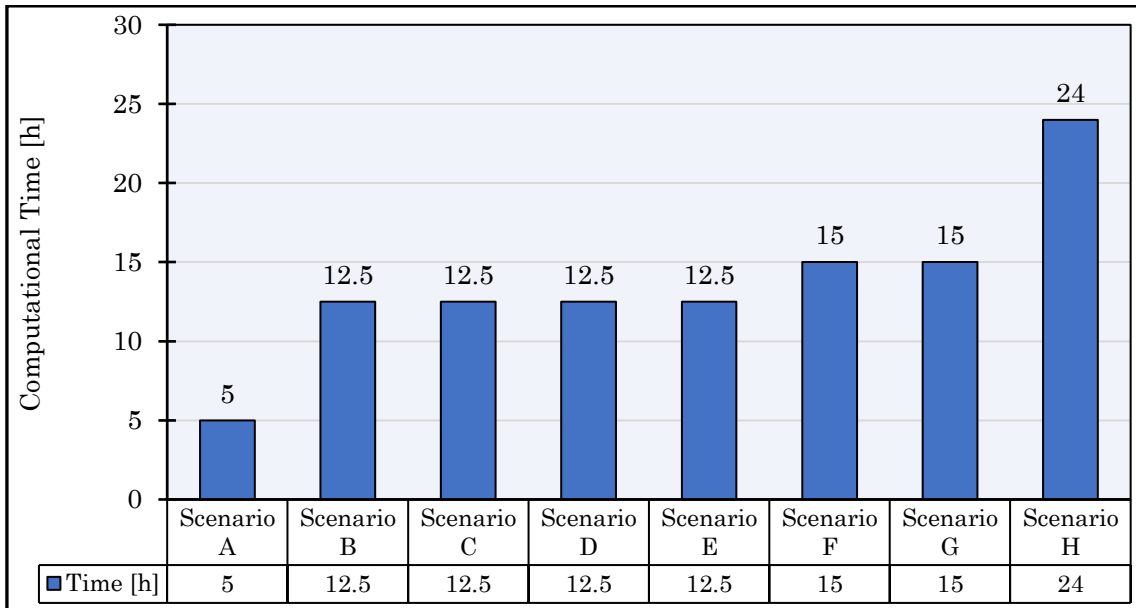


Figure 156. Computational efforts, knowing $t = 18$ seconds for each iteration

The Mass reduction, or Mass-Dropping resulted by optimization process is evaluated as follows:

$$\Delta M = M_0 - M_{opt}$$

where $M_0 = 1440 \text{ kg}$ is the initial mass before the optimization, M_{opt} is the optimized mass obtained at the end of the optimization process.

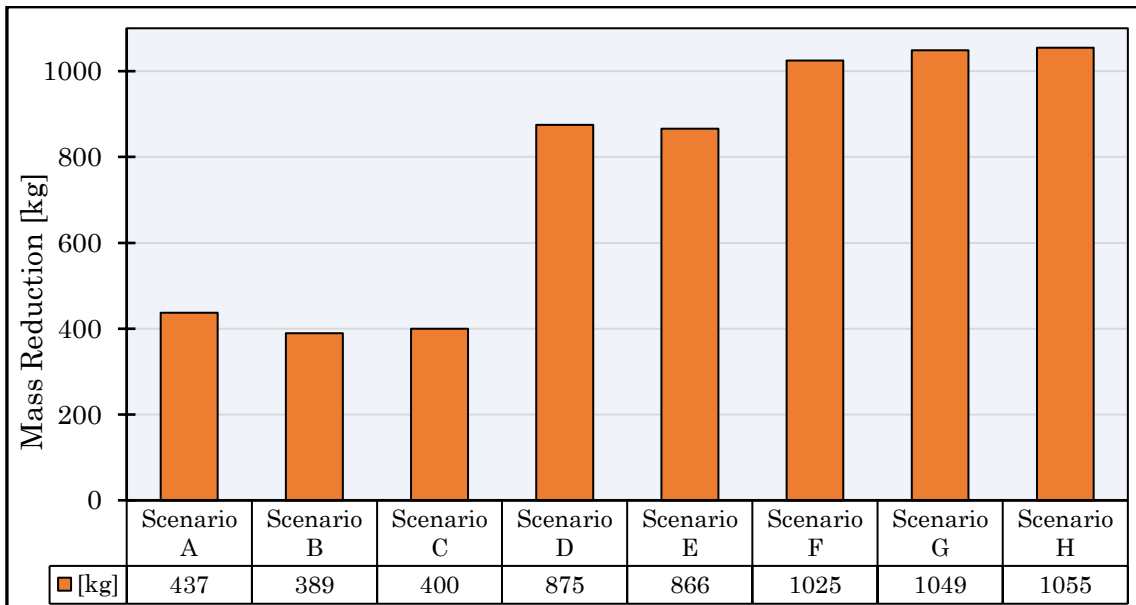


Figure 157. Mass Reduction $\Delta M = M_0 - M_{opt}$.

We can introduce a new mark, simply called ‘performance’ P , as an indicator that measures the optimization rate, expressed in $[kg/h]$. It explains the quantity of optimized material for unit time, and it is different for each scenario.

$$P = \frac{\Delta M}{T}$$

	A	B	C	D	E	F	G	H
T [h]	5	12.5	12.5	12.5	12.5	15	15	24
M _{opt} [kg]	1003	1051	1040	565	574	415	391	394
ΔM [kg]	437	389	400	875	866	1025	1049	1055
P [kg/h]	87.4	31.1	32.0	70.0	69.3	68.3	69.9	44.0

Table 58

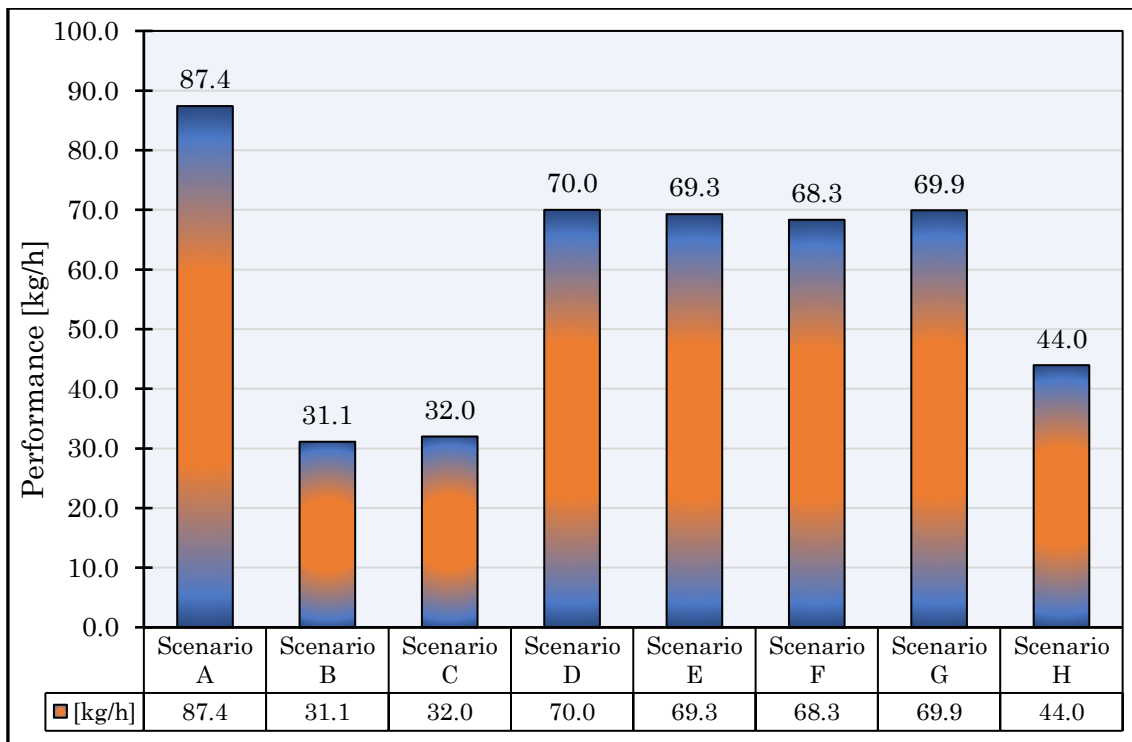


Figure 158. Providing the ratio between the mass reduction and the computational time, the quantity of structural material saved per unit of time is founded.

Despite these results, that highlight the computational effort for each scenario, we want to choose a scenario independently from the computational times. In fact, the computational times showed above are dependent from the Computer Processor used. So now we try to reason by number of iterations, that is independent from the technology employed. The objective is to provide the most likely number of iterations needed to achieve the minimum value of the OF, for each scenario. That number will not be affected by N_{Trial} , as the latter only makes our analysis more robust. Just to remember, N_{Trial} is the

number of whole procedures executed. In our case, N_{Trial} is set to 3 or 5. At the end of the following discussion they will be provided the number of iterations needed to Customers to optimize their structures avoiding loses of time related to N_{Trial} , assuring a certain level of confidence in the number of generations. Actually, in this thesis, a sufficient number of N_{Trial} s, that provide a robust statistical basis, has not been used due to lack of time. Anyway, the procedure has been done to explain the criteria that should be used. Once collected the OF for each N_{Trial} , the mean value μ , the variance σ^2 , and standard deviation σ have been computed for each scenario. Then $\mu + \sigma$ is computed, and it represents the value of the Objective Functions with the probability of $\sim 32\%$ to be exceeded. $\mu + \sigma$ is now compared with each single trial looking for the corresponding value of number of generations, as illustrated in Figure 159 in the specific case of Scenario ‘G’.

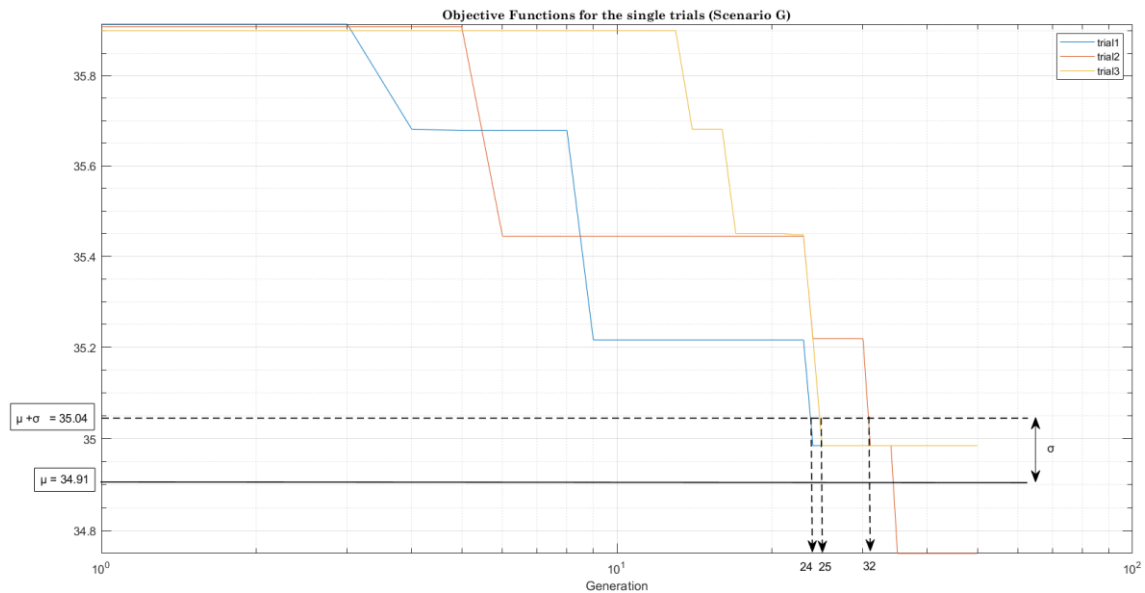


Figure 159. Objective Function for the single trial. Figure taken from Scenario ‘G’.

Once collected number of generations, the mean value, variance, and standard deviation are computed. The value $\mu + 3\sigma$ represents the number of generations that has a level of probability of $\sim 0.3\%$ to be exceeded. Multiplying that value by the *population size*, the total number of iterations needed to achieve the expected value of OF is obtained. All that procedure is summarized in Table 59.

n°variables- Scenarios	1-A	2-B	3-C	3-D	4-E	5-F	5-G	8-H
OF(N _{trial} 1)	40.76	41.25	41.39	36.46	37.77	35.14	34.98	34.79
OF(N _{trial} 2)	40.76	41.47	41.34	37.39	36.96	34.99	34.75	34.84
OF(N _{trial} 3)	40.76	41.25	41.23	36.49	36.55	35.06	34.98	34.70
OF(N _{trial} 4)	40.76	41.47	41.61	36.49	37.29	-	-	-
OF(N _{trial} 5)	40.85	41.23	41.12	36.52	38.34	-	-	-
mean value [μ]	40.78	41.33	41.34	36.67	37.38	35.06	34.91	34.77
variance [σ^2]	0.001	0.012	0.027	0.129	0.387	0.004	0.012	0.004
std. Dev [σ]	0.041	0.123	0.184	0.402	0.695	0.074	0.135	0.073
[$\mu + \sigma$]	40.82	41.45	41.52	37.07	38.08	35.14	35.04	34.85
n° Generations for [$\mu + \sigma$]	14	3*	18	1*	1*	29	23	14
	17	3*	42	5	48	34	24	28
	28	49	24	37	4	46	34	27
	48	23	36	25	8	-	-	-
	44	48	48	47	1*	-	-	-
mean value [μ]	30.2	40.0	33.6	28.5	20.0	36.3	27.0	23.0
variance [σ^2]	189.8	144.7	123.8	244.8	394.7	50.9	24.7	40.7
std. Dev [σ]	15.4	14.7	12.4	18.1	24.3	8.7	6.1	7.8
Pop.Size	4	10	10	10	10	20	20	32
($\mu+3\sigma$)·Pop.Size	306	842	709	827	930	1251	905	1486

Table 59.

Finally, in Figure 160, the weight of the structure at the end of the optimization procedure and the n° of iterations for each scenario are plotted. It can be recognised an expected reduction in the usage of material, as it has been discussed previously. Actually, we expect to have a different trend in scenarios *B* and *C* regarding mass reduction, in fact the weight increases a little bit with respect scenario *A*. Essentially in the latter only one diameter optimizes the structure, while in the other two, the tapering is not sufficient, being also a minimum diameter imposed (100 mm) that does not allow to fit well the problem. The difference between these scenarios is the order of about 4% in weight, that is negligible for our purposes. *By the way, we do not want to prove that using more variables certainly means getting best results.* In the same way the expected trend of the number of iterations should be monotonically increasing with the number of variables. Instead, a very noticeable exception occurs in scenario *G*, in which a quick reduction of iteration is highlighted. To summarize, in this situation the design variables involved are t_1, t_2, t_3, t_4, t_5 , which are the thicknesses of the five segments that compose the main pole. In this case, the search-space of the solutions is much

smaller, and therefore the search for the optimum one involves lower computational costs.

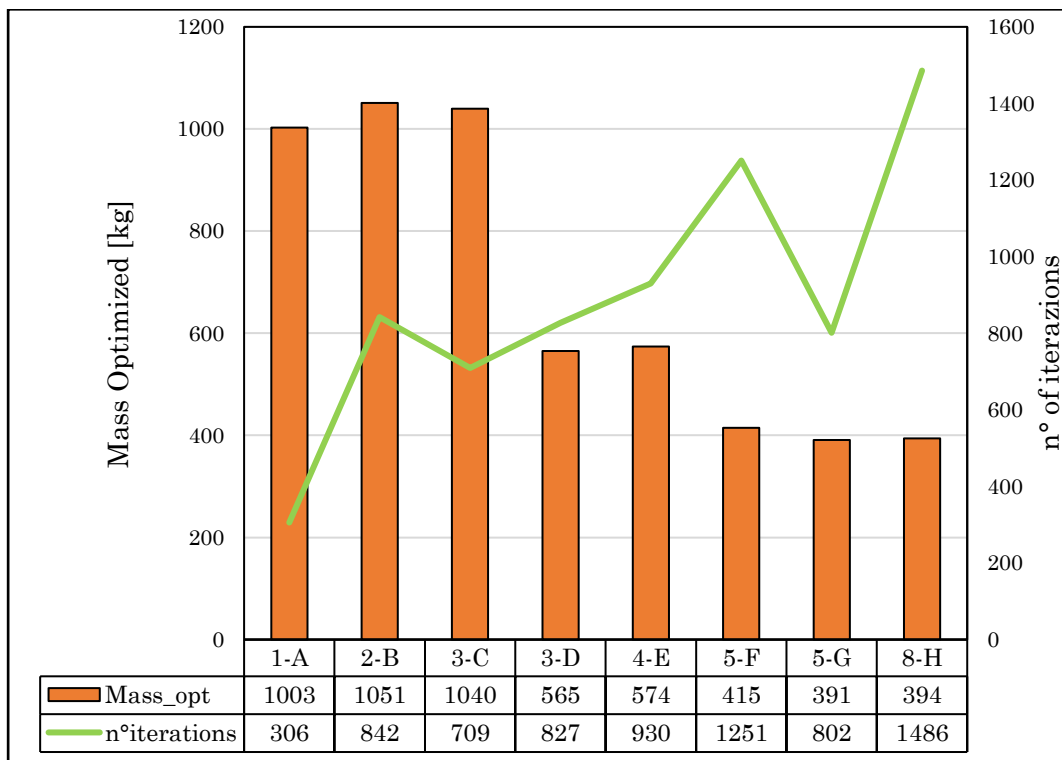


Figure 160.

9 Conclusions and future developments

In this thesis, a size optimization process on Guyed Radio Mast was performed with the aim to identify the equilibrium solution which guarantees the lighter optimized model verifying the strength and instability safety of the structure. The well-known OAPI was used to perform structural analysis with software FEM SAP2000 on the optimized structure considering the non-linearity of the cables. The optimization strategy was conducted using GA algorithm, which was tested on specific structure and varying different parameters such as the investigated case study.

A parametric modelling has been performed to investigate the variables that mainly affect the industrial solution considered as the target of this work.

Several scenarios were investigated considering different optimization strategies varying geometric characteristics respectively of the main pile and cables. The number of the input parameters to perform the optimization was increased from the scenario *A* to *H* since best fitness value of the self-weight was found. In this way, a well-oriented research area was guaranteed since the beginning of the first iterations algorithm.

As we expected, observing the results of the optimization for each scenario a positive trend of the *OF* was recognised. From Scenario *A* to *H* the mass reduction index generally increases as the computational effort with the exception of scenarios B and E, in which the input parameter do not represent the best vector design for the structural optimization.

At this stage, the best industrial solution was evaluated from the Database section of the Software *FEM* in terms of distance gap from the optimized one. Moreover, a performance index was calculated for evaluating the best compromise solution between Mass reduction and Computational effort. Though the Scenario *A* provides the worst structural solution in terms of *OF*, it represents the most convenient optimization strategy due to its low computational effort; on the contrary, Scenario *H* exhibits the best fitness value with the lowest self-weight, but it represents the most time-consuming solution. For these reasons, a compromise solution might be offered by Scenario *D* which provides Mass reduction index which is very close to the highest obtained among the scenarios investigated with reasonable computational burden.

In conclusion, the best solution is reached when thickness values of each member, which compose the main pole is taken into account during the Optimization process. Increasing thickness, an improvement of the sectional behaviour respect to the instability problem is observed. This verification, in fact, represents the most critical one for this type of structure which are mainly subjected to normal stress resulting from self-weight and prestressing cable force. The entire optimization process seems to be not sensible considering diameter as input parameter of the design vector.

As future development, exchanging circular hollow sections with steel built-up solutions could provide best solution in terms of structural performance and assemblage procedures. Especially for higher structures, it is usual to recognize guyed radio masts consisting of truss skeleton.

Another possible development may be a structural optimization for a cable-stayed radio antenna adopting other optimization strategies, as Particle Swarm Optimization *PSO* and Evolution Differential Algorithm *EDA* which could be less time-consuming.

Finally, it could perform a typological optimization by managing the position of the cables connection, trying to find the best attachment points.

10 References

- [1] TIMOSHENKO, STEPHEN & GERE, JAMES M. (1961). *Theory of Elastic Stability*. 2, rev. ed. New York: McGraw-Hill.
- [2] GIULIO BALLIO, FEDERICO M. MAZZOLANI, CLAUDIO BERNUZZI, RAFFAELE LANDOLFO, *Strutture di Acciaio_Teorica e Progetto*, 2nd Edition, Hoepli (2020).
- [3] MINISTERO DELLE INFRASTRUTTURE E DEI TRASPORTI, *Norme Tecniche per le Costruzioni*, Decreto ministeriale 17 gennaio 2018.
- [4] EUROPEAN COMMITTEE FOR STANDARDIZATION (CEN / TC250), *Eurocode 3: Design of Steel Structures*.
- [5] K. HAILEMICHAEL, B. LIIVO, «*Stability of Slender Columns*», Division of Structural Engineering, Faculty of Engineering, LTH, Lund University, (2014).
- [6] J.A. YURA, T.H. HELWIG, «*Bracing for Stability*», University of Texas at Austin, University of Houston, Structural Stability Research Council, American Institute of Steel Construction, (1995).
- [7] J.A. YURA, T.H. HELWIG, «*Continuous Bracing System for Columns and Beams*», M.ASCE, American Society of Civil Engineers , (2021).
- [8] ALBERTO CARPINTERI, «*Instabilità Statica e Dinamica delle Strutture*», dispense, Dipartimento di Ingegneria Strutturale e Geotecnica, Politecnico di Torino.
- [9] ALBERTO CARPINTERI, «*Scienza delle Costruzioni*», Pitagora Editrice Bologna.
- [10] ALBERTO CARPINTERI, «*Advanced Structural Mechanics*», CRC Press, Taylor & Francis Group, 2017.
- [11] RAPHAEL T. HAFTKA, ZAFER GÜRDAL, «*Element of Structural Optimization*», G.M.L. Gladwell, Solid Mechanics Division, Faculty of Engineering, University of Waterloo, Ontario, Canada.
- [12] PETER W. CHRISTENSEN, ANDERS KLARBRING, «*An Introduction to Structural Optimization*», Springer, Solid Mechanics and its Applications.
- [13] LINFENG MEI, QUIAN WANG, «*Structural Optimization in Civil Engineering: A Literature Review*», MDPI, Department of Building, School of Design and Environment, National University of Singapore, 2021.
- [14] TUAN Q. PHAM, T. T. H. LUONG, «*A comparison of the performance of Classical Methods and Genetic Algorithms for Optimization Problems involving Numerical Models*», Conference Paper, Australia, 2004.

- [15] J. J. DURILLO, E. ALBA, Y. ZHANG, A. J. NEBRO, «*A Study of the Multi-objective Next Release Problem*», Genetic and Evolutionary Computation Conference, GECCO 2007, Proceedings, London, England, UK, July 7-11, 2007.
- [16] G. DHIMAN, V. KUMAR, «*Spotted hyena optimizer: A novel bio-inspired based metaheuristic technique for engineering applications*», *Advances in Engineering Software* 114, 2017.
- [17] C. BLUM, A. ROLI, «*Metaheuristics in Combinatorial Optimization: Overview and Conceptual Comparison*», *ACM Computing Surveys*, 2003.
- [18] X. S. YANG, «*Metaheuristic Optimization*», Scholarpedia, 2011.
- [19] M. P. SAKA, O. HASANCEBI, Z. W. GEEM, «*Metaheuristics in structural optimization and discussion on harmony search algorithm*», *Swarm Evolutionary Computation*, 2016.
- [20] S. MAHDAVI, M. E. SHIRI, S. RAHNAMAYAN, «*Metaheuristics in large-scale global continues optimization: A survey*», *Information Sciences*, 2014.
- [21] D. SONI, «*Introduction to Evolutionary Algorithms*», *Towards Data Science*, 2018.
- [22] T. B. BEIELSTEIN, J. MEHNEN, J. BRANKE, «*Evolutionary Algorithms*», *Wiley Interdisciplinary Reviews: Data Mining and Knowledge Discovery*, 2014.
- [23] K. C. WONG, «*Evolutionary Algorithms: Concepts, Designs, and Applications in Bioinformatics*», arXiv:1508.00468, 2015.
- [24] V. MALLAWAARACHCHI, «*Introduction to Genetic Algorithms*» *Towards Data Science*, 2017.
- [25] Z. HUANG, Y. CHEN, «*An Improved Differential Evolution Algorithm based on Adaptive Parameter*», *Hindawi Publishing Corp., Journal of Control Science and Engineering, China*, 2013.
- [26] R. MARTÌ, P. M. PARDALOS, , M. G. C. RESENDE, «*Handbook of Heuristics*», *Springer Nature, Switzerland*, 2018.
- [27] A. ELKASABY, A. SALAH, E. Z. ELFEKY, «*Multiobjective Optimization using Genetic Programming: Reducing Selection Pressure by Approximate Dominance*», 6th *International Conference on Operations Research and Enterprise Systems*, 2017.
- [28] B. MORGAN, «*Genetic Programming*», *Towards Data Science*, 2021.
- [29] N. HANSEN, D. A. ARNOLD, A. AUGER, «*Evolution strategies*», *Hand. of Comput. Intellig.*, Springer, <http://www.cmap.polytechnique.fr>, 2015
- [30] H. G. BEYER, H. P. SCHWEFEL, «*Evolution strategies: A comprehensive intoduction*», *Natural Computing*, 2002.

- [31] RAO SINGIRESU, *Engineering Optimization Theory and Practice*, John Wiley & Sons, Fifth Edition, 2019.
- [32] M. M. ROSSO, «*Structural Optimization with Swarm-based Algorithms*», Master Degree Thesis, Politecnico di Torino, Oct. 2020.
- [33] <https://www.azionadigitale.com> «*API cosa sono e come funzionano*».
- [34] «*Technical Standards and Infrastructure Requirements*», Malaysian Technical Standards Forum Bhd.
- [35] R. BELEVICIUS, D. JATULIS, D. ŠEŠOK, «*Optimization of tall guyed masts using genetic algorithms*», *Engineering Structures* 56 (2013) 239–245.
- [36] CONSIGLIO NAZIONALE DELLE RICERCHE, «*Istruzioni per la valutazione delle azioni e degli effetti del vento sulle costruzioni*», ROMA – CNR 06 febbraio 2019.
- [37] R. CUCUZZA, C. COSTI, M. M. ROSSO, M. DOMANESCHI, G. C. MARANO, «*Optimal strengthening by steeltruss arches in prestressed girder bridges*», *Proceedings of the Institution of Civil Engineers - Bridge Engineering* 0 0:0, 1-21.
- [38] K. PARSOPOULOS, M. VRAHATIS, «*Unified Particle Swarm Optimization for Solving Constrained Engineering Optimization Problems*», *International Conference on Natural Computation*; Springer: Berlin/Heidelberg, Germany, 2005; Volume 3612, pp. 582–591.
- [39] M. M. Rosso, R. Cucuzza, A. Aloisio, G. C. Marano, «*Enhanced Multi-Strategy Particle Swarm Optimization for Constrained Problems with an Evolutionary-Strategies-Based Unfeasible Local Search Operator*», *Appl. Sci.* 2022, 12, 2285. <https://doi.org/10.3390/app12052285>.